USGS
science for a changing world

Use of Environmental Tracers to Estimate Parameters for a Predevelopment Ground-Water-Flow Model of the Middle Rio Grande Basin, New Mexico

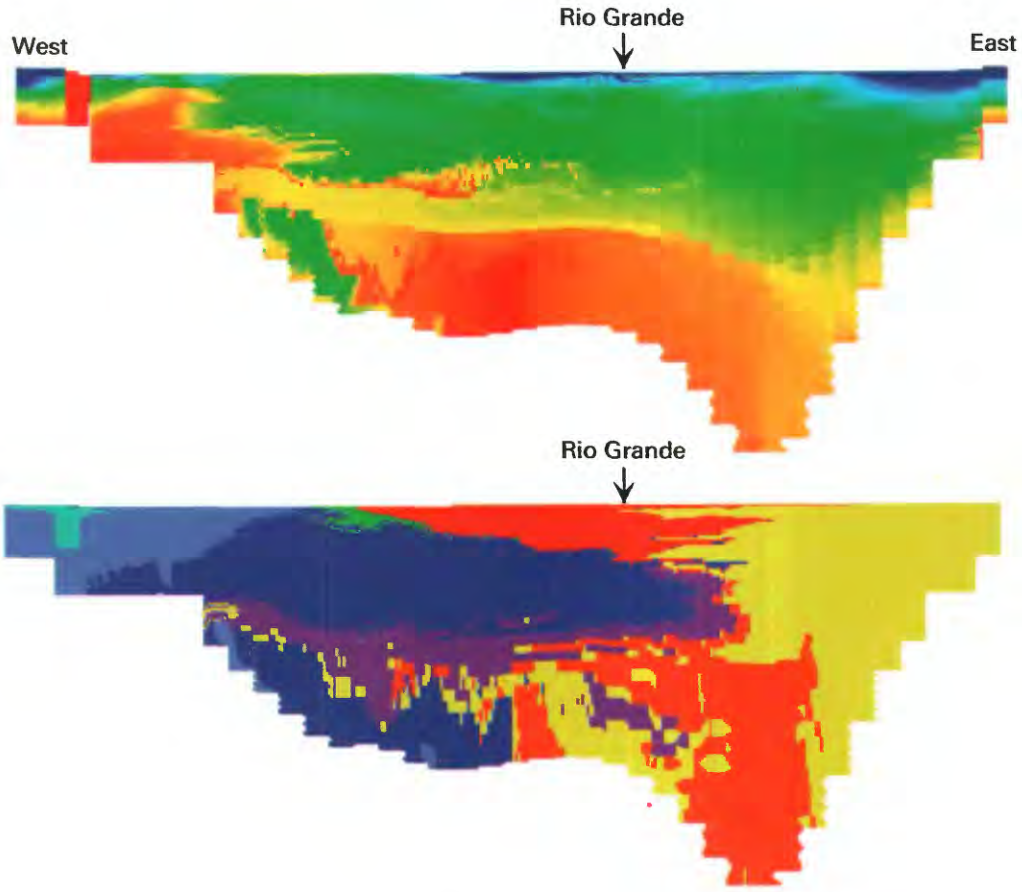

Water-Resources Investigations Report 03-4286

U.S. Department of the Interior
U.S. Geological Survey

Use of Environmental Tracers to Estimate Parameters for a Predevelopment Ground-Water-Flow Model of the Middle Rio Grande Basin, New Mexico

Ward E. Sanford, L. Niel Plummer, Douglas P. McAda, Laura M. Bexfield, and Scott K. Anderholm

Water-Resources Investigations Report 03-4286

U.S. Department of the Interior
U.S. Geological Survey

U.S. Department of the Interior
Gale A. Norton, Secretary

U.S. Geological Survey
Charles G. Groat, Director

U.S. Geological Survey, Reston, Virginia: 2004

For sale by U.S. Geological Survey, Information Services
Box 25286, Denver Federal Center
Denver, CO 80225

For more information about the USGS and its products:
Telephone: 1-888-ASK-USGS
World Wide Web: http://www.usgs.gov/

CONTENTS

FIGURES

TABLES

CONVERSIONS FACTORS AND DATUM

Multiply	By	To obtain
	Length	
inch (in.)	2.54	centimeter (cm)
foot (ft)	0.3048	meter (m)
mile (mi)	1.609	kilometer (km)
	Area	
acre	4,047	square meter (m^2)
acre	0.004047	square kilometer (km^2)
square foot (ft^2)	0.09290	square meter (m^2)
square mile (mi^2)	2.590	square kilometer (km^2)
	Volume	
gallon (gal)	3.785	liter (L)
cubic foot (ft^3)	0.02832	cubic meter (m^3)
acre-foot (acre-ft)	1,233	cubic meter (m^3)
	Flow rate	
acre-foot per year (acre-ft/yr)	1,233	cubic meter per year (m^3/yr)
cubic foot per second (ft^3/s)	0.02832	cubic meter per second (m^3/s)
gallon per day (gal/d)	0.003785	cubic meter per day (m^3/d)
	Mass	
ounce, avoirdupois (oz)	28.35	gram (g)
pound, avoirdupois (lb)	0.4536	kilogram (kg)
	Hydraulic conductivity	
foot per day (ft/d)	0.3048	meter per day (m/d)

Temperature in degrees Celsius (°C) may be converted to degrees Fahrenheit (°F) as follows:

$$°F=(1.8×°C)+32$$

Temperature in degrees Fahrenheit (°F) may be converted to degrees Celsius (°C) as follows:

$$°C=(°F-32)/1.8$$

Use of Environmental Tracers to Estimate Parameters for a Predevelopment Ground-Water-Flow Model of the Middle Rio Grande Basin, New Mexico

Ward E. Sanford, L. Niel Plummer, Douglas P. McAda, Laura M. Bexfield, and Scott K. Anderholm

ABSTRACT

The question of the availability of ground water as a long-term resource in the Middle Rio Grande Basin of central New Mexico has been addressed recently by the development of ground-water-flow models by the U.S. Geological Survey. An initial model constructed in 1994 was updated by Kernodle and others (1995), and then calibrated by Tiedeman and others (1998) using nonlinear regression methods and additional hydrologic observations. A new model was constructed using some of the results from the Middle Rio Grande Basin initiative by McAda and Barroll (2002). This report documents the use of ^{14}C activities and the location of hydrochemical zones to constrain parameter values used in a predevelopment ground-water-flow model of the Middle Rio Grande Basin. The universal inverse modeling code, UCODE, was used to help estimate hydraulic conductivities of hydrogeologic units and current and past recharge along the basin margins and tributary rivers. The water levels in the basin were simulated using MODFLOW, and travel times to wells and source-area delineation were simulated using MODPATH.

A three-dimensional geologic model was discretized into a three-dimensional MODFLOW grid of the basin. Major hydrogeologic units in the geologic model included volcanic rocks, and several units that represent the Santa Fe Group sediments, including ancestral gravels from the Rio Grande and some finer grained units that represent the middle and lower Santa Fe Group. The MODFLOW grid represented the hydrogeologic units with nine layers of variable thickness totaling up to 12,000 feet in places, and a uniform horizontal grid resolution of one square kilometer (0.386 square miles). The bottom of the model was considered to be the base of the poorly to semiconsolidated basin-fill sediments as defined by geophysical observations. Observations that were used to calibrate a steady-state predevelopment model, and then a transient paleohydrologic model, included 200 water levels and 200 ^{14}C activities. Observed water levels were compared with simulated water levels, and observed ^{14}C activities were compared with simulated ^{14}C activities based on travel times to individual wells. In addition, the distributions of ground water that originated from the Rio Grande and Rio Puerco were also used as constraints by comparing the percentage of river water in certain hydrochemical target regions with the percentage is simulated river water. The ^{14}C activities were adjusted for chemical reactions along the flow paths and for long-term variation in atmospheric input.

Hydraulic conductivities estimated for the model using the inverse procedure were similar to values that had been estimated in the previous models. The best-fit value of hydraulic conductivity of the Rio Grande alluvium and the volcanic rocks averaged about 30 feet per day, which is in agreement with field tests and earlier models. The best-fit hydraulic conductivity of a silty layer identified in the geologic model was estimated to be about 0.4 feet per day, which is also in agreement with field tests. The ratio of horizontal to vertical hydraulic conductivity was estimated for 12 different regions of the basin, with the best-fit ratios for the different regions ranging from 230:1 to 3,400:1.

Basin-margin and tributary recharge estimates were lower than estimates used in previous models. The 1995 ground-water-flow model assigned total margin and tributary recharge values of 138,600 acre-feet per year, based primarily on previous estimates using the water-budget method. The 1998 version of the model estimated this external recharge to be 95,500 acre-feet per year, based on inverse modeling using primarily water levels. The 2002 version of the model used a combination of estimates from previous sources and those from a chloride mass-balance study to arrive at a recharge of 67,500 acre-feet per year. The present study estimates recharge at 35,700 acre-feet per year, based on inverse modeling that includes 200 ground-water ages and the distribution of river waters within the basin.

The water-budget methods used to estimate recharge in the earlier models do not account for runoff that enters the

Rio Grande, or evapotranspiration of runoff once it enters the subsurface. In addition, recharge estimates for the mountain fronts on the eastern side of the basin have been made independently using the chloride mass-balance method. Estimates by the chloride method were used in the 1998 model and are close to the estimates made in the present study. The lower recharge estimates from the current model are also consistent with the simulated water levels and source-area delineation. A ground-water trough is simulated west of the Rio Grande that is partially occupied by ground water that is derived from the Rio Grande. A ground-water trough and the Rio Grande-derived ground water have been observed using water levels and hydrochemistry, respectively. The 1995 model with the greatest recharge did not reproduce these features, and the 1998 and 2002 models used hydraulic conductivity zones or barriers to produce the trough.

In addition to the steady-state predevelopment model, a transient paleohydrologic model was calibrated to determine if the ^{14}C activities could indicate whether recharge rates had changed during the past 30,000 years. Paleolimnological evidence from central New Mexico has indicated that the climate in the region was wetter during the last glacial maximum (20,000 to 25,000 years ago). The paleohydrologic simulation involved a period of 30,000 years, with an separate value of recharge estimated every 2,500 years. These paleorecharge values were estimated simultaneously with the parameters from the original steady-state model. The transient, paleohydrologic simulation suggests that recharge to the basin during the last glacial maximum was 7 to 15 times greater than that at present, and after the end of the Ice Age was as little as half that at present. However, substantial uncertainties are associated with these paleorecharge estimates.

INTRODUCTION

In the Middle Rio Grande Basin (MRGB) of central New Mexico (fig. 1), ground water is a primary water source for all municipal, industrial, and domestic uses except agricultural irrigation. Ground-water withdrawals around the city of Albuquerque steadily increased from the 1940s through the 1990s, resulting in large declines in water levels. Since the beginning of the last century (Lee, 1907; Bryan, 1938), regulatory, scientific, and academic institutions have been studying the hydrogeology of the basin. Since the 1980s, numerical models of ground-water flow within the basin have been constructed. The goals of these hydrogeologic and modeling studies have been to characterize the basin geology and the ground-water-flow system and to provide this information to water-resources managers involved with the basin.

In the early 1990s, in cooperation with the City of Albuquerque, the New Mexico Bureau of Mines and Mineral Resources synthesized the hydrogeologic framework of the MRGB (Hawley and Haase, 1992), and the U.S. Geological Survey (USGS) synthesized the knowledge of the basin geohydrology (Thorn and others, 1993). Following this, the USGS developed a numerical ground-water-flow model of the basin on the basis of this geologic and hydrologic understanding (Kernodle and others, 1995). To realistically represent basin features and the hydrologic record, the spatial and temporal discretization used in the model was relatively fine. Consequently, obtaining the model solution, which is the spatial and temporal distribution of hydraulic heads and flows within the basin, was computationally intensive and required a large number of hours with the computers available at the time. Because of this large computational requirement, the model was not rigorously calibrated. Instead, reasonable values of model parameters were assumed, using field estimates and knowledge of and inferences about geologic and hydrologic conditions in the basin.

Between 1995 and 2002 the U.S. Geological Survey undertook a multi-year MRGB initiative to improve the understanding of the water resources in and around the MRGB (Bartolino and Cole, 2002). The MRGB study included geologic and fault mapping, geophysical investigations of the subsurface, and generation of high-resolution cartographic data to aid geologic mapping and land-surface analysis within the basin. Hydrologic studies included several investigations of recharge along mountain fronts and tributaries to the Rio Grande (Nimmo, 1997; Constantz, 1998; Stonestrom and Atkins, 1998; Anderholm, 2001), field studies of the interaction of ground water and surface water in the basin (Bartolino and Niswonger, 1999), collection and interpretation of ground-water chemistry and age data (Plummer and others, 2004), a modeling study using nonlinear regression methods for calibration (Tiedeman and others, 1998), and a model that included much of the new information that was gathered during the MRGB study (McAda and Barroll, 2002). The work described in this report was also funded as part of the MRGB study, and involves using the ground-water chemistry and age data and inverse modeling to further improve estimates of the recharge and hydraulic conductivity parameters that have been used in the ground-water-flow models of the MRGB.

Purpose and Scope

The purpose of this report is to document the use of environmental tracers to estimate parameters being used in ground-water-flow models of the MRGB. To estimate these parameters a predevelopment model was calibrated using the environmental tracers. A transient model that included pumping was not constructed because the primary focus was on using naturally occurring long-term tracers, and accounting for the effects of recent manmade stresses was secondary. The primary focus of this work was to improve estimates of model parameters, including recharge values, that can be constrained by ground-water ages and other hydrochemical observations. Several steps were involved in accomplishing this goal. Collection and analysis of the ground-water chemistry and age data were done first, and have been reported by Plummer and others (2004). The finite-difference grids representing the model that were developed by Kernodle and others (1995) and by Tiedeman and others (1998) were modified to give a

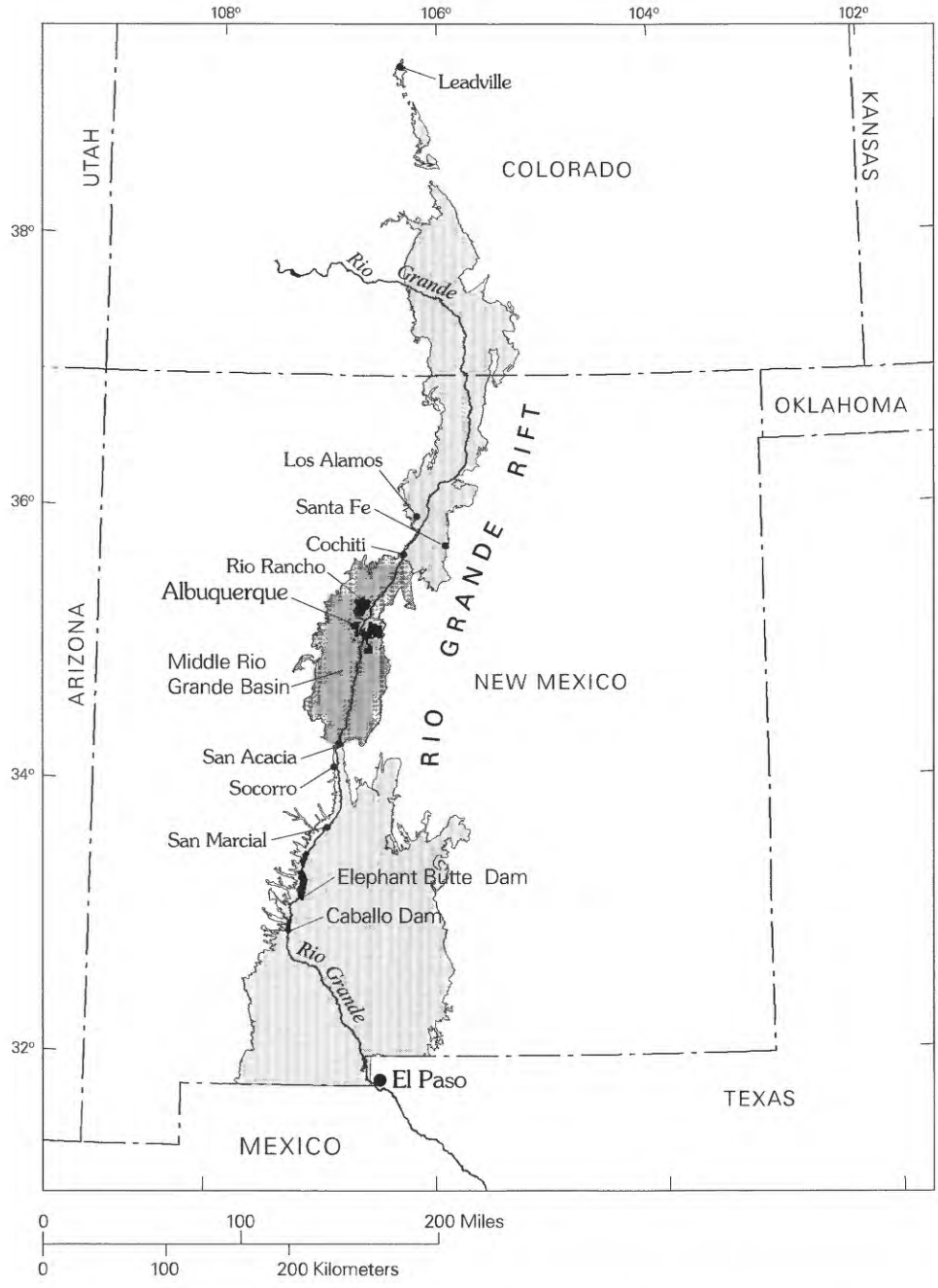

Figure 1. Location of the Middle Rio Grande Basin in central New Mexico (modified from Thorn and others, 1993, fig. 1).

more even resolution over the entire basin, and to extend the lower layers of the model to the base of the unconsolidated Cenozoic sediments. The three-dimensional geologic model of Cole (2001b) was used to define hydraulic conductivity zones within the three-dimensional ground-water-flow model.

The calibration was performed first assuming steady-state predevelopment hydrologic conditions. Second, a paleohydrologic simulation was calibrated to estimate paleorecharge rates based on the distribution of ^{14}C ages. Water-level data were chosen that best represented predevelopment conditions. This data set was reduced to a set of 200 water-level observations that were used to calibrate the flow model. Ground-water ages based on ^{14}C activities were also compiled into a data set of 200 observations. Finally, hydrochemical zones mapped by Plummer and others (2004) were used to constrain source-area delineation of the ground water within selected areas of the basin. These three sets of observations were used to make best estimates for the values of hydraulic conductivity and recharge. The estimates were made by calibrating the model with an inverse modeling code that uses nonlinear regression to minimize the residuals in an objective function that includes, in this case, the three types of observations. The inverse modeling was also used to estimate paleorecharge rates over the past 30,000 years. Nonlinear methods were used initially to minimize the model error for the steady-state and transient recharge models. Final minimization of the error was obtained by additional manual adjustment of the individual model parameters.

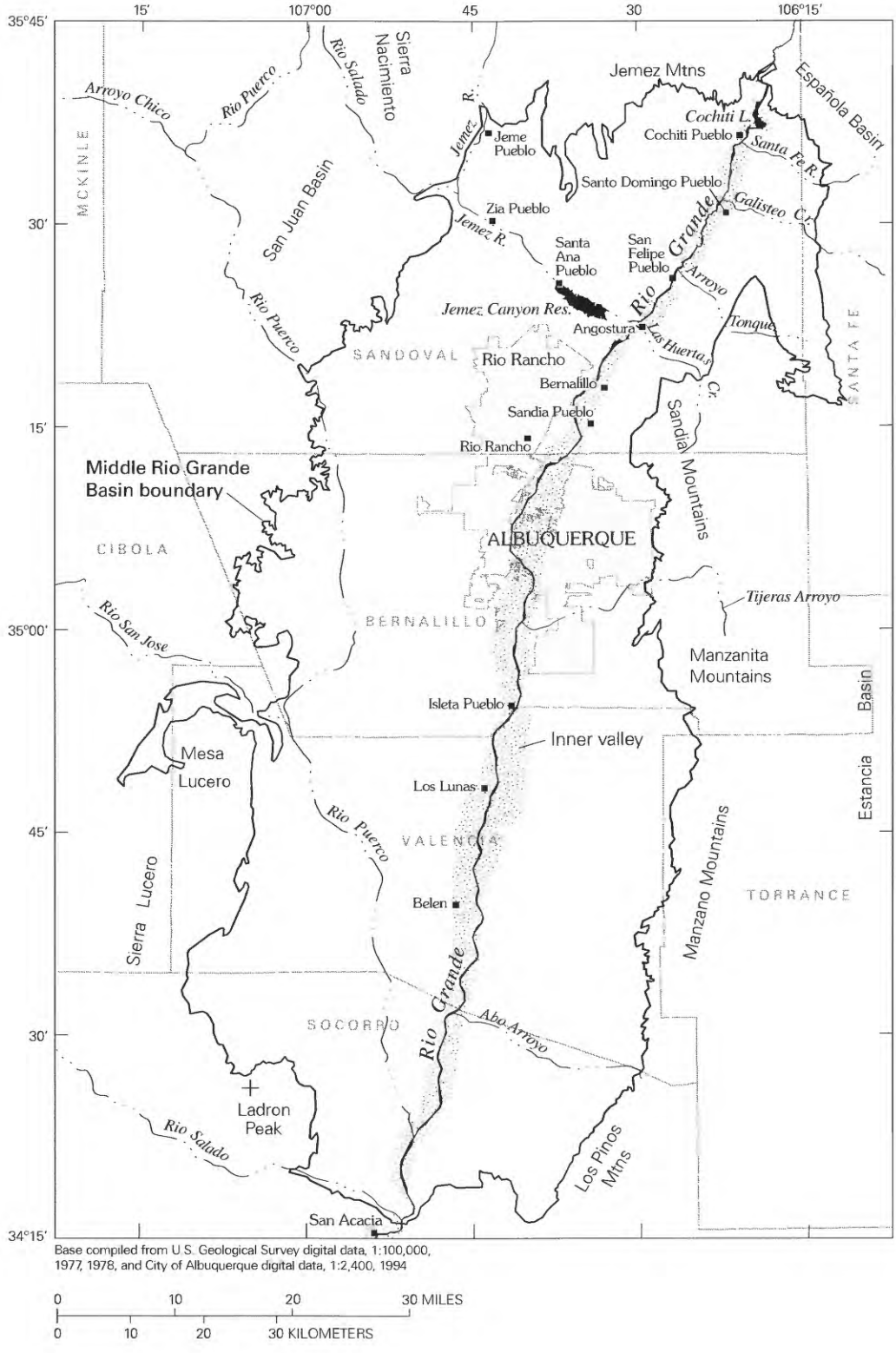

Figure 2. Physiographic features in the vicinity of the Middle Rio Grande Basin.

Description of the Study Area

The MRGB (also known as the Albuquerque Basin) occupies about 3,000 square miles in central New Mexico (fig. 1). The basin is one in a series of north-trending structural basins within the Rio Grande Rift, a region of Cenozoic crustal extension reaching from central Colorado into northern Mexico. The Rio Grande enters the basin from the northeast near Cochiti Pueblo, and exits the basin through a basin-fill constriction near San Acacia in the south (fig. 2). Major tributaries to the Rio Grande include the Santa Fe River, the Jemez River, and the Rio Puerco. Major arroyos entering the Rio Grande include Tijeras and Abo Arroyos. Land-surface altitudes of the basin-fill deposits range from about 4,800 feet above sea level at the southern end of the basin to about 6,000 feet above sea level at the northern end near the Jemez Mountains.

The climate is semiarid, with long-term average precipitation ranging from about 8 inches per year near the Rio Grande to about 23 inches per year at the crest of the Sandia Mountains (Thorn and others, 1993, table 1), which form part of the eastern boundary of the basin. Mean annual temperatures range from about 56°F in the lower elevations to about 38°F near the crest of the Sandia Mountains. Mean annual potential evapotranspiration ranges from less than 50 inches in the mountains to more than 60 inches near the Rio Grande (Thorn and others, 1993, fig. 10). Vegetation in the region consists predominantly of evergreen trees in the mountains, rangeland grasses and shrubs in the basin, and phreatophytes and irrigated crops in the inner valley of the Rio Grande. The metropolitan area associated with the city of Albuquerque lies in the north-central part of the basin and has been growing rapidly since the mid-20TH century, with a population of greater than 700,000 in 2000.

Previous Investigations

Investigations of geologic and hydrologic conditions in the MRGB began in the early 20TH century, but began to increase in frequency during the 1960s. Thorn and others (1993) and McAda (1996) provide fairly comprehensive summaries of these investigations. The geology and hydrology of the MRGB were recently described by Hawley and Haase (1992), Thorn and others (1993), and Hawley and others (1995). Several three-dimensional numerical models of ground-water flow in the basin have been developed. Kernodle and Scott (1986) constructed a model of steady-state ground-water flow, and Kernodle and others (1987) expanded this model to simulate transient conditions. Later, Kernodle and others (1995) constructed a new transient model of ground-water flow in the basin. Compared with earlier flow models, this model incorporated more recent interpretations of the subsurface and more realistically represented the interaction of the ground-water- and surface-water-flow system in the inner valley. The model by Kernodle and others (1995) was never calibrated rigorously because of the fine grid and computational requirements at the time. Kernodle (1998) presented revisions to the 1995 model in which the representation of some hydrogeologic conditions was updated.

Tiedeman and others (1998) constructed another model using a coarser grid that could be calibrated using nonlinear regression methods. That study used primarily transient water-level data from across the basin as observations with which to fit the simulations using the USGS code MODFLOWP (Hill, 1992). One major purpose of the study was to determine the potential cause of a water-table trough in the west-central part of the basin discovered originally by Meeks (1949), Bjorklund and Maxwell (1961), and Titus (1963). Six different subsurface configurations were simulated by Tiedeman and others (1998) to reproduce the trough assuming either the presence of (1) a high hydraulic conductivity zone, (2) a low-permeability north-south trending fault, or (3) a greater total sediment thickness for the basin. Results indicated that the first two configurations resulted in a significantly better fit to the data, but no field evidence has yet been produced to conclusively support the existence of any of these configurations.

McAda and Barroll (2002) incorporated the geologic information from Cole (2001b) to construct an improved version of the model of Kernodle and others (1995). They also incorporated recent estimates of recharge from the eastern mountain front from Anderholm (2001), and some of the results from this study and the recent ground-water chemistry and age study by Plummer and others (2004).

Many investigations have been conducted in association with the MRGB study (Bartolino and Cole, 2002). Geophysical studies of the basin by the USGS have included electromagnetic surveys (Deszcz-Pan and others, 1999), and aeromagnetic and gravity surveys (Grauch, 2000). Geologic studies have included the mapping of faults (Minor and Shock, 1998) and stratigraphy (Stone and Allen, 1998), and the construction of a three-dimensional geologic model of the basin (Cole, 2001b). Field-based estimates of recharge have been conducted for the Rio Grande (Bartolino and Niswonger, 1999), the eastern mountain front (Anderholm, 2001), and several prominent arroyos (Constantz, 1998; Stonestrom and Atkins, 1998; Thompson and others, 1999; Stewart and Constantz, 2000). Geochemical studies have focused on sampling the ground water and surface water to analyze for major chemical constituents and environmental tracers such as stable isotopes and radiocarbon (Plummer and others, 2004). The parameter estimates described in this report are based on a model that incorporates data from the recent geologic and hydrochemical studies.

HYDROGEOLOGY AND HYDROCHEMISTRY OF THE MIDDLE RIO GRANDE BASIN

Geologic Setting

The MRGB is one of several structural basins that are part of the Rio Grande Rift, a region formed by Cenozoic extension that stretches from Colorado through the length of central New Mexico into northern Mexico (figs. 1, 3). The main period of extension occurred from about 30 million years ago (Ma) to

Table 1. Median values of selected water-quality parameters by hydrochemical zone (from Plummer and others, 2004).

[nd, not determined; µS/cm, microsiemens per centimeter at 25 degrees Celsius; deg. C, degrees Celsius; mg/L, milligrams per liter; µg/L, micrograms per liter; pmC, percent modern carbon; no., number]

Hydrochemical zone	Hydrochemical zone no.	Specific conductance (µS/cm)	Field pH	Water temperature (°C)	Dissolved oxygen (mg/L)	Calcium (mg/L as Ca)	Magnesium (mg/L as Mg)	Sodium (mg/L as Na)	Potassium (mg/L as K)	Alkalinity (mg/L as HCO_3)	Sulfate (mg/L as SO_4)	Chloride (mg/L as Cl)	Fluoride (mg/L as F)	Bromide (mg/L as Br)	Silica (mg/L as SiO_2)	Nitrate (mg/L as N)	Aluminum (mg/L as Al)	Arsenic (mg/L as As)
Northern Mountain Front	1	340	7.49	18.9	5.12	38.5	6.1	20.0	4.9	137.	19.5	5.6	0.35	0.08	53.3	0.56	nd	3.2
Northwestern	2	400	7.84	20.6	6.68	33.9	4.2	49.9	5.7	160.	44.8	8.5	0.61	0.07	30.1	2.44	nd	9.8
West Central	3	535	8.22	23.8	3.00	12.0	2.5	103.	4.2	174.	92.0	13.4	0.99	0.11	34.5	1.24	6.76	23.3
Western Boundary	4	4,572	7.70	22.0	4.09	135.	56.4	589.	15.2	300.	793.	820.	1.64	0.38	22.5	0.86	5.00	1.8
Rio Puerco	5	2,731	7.50	20.0	3.73	135.	42.7	290.	10.4	190.	1,080.	185.	0.63	0.64	21.8	0.88	5.00	1.0
Southwestern Mountain Front	6	462	8.11	19.1	4.43	52.6	13.5	27.8	2.5	202.	53.0	15.	1.02	0.21	17.6	1.12	3.31	0.2
Abo Arroyo	7	1,055	7.45	20.7	6.23	92.5	34.4	49.2	3.1	148.	346.	25.9	0.90	0.17	24.0	1.40	4.14	5.2
Eastern Mountain Front	8	382	7.67	22.0	5.16	45.0	5.1	29.2	2.2	157.	31.0	10.5	0.60	0.17	28.4	0.31	5.56	2.0
Tijeras Fault Zone	9	1,406	7.42	18.5	4.66	171.	36.0	95.1	6.1	599.	100.	139.	1.27	0.69	18.9	1.09	5.22	2.2
Tijeras Arroyo	10	677	7.39	16.1	6.97	89.4	24.5	29.3	3.8	240.	115.	56.6	0.60	0.35	19.5	3.79	4.09	1.0
Northeastern	11	1,221	7.50	19.4	6.44	141.	29.5	81.8	4.8	208.	390.	22.7	0.51	0.19	38.5	0.64	4.34	2.7
Central	12	436	7.74	18.1	0.12	42.9	8.0	31.0	6.4	158.	66.0	16.6	0.44	0.09	47.0	0.08	6.00	5.4
Discharge	13	1,771	7.70	20.6	0.08	93.0	31.0	190.	10.5	157.	290.	280.	1.40	0.47	39.0	0.42	4.50	9.9

Hydrochemical zone	Hydrochemical zone no.	Barium (mg/L as Ba)	Boron (mg/L as B)	Chromium (mg/L as Cr)	Copper (mg/L as Cu)	Iron (mg/L as Fe)	Lead (mg/L as Pb)	Lithium (mg/L as Li)	Manganese (mg/L as Mn)	Molybdenum (mg/L as Mo)	Strontium (mg/L as Sr)	Uranium (mg/L as U)	Vanadium (mg/L as V)	Zinc (mg/L as Zn)	∂D (per mil)	∂18O (per mil)	∂13C (per mil)	^{14}C (pmC)
Northern Mountain Front	1	0.062	0.043	1.2	0.8	0.060	0.20	0.058	0.005	1.7	0.31	1.0	6.4	258.	-77.7	-10.9	-8.50	33.4
Northwestern	2	0.056	0.118	nd	0.4	0.030	0.10	0.068	0.002	3.4	0.57	2.7	15.6	9.0	-64.7	-8.73	-6.93	29.6
West Central	3	0.032	0.239	5.7	0.5	0.028	0.11	0.045	0.002	8.2	0.20	3.7	27.9	5.0	-96.7	-12.7	-7.18	8.80
Western Boundary	4	0.014	0.900	10.6	3.0	0.213	0.12	0.251	0.041	9.9	2.09	4.4	5.7	118.	-64.4	-9.12	-4.70	6.19
Rio Puerco	5	0.014	0.291	nd	3.4	0.130	0.10	0.253	0.015	7.0	3.92	6.1	3.4	117.	-61.6	-8.51	-7.65	36.4
Southwestern Mountain Front	6	0.045	0.094	1.9	9.3	0.030	0.41	0.041	0.007	3.0	0.86	0.9	1.0	252.	-53.5	-7.74	-5.76	40.0
Abo Arroyo	7	0.017	0.130	nd	2.0	0.105	0.10	0.031	0.004	3.4	1.48	5.4	9.5	8.1	-65.2	-9.05	-6.72	24.1
Eastern Mountain Front	8	0.084	0.050	1.0	1.7	0.031	0.27	0.020	0.003	2.0	0.32	3.6	7.5	6.7	-81.0	-11.4	-8.70	47.2
Tijeras Fault Zone	9	0.046	0.347	1.7	4.3	0.111	0.34	0.227	0.023	3.7	1.11	7.3	6.3	61.5	-74.2	-10.3	-0.98	9.70
Tijeras Arroyo	10	0.057	0.060	1.1	1.0	0.050	0.10	0.017	0.005	1.9	0.47	3.7	3.0	4.5	-75.7	-10.3	-6.80	72.8
Northeastern	11	0.018	0.215	nd	3.7	0.170	0.11	0.040	0.004	6.7	1.72	8.5	3.8	99.5	-68.6	-9.72	-6.40	28.5
Central	12	0.083	0.085	1.0	0.8	0.041	0.10	0.040	0.015	5.0	0.40	3.6	9.3	5.0	-95.4	-12.8	-8.87	61.0
Discharge	13	0.030	0.630	10.2	1.7	0.080	0.15	0.326	0.010	10.3	3.02	3.9	7.1	16.2	-90.8	-12.1	-7.00	10.8

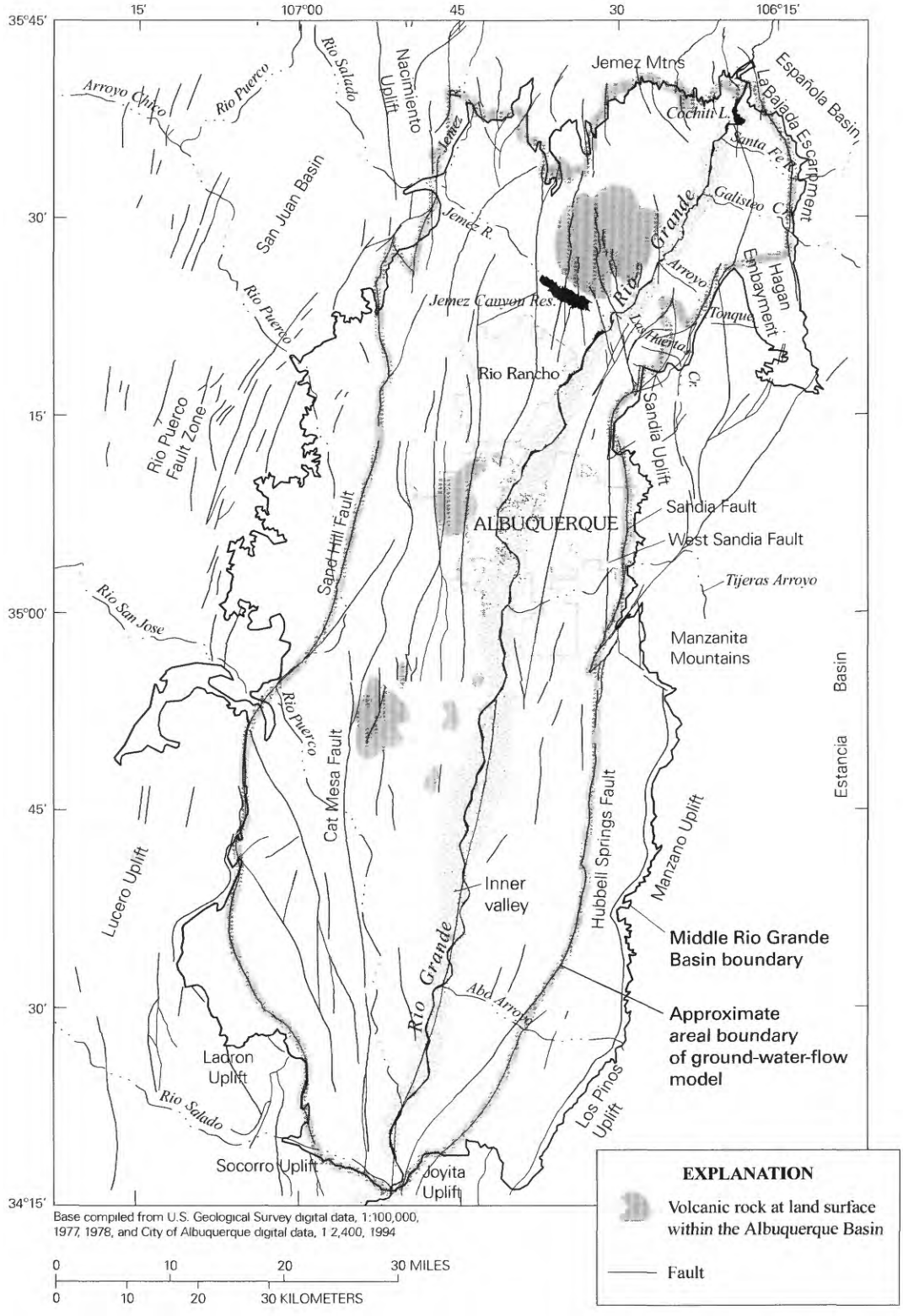

Figure 3. Major geologic and tectonic features in the vicinity of the Middle Rio Grande Basin (modified from Kelley, 1977; Thorn and others, 1993, fig. 4; Kernodle, 1998, fig. 14).

about 5 Ma, with tectonism active mostly from about 15 Ma to 5 Ma (Thorn and others, 1993). Structural boundaries of the basin are the Nacimiento Uplift to the northwest, the Jemez Mountains to the north, the La Bajada Escarpment to the northeast, the Sandia and Manzano Uplifts to the east, the Los Pinos Uplift to the southeast, the Socorro and Joyita Uplifts to the south, the Ladron Uplift to the southwest, and the Lucero Uplift and the Rio Puerco Fault Zone to the west (fig. 3). The MRGB is defined as the extent of Cenozoic deposits within these structural boundaries. The Rio Grande flows into the basin through the northeastern constriction and out of the basin through the southern constriction, where eastern and western structural features converge. Basin fill is continuous across the northeastern and southern boundaries (Hawley and Haase, 1992).

Rock units in the MRGB include pre-Santa Fe Tertiary deposits, Tertiary Santa Fe Group basin fill, post-Santa Fe Pleistocene volcanic rock, and post-Santa Fe Quaternary sediments. The following discussion of the depositional history, lithology, and thicknesses of the Santa Fe and post-Santa Fe deposits is condensed from Hawley and Haase (1992) and Thorn and others (1993); these works describe the understanding of the geologic history and depositional structure of the basin as of the mid-1990s. The predominant basin deposit is the Santa Fe Group, the thickness of which ranges from about 3,000 feet along the basin margins to greater than 14,000 feet in the basin center. The lower units in the Santa Fe Group were deposited during the Oligocene and Miocene from about 30 Ma to 15 Ma, when the basin was internally drained, and contain piedmont-slope, eolian, and basin-floor playa deposits. The middle units of the Santa Fe Group were deposited during the Miocene and early Pliocene from about 15 Ma to 5 Ma, the time of greatest accumulation of sediments in the basin. During that time, piedmont-slope deposition continued and fluvial systems developed, transporting sediment into the basin, but most likely terminating in playa lakes within the basin. The upper units of the Santa Fe Group were deposited during the Pliocene from about 5 to 2.7 Ma. The ancestral Rio Grande developed at the end of this time, entering the basin from the north and flowing out to the south. The axial-channel sands and gravels associated with the ancestral Rio Grande are especially coarse and well sorted, but thin. The sands of the middle and lower units of the Santa Fe Group tend to be finer-grained and less well sorted.

Geologic and geophysical studies have since been conducted to further characterize the location, extent, and properties of the depositional units in the basin (Bartolino and Cole, 2002). Much of that work was compiled into a three-dimensional geologic model of the basin (Cole, 2001b), upon which the hydraulic conductivity zonation of the ground-water-flow model in this study has been based.

The crustal extension that formed the Rio Grande Rift caused normal faults to develop throughout the MRGB during deposition of the Santa Fe Group. Pliocene and younger faults have a predominantly north-south orientation (fig. 3). At the basin margins and at depth in the central parts of the basin, the normal faulting placed older, less permeable rock adjacent to parts of the Santa Fe Group. Total vertical displacements along these faults are up to 30,000 feet (Hawley and others, 1995, p. 45). Normal faulting also occurred within the Santa Fe Group deposits, and some of these faults have been cemented and act as partial barriers to horizontal ground-water flow. Basalt flowed to the land surface along presumed fault zones and was emplaced in the central part of the basin from about 4 to 2.5 Ma (Love and others, 1994). Outcrops of this rock occupy a small percentage of the basin surface area, although recent aeromagnetic studies indicate that the basalt is much more extensive in the subsurface (Grauch and others, 2001).

Hydraulic Properties

Many aquifer tests have been performed and analyzed to estimate the hydraulic conductivity and transmissivity of deposits within the Santa Fe Group. Most tests were conducted in public-supply wells with screens that are a few hundred feet long. Thorn and others (1993, table A1, pages 75–81) summarized the results of several of these aquifer tests and reported the hydraulic-conductivity estimate for each well as the transmissivity divided by the screen length. Hydraulic-conductivity estimates for over 20 wells completed only in the upper part of the Santa Fe Group range from 4 to 130 feet per day. Sandy, pebble-gravel deposits of the upper part of the Santa Fe Group that are beneath the City of Albuquerque generally have the highest hydraulic conductivities. Hydraulic-conductivity estimates for nine wells with screens that penetrate both the upper and middle Santa Fe Group range from 7 to 71 feet per day. Additional tests were performed in several wells for which the lithology is unknown. Deposits in the Rio Grande alluvium can vary from silty clay to coarse gravel. Cummins (1997) estimated the hydraulic conductivity of coarse-grained alluvium deposits to be between 90 and 350 feet per day. Willis (1993) estimated the hydraulic conductivity for silty clay and gravelly coarse sand within the alluvium to be 0.2 and 65 feet per day, respectively.

In their models of ground-water flow within the basin, Kernodle and others (1995) assigned horizontal hydraulic conductivities on the basis of field tests and on compiled unit descriptions from Hawley and Haase (1992). These assigned values ranged from 2 feet per day for the lower Santa Fe Group deposits to 70 feet per day for the axial-channel gravel deposits. Tiedeman and others (1998) calibrated a ground-water-flow model of the basin based on water levels and seepage estimates from the Rio Grande in the vicinity of Albuquerque. These calibrated hydraulic conductivities ranged from about 2 feet per day for the lower Santa Fe Group deposits to about 100 feet per day for the Rio Grande alluvium and the axial-channel deposits. McAda and Barroll (2002) used values in their recent model that varied between 0.5 and 45 feet per day. Presently, there are no field measurements of the ratio of horizontal to vertical hydraulic conductivity for deposits in the MRGB. The ratio used by Kernodle and others (1995) was 300:1, that used by McAda and Barroll (2002) was 150:1,

whereas the value calibrated by Tiedeman and others (1998) ranged from 330:1 to 3,500:1, depending upon the other assumptions made in the model.

Hydrologic Conditions

The following discussions of the hydrologic conditions of the MRGB are condensed from the more detailed descriptions given by Thorn and others (1993), McAda (1996), Bexfield and Anderholm (2000), and McAda and Barroll (2002).

Ground-Water Levels

Regional ground-water levels that represent predevelopment conditions have been compiled by Bexfield and Anderholm (2000), and are shown in figure 4. The ground-water levels that were used to construct this figure were from different depths and have different screened interval lengths; thus, the water-level contours depict large-scale horizontal ground-water movement through the basin, but do not accurately represent smaller scale ground-water-flow conditions. In addition, uniformly spaced contours are shown in some areas of sparse data, whereas the horizontal hydraulic gradient may be more variable in the true flow system. Some ground water flows from the flanks of the basin inward toward the Rio Grande, but the predominant direction of flow is through the basin from north to south. The Rio Grande was losing water to the basin aquifer under predevelopment conditions in a reach just north of the city of Albuquerque. This water moves into the aquifer system away from both sides of the Rio Grande and flows southward parallel to the river until it discharges back into the Rio Grande along an extended reach in the southern part of the basin. The extent of the losing reach of the Rio Grande has increased toward the south as increasing ground-water extractions over the last 50 years in the vicinity of the city of Albuquerque have induced more leakage. In one region west of the Rio Grande and the city of Albuquerque, ground-water levels are lower than those in the Rio Grande just to the east. This area, known as the "trough," was originally described by Meeks (1949), Bjorklund and Maxwell (1961), and Titus (1963), and has been the subject of speculation ever since as to its cause. Tiedeman and others (1998) performed numerical experiments to test different hypotheses, including a north-south-trending fault zone, the presence of a unit of greater hydraulic conductivity, and a greater thickness of permeable sediments. The results were equivocal and no single hypothesis could be supported fully by the field evidence.

Today, the inner valley (fig. 2) of the MRGB is networked with an extensive system of canals and drains that greatly affect and control the ground-water levels there, but these effects are not shown in the predevelopment map (fig. 4) because their impact on more regional water levels is limited. Although irrigation practices have been undertaken in the inner valley for more than a century, extensive ground-water development for public supply in the Albuquerque area began in the 1950s. Thus for the present study, a predevelopment water-level configuration refers to levels occurring before approximately 1950. The Cochiti and Jemez Canyon Dams in the northern part of the basin are relatively recent and are not predevelopment features. Because the focus of this study is on the calibration of a ground-water model to predevelopment conditions, all of the manmade hydrologic features will receive no further discussion in this report.

Rio Grande

The position and geometry of the Rio Grande channel have changed over time because of natural and anthropogenic activities, as evidenced by data back to 1935 that are stored in Geographical Information Systems (GIS) of the USGS and the Bureau of Reclamation. The river channel is locally incised into the inner valley of the basin, and the Rio Grande water level generally is within a few feet of the land surface. Land-surface altitude is available from USGS 1:24,000-scale topographic maps and varies at the river channel from about 4,690 feet above sea level at the southern edge of the basin to about 5,240 feet above sea level at the northern edge of the basin. The mean annual flow in the Rio Grande in the MRGB between the years of 1974 and 1992 was about 1 million acre-feet. The bottom consists of coarse sand that is about 3 feet thick (Gould, 1997), usually underlain by finer grained deposits. Although reliable field estimates of the vertical hydraulic conductivity of the river bed have not been made, the location and extent of some clay-rich layers beneath the flood plain have been mapped in the vicinity of Albuquerque (Bartolino and Sterling, 1999).

Recharge

The ground-water flow system of the MRGB has several sources of recharge. Precipitation in the mountains infiltrates along mountain fronts bordering the basin, and surface water infiltrates along streams and arroyos that are tributaries to the Rio Grande. Ground-water inflow from adjacent basins and mountains recharges as underflow to the northern and southwestern parts of the basin. Substantial ground-water withdrawals in the Albuquerque area have lowered water levels beneath the Rio Grande and subsequently induced recharge from the river. Recharge also occurred naturally as leakage from the Rio Grande along reaches from just north of Albuquerque to as far south as Belen.

Recharge along the mountain fronts and tributaries to the Rio Grande was estimated in the past using the rainfall-runoff and water-budget methods described by Hearne and Dewey (1988) and Waltemeyer (1994). Kernodle and Scott (1986) and Kernodle and others (1995) used and modified this type of data for values of recharge that were input to their ground-water-flow models (fig. 5). Using these methods, the total recharge along the eastern side of the basin was estimated to be 71,700 acre-feet per year. Tiedeman and others (1998) calibrated a ground-water-flow model of the basin and adjusted some of the recharge values to obtain a better fit with the water-level and streamflow data. Their estimates

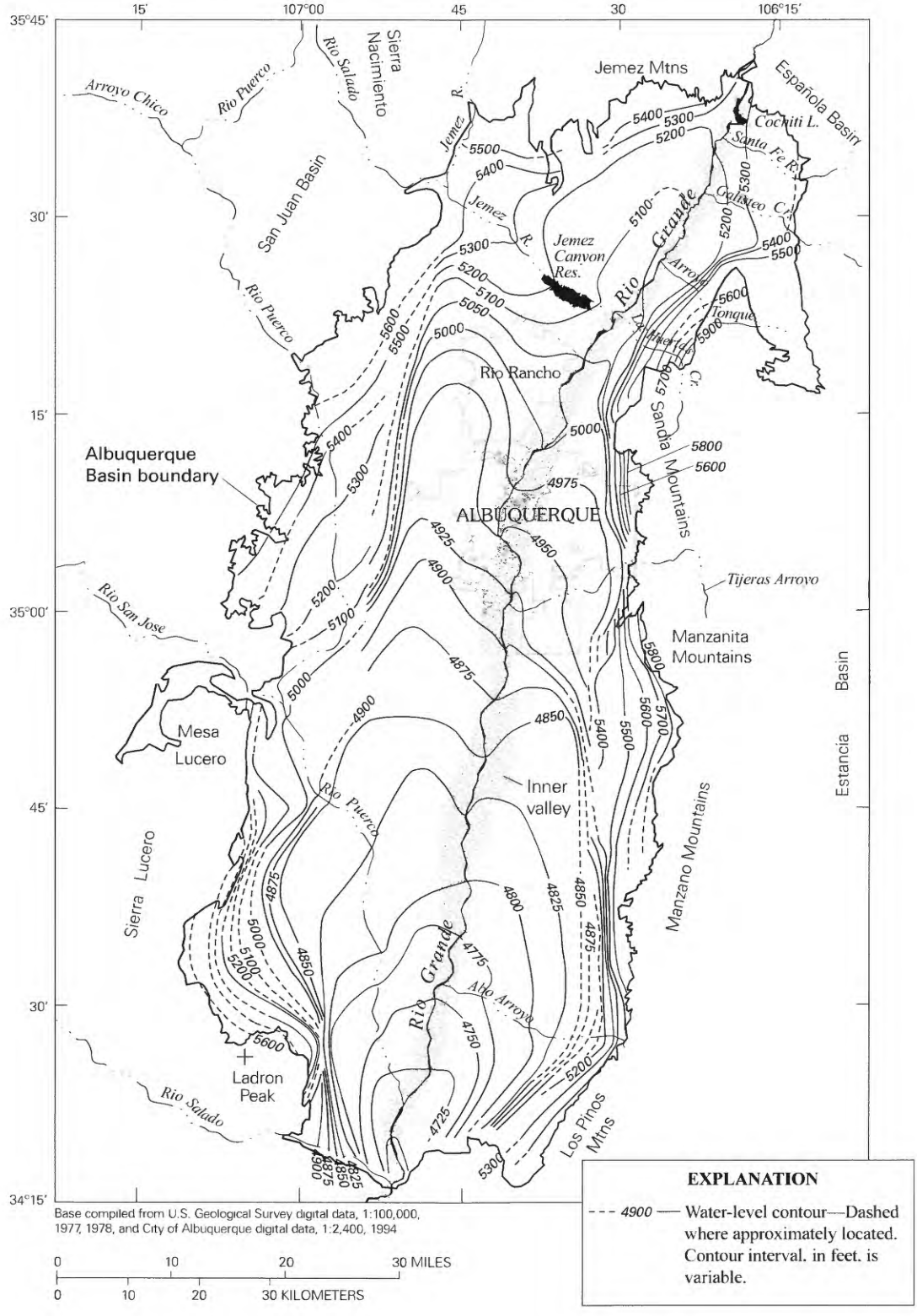

Figure 4. Water table in its predevelopment configuration (modified from Bexfield and Anderholm, 2000).

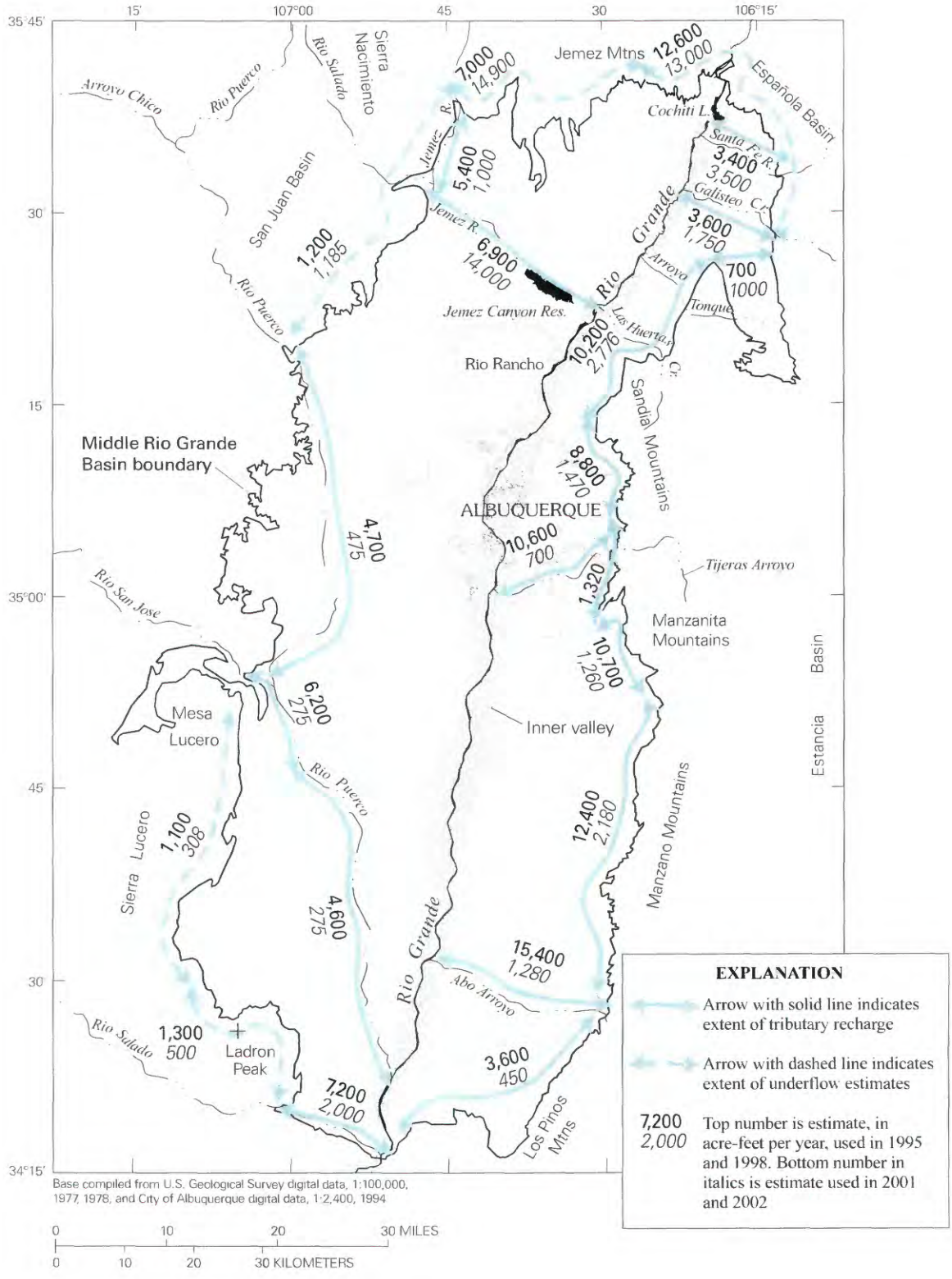

Figure 5. Mountain-front recharge, tributary recharge (solid lines), and underflow estimates (dashed lines), in acre-feet per year, used by Kernodle and others (1995) and Tiedeman and others (1998), and estimates used by McAda and Barroll (2002) (italics) that include those of Anderholm (2001).

were typically from one-half to three-fourths of those from the water-budget methods. Anderholm (2001) estimated recharge along the eastern mountain fronts by using the chloride mass-balance method. His estimates of recharge were significantly lower, with a total recharge value for the eastern side of the basin being about 11,200 acre-feet per year. The difference in the estimates between the water-budget and chloride mass-balance methods can be explained if surface-water runoff from the mountains that is initially recharged undergoes significant loss due to evapotranspiration (Anderholm, 2001), because the water-budget methods assume these evaporation losses are negligible. McAda and Barroll (2002) used a combination of recharge estimates from the water-budget and chloride mass-balance methods (fig. 5).

Numerical modeling of ground-water flow in basins adjacent to the MRGB suggests that there is ground-water inflow to the northern and western parts of the basin (Frenzel, 1995; Hawley and Grant, 1997). Using a model of ground-water flow in the Española Basin, McAda and Wasiolek (1988) estimated ground-water flow from that basin to the MRGB to be 12,600 acre-feet per year. Kernodle and others (1995) estimated ground-water inflow from the Jemez Mountains by assuming the ground-water inflow per unit length of the boundary was the same as that entering from the Española Basin. In their model of ground-water flow in the San Juan Basin, Frenzel and Lyford (1982) estimated ground-water underflow to the MRGB to be 1,200 acre-feet per year. Using a water-budget method, J. D. Dewey (Hydrologist, U.S. Geological Survey, written commun., 1982) estimated total underflow from the Sierra Lucero and Ladron Peak region into the MRGB to be about 2,400 acre-feet per year.

Discharge

Under predevelopment conditions, ground water discharged from the MRGB by flow into the Rio Grande, by underflow to the Socorro Basin at the southern end of the basin near San Acacia, and by evapotranspiration in the inner valley. Discharge to the Rio Grande contributes base flow to the river, especially in the northernmost and southernmost reaches in the basin, but because this amount is small relative to the entire flow in the river, the amount has not been measured in the field. Underflow to the Socorro Basin has been considered small compared to other budget components (Kernodle and Scott, 1986) and therefore has been neglected in all modeling studies. The Bureau of Reclamation (1973) estimated in field studies that about 3 feet per year of water is evapotranspired by tamarisk and Russian olives, two riparian species that grow in the inner valley. Using this rate, Thorn and others (1993) estimated that transpiration by riparian vegetation in the inner valley is 112,000 acre-feet per year. Similarly, they used rates from a study by Blaney and others (1938) and estimated evapotranspiration from wetlands to be 13,500 acre-feet per year. Much of this evapotranspired water would originate from the adjacent Rio Grande and not necessarily be water that had recharged along distant boundaries of the basin.

Geochemical Conditions

Geochemical data for ground water in the MRGB has been compiled, collected, and analyzed by Anderholm (1988) and Logan (1990), and more recently and extensively by Bexfield and Anderholm (2002) and Plummer and others (2004) as part of the multi-year MRGB study. The data by Plummer and others (2004) include major and minor-element chemistry (30 elements), ^{18}O and δ^2H in water, ^{13}C and ^{14}C of dissolved inorganic carbon (DIC), ^{34}S of dissolved sulfate, tritium (^3H), and selected dissolved gases (including dissolved oxygen, nitrogen, argon, methane, helium, tritiogenic helium-3 (^3He), chlorofluorocarbons (CFCs: CFC-11, CFC-12, CFC-113), sulfur hexafluoride (SF_6), neon, and carbon dioxide). Most of the chemical and isotopic data are from relatively shallow depths—typically the upper 150 feet of aquifer—but some data are from depths of more than 1,500 feet below the water table. The chemical and isotopic composition of ground water in the MRGB was mapped (for example, see figs. 6–8) and used to identify 13 water-quality zones that have unique chemical and isotopic characteristics (fig. 9). The water-quality zones were interpreted as representing sources of recharge to the basin (zones 1–12) or ground-water discharge from the basin (zone 13). The classification is based on existing water-quality data and new analyses from 288 wells and springs.

Most of the discussion that follows is a summary from Plummer and others (2004). Most chemical and isotopic data align parallel to the predominant north to south direction of ground-water flow throughout the basin and show a small but distinguishable effect of geochemical reactions on radiocarbon activity. The ^{14}C ages of DIC were adjusted for the geochemical reactions, and the ages ranged from modern to more than 30,000 years before present. Deuterium, δ^2H, was useful in delineating sources of ground water in the basin (fig. 7). Based on 72 samples collected between 1996 and 1999, the median δ^2H content of Rio Grande water is –89.9 ‰, and based on 20 samples from the same time period, the median δ^2H content of mountain-front recharge water at the base of the Sandia Mountains is –83.5 ‰. More limited isotopic data from the Jemez River near Jemez and the Rio Puerco near Highway 6 indicate mean δ^2H values of –83.6 and –58.6 ‰, respectively.

The median values for selected water-quality parameters that are characteristic for each hydrochemical zone are summarized in table 1. Zone recognition was based on varied subsets of the chemical and isotopic constituents. Zone 1 (northern mountain-front recharge) is in the northeast part of the basin and is thought to be water recharged along the southern flanks of the Jemez Mountains (fig. 9). Zone 1 water is characterized by relatively low specific conductance and pH, and higher than average δ^2H and dissolved SiO_2 for the basin, and has a median radiocarbon age of 8,800 years. The saturated thickness of zone 1 is greater than 200 feet at the northeast basin margin but may be relatively thin (50 feet) elsewhere. Zone 2 (northern intra-basin recharge) is thought to represent lower elevation recharge from arroyos in the northern part of the basin (fig. 9). Some distinguishing characteristics of

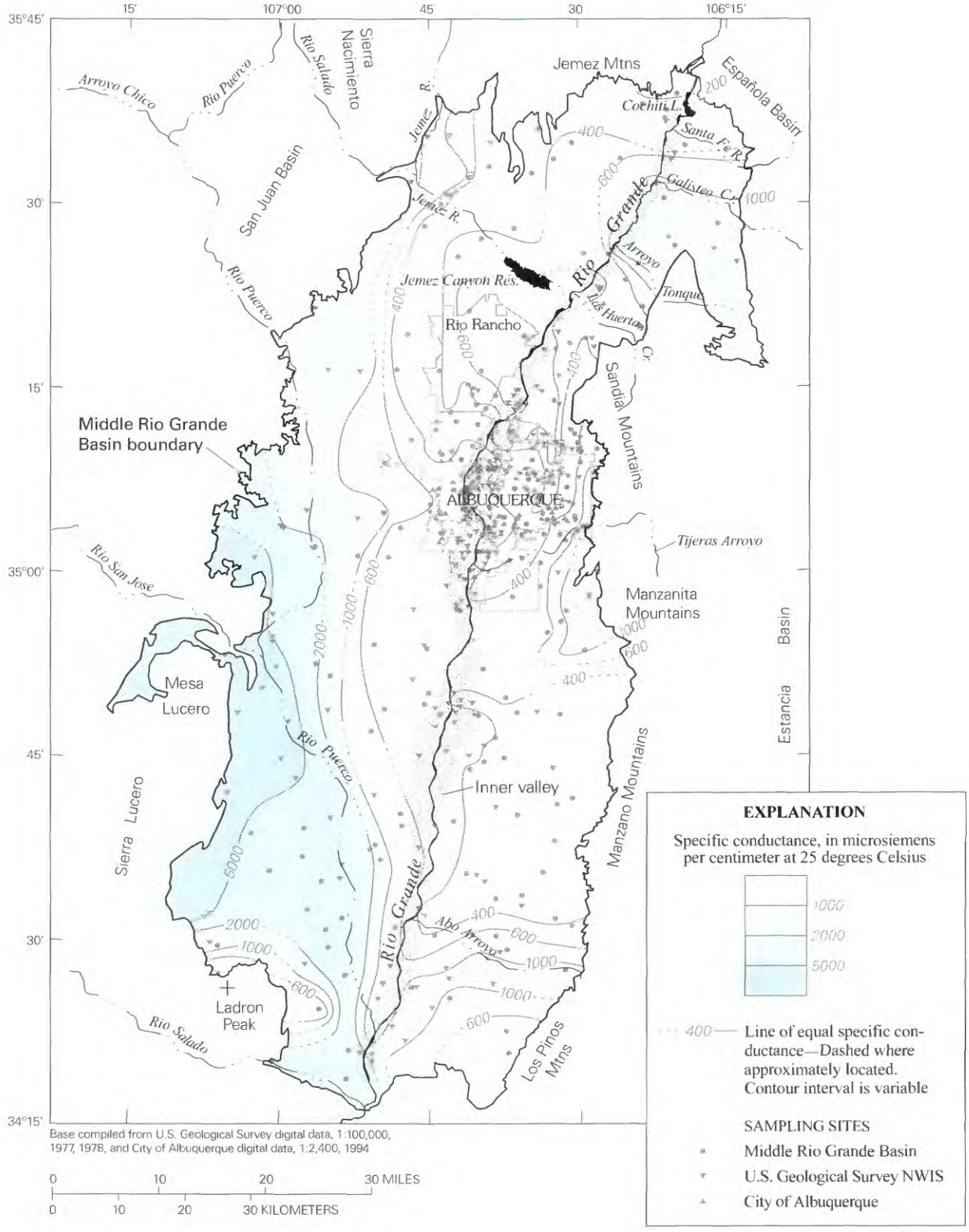

Figure 6. Specific conductance in ground water of the Middle Rio Grande Basin (from Plummer and others, 2004).

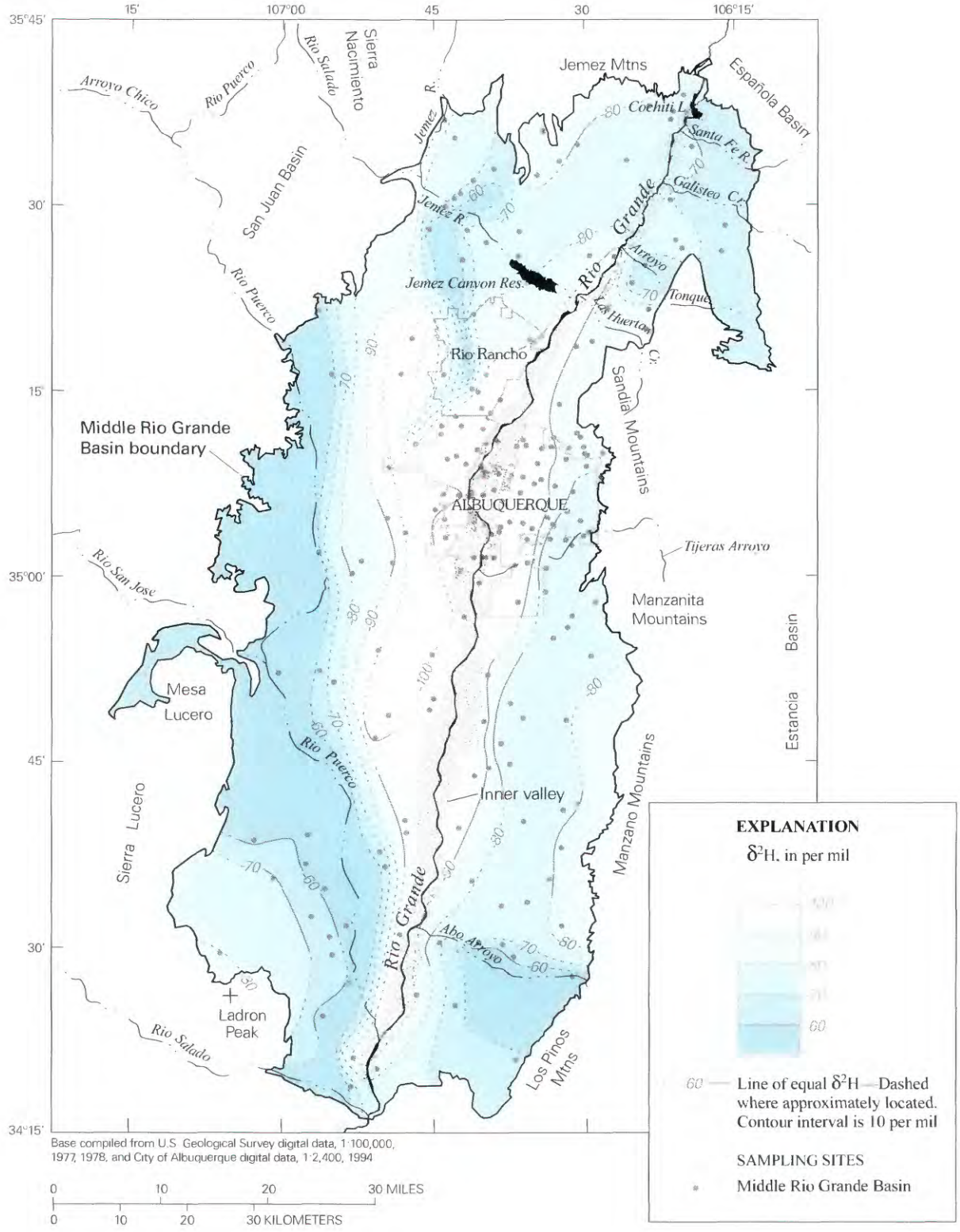

Figure 7. Contours of deuterium composition, δ^2H, for ground water of the Middle Rio Grande Basin (from Plummer and others, 2004).

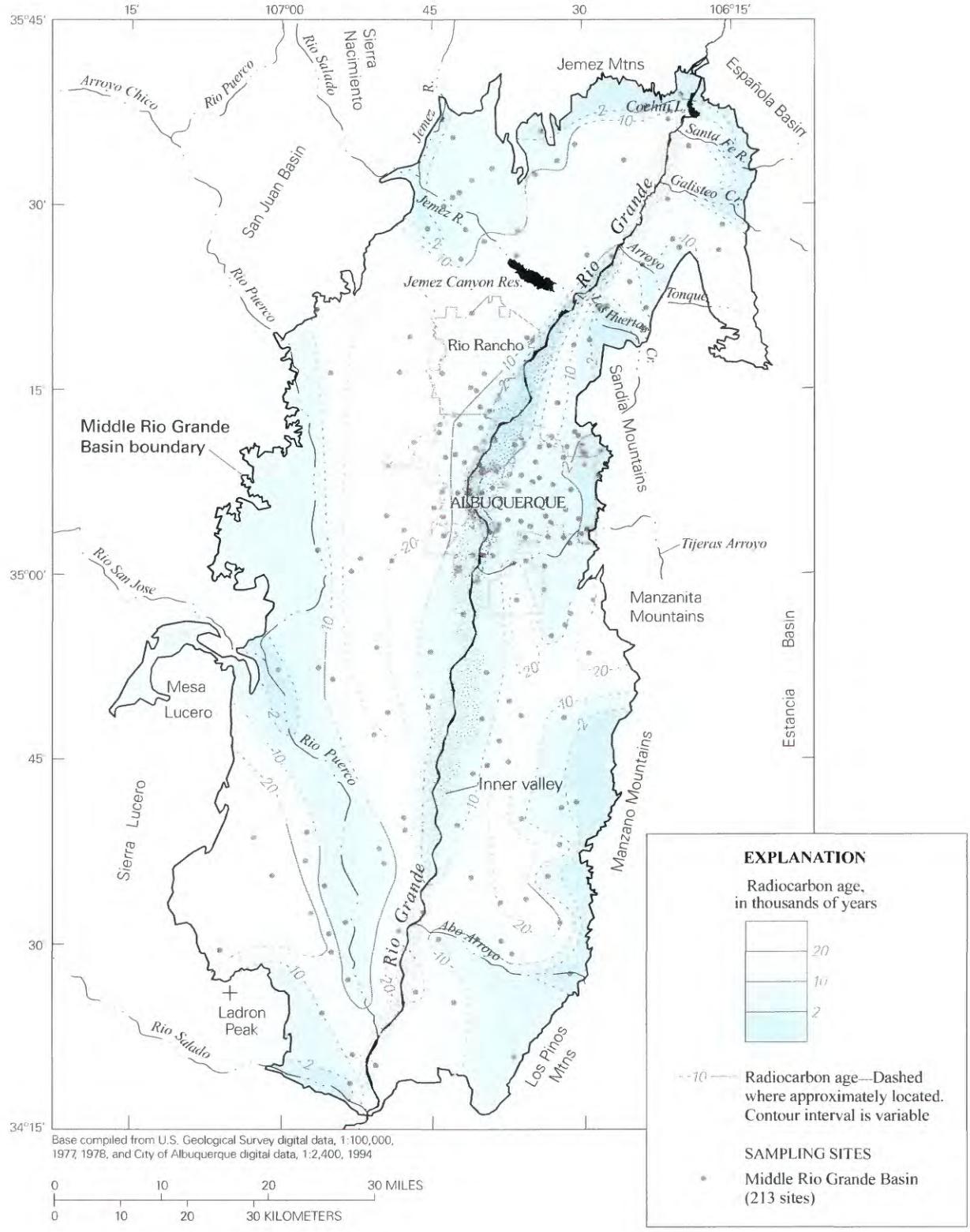

Figure 8. Contours of conventional radiocarbon age of DIC (dissolved inorganic carbon) in ground water of the Middle Rio Grande Basin (from Plummer and others, 2004).

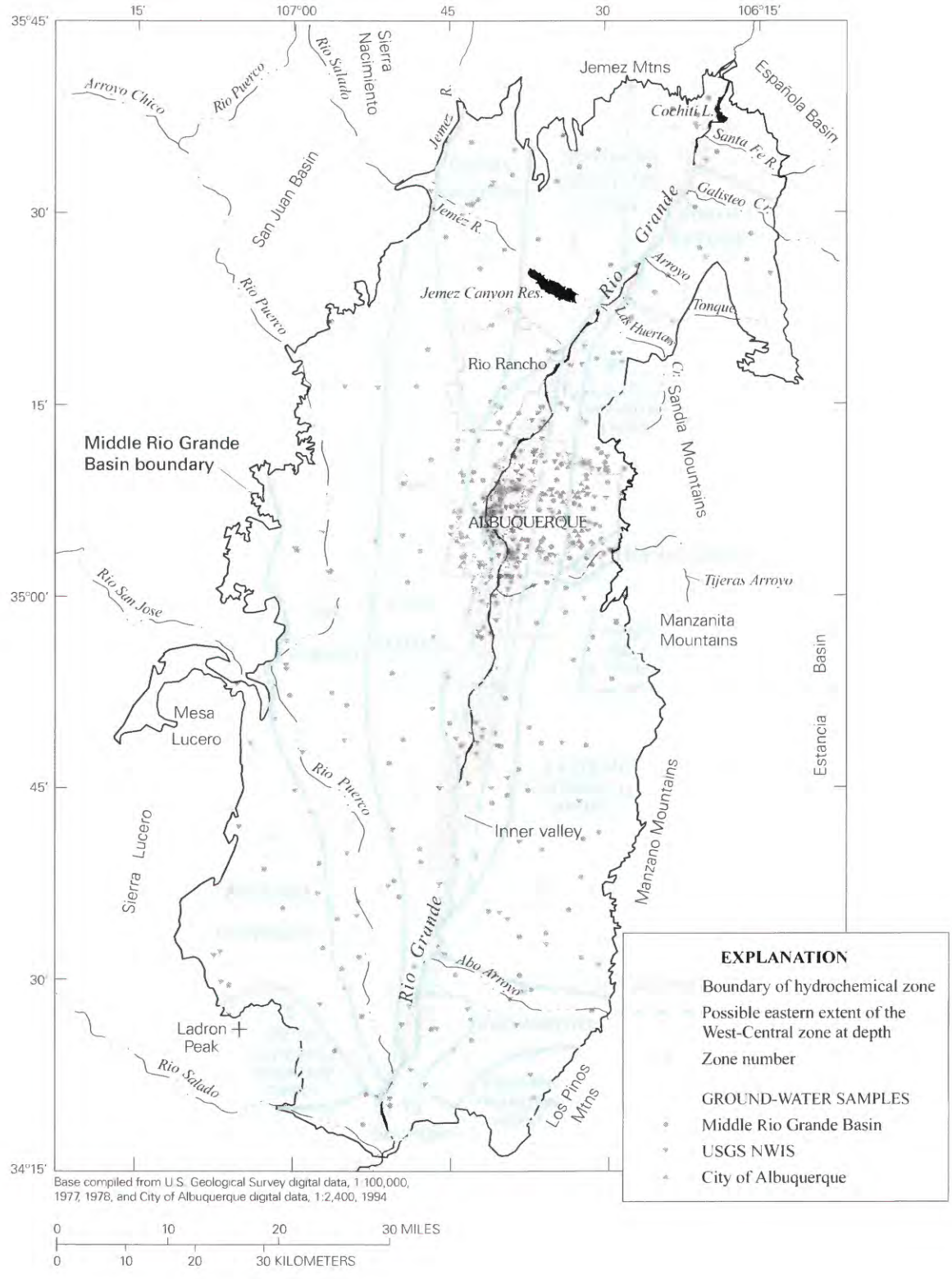

Figure 9. Hydrochemical zones in the Middle Rio Grande Basin (from Plummer and others, 2004).

zone 2 water are lower than average specific conductance and dissolved SiO_2, and higher than average δ^2H and dissolved nitrate. Zone 2 has a median age of water of 8,800 years, and a saturated thickness of possibly less than 200 feet.

Zone 3 (inflow along the northern basin margin) occurs beneath zones 1 and 2 in the northern part of the basin, extends under part of zone 12 that parallels the Rio Grande, and occurs at the water table throughout the central part of the basin, converging at the Rio Grande in the southern basin (fig. 9). Zone 3 contains some of the oldest waters sampled in the basin, with a median age of 19,900 years, and is thought to represent recharge from the Jemez Mountains north of the basin, primarily during the last glacial period. Zone 3 water is a Na-HCO_3-SO_4-type water with higher than average specific conductance, arsenic, vanadium, and pH. Relative to zones 1 and 2, zone 3 water is high in dissolved sulfate, but very depleted in δ^2H. Zone 4 (inflow from the western basin margin) contains old ground water that seeps into the basin from Pennsylvanian through Cretaceous sedimentary rocks along the western basin margin (fig. 9). Zone 4 water has some of the highest specific conductance values in the basin, along with higher than average δ^2H and chloride, and is predominantly a Na-Cl-SO_4-type water. The median age of zone 4 water is 20,400 years. Zone 4 water is likely to occur to considerable depth in the southwest part of the basin, but this cannot be directly determined from the relatively shallow windmills sampled. Water in zone 4 may become diluted by infiltration water in the basin and mixing with water from the Rio Puerco.

Zone 5 occurs parallel to the Rio Puerco throughout the basin and contains water infiltrated from it. It is predominantly a Na-SO_4-type water , and is characterized by higher than average δ^2H, specific conductance, and sulfate. The median age is 8,100 years, but the water is younger nearer the Rio Puerco. Zone 5 water occurs down to at least 250 feet below the water table. Zone 6 (southwestern mountain-front recharge) occurs in the southwest corner of the basin and probably represents recharge occurring along the flanks of Ladron Peak. Only two water samples were identified from this source; they have lower than average specific conductance and dissolved sulfate. The water appears to be a Na-Ca-Mg-HCO_3-type water, with higher than average δ^2H. Total saturated thickness of this zone is unknown. The mean radiocarbon age is 7,700 years.

Zone 7 (recharge from Abo Arroyo) occurs in the southeastern part of the basin and appears to be eastern mountain-front recharge affected by infiltration from Abo Arroyo. The water is a Ca-SO_4 type, and is characterized by higher than average specific conductance, sulfate, and chloride. The median age is 9,400 years and flow is generally to the west-southwest to the Rio Grande. The limited depth information indicates total saturated thickness of at least 80 feet. Zone 8 (eastern mountain-front recharge) occurs along the entire eastern mountain front and represents recharge from that source (fig. 9). The water is a Ca-Na-HCO_3 type, and is characterized by lower than average specific conductance, δ^2H, chloride, and $\delta^{13}C$. Elevated concentrations of sulfur hexafluoride released from fluid inclusions in granitic rock were detected along the eastern mountain front. Eastern mountain-front water has a median age of 5,200 years. The saturated thickness in zone 8 may be more than 800 feet.

Zone 9 (ground-water inflow from the Tijeras Fault Zone) occurs along the eastern mountain front south of Tijeras Arroyo, and appears to represent water from crystalline rocks along the Tijeras Fault Zone that have mixed with eastern mountain-front recharge water (zone 8). Zone 9 water is characterized by higher than average specific conductance, δ^2H, boron, $\delta^{13}C$, chloride, bicarbonate, and lithium. The median age is 16,300 years. Zone 10 (recharge from Tijeras Arroyo) occurs in a narrow zone along Tijeras Arroyo and appears to be mountain-front recharge affected by infiltration from Tijeras Arroyo. This water is a Ca-HCO_3-type water, and is characterized by higher than average specific conductance, sulfate, nitrate, and δ^2H. The median age of waters sampled from zone 10 was only 3,200 years, and some waters contained tritium and chlorofluorocarbons.

Zone 11 (inflow from the northeast basin margin) occurs along the northeast side of the basin and appears to be a mixture of inflow from the Hagan Embayment (fig. 3), mountain-front recharge, and arroyo recharge. The water is characterized by higher than average specific conductance, chloride, calcium, sulfate, δ^2H, sodium, and $\delta^{13}C$. The median radiocarbon age is 10,000 years but appears older nearest the basin margin, suggesting that inflow from the adjacent Hagan Embayment contains relatively old water. Zone 12 (recharge from the Rio Grande) occurs parallel to the Rio Grande from about San Felipe Pueblo (fig. 4) in the northern basin to Abo Arroyo in the south. Zone 12 appears to represent infiltration from the Rio Grande and occurs slightly west of the Rio Grande and as much as 7 miles east of the Rio Grande at Albuquerque. The zone is relatively narrow in its extreme northern and southern extents (fig. 9). The water from zone 12 contains lower than average δ^2H, $\delta^{34}S$ of sulfate, dissolved oxygen, and sulfate. Zone 12 water contains higher than average dissolved SiO_2 and potassium, with calcium elevated relative to sodium. The median age is 4,300 years, and the saturated thickness in zone 12 is more than 1,400 feet beneath parts of Albuquerque. Zone 12 water has lower pH, sulfate, radiocarbon age, and higher calcium than water from zone 3, which occurs under about the western third of zone 12.

Zone 13 (basin discharge) was recognized in seven samples from the southern tip of the basin (fig. 9) and is thought to represent an area of convergence of flow lines due to reduction in thickness and lateral extent of basin-fill material. Zone 13 water has higher than average specific conductance, sulfate, chloride, lithium, and boron. The median chloride content is elevated relative to chloride in adjacent zones, possibly indicating upward movement of water from deeper parts of the basin. Zone-13 water has lower than average δ^2H, and lower than average dissolved oxygen. The median age of zone 13 water is 17,900 years.

GROUND-WATER-FLOW MODEL

Numerical Methods

Transient, three-dimensional ground-water flow through heterogeneous, anisotropic, porous media is governed by the following partial differential equation (Freeze and Cherry, 1979):

$$\frac{\partial}{\partial x}\left(K_{xx}\frac{\partial h}{\partial x}\right)+\frac{\partial}{\partial y}\left(K_{yy}\frac{\partial h}{\partial y}\right)+\frac{\partial}{\partial z}\left(K_{zz}\frac{\partial h}{\partial z}\right)-W=S_s\frac{\partial h}{\partial t} \quad (1)$$

where

x, y = cartesian coordinates in the horizontal direction (L);
z = cartesian coordinate in the vertical direction (L);
K_{xx}, K_{yy}, K_{zz} = hydraulic conductivity in the x, y, and z directions (LT-1);
h = hydraulic head, or water level (L);
W = volumetric flux of an external source or sink, per unit volume (L);
Ss = specific storage (L^{-1}); and
t = time.

The USGS MODFLOW model (McDonald and Harbaugh, 1988) implements an integrated finite-difference approximation of equation 1. The MODFLOW model was used to simulate ground-water flow in the MRGB using the preconditioned conjugate-gradient solver (Hill, 1990). The hydrogeologic deposits are allowed to be anisotropic in the horizontal direction, but only by a single constant factor for each layer. Vertical anisotropy can vary horizontally, though, as vertical and horizontal conductivity can be specified independently throughout the three-dimensional domain. A steady-state assumption was made in the first part of this study for simulating predevelopment conditions, but later transient simulations were made to accommodate possible varying past rates of recharge. Travel times to wells sampled for ^{14}C were calculated using the USGS MODPATH model (Pollock, 1994). The model uses the cell-by-cell fluxes calculated with MODFLOW to track flow lines backward from wells to recharge locations. The curvatures of the flow lines are calculated through each cell by assuming a linear change in velocity between the cell faces along each coordinate direction. The MODPATH model was also used to delineate how waters from different source regions were simulated by MODFLOW to be distributed across the basin. The MODFLOW and MODPATH representations of the basin were calibrated in part using nonlinear regression methods implemented in UCODE (Poeter and Hill, 1998).

Spatial Discretization

Although the MRGB is defined as the extent of Cenozoic deposits within the bounding structural uplifts, the model domain covers a somewhat smaller area. The eastern and western model boundaries are mostly coincident with faults thought to be partial barriers to horizontal ground-water movement (fig. 3). The model boundaries in the north and south coincide with the boundaries of the MRGB, which are defined by mountains and uplifts. The areal model extent is the same as in the earlier models of Kernodle and others (1995) and Tiedeman and others (1998). The overall horizontal discretization is somewhat coarser than that of Kernodle and others (1995), yet somewhat finer than that of Tiedeman and others (1998). The model area is divided into a rectilinear grid of equally spaced 1-kilometer-size cells composing 156 rows and 80 columns (fig. 10).

The vertical extent of the aquifer system is represented by nine model layers. Kernodle and others (1995) used 11 layers, whereas Tiedeman and others (1998) used 6 to 9. The bottom of layer 1 is 20 feet below the bed of the Rio Grande, and the altitude of the bottom of layer 1 is constant in an orthogonal direction away from the trend of the inner valley (fig. 11). The upper seven layers range in thickness from 20 to 1,000 feet and extend to a depth of about 2,400 feet below the elevation of the Rio Grande. Layers 8 and 9 are of variable thickness and represent the aquifer system from the bottom of model layer 7 to the base of the Santa Fe Group (fig. 12). Layer 8 ranges in thickness from about 400 to 3,000 feet, and layer 9 ranges in thickness from about 800 to 6,000 feet. The total thickness of the model is about 12,000 feet, although the deeper depths are represented by coarser layering because geologic data there are sparse, and water-level data are nonexistent. This is a significant change from the earlier models of Kernodle and others (1985) and Tiedeman and others (1998), which extended to depths of only 1,730 feet and 5,000 feet, respectively. The basin thins near its margins; therefore, the number of active cells in each model layer is smaller for successively deeper layers. Layer 1 contains about 6,200 active cells, and layer 9 contains about 4,500 active cells. The model contains a total of about 51,000 active cells.

Boundary Conditions

Boundary conditions include no flow on the bottom of the model domain, no flow and specified flow on the sides of the model domain, and head-dependent flow and specified flow on the top of the model domain. For each boundary condition, an associated parameter was estimated during model calibration with aid of the nonlinear regression procedure within UCODE. Manual adjustments of individual parameters were also made to further minimize the model error. The best parameter estimates from Tiedeman and others (1998) were used as the initial parameter values at the outset of the calibration procedure.

Head-Dependent River Boundary Conditions

Head-dependent boundaries are implemented in the inner valley of the MRGB to represent the interaction of the Rio Grande with the ground-water-flow system. Likewise, head-dependent boundaries are implemented along the Jemez

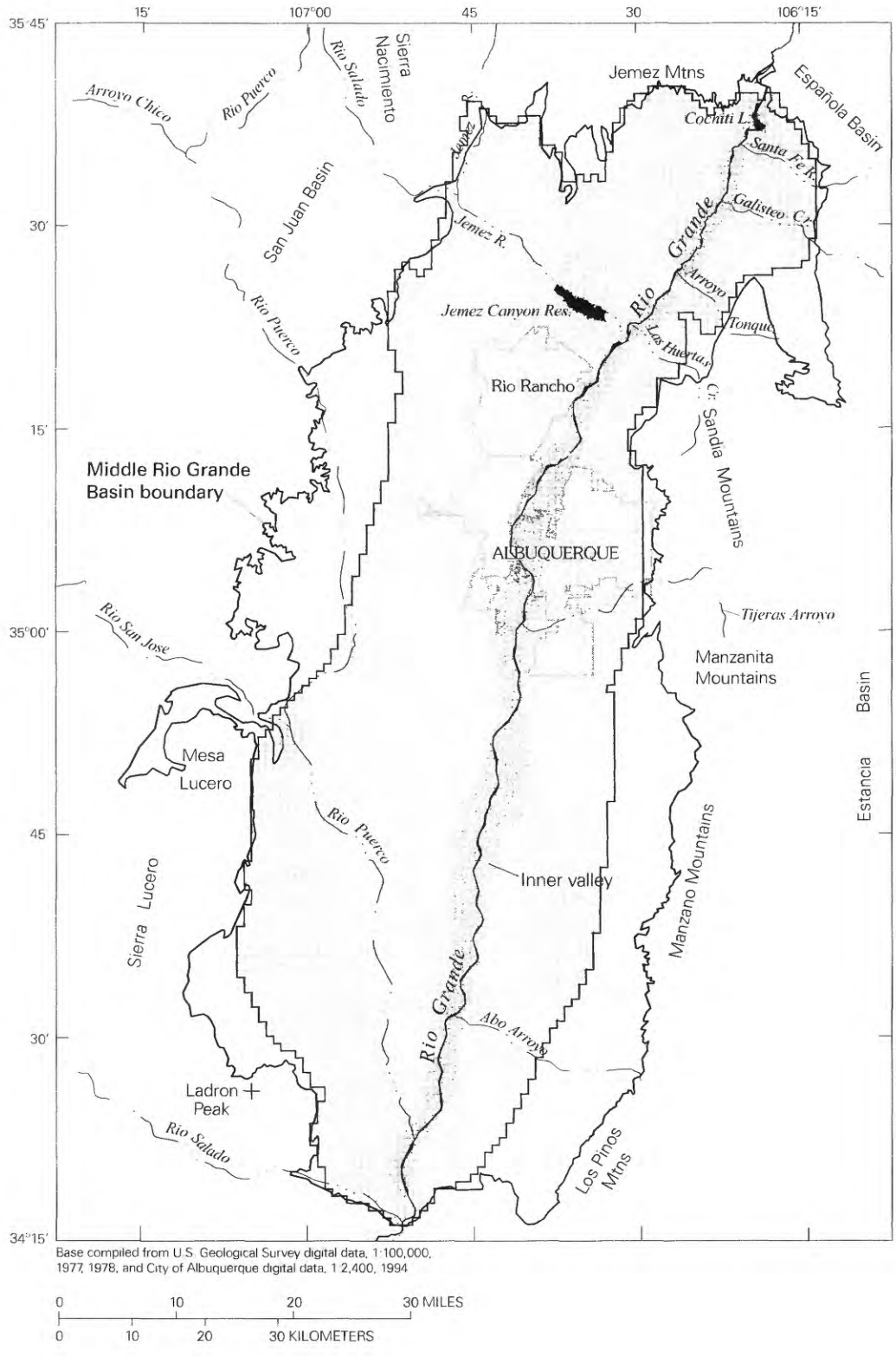

Figure 10. Plan view of finite-difference grid for the ground-water-flow model.

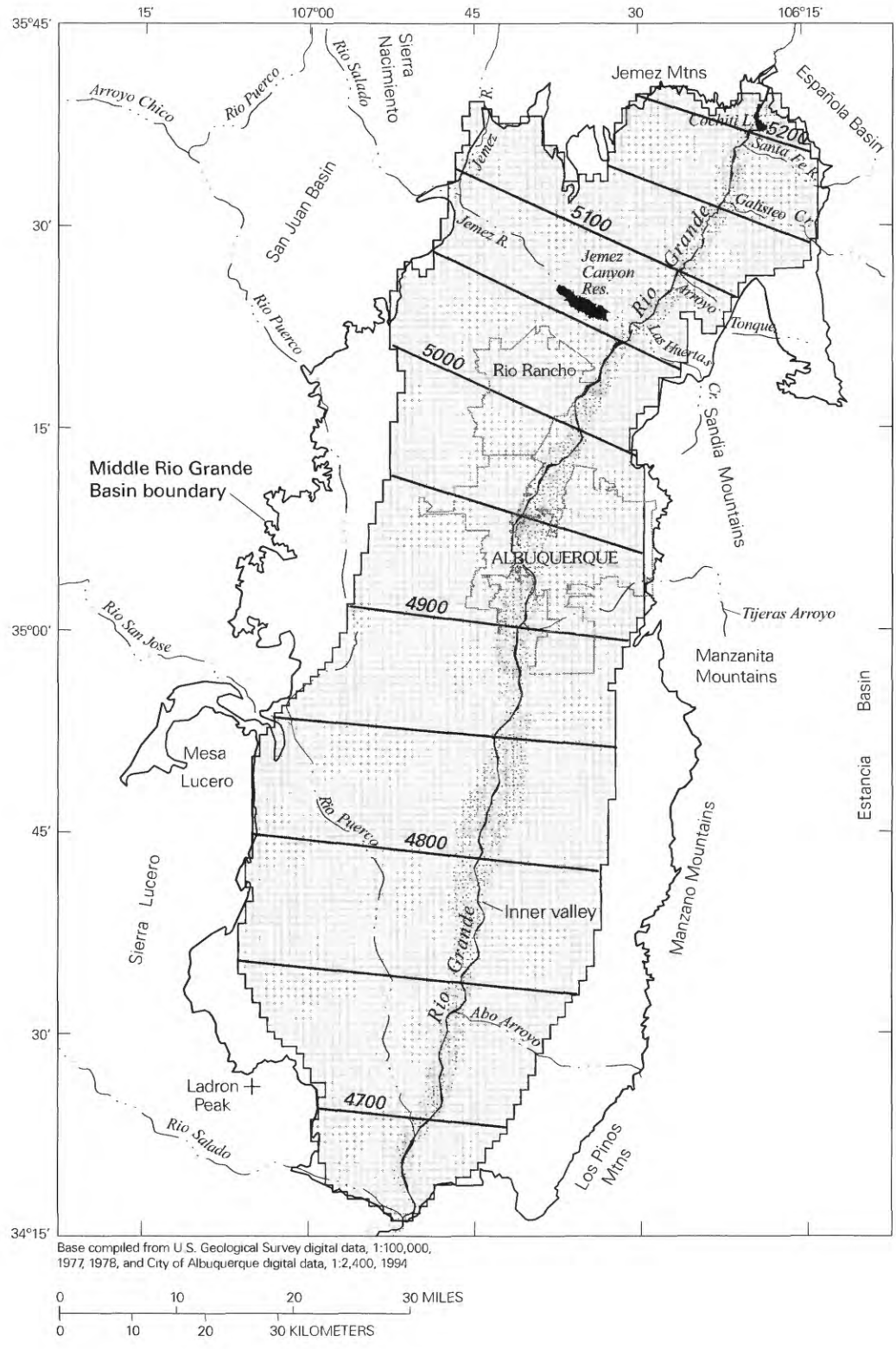

Figure 11. Altitude, in feet above sea level, of the base of model layer 1.

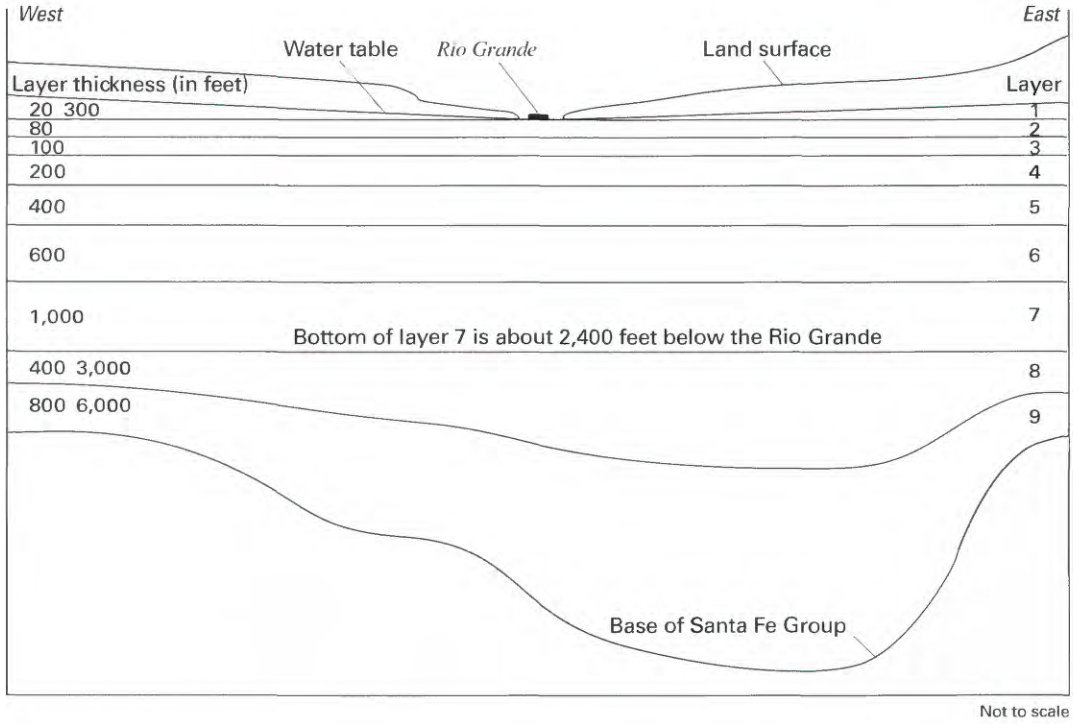

Figure 12. Configuration of model layers.

River and Rio Puerco to represent ground-water/surface-water interaction along those waterways. The manmade waterways and reservoirs within the basin were not included in this study because the simulations represent predevelopment conditions within the basin. The head-dependent boundary is simulated using the river package of MODFLOW (McDonald and Harbaugh, 1988). In the river package, flow between a surface-water body and the underlying cell of the ground-water-flow model is a function of the altitude of the stage of the river; the simulated hydraulic head in the cell; the length and width of the river in the cell; and the altitude, vertical hydraulic conductivity, and thickness of the riverbed. The river dimensions, hydraulic conductivity, and thickness are combined into a single parameter referred to as the riverbed conductance. A separate riverbed conductance was estimated for the central Rio Grande, the Jemez River, the northern Rio Puerco, and the southern Rio Puerco. The northern and southern Rio Grande riverbed conductances were assigned large arbitrary values, because the inverse procedure indicated they should be high, but the procedure also indicated that the simulation results were very insensitive to their exact values.

The cells specified using the river package in this study included all of the regions within the flood plains of the Rio Grande, Jemez River, and Rio Puerco (fig. 13). This approach was used instead of treating the evapotranspiration (ET) boundary condition and Rio Grande boundary condition in these regions separately, as was done in the previous models. There were two main reasons for using this approach. The first reason for adopting this method was that rivers migrate across their flood plains over the course of several thousand years. This effect needed to be accounted for in the paleohydrologic simulation and in the steady-state, predevelopment simulation where the goal was to represent long-term average hydrologic conditions. This was especially critical because of the travel-time calculations made for wells near the flood plains. For a well immediately adjacent to a flood plain, the simulated distance from the well to the exact recharge cell within the valley may vary greatly depending on which side of the flood plain that reach of the river was on at the time the water was recharged. If the water is more than several decades old, this position cannot be determined. For this reason, the river fluxes were spread across the entire flood plain by assigning river cells across the entire flood plain. The second reason was that in this study the objective did not include distinguishing between the river and ET fluxes in the hydrologic budget of the basin. Including ET in a simulation affects mostly the calibrated position of the local water table and the distribution of the local ground-water to surface-water fluxes. For a flood plain with low relief, excluding ET has little effect on the total flux between the basin and the inner valley and river system.

Specified-Inflow Boundary Conditions

Recharge of precipitation and stream water is simulated as a specified flux to the uppermost active cell of the model, using the recharge package of MODFLOW. This recharge is divided into geographic zones, each of which generally corresponds to a basin-boundary segment, a group of basin-boundary segments, or a small stream or arroyo that is known to carry a significant volume of water at various times. There were nine major zones specified, and the zone along the Sandia Mountains was later divided into four

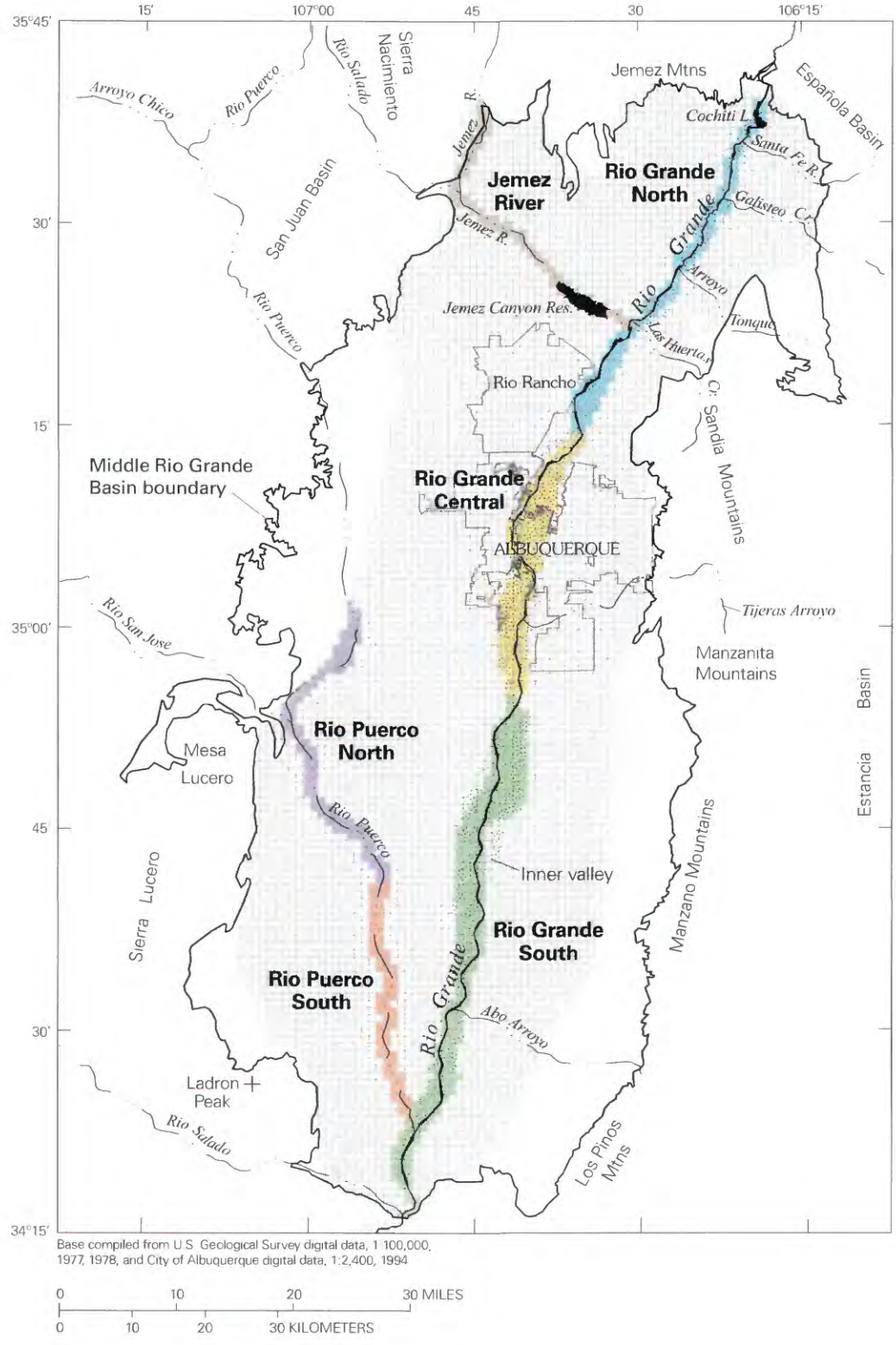

Figure 13. Location of head-dependent river cells in the ground-water-flow model.

zones, giving 12 recharge zones in all (fig. 14). These 12 zones are: (1) mountain-front recharge along the Jemez Mountains; (2) tributary recharge along the Santa Fe River, Galisteo Creek, and Las Huertas Creek; (3) mountain-front recharge at the northern end of the Sandia Mountains; (4) mountain-front recharge at the north-central section of the Sandia Mountains; (5) mountain-front recharge at the south-central section of the Sandia Mountains; (6) mountain-front recharge at the southern end of the Sandia Mountains; (7) tributary recharge along Tijeras Arroyo; (8) mountain-front recharge along the Manzano Mountains; (9) tributary recharge along Abo Arroyo, (10) mountain-front recharge along the Los Pinos Mountains; (11) tributary recharge along the Rio Salado; and (12) mountain-front recharge along Ladron Peak. No recharge is specified across the top surface of the model, because the amount of rainfall during the year is exceeded by the amount of evaporation. Eventually mountain-front recharge along the Jemez Mountains was set to zero because as the inverse model estimated low values and could not distinguish between it and underflow at the same location. Some of the final estimate for the underflow there could also include mountain-front recharge.

Underflow along the basin boundaries is simulated using the well package of MODFLOW as a specified flow into layers 2, 3 and 4 of the model. The depth distribution of ground-water flow across the MRGB boundaries is uncertain. Underflow was specified in layers 5–9 in Kernodle and others (1995), in layer 3 in Tiedeman and others (1998), and in layers 1–3 in McAda and Barroll (2002). The current model specifies these fluxes at similar average depths to those in the previous models, and the influx is spread out vertically so that travel times to wells near those borders would not reflect an arbitrary influx in one layer only. The influx for layers 2, 3, and 4 was allocated in proportion to their thickness to maintain a consistent horizontal velocity throughout the vertical thickness of the inflow zone. The seven underflow zones (fig. 15) are: (1) along the Sierra Lucero Uplift, (2) along the Sand Hill Fault Zone, (3) along the boundary with the San Juan Basin, (4) along the western part of the Jemez Mountains, (5) along the eastern part of the Jemez Mountains, (6) along the boundary with the Espanola Basin, and (7) along the boundary with the Hagan Embayment.

Hydraulic Properties

The ground-water-flow model requires values of horizontal and vertical hydraulic conductivity to be specified throughout the domain. The degree to which these values vary across the basin is accounted for in the model by specifying hydraulic conductivity zones, with a single value of horizontal and/or vertical hydraulic conductivity associated with each zone. To create a more realistic and accurate model, the zone boundaries should follow the boundaries between the geologic formations or facies (Hill, 1998). In this study, a three-dimensional geologic model was used to create the pattern of hydraulic conductivity zones in the model.

Geologic Model

The geologic framework for the ground-water-flow model is based on a revised geologic model (Cole, 2001b) that was in turn based on detailed geologic mapping that had been conducted by the USGS, the New Mexico Bureau of Geology and Mineral Resources, and the University of New Mexico. Considerable insight to the three-dimensional distribution of geologic units within the model was made possible by recent geophysical investigations (Grauch and others, 2001; Rodriguez and others, 2001) and reinterpretations of existing data. The revised geologic model was also based on stratigraphic and lithologic interpretations of the sediments penetrated by numerous wells in the basin. In particular, careful consideration was given to the stratigraphic interpretations of Lozinsky (1988, 1994) for 12 deep oil-exploration wells from the central and southern parts of the system, and to interpretations from dozens of water wells in the central part of the system around Albuquerque and Rio Rancho (Hawley and Haase, 1992; Hawley and others, 1995; Connell and others, 1998). An independent interpretation of drill-hole geophysical logs was performed for many of the wells, using an empirical semiquantitative method to identify dominant grain-size characteristics of rift-fill sediments (Cole, 2001b). The goal of creating the geologic model was to define regional-scale hydrostratigraphic units that could be delimited in the subsurface across the structural subbasins from drill-hole data and geophysical constraints, where available. However, such data and constraints were lacking for major parts of the geologic model, such that the delimitation of hydrostratigraphic units was based on a conceptual understanding of overall rift history and the expected relationships between tectonic deformation and sedimentation (Stone, 2001; Stone and others, 2001).

The higher density of pre-rift sediments allowed the regional gravity data (Grauch and others, 2001) to be used to calculate the bottom of the aquifer system. This procedure dramatically revealed the important substructure of the Middle Rio Grande "Basin," which consists of discrete deep subbasins in the northern and central areas and a highly irregular subbasin complex in the south (fig. 16). This irregular surface was specified as the bottom of the aquifer system, and it was used to define the bottom of the ground-water-flow model (fig. 17).

Faults are important structural and hydrologic elements in the aquifer framework, and several sources of data were used to identify the principal fault zones in the basins. Sharp gradient zones in the gravity data indicate boundaries of major blocks of basement-density material, and these zones largely coincide with north- and northwest-trending margins of the deeper (older) parts of the structural subbasins. Younger faults that are manifest in the near surface chiefly trend north-south (fig. 3) and reflect the dominant extension direction during the last 5 million years. A final set of fault trends for the geologic model of the basin was determined by comparing independent compilations based on aeromagnetic lineament data (Grauch and others, 2001), topographic scarps defined by digital elevation data, mapped fault zones (Hudson and others, 1999), and fault scarps known or inferred to reflect Quaternary offset

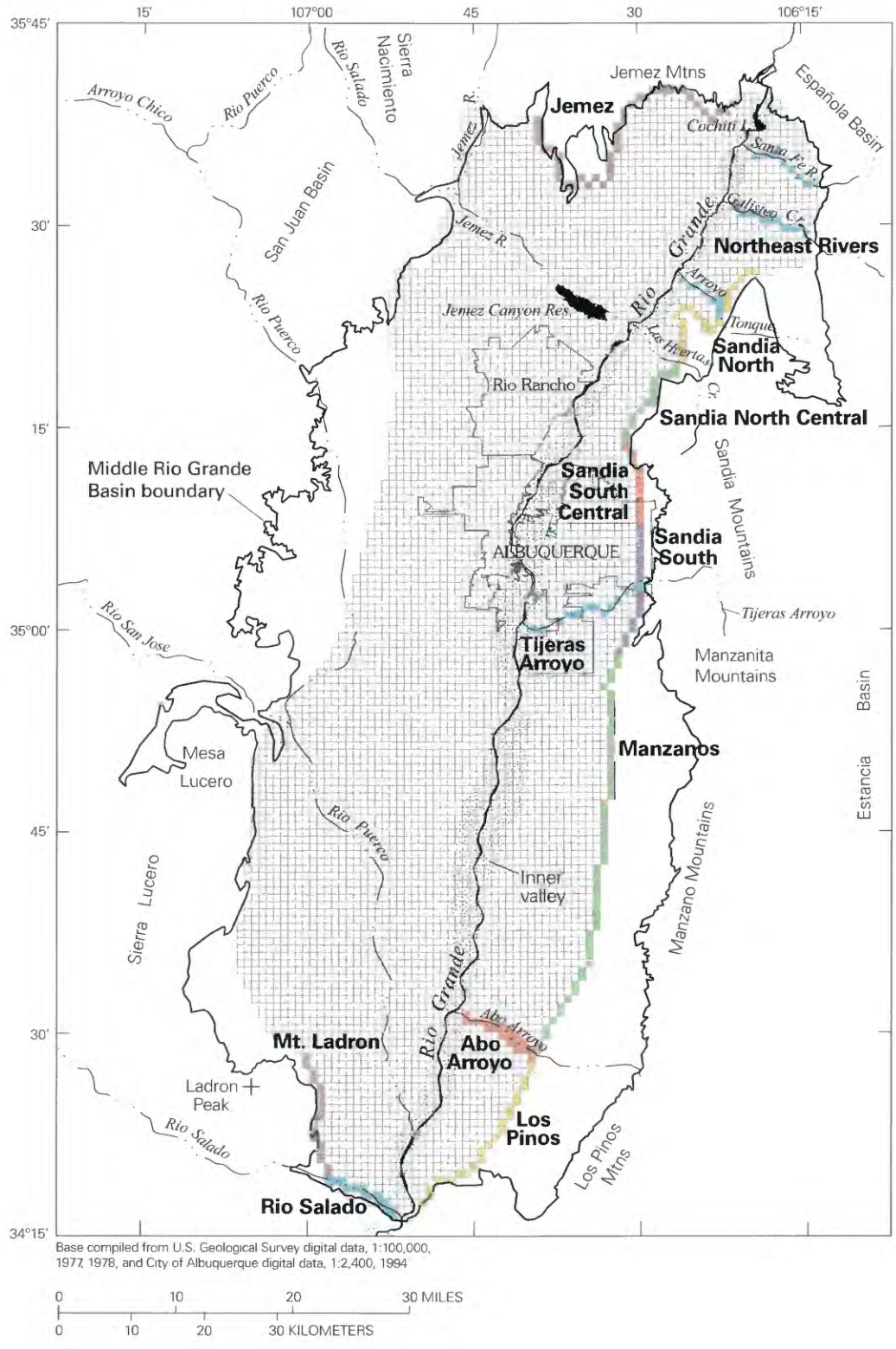

Figure 14. Location of mountain-front and arroyo recharge cells in the ground-water-flow model.

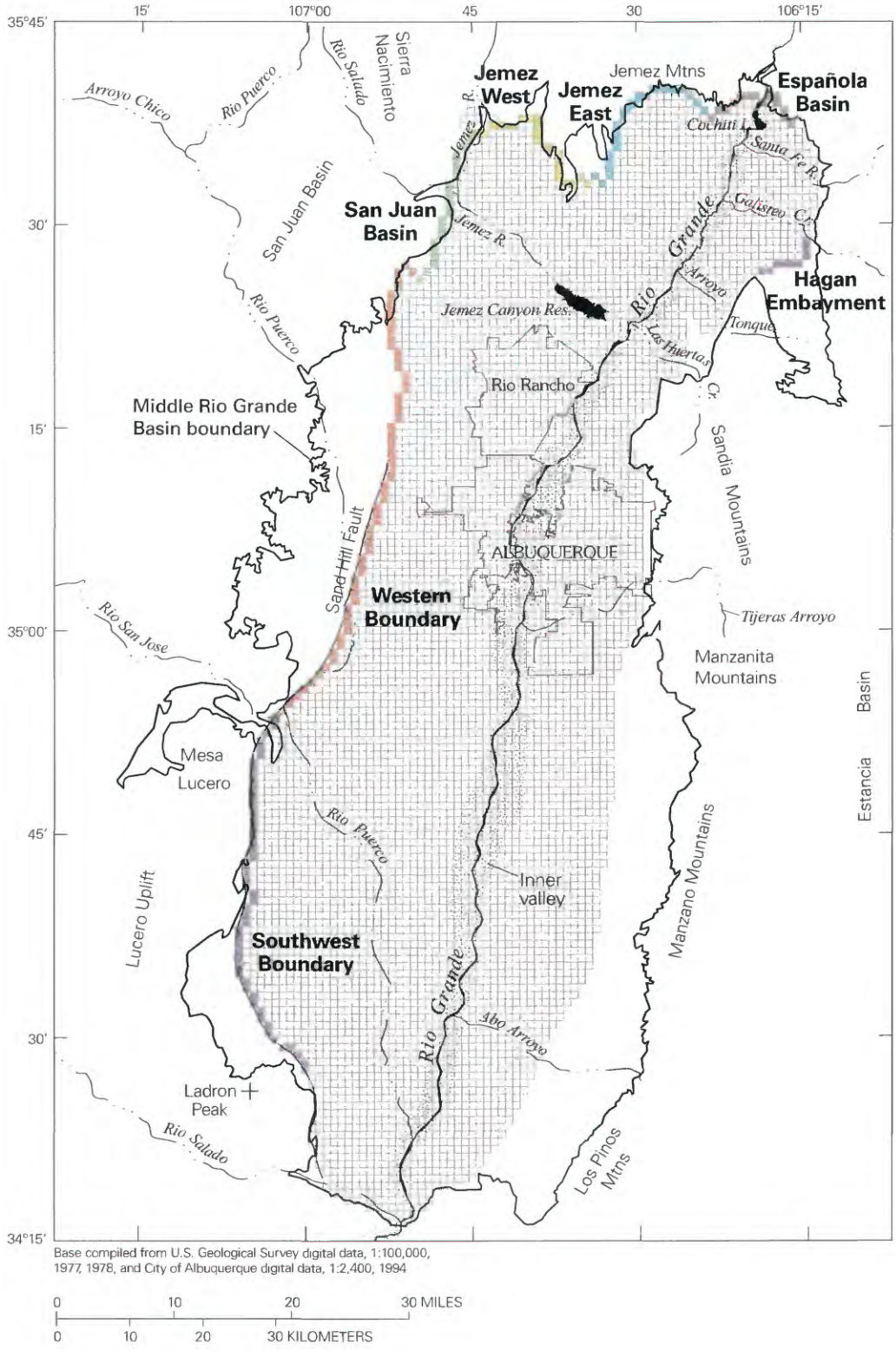

Figure 15. Location of specified underflow cells in the ground-water-flow model.

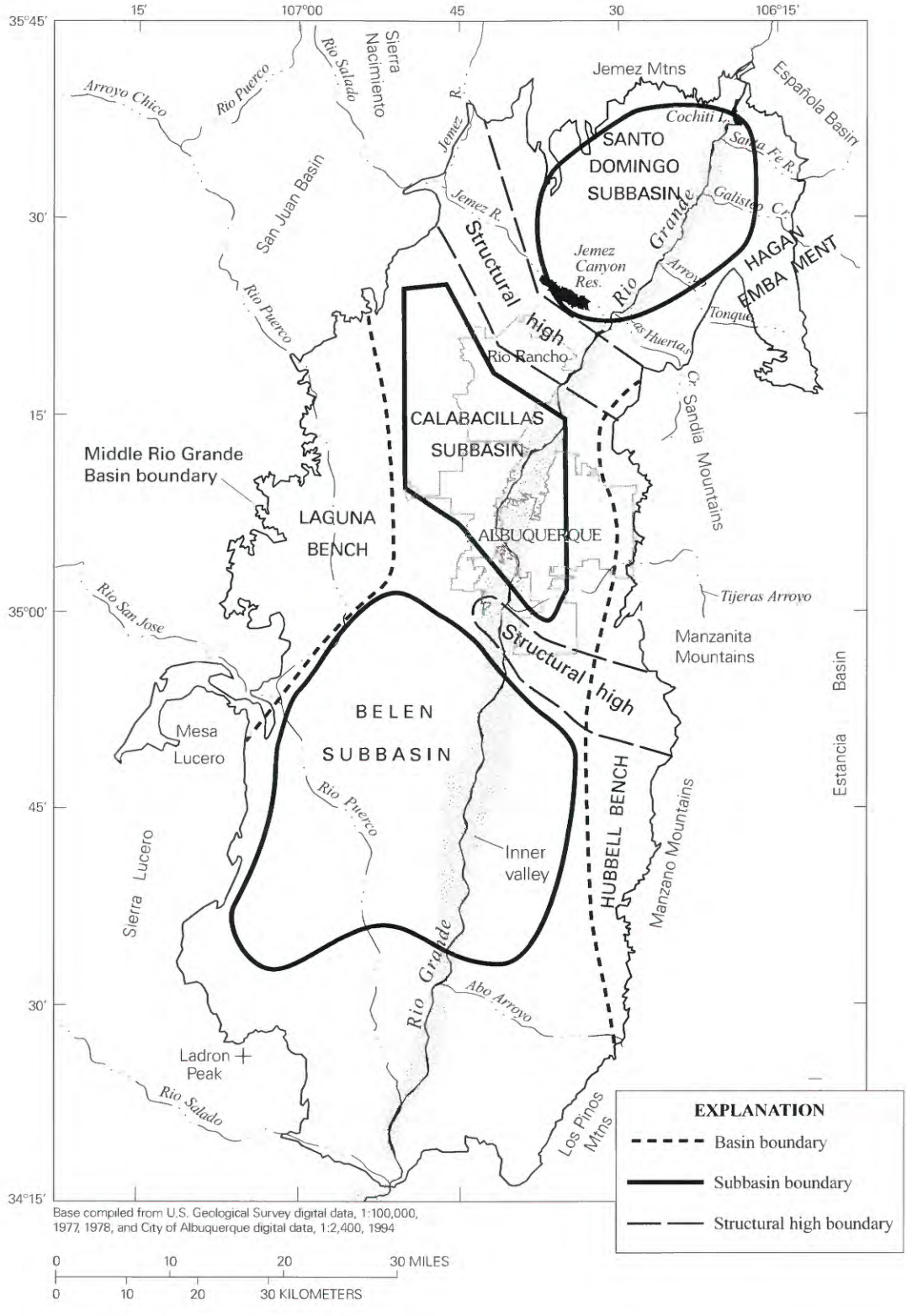

Figure 16. Simplified structure of the Albuquerque Basin, showing subbasins identified from gravity data in Grauch and others (2001).

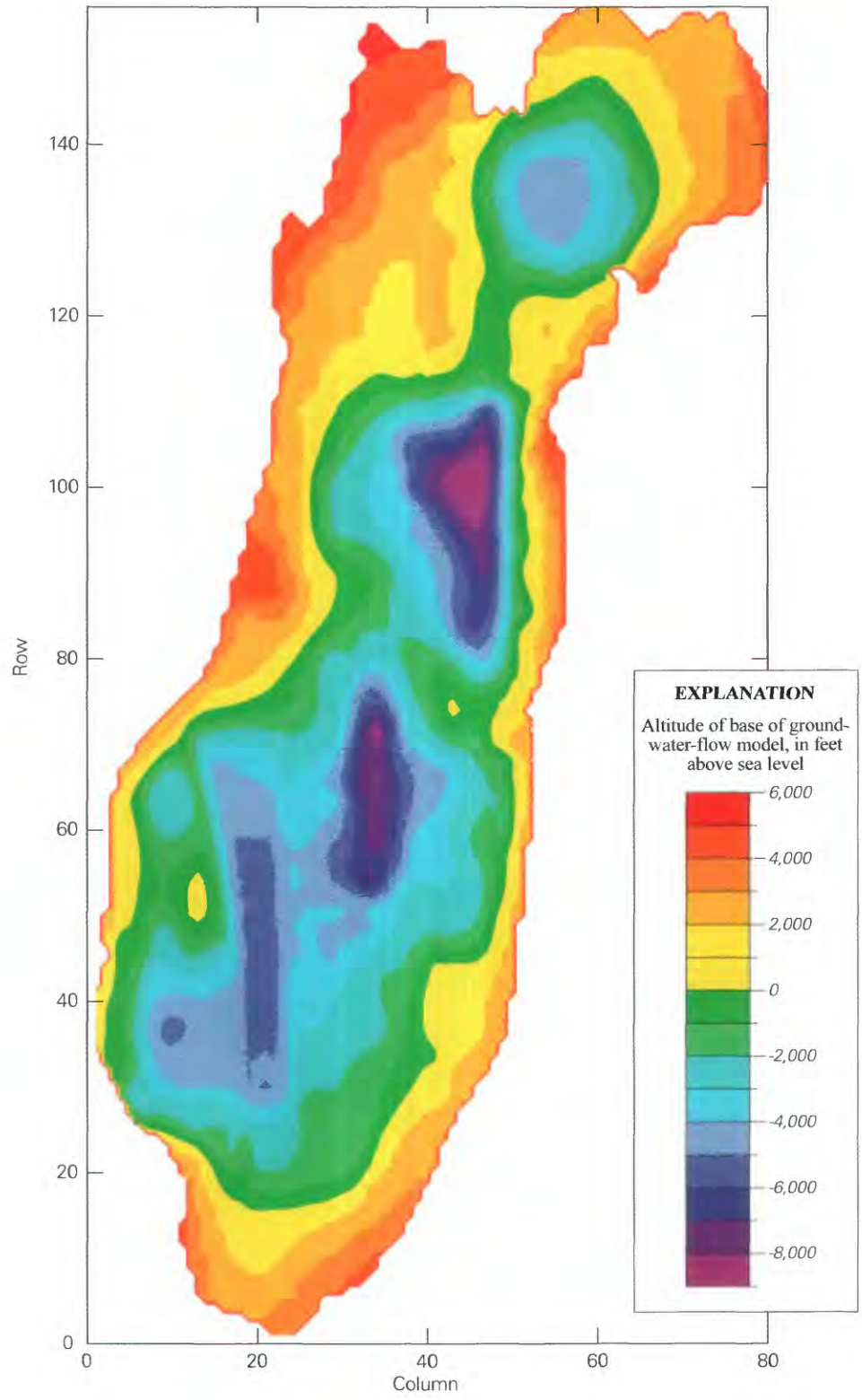

Figure 17. Altitude of the base of the ground-water-flow model. Surface is based on geophysical data in Cole and others (2001) and Grauch and others (2001).

(Machette and others, 1998). Of all the faults in the geologic model, only two were treated explicitly in the model in this study—the Cat Mesa Fault Zone and the Sandia Fault Zone. These were the only two zones across which large discontinuities in water levels could be observed in the model region.

The hydrostratigraphic units distributed through the three-dimensional geologic model were necessarily simple and coarsely defined, as required for the regional scale of the model. Nonetheless, they were consistently defined on the basis of overall grain size and bedding characteristics that reflect the conceptual sedimentological controls on deposition during rift-basin subsidence (Stone, 2001; Stone and others, 2001). The lowest units in the northern and southern subbasins are dominantly volcaniclastic sand and gravel reflecting erosion of volcanic-source terranes outside the rift basin; the oldest unit in the central subbasin is chiefly eolian sand and playa silt and clay. The thick and variable middle section of all three subbasins is composed of fluvial sand and silt derived from various external sources and accumulated in depositional centers through much of Miocene time while faulting was quite active and climate was temperate. The uppermost blanketing unit in all three subbasins consists of coarse gravel and sand that reflects a regional change to wetter climate at about 5 Ma (Raymo and Ruddiman, 1992). Sometime after 2.7 Ma (Kelley and Kudo, 1978), the ancestral Rio Grande drainage was integrated through and downstream of this region and the river system began to incise the existing basin fill (Cole, 2001b).

Hydraulic Conductivity Zones

The hydraulic conductivity zones of the ground-water-flow model were based directly on the hydrostratigraphy as represented in the three-dimensional geologic model (Cole, 2001b). The geologic model of the MRGB was constructed from the geologic data described above using Earth Vision geologic modeling software by Dynamic Graphics, Inc. Gridded data points were exported from the Earth Vision model listing the elevation of the top of each hydrostratigraphic unit at the UTM grid locations of cell boundaries in the MODFLOW ground-water-flow model (McAda and others, 2001). Similarly, gridded data were exported from the geologic model that defined the location and extent of each of the major faults in the model. In this fashion, the Earth Vision geology model was converted into input for the MODFLOW model with little distortion or loss of detail (figs. 18–27).

A total of 12 hydrostratigraphic units from the geologic model were converted to 18 hydraulic conductivity zones within the ground-water-flow model. Most of the zone refinement was based on the sensitivity of the model results to the different hydrostratigraphic zones. Where sensitivity was high, hydrostratigraphic zones were subdivided further into geographic subzones. In this way, the medium-to-coarse-sand unit that covers a large section of the basin was subdivided into six geographic subzones. Likewise the medium-sand unit and the proximal-volcanic-sand unit were subdivided into northern and southern subzones. Where sensitivity of the model results was low, hydrostratigraphic zones were combined. In this way extrusive and intrusive volcanics were combined, and the fine and very fine (eolian) sand were combined. In the case of the river alluvium, a recombination was made of the ancient and modern alluvium geologic zones into northern, central, and southern alluvium zones.

Vertical conductances in the ground-water-flow model were divided into 12 zones as values of vertical anisotropy. Each of the three Rio Grande alluvium zones was assigned a separate anisotropy; six of the medium-to-coarse sand-unit zones were each assigned an anisotropy value; the remaining three anisotropy values were assigned to the remaining units in the basin as northern, central, and southern values. The boundaries between these final three zones correspond roughly to the boundaries between the different subbasins (fig. 16). The north-south-trending faults within the basin (fig. 18) suggest there may be a regional north-south to east-west anisotropy in the basin. For this reason, a single value of north-south to east-west anisotropy was assigned to the entire basin in the ground-water-flow model. Best-fit values of the vertical anisotropies and vertical and horizontal hydraulic conductivities were estimated during the model calibration.

GROUND-WATER PATH LINE MODEL

The main purpose of this study is to use environmental tracer data to help improve estimates of parameters used in ground-water-flow models of the MRGB. To achieve this, a predevelopment ground-water-flow model of the basin was calibrated using parameter estimation methods and the environmental tracer data collected by Plummer and others (2004). Ground-water ages obtained from ^{14}C activities are one set of these data. When these observed ages are compared with equivalent simulated ages, the residuals can be used to directly influence the model calibration. The simulated ages are obtained by using MODPATH (Pollock, 1994) to track the line of travel of a parcel of water from an observation well backward to a recharge location. MODPATH is a post-processing program that is used in conjunction with the cell-by-cell flow rates calculated with MODFLOW. Time of travel can be integrated backward along a path line to obtain a simulated ground-water age. Another source of tracer information that is useful for calibration is the identification of the hydrochemical zones (fig. 9). These zones identify waters with different source areas. A delineation of waters with different source areas can also be simulated using MODPATH. A map of the distribution of ground water originating from different sources can be constructed by tracking a parcel of water backward from every cell in the model, and then plotting a symbol for the source areas at the cell centers. Such a simulated map can be compared with the hydrochemical zone map to help calibrate the model.

Porosity

The calculation of ground-water age by backward path line tracking requires the calculation of the seepage velocity at each cell face. Whereas the ground-water-flow model can

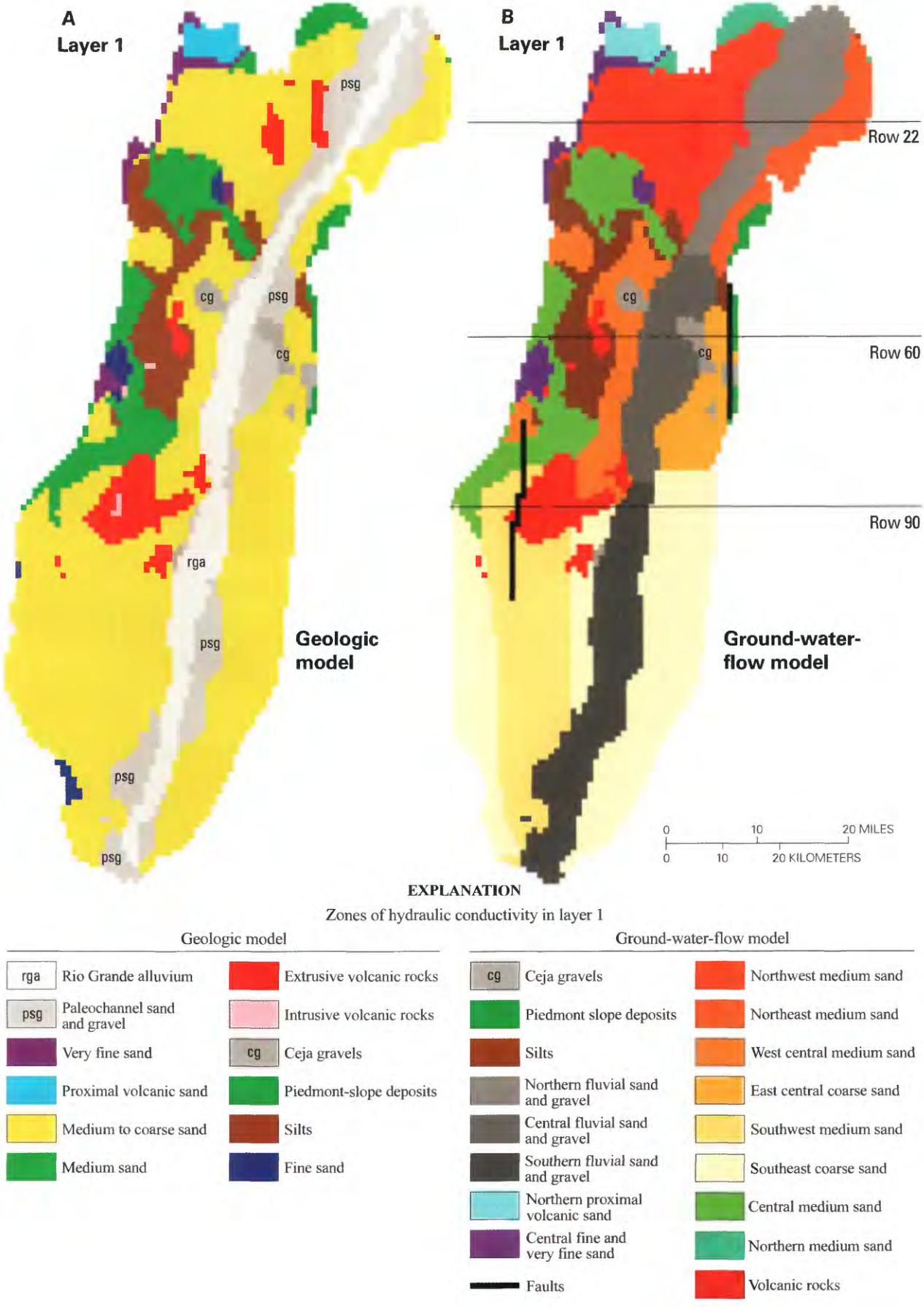

Figure 18. Hydraulic conductivity zones of layer 1 as defined in (A) the geologic model of Cole (2000b), and (B) the ground-water-flow model.

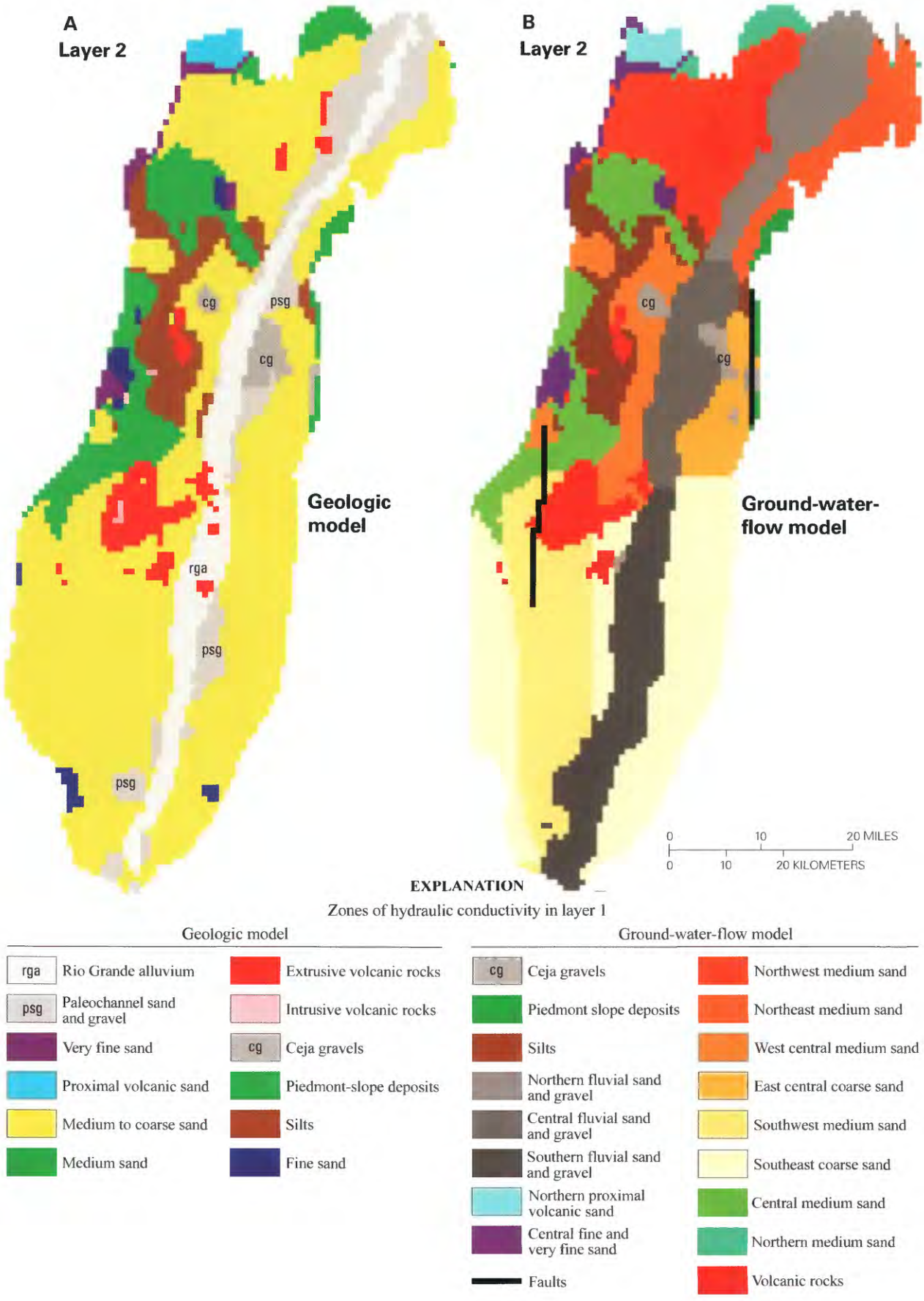

Figure 19. Hydraulic conductivity zones of layer 2 as defined in (A) the geologic model of Cole (2000b), and (B) the ground-water-flow model.

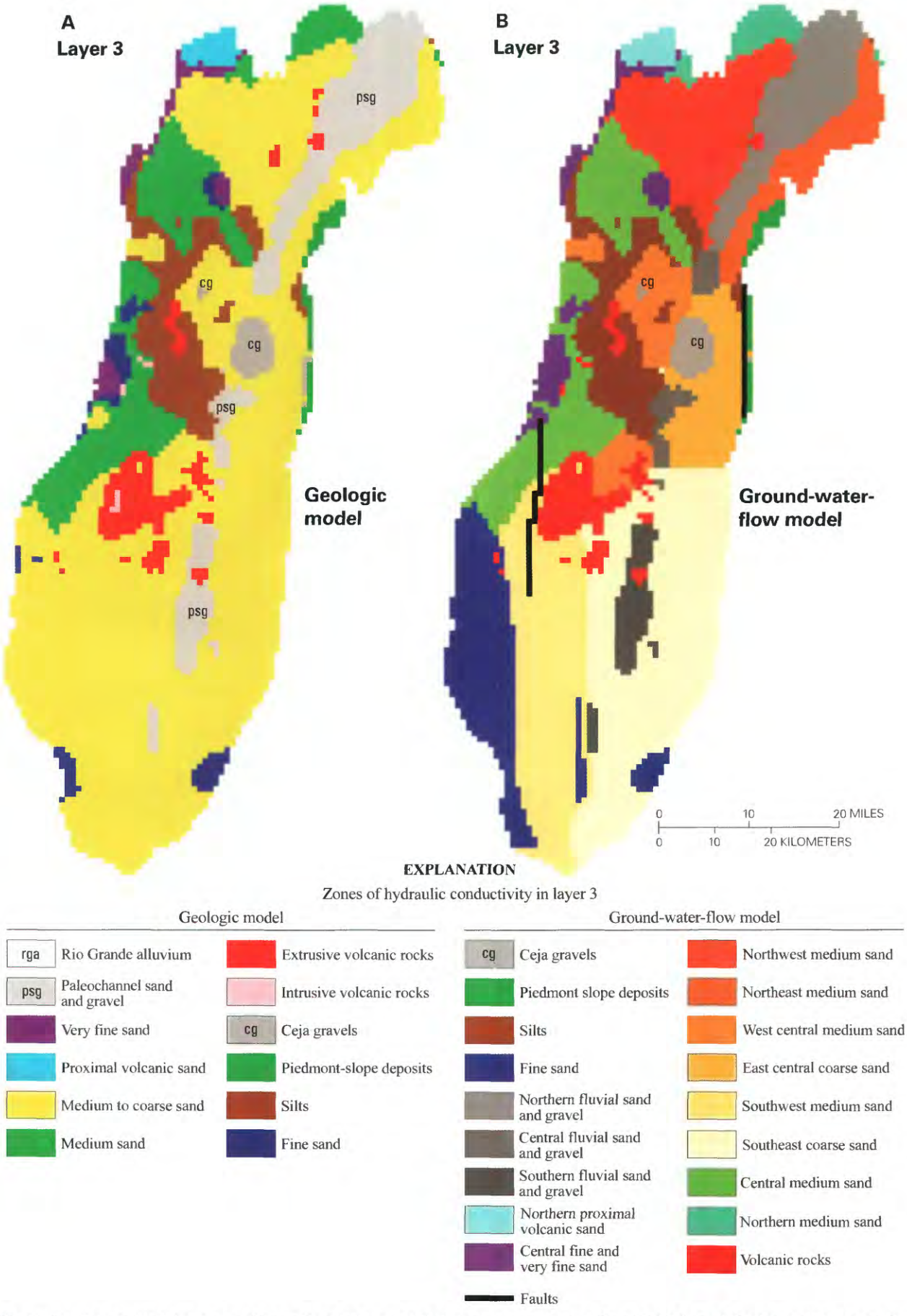

Figure 20. Hydraulic conductivity zones of layer 3 as defined in (A) the geologic model of Cole (2000b), and (B) the ground-water-flow model.

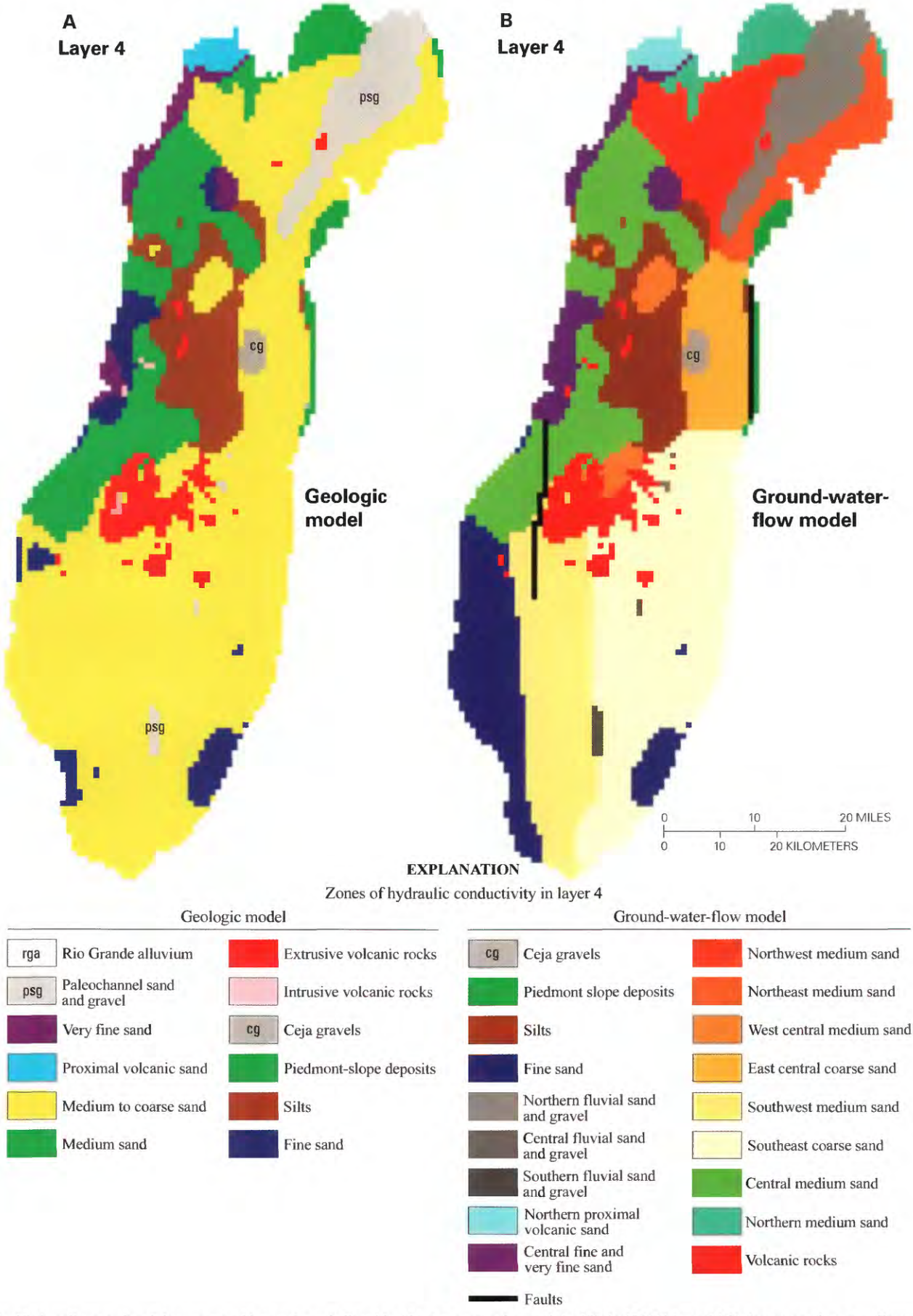

Figure 21. Hydraulic conductivity zones of layer 4 as defined in (A) the geologic model of Cole (2000b), and (B) the ground-water-flow model.

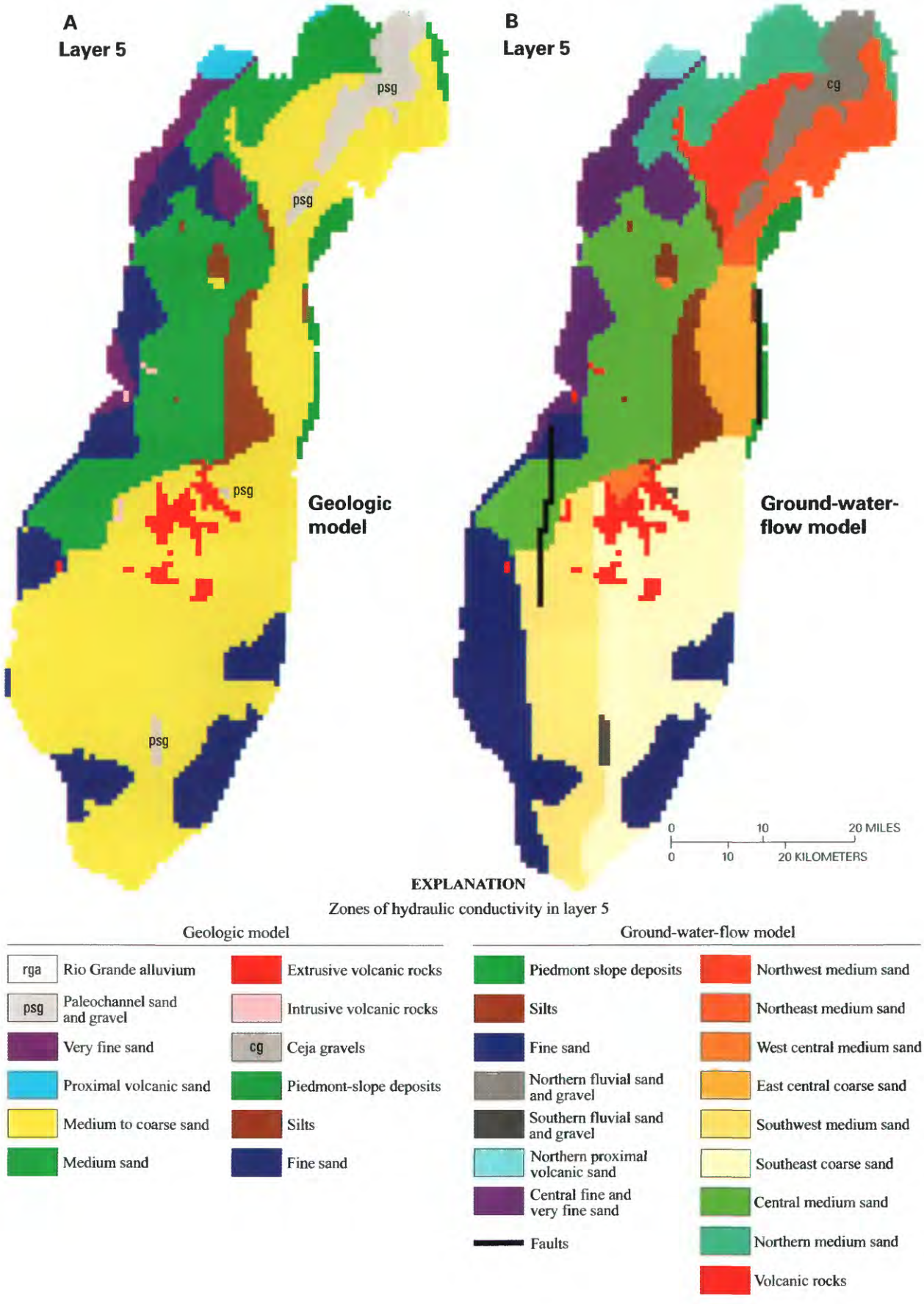

Figure 22 Hydraulic conductivity zones of layer 5 as defined in (A) the geologic model of Cole (2000b), and (B) the ground-water-flow model.

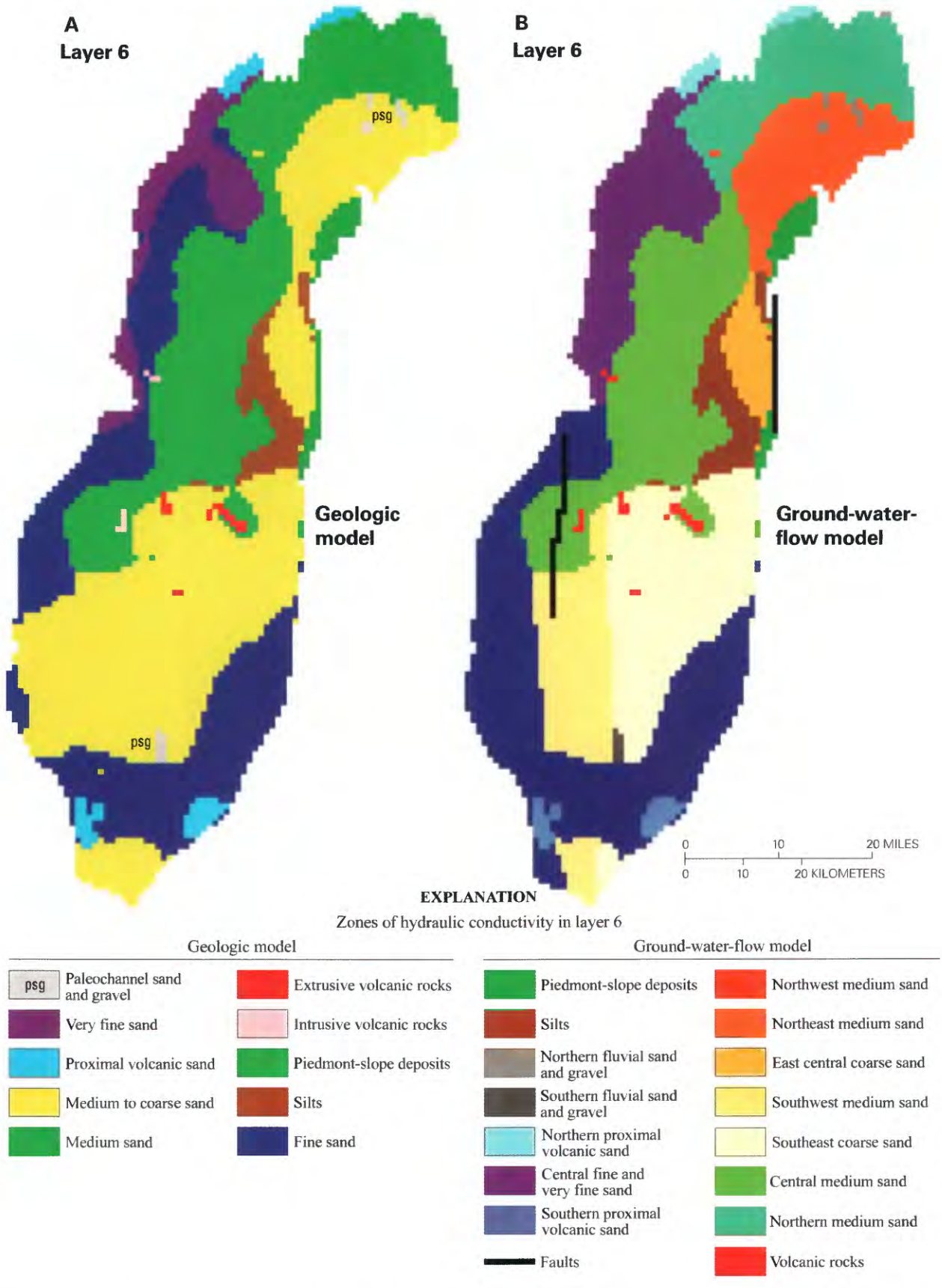

Figure 23. Hydraulic conductivity zones of layer 6 as defined in (A) the geologic model of Cole (2000b), and (B) the ground-water-flow model.

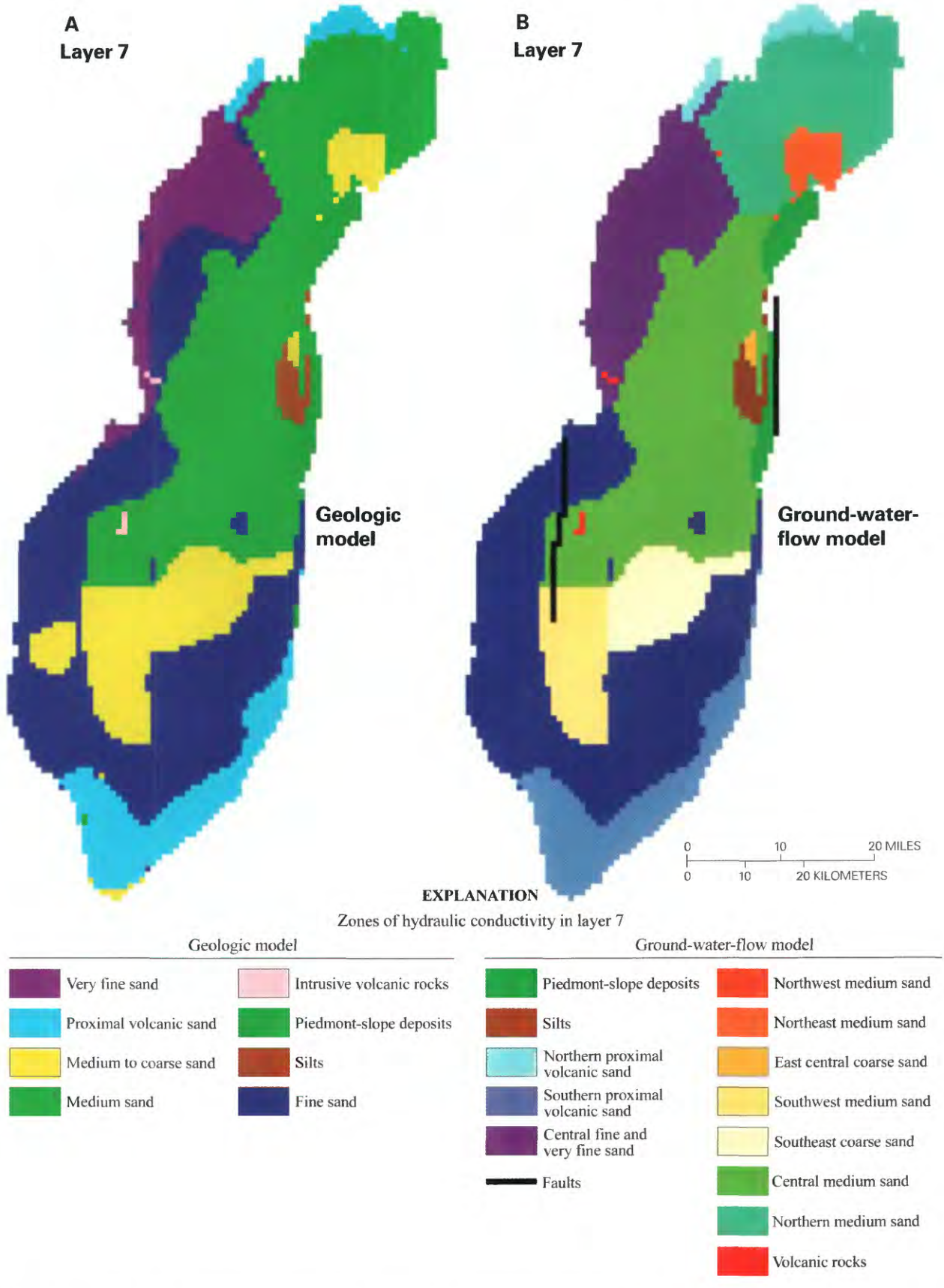

Figure 24. Hydraulic conductivity zones of layer 7 as defined in (A) the geologic model of Cole (2000b), and (B) the ground-water-flow model.

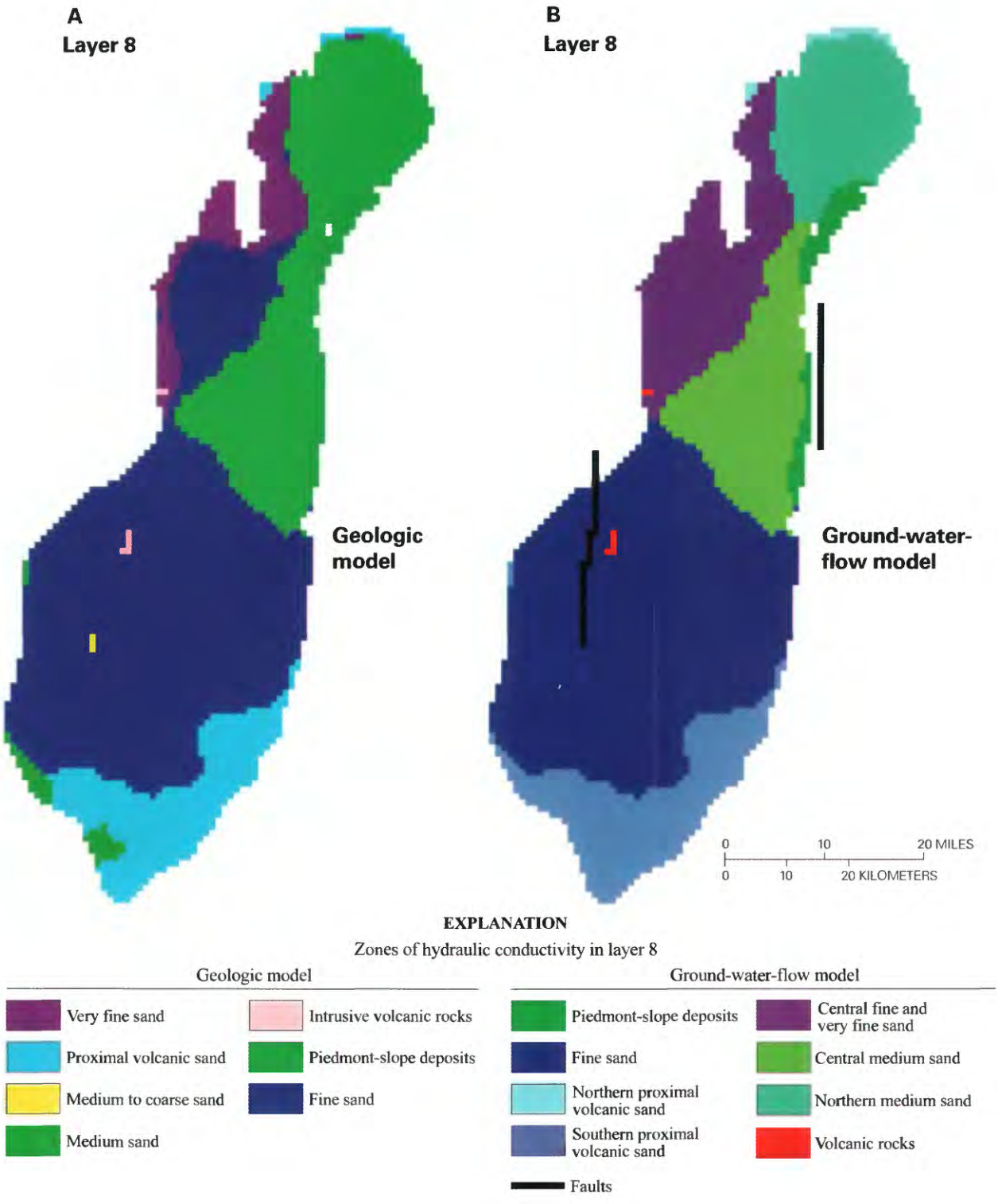

Figure 25. Hydraulic conductivity zones of layer 8 as defined in (A) the geologic model of Cole (2000b), and (B) the ground-water-flow model.

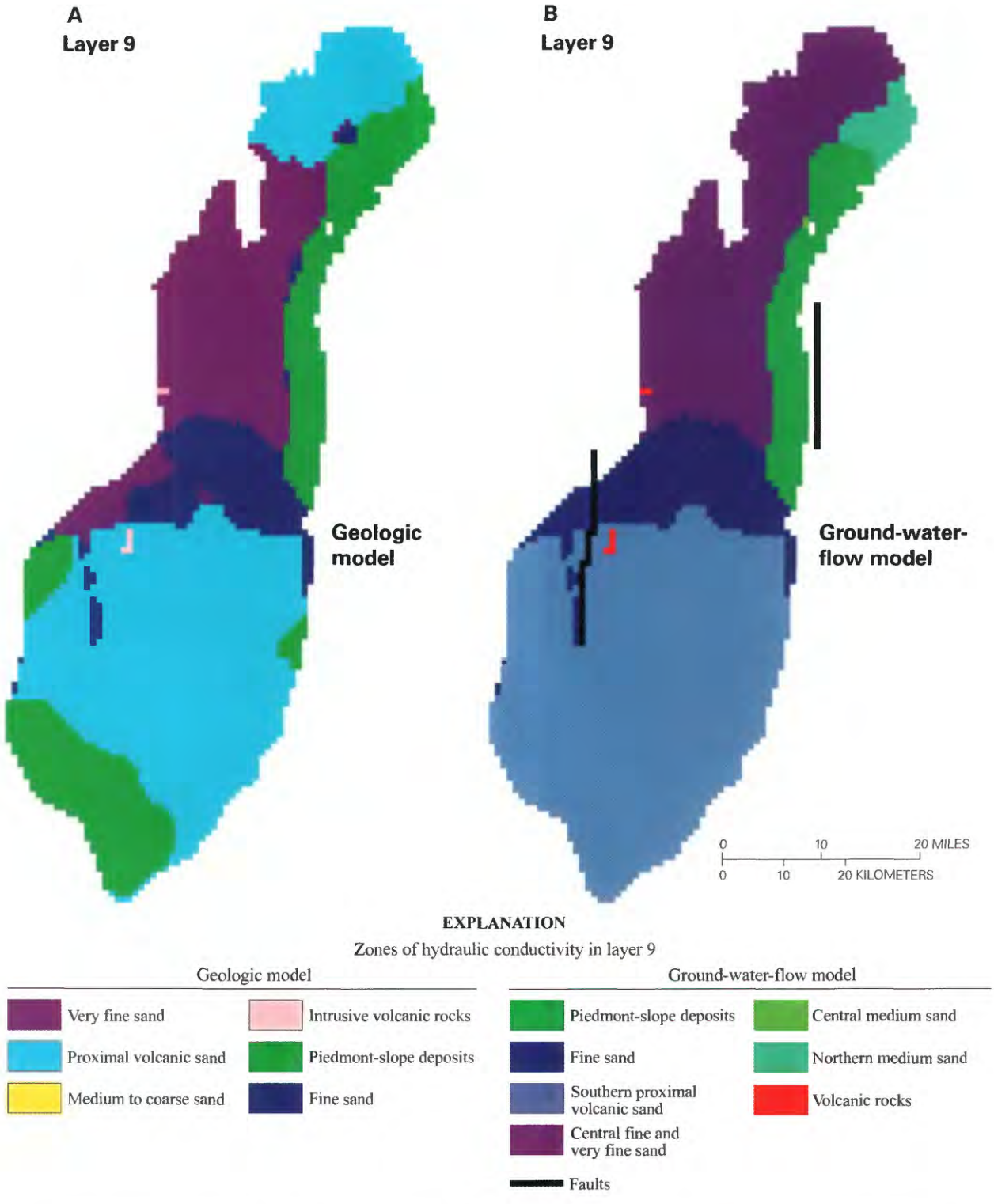

Figure 26. Hydraulic conductivity zones of layer 9 as defined in (A) the geologic model of Cole (2000b), and (B) the ground-water-flow model.

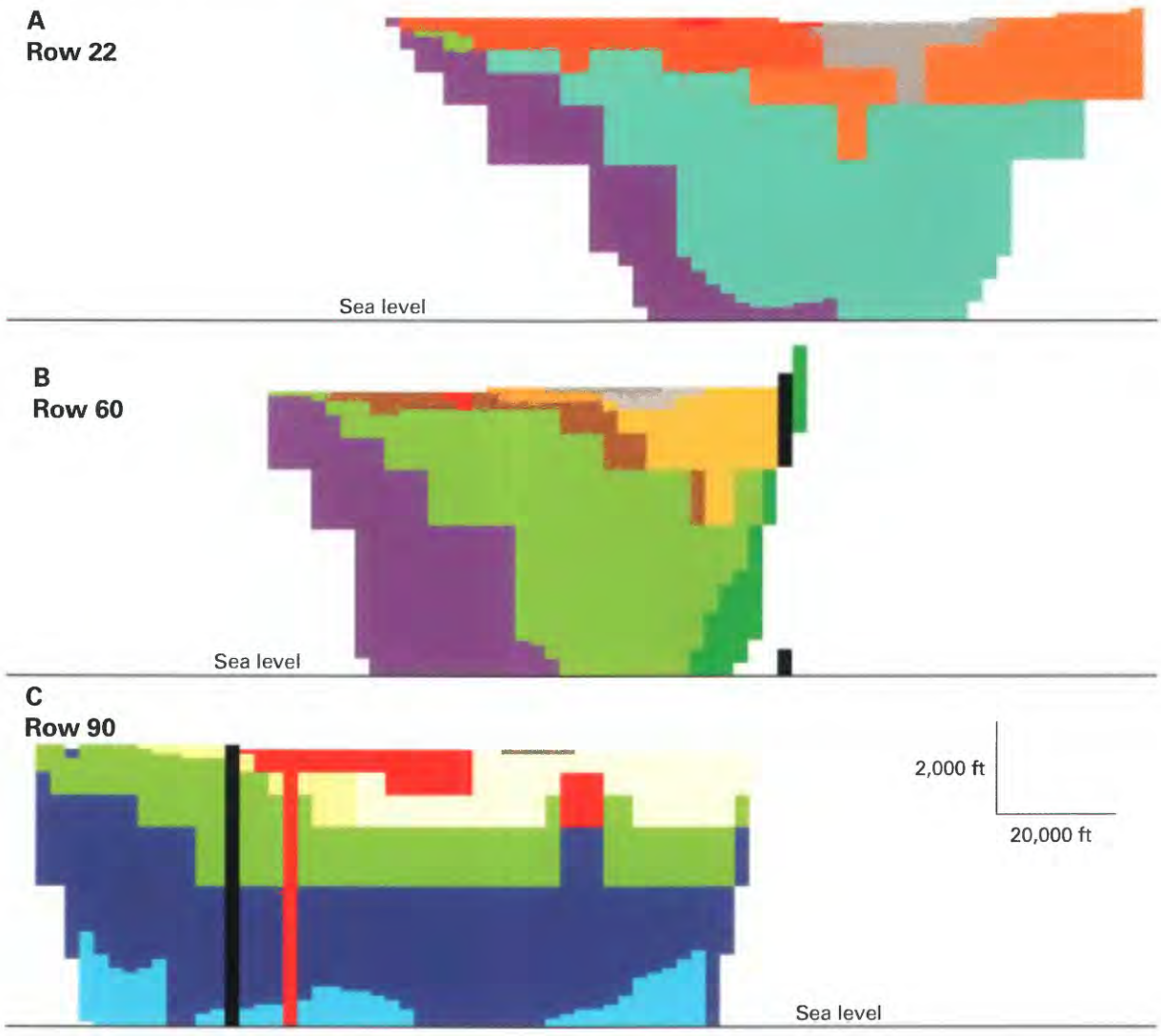

EXPLANATION

Cross-sectional zones of hydraulic conductivity zones along rows (A) 22 (B) 60, and (C) 90

Ground-water-flow model

cg Ceja gravels	Northwest medium sand
Piedmont-slope deposits	Northeast medium sand
Silts	West central medium sand
Fine sand	East central coarse sand
Northern fluvial sand and gravel	Southwest medium sand
Central fluvial sand and gravel	Southeast coarse sand
Southern fluvial sand and gravel	Central medium sand
Southern proximal volcanic sand	Northern medium sand
Central fine and very fine sand	Volcanic rocks
Faults	

Figure 27. Cross-sectional views of the hydraulic conductivity zones along rows (A) 22, (B) 60, and (C) 90 of the ground-water-flow model. See figure 18 for locations of section lines.

be used to calculate a Darcian flux, the path line tracking routine uses the seepage velocity. The seepage velocity is equal to the Darcian flux divided by the effective porosity of the porous medium. Effective porosity is therefore a necessary parameter to specify or estimate in the calibration procedure. Ground-water ages provide inherent information on the ground-water flux, and therefore also on recharge rates. They do not, however, provide independent information on the recharge rate and the effective porosity (Medina and Carrera, 1996). On the other hand, porosities for the unconsolidated sediments of the MRGB can be constrained from field measurements with a degree of certainty that is significantly greater than that for recharge rates. In addition, effective and total porosity for granular porous media have very similar values. For these reasons, the effective porosity of the model was specified, rather than estimated during the calibration procedure.

Stone and Allen (1998) report total porosity values between 30 and 40 percent from a 1,500-foot core of the Santa Fe Group. Haneberg (1995) reports porosity values derived from geophysical logs that range from about 40 percent at the land surface to about 30 percent at a depth of 1,000 feet. These values are in agreement with values that are typical for unconsolidated silt- and sand-sized material (Driscoll, 1986). In addition, it is well established that porosity values trend lower in an exponential manner with increasing depth in sedimentary rocks (Athy, 1930). Based on this information, and on compilations of porosity-depth curves for the MRGB (Haneberg, 1995) and for sandstones (Giles, 1997, p. 224), porosities were assigned by layer, beginning with 36 percent for layer 1 and decreasing by 2 percent per layer down to 20 percent for layer 9. Given that each deeper layer increases in thickness, the assigned porosities decrease in a fashion similar to an exponential decay curve.

Simulated ^{14}C Activity Calculations

There is more than one approach to using ground-water ages to calibrate a ground-water-flow model. One approach is to compare the simulated travel time with the ground-water age calculated from the ^{14}C activity. A second approach is to compare the ^{14}C activity with a simulated ^{14}C activity calculated from the simulated travel time. In this study the latter approach was used for two reasons. The first reason was based upon the degree to which the residuals (the difference between the simulated and observed values) influence the objective function in the linear regression model. For comparisons of ages, a 1,000-year difference for a 30,000-year age would carry the same influence as a 1,000-year difference for a 1,000-year age. Alternatively, for comparisons of ^{14}C activities, a 1-pmC (percent modern carbon) difference at 5 pmC would carry the same influence as a 1-pmC difference at 90 pmC. The pmC differentials better reflect the relative uncertainty between old and young ages that exists in the ^{14}C dating method than the age differentials. The weights could not be used to reflect the age-related uncertainties because the weights were used to reflect uncertainty associated with mixing in long-screened wells. The second reason was because of mixing that occurs in long-screened wells. More than one path line was often used per well, and to properly calculate one value for the well, activities need to be averaged rather than ages of the individual flow lines.

The relation between the simulated ^{14}C activity and ground-water age is based on exponential decay, and is given by the equation:

$$pmC = A_o/(\exp(time*\ln(2.)/5{,}730.)) \quad (2)$$

where pmC is the simulated ^{14}C activity; A_o is the ^{14}C activity at the recharge location; "time" is the simulated travel time from MODPATH plus, when necessary; initial age is as described below; and 5,730 is the half-life of ^{14}C, in years. Activities of ^{14}C also are affected along their flow paths by geochemical reactions. The ^{14}C activities in the study were all adjusted for geochemical reactions, and the results are described in detail by Plummer and others (2004). In addition, ^{14}C activities in the atmosphere varied over the past 24,000 years. Based on data by Stuiver and others (1998) and a calibrated curve by Kalin (2000), Plummer and others (2004) used a polynomial expression to relate calendar years to ^{14}C years. The geochemical reactions and the transient atmospheric effects were incorporated into a value of A_o assigned to each individual ^{14}C activity (eq. 2). In MODPATH one parcel of water was tracked backward for each 100 feet of observation well screen. The simulated ^{14}C age for each parcel was calculated individually and then the average age was calculated for the entire observation well. For long-screened city production wells, as many as 12 parcels were used. In this manner, a mixing effect was added to the final simulated ^{14}C age for long-screened wells.

The backward tracking in MODPATH brings the particles or path lines to the location where that water would have entered the model of the basin. In many circumstances this boundary of the basin does not coincide with a recharge location for the water where the ^{14}C activity would obtain its initial value. Underflow boundaries from bounding basins are the most common example of this, but also along the eastern mountain front, there are stretches where the water would actually have entered the subsurface many miles to the east of the model boundary (fig. 14). For these situations, an initial age has to be assigned for the water as it enters the basin. This initial age must be added to the path line age calculated by MODPATH. These initial ages were treated as parameters in the model that were estimated during the inverse procedure. Such inflow ages may vary along any one boundary, but no field data are available for comparisons, and in order for the number of estimated parameters not to become too large, a single value was estimated for each boundary.

MODEL CALIBRATION

The ground-water-flow model was calibrated using a combination of nonlinear least-squares regression method as it is implemented in the computer code UCODE (Poeter and Hill, 1998), and manual adjustment of individual parameters. UCODE is designed for inverse modeling of problems posed as parameter-estimation problems. Any application model or models can be used; the only requirement is that they have ASCII input and output files. UCODE acts as a shell that repeatedly calls the application models, automatically adjusting input parameters and extracting and comparing output values until a minimum is reached in the error between observed and simulated data. For this study MODFLOW, MODPATH, and a small number of pre- and post-processing routines were called by UCODE for each iteration.

Nonlinear Regression Method

In the regression procedure, optimal parameter values are estimated by minimizing the squared weighted differences between observed and simulated values in an objective function (Hill, 1998):

$$S(b) = \sum_{i=1}^{n} \left[w_i^{1/2} e_i \right]^2 \qquad (3)$$

where b = vector of parameters to be estimated;
n = number of measurements;
w_i = weight on difference e_i; and
e_i = residual (difference between observed and simulated value) for measurement i.

The residual e_i is equal to the difference between an observed (y_i) and simulated ($\hat{y}_i(b)$) quantity. In this study, y_i represents a measured hydraulic head, ^{14}C activity, or percentage of ground water originating from a particular source, and $\hat{y}_i$ represents the simulated equivalent of y_i. The minimization of the objective function (eq. 3) is performed by the modified Gauss-Newton method (Cooley and Naff, 1990; Hill, 1992).

The weight given to any residual reflects the relative importance of matching that particular observation, and often is related to the accuracy of the measurement. In this study w_i is generally calculated as the inverse of the estimated variance of the measurement error, following procedures suggested by Hill (1992, 1998). By using this method, highly accurate measurements, which have small variance, have relatively large weights, whereas less accurate measurements, with large variance, have relatively small weights. Furthermore, the weighted differences, $w_i e_i$, are dimensionless numbers; therefore, squared weighted differences for quantities with different units, such as hydraulic head and ^{14}C activity, can be summed in the objective function (eq. 3).

In the process of minimizing the objective function, the regression procedure computes the sensitivity of simulated head or activity i at observation location i to each model parameter b_j. These sensitivities, $\partial_i / \partial b_j$, are a measure of the change in the simulated observation resulting from a small change in the parameter value. In terms of regression, the sensitivities indicate how much information a particular observation provides toward estimating a particular parameter. The amount of information all observations provide toward estimating a single parameter can be expressed by a summary statistic, the composite scaled sensitivity (CSS). The CSS for parameter j is expressed as (Hill, 1998):

$$CSS_j = \left\{ \frac{\sum_{i=1}^{n} w_i \left(\frac{\partial \hat{y}_i}{\partial b_j} b_j \right)^2}{n} \right\}^{\frac{1}{2}} \qquad (4)$$

Because this measure is scaled by the parameter value b_j, its value for different parameters can be compared and used to choose the set of parameters to estimate in the regression procedure. Parameters with larger values of CSS are those to which the data as a whole are more sensitive and therefore more likely to be estimated by the regression. Parameters with smaller values of CSS are those to which the data as a whole are less sensitive.

In this study, six programs were called by UCODE. The code names were PREP, MODFLOW, MODPATH, ENDYEAR, POST, and GETHEADS (appendix B). The code PREP was used to create the MODFLOW input files from the parameter values of recharge, hydraulic conductivities, and underflows as they were to be assigned to different regions within the model domain. A parameter-input file, PARAMS, was created that could be modified easily by hand between calibration runs. This PARAMS file contained a list of all of the parameters that would be perturbed or modified by UCODE during the calibration procedure. During each UCODE iteration cycle, PREP would read the PARAMS file to create the MODFLOW input files. MODFLOW was run to produce simulated heads and cell-by-cell flow rates. MODPATH was run using the cell-by-cell flow rates to calculate a travel time, or ground-water age, for each 100-foot section within an observation well. MODPATH was also run to determine the recharge or source location of each particle within the hydrochemical-target regions. ENDYEAR was used to convert MODPATH output into simulated ^{14}C activities for each of the calculated MODPATH ages. POST was used to compile the individual simulated ^{14}C activities into a composite simulated ^{14}C activity for each well. POST was also used to determine the percentage of a hydrochemical-targeted region whose water originated from a local river (the Rio Grande or Rio Puerco). This technique is described further in the section on "Hydrochemical-Zone Observations."

After the UCODE run, individual parameters were adjusted further to obtain a better fit. Accuracy of the sensitivity calculations was limited by the discrete nature of the path

line calculations. Small changes in the parameters could make sudden shifts in path lines from wells to new source areas, creating an associated jump in travel time. UCODE was also used to run multiple simulations varying only one parameter at a time over a finite range of values. In this way, the discrete jumps in the global error were observed, and the minimum error and associated value for each parameter could also be determined. All of the individual parameters were examined in this way, adjusting the value of each one in order to lower the global error. The entire set of parameters was reevaluated consecutively in this fashion three times, after which the global error no longer decreased by an appreciable amount.

Calibration Data Sets

Multiple types of data were used in this study to calibrate the ground-water-flow model. Hydraulic heads, ^{14}C activities, and the locations of the hydrochemical zones were all used as observations in the objective function (eq. 3). These values were all given weights in accordance with their perceived or estimated accuracy. A total of 200 hydraulic heads, 200 ^{14}C activities, and the locations of two of the river-water hydrochemical zones within nine hydrochemical-target regions were used as observations, making a total of 409 observations.

Water-Level Observations

The ground-water-flow model was designed to simulate steady-state ground-water flow prior to the development of ground water as a resource within the basin. To calibrate the model, hydraulic-head data were needed that did not show the influence of any appreciable ground-water withdrawals that have occurred within the basin over the last half century. The data were compiled from many sources; these various sources are described by Bexfield and Anderholm (2000), and much of the data are presented in their map of the predevelopment water table. The sources of the data include domestic wells, windmills, pueblo wells, and monitoring wells. Data from wells within the vicinity of the city of Albuquerque were used only if they were measured before 1960. Those that were measured during the 1950s were chosen carefully to exclude wells cited close to visible cones of depression. Wells far from the city were assumed to have water levels that contained negligible effects from anthropogenic stresses. Only water levels from the time of well installation were used at producing wells.

Two hundred hydraulic-head values were used in total (table A1; fig. 28). The screen depths from the wells were used to determine the layer in which the well would be located in the ground-water-flow model. Well locations typically do not fall exactly on cell-center coordinates, so to obtain the equivalent simulated value, hydraulic heads were calculated using heads from several cells. A trilinear interpolation scheme was used that interpolated the head value between the cells of the nearest two rows, columns, and layers. A separate FORTRAN code was written called GETHEADS (appendix B) that read all of the heads from the MODFLOW output file and then performed the interpolation calculations to obtain the 200 simulated hydraulic-head observations. These simulated observations were then written to another output file with the prefix "heads." This heads file was the file from which UCODE extracted the simulated observations. The expected measurement errors for the hydraulic heads in the data set were estimated as expected standard deviations, and were assigned values between 1 foot for recent surveyed monitoring wells, to 10 feet or more for domestic wells where the measuring-point altitude was estimated from a topographic map. These estimated measurement errors were used to assign weights to the head observations.

^{14}C-Activity Observations

The activity of ^{14}C was measured in samples taken from over 200 wells and river locations throughout the basin. Locations of the 200 well-sample sites used for observations are shown in figure 29, and the ^{14}C activities and the associated ages are given in table A2 (p. 82–87). These sites include areas of active pumping because the withdrawals only remove water within close proximity of the wells, and ages will still reflect patterns of regional ground-water movement. Estimates of the geochemical reactions that occurred within the basin to alter the ^{14}C activities were made by Plummer and others (2004), who compiled a list of values for A_o that account for these reactions and long-term atmospheric variations. These A_o values, listed in table A2, were used to calculate the simulated ^{14}C activities from the simulated travel times (eq. 2). In addition to the activities and ages, information is given in table A2 on the cell location with the flow model, the number of MODPATH flow lines tracked from each well, and the uncertainty assigned to each age estimate. For each ^{14}C-age observation, a simulated age observation was determined using the backward-tracking option in MODPATH. Because wells can produce mixtures of waters that have traveled along different flow paths, multiple flow paths were simulated for long-screened wells.

Observations should be weighted based on the relative uncertainty associated with each measurement (Hill, 1998). Plummer and others (2004) made estimates of uncertainties in the ^{14}C activities measured at the wells (table A2). Additional uncertainty is related to how the influx of water to a well varies vertically within the well screen. This variation in vertical influx makes the full uncertainty difficult to evaluate on a well-by-well basis, and thus a simple scheme was adopted where an uncertainty of 1 or 5 pmC was assigned to short- and long-screened wells, respectively. These uncertainty values, rather than those from Plummer and others (2004), were assigned to the observations in the UCODE files, and each ^{14}C observation was weighted based upon these values. The uncertainties in the ^{14}C activities (table A2) are expressed in terms of the standard deviation for the activity. The weights for each of these observations are a function of the inverse of the standard deviation. Thus the short-screened wells with a

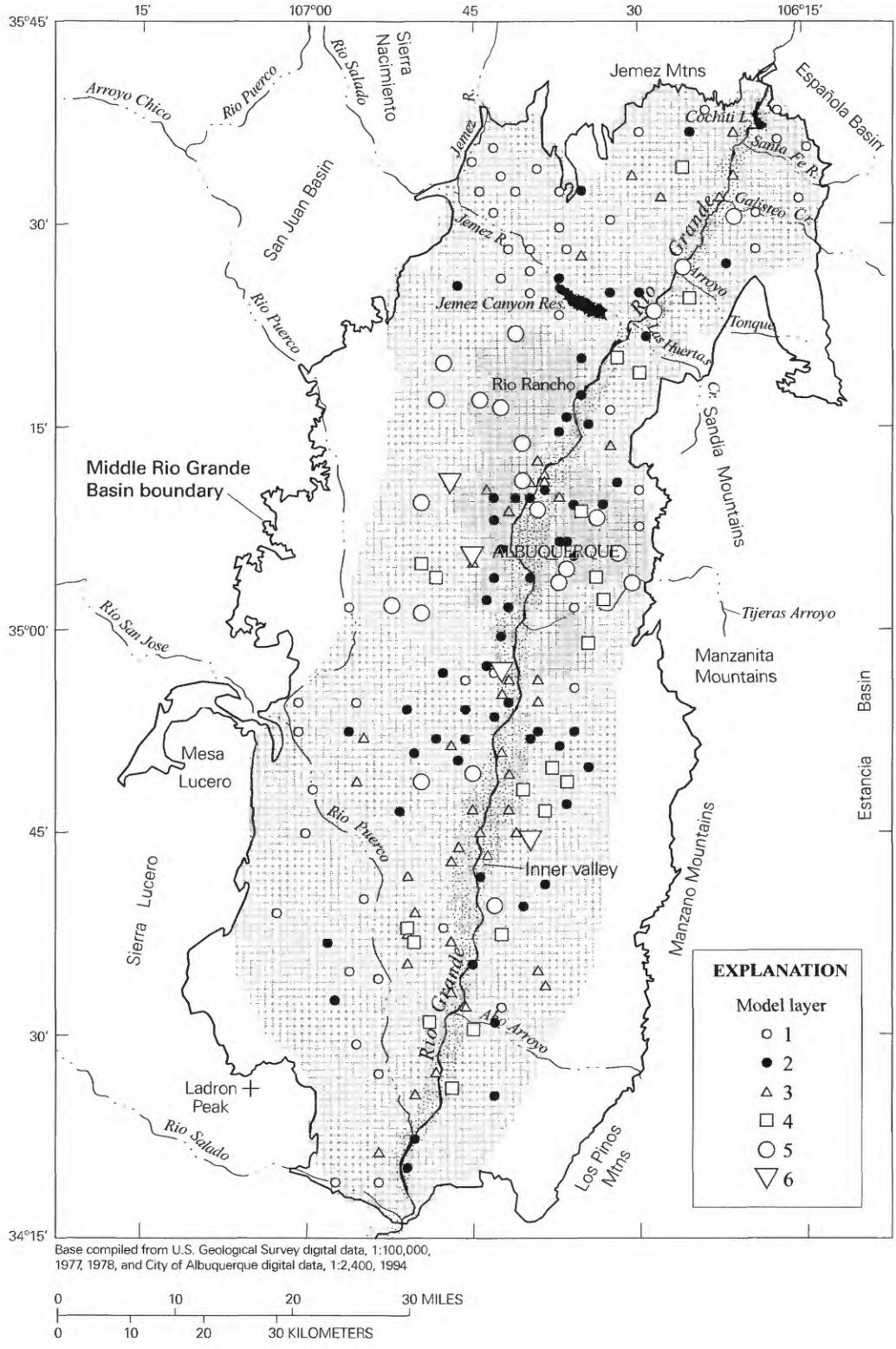

Figure 28. Location of hydraulic-head observations used to calibrate the predevelopment ground-water-flow model.

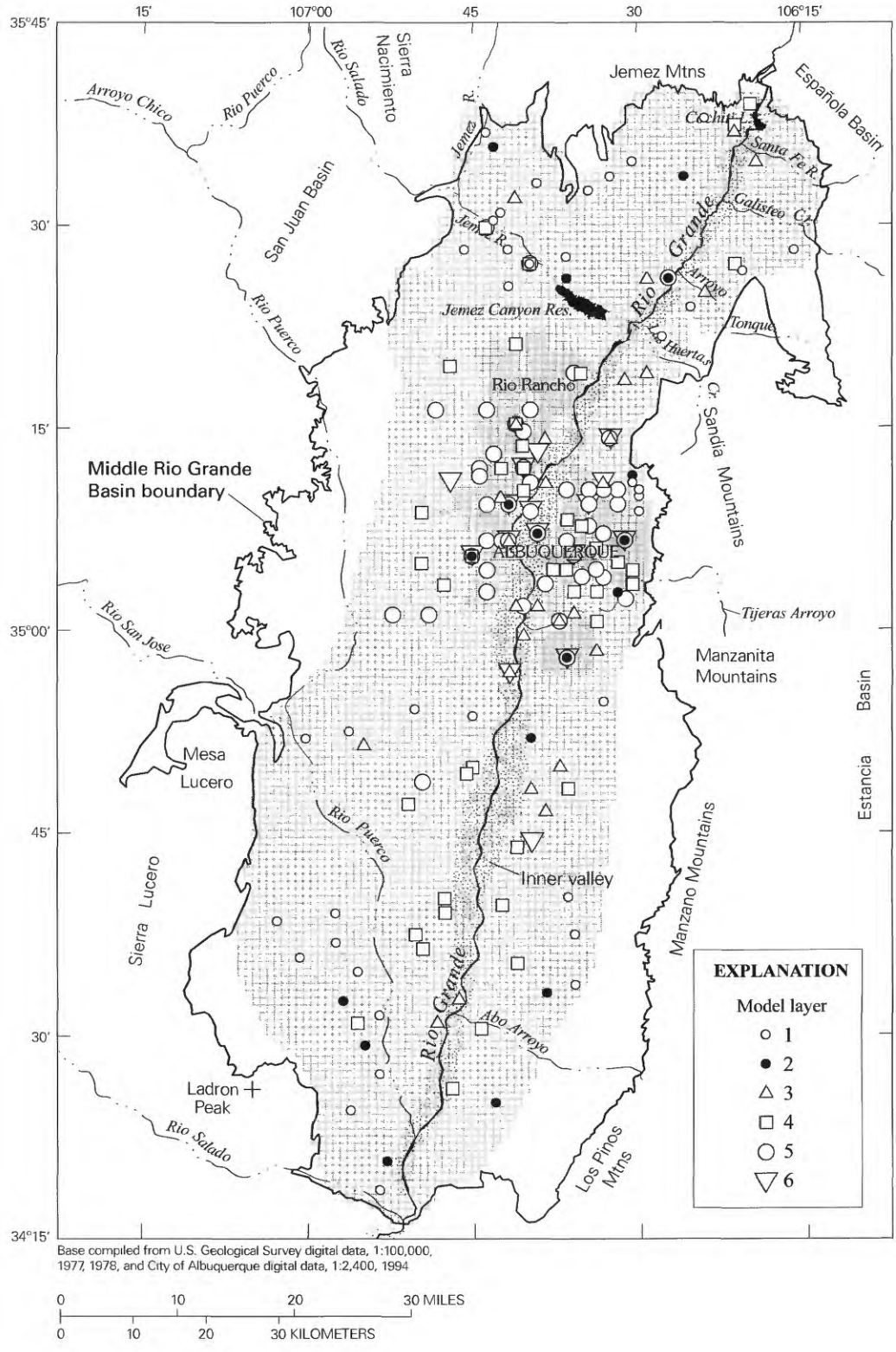

Figure 29. Location of carbon-14 samples used to calibrate the predevelopment ground-water-flow model.

standard deviation of 1 pmC are weighted five times more than the long-screened wells with a standard deviation of 5 pmC.

Hydrochemical-Zone Observations

In addition to water levels and ^{14}C activities, the location and extent of selected hydrochemical zones were used as observations. Earlier pilot simulations (Sanford and others, 1998) indicated that the volume of Rio Grande and Rio Puerco water in the basin aquifer system would depend upon the recharge and hydraulic conductivity parameters of the model. The less the recharge along the margins of the basin, or the higher the hydraulic conductivity of the aquifer, the broader is the areal extent of the recharged river water that is adjacent to the river. In the case of the Rio Puerco and the Jemez River, the extent of river water in the basin is also very sensitive to the vertical hydraulic conductance of the riverbed. Zones of river water can be observed based on their geochemical signature. The hydrochemical zones described by Plummer and others (2004) and in table 1 include zones described as Rio Grande water (zone 12), and Rio Puerco water (zone 5). Jemez River water was not considered as a separate zone because it was found only in a few wells very near the river. The boundaries between the river-water zones and the other hydrochemical zones in the basin are shown in figure 9. The positions of such boundaries are known (from the earlier pilot studies) to be a function of recharge, hydraulic conductivity, and riverbed conductance, and the simulated positions of the boundaries could, therefore, also be used as observations in the model calibration using UCODE.

The nonlinear regression routine requires that simulated observations be continuous functions of the parameter values, because small perturbations of the parameter values must register as a finite change in the simulated observations. The hydrochemical zones, however, represent discrete regions where water simulated to migrate to a certain point in the aquifer system either did, or did not, originate from a source location with a recognizable geochemical signature. A method was needed whereby path lines simulated using MODPATH would register the source location of the water in such a way as to make a continuous or near-continuous function. To accomplish this, nine rectangular hydrochemical "target regions" were created that partially encompassed river-water zones defined by the geochemistry (fig. 30). These hydrochemical-target regions were used as observations, bringing the total number of observations for the regression analysis to 409. The observation value was the percentage of river water observed to be in any target region based on the hydrochemical zones. To simulate this, a fine array of particles covering evenly each target region was tracked backward to their sources (table 2) using MODPATH. The number of paths that tracked to river cells was then divided by the total number of paths for that target region. The very large number of particles allowed this simulated percentage to vary by finite and significant amounts when each parameter was perturbed by only a few percent. Therefore, although the responses of the simulated observations are not continuous at an infinitesimally small parameter perturbation, they are continuous at the size of perturbations used in these simulations, and thus allow for the use of the nonlinear regression methods.

Sensitivities

The composite scaled sensitivities were calculated for each of the parameters from the MODFLOW and MODPATH model simulations (fig. 31 and 32). Based partially on the magnitude of the sensitivity and partially on the availability of prior information, some parameters were assigned values and others were estimated using the nonlinear regression. The parameters with the highest sensitivity were the hydraulic conductivities in the northeastern, central, and southern basin (hcsfne, hcsfsw, hcsfse, hcsfce, hcalal, hcsfcw, and hclsfs), the anisotropy of the Rio Grande alluvium near Albuquerque (analal), recharge values for the southern Sandia Mountain front (snsandias, sssandias), and underflow from the northern

Table 2. Information on geochemical-target regions (fig. 30) defined for use in calibration against the geochemical zones.

Region number	Region name	Layer number	Ending row number	Beginning row number	Beginning column number	Ending column number	Total number of path lines in region	Approximate number of path lines with river origin	Fraction of region containing river water
1	Rio Grande Northwest	2	47	76	26	45	5,400	2,160	0.40
2	Rio Grande Northeast	2	47	76	46	55	2,583	1,350	0.52
3	Rio Grande Southwest	2	77	106	26	40	4,050	1,890	0.47
4	Rio Grande Southeast	2	77	106	41	50	2,634	900	0.34
5	Rio Grande South	2	107	136	26	40	3,843	500	0.13
6	Rio Puerco North	2	72	96	1	25	4,725	1,800	0.38
7	Rio Puerco West	2	97	121	1	15	3,096	540	0.17
8	Rio Puerco East	2	97	121	16	25	2,250	1,800	0.80
9	Rio Puerco South	2	122	146	11	25	3,330	1,440	0.43

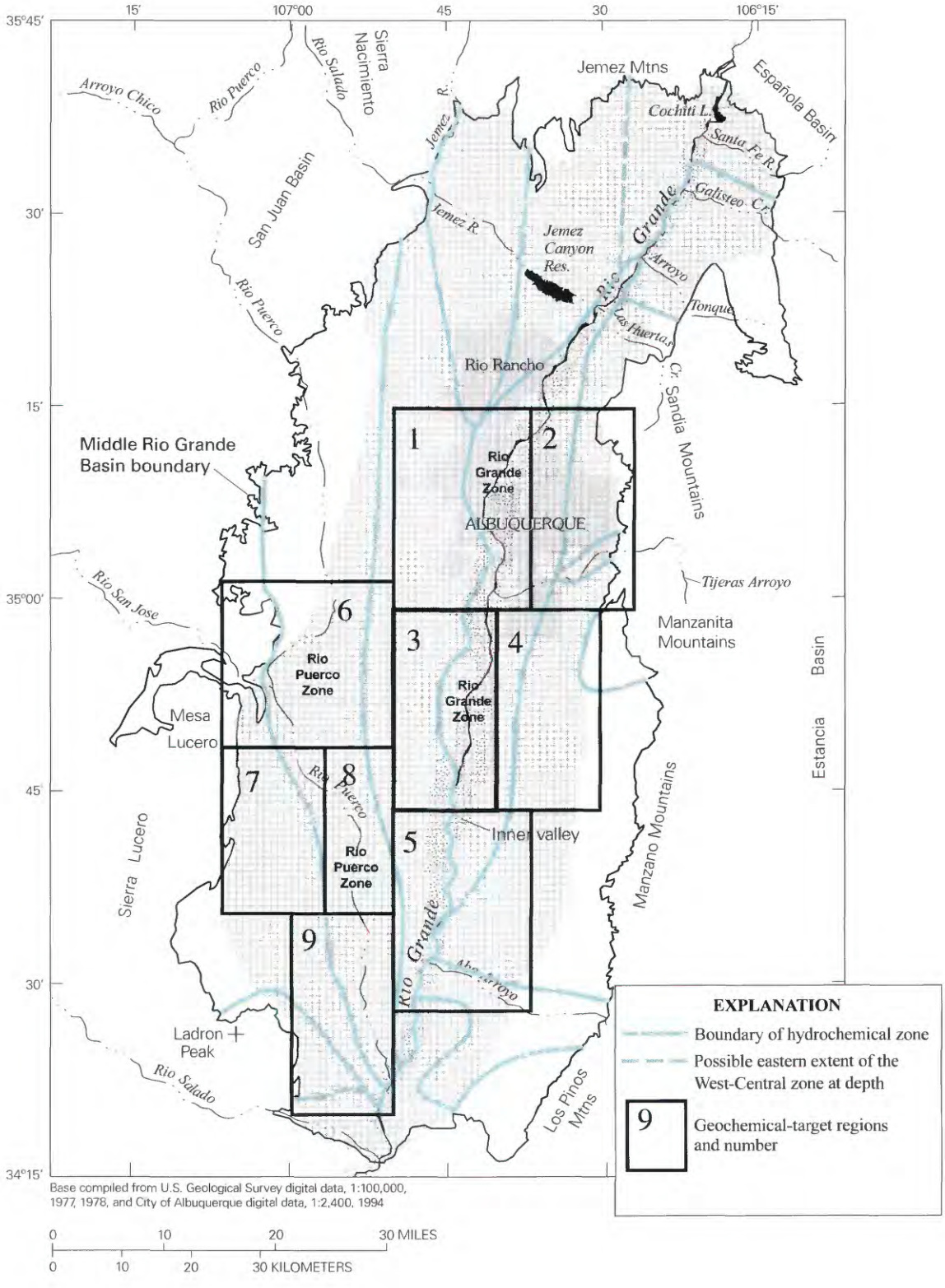

Figure 30. Location of geochemical-target regions used to calibrate the ground-water flow model.

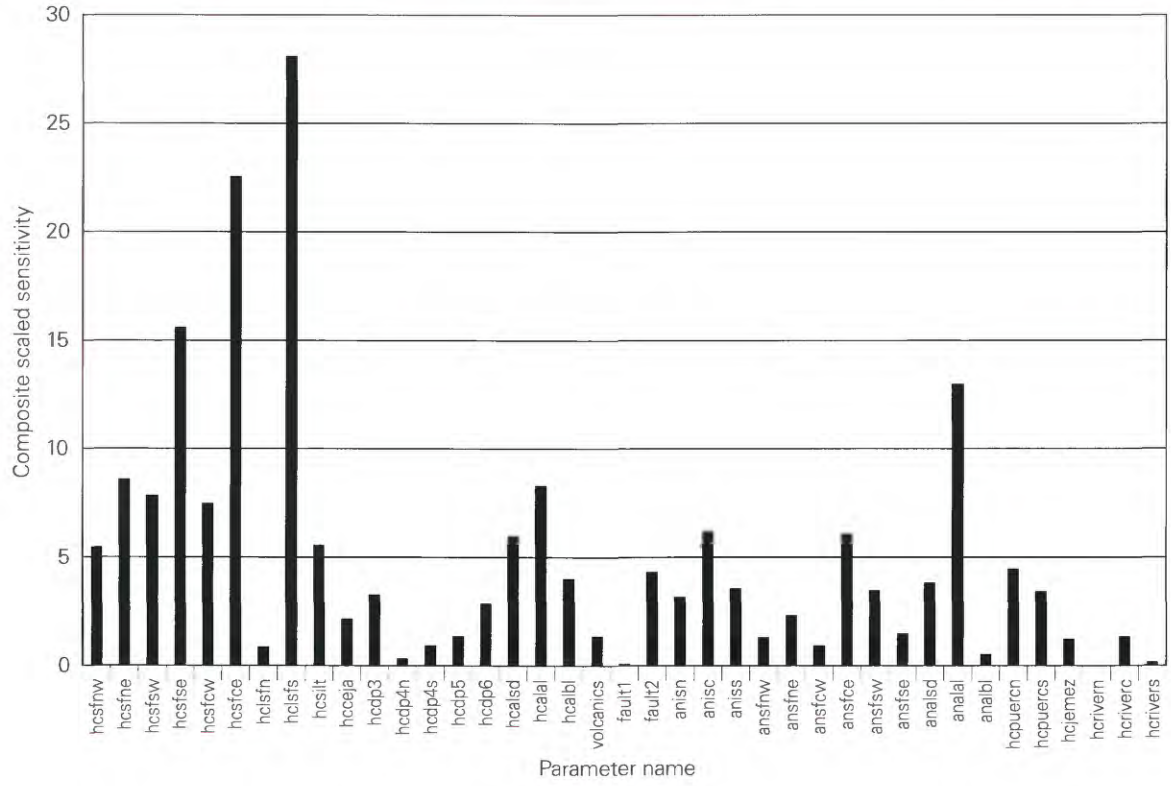

Figure 31. Composite-scaled sensitivities for parameters of hydraulic conductivity, anisotropy, and riverbed conductance at the optimized or specified values (see table 3 for parameter descriptions, locations, and values).

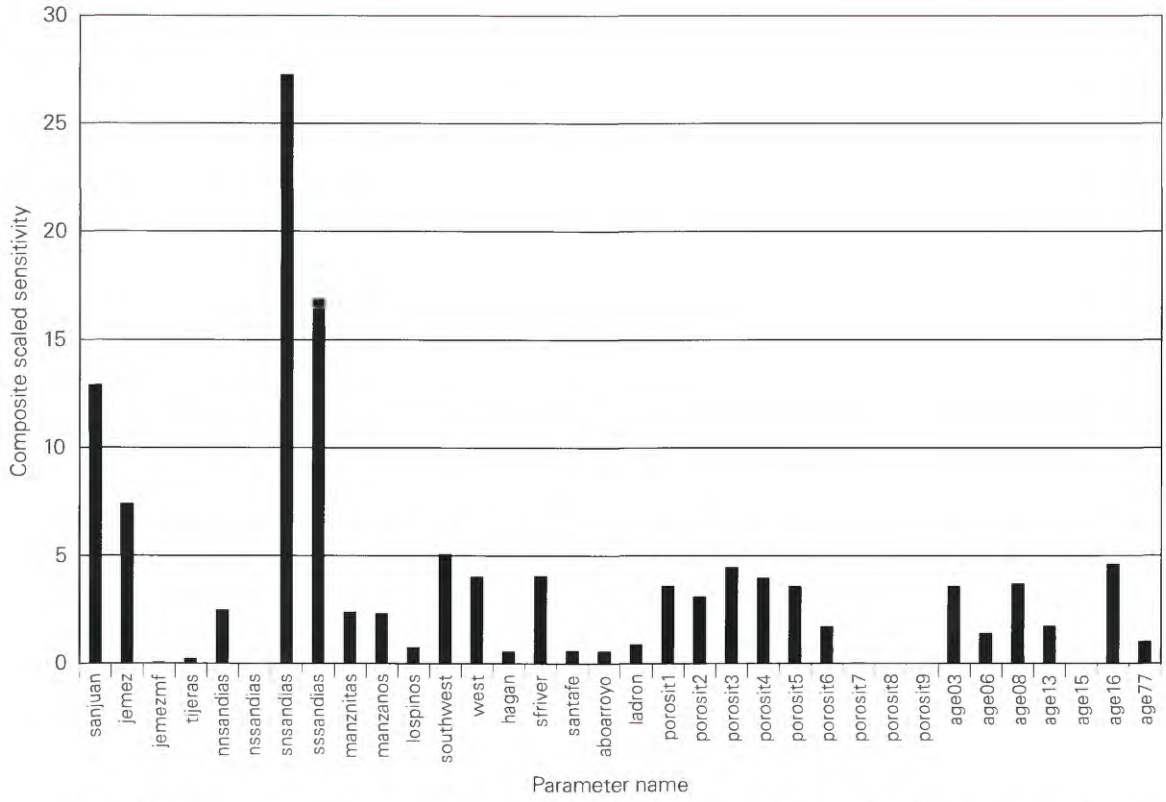

Figure 32. Composite-scaled sensitivities for parameters of recharge, porosity, and initial underflow age at the optimized or specified values (see table 3 for parameter descriptions, locations, and values).

(jemez) and northwestern (sanjuan) boundaries. More detailed descriptions of the parameters are provided in table 3. The composite scaled sensitivity values shown in figures 31 and 32 were calculated based on the best-fit parameter values for the simulations. Based on low sensitivity values, values were assigned to the vertical leakance of the northern (hcrivern) and southern (hcrivers) sections of the Rio Grande (1,000,000 feet per day), and to the hydraulic conductivity of the Cat Mesa Fault Zone (fault1) (0.000001 feet per day). Beyond the fact that the model indicated that the values of hcrivern and hcrivers should be very high, and the value of fault1 very low, the observation data did not provide enough information to the model for these values to be estimated with any certainty. Porosity values were assigned because reasonable estimates could be made from field data.

MODEL RESULTS

Simulations of ground-water levels and path line tracks were completed in two stages. The goal for these stages was to obtain a set of parameters for the flow model that would yield a best fit with the observed data. The nonlinear regression methods in UCODE improved the fit of the model considerably relative to fit based on the initial guesses. After a point of convergence was reached, individual parameters were adjusted further manually to obtain a better fit. The results presented here are from the simulation with the final best fit of parameter values to the data.

Hydraulic Heads

The hydraulic heads from the final simulation are shown for layers 2 and 6 in figures 33 and 34. Values of heads at individual wells are given in table A3 (pages 88–92). One of the features in the water levels that has been an enigma for years is the presence of a lower region in the potentiometric surface in the west-central section of the basin (see the observed predevelopment water table map, fig. 4) often referred to as the "trough." The current model configuration reproduces this feature, although not as far north as the some of the observed water levels indicate. The observed trough is still much deeper north of Albuquerque than this model shows. This region is one of sparse field data, and hydrogeologic conditions likely exist there that have not been included in any of the models. The current model also shows just a hint of the trough in the deeper section (layer 6) in the region of Rio Rancho. The geochemical zones are partly consistent with the presence of a trough. This partial consistency is discussed later in the "Hydrochemical Zones" section.

Earlier prototype models by Sanford and others (1998) demonstrated that by lowering basin underflow or mountain-front recharge in the model, the system changed from one dominated by the movement of water from the basin boundaries toward the Rio Grande to one dominated by water leaking from and back into the Rio Grande. This conceptual system of low recharge would create heads to the west of the Rio Grande that are lower than the river, such as are present in the trough. Low recharge is also a condition consistent with results of this study (reported in a later section). McAda and Barroll (2002) included in their model some lower values of recharge, some additional north-south-trending faults, and zones of increased north-south hydraulic conductivity in the region of the trough, but the trough is not readily apparent in the hydraulic head map for their predevelopment simulation.

Another main feature visible from the hydraulic head maps is the barrier specified at the Cat Mesa Fault Zone in the southwestern quadrant of the model. Water levels in wells a short distance from each other across this fault zone differ by more than 100 feet, suggesting the fault zone acts as a barrier to flow. The zone was simulated with a very low permeability. Early attempts to estimate the permeability of the zone with nonlinear regression were unsuccessful. The model continued to suggest the permeability value to be lower, and the sensitivity of the data to the low value also continued to decrease. The West Sandia Fault Zone, on the east side of the city of Albuquerque, also acts as a detectable barrier to flow. Water levels change abruptly by more than 200 feet across the fault zone. This feature can be reproduced readily in the model by an adjustment to the hydraulic conductivity of the fault zone and the recharge along that section of the mountain front. Both the hydraulic conductivity and recharge can be adjusted independently by the inverse model because ground-water ages there give additional data that are independent of water levels.

The model in this study reproduces the losing section of the Rio Grande just north of Albuquerque (fig. 35). From the contours one can see that water from the Rio Grande moves out of the Inner valley not only to the west toward the trough, but also to the south beneath the city of Albuquerque, as is also shown in the predevelopment water-table map (fig. 4). The zone of Rio Grande water beneath the city is also corroborated by the geochemical data (fig. 9). The earlier version of the model did not reproduce this feature (Kernodle and others 1995, p. 41)—the difference being that the high eastern mountain-front recharge values in the older model overwhelmed any tendency for water to move from the Inner valley into the regional aquifer system. Tiedeman and others (1998) also used high recharge values and showed water beneath the city moving toward the Inner valley. McAda and Barroll (2002) used lower eastern mountain-front recharge values, and their results indicate flow parallel to the river.

^{14}C Activities

Ground-water travel times and activities of ^{14}C at wells were simulated using MODPATH and results from MODFLOW. Results for individual wells are given in table A3. Although ^{14}C activities were used as the simulated observations, the distribution of simulated ages is shown for layers 2 and 6 in figure 36, because such ages can often more intuitively reveal model behavior. The model ages are converted to simulated ^{14}C activities using equation 2. The simulated ages

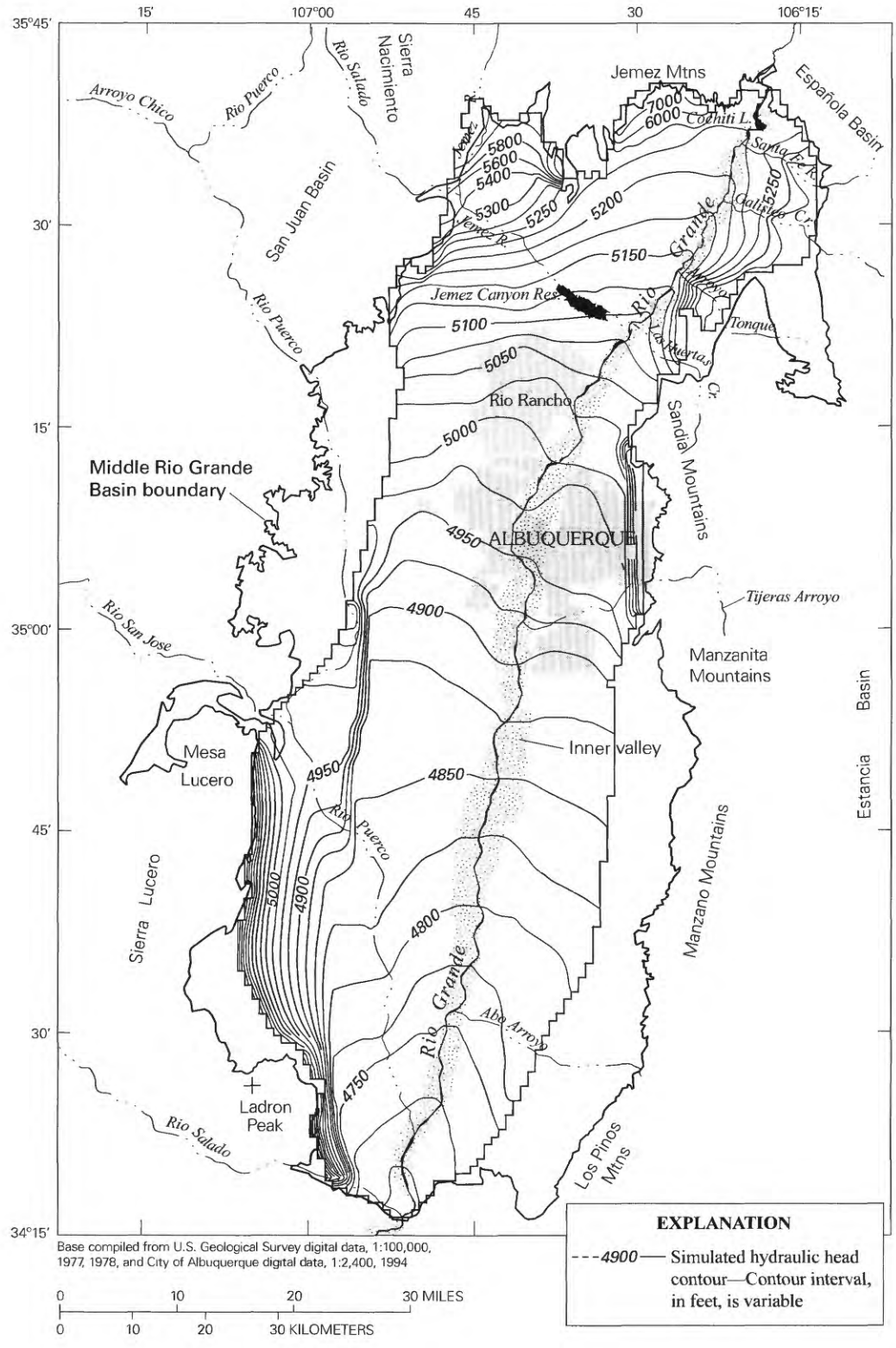

Figure 33. Simulated water levels in layer 2 of the steady-state ground-water-flow model.

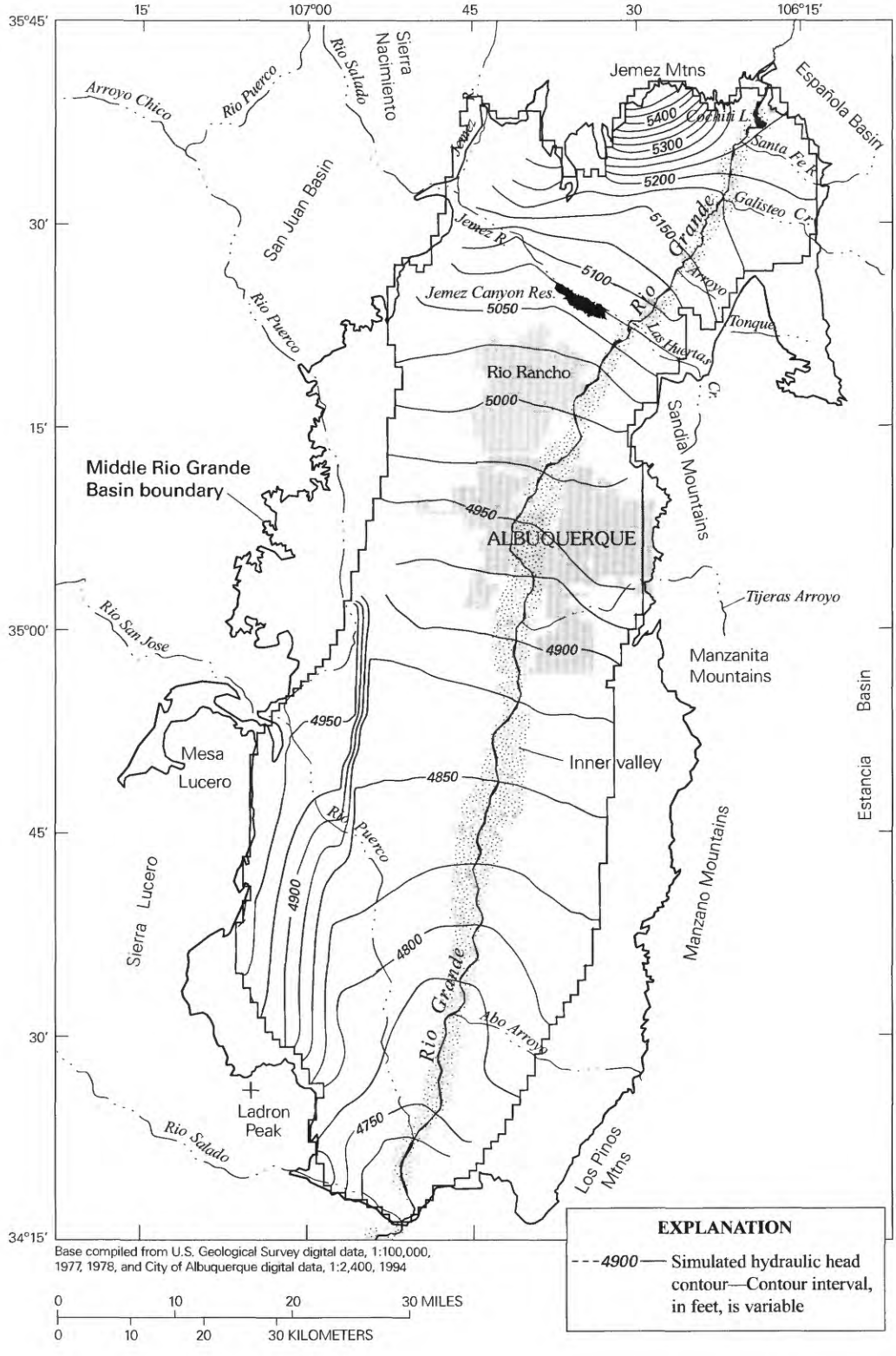

Figure 34. Simulated water levels in layer 6 of the steady-state ground-water-flow model.

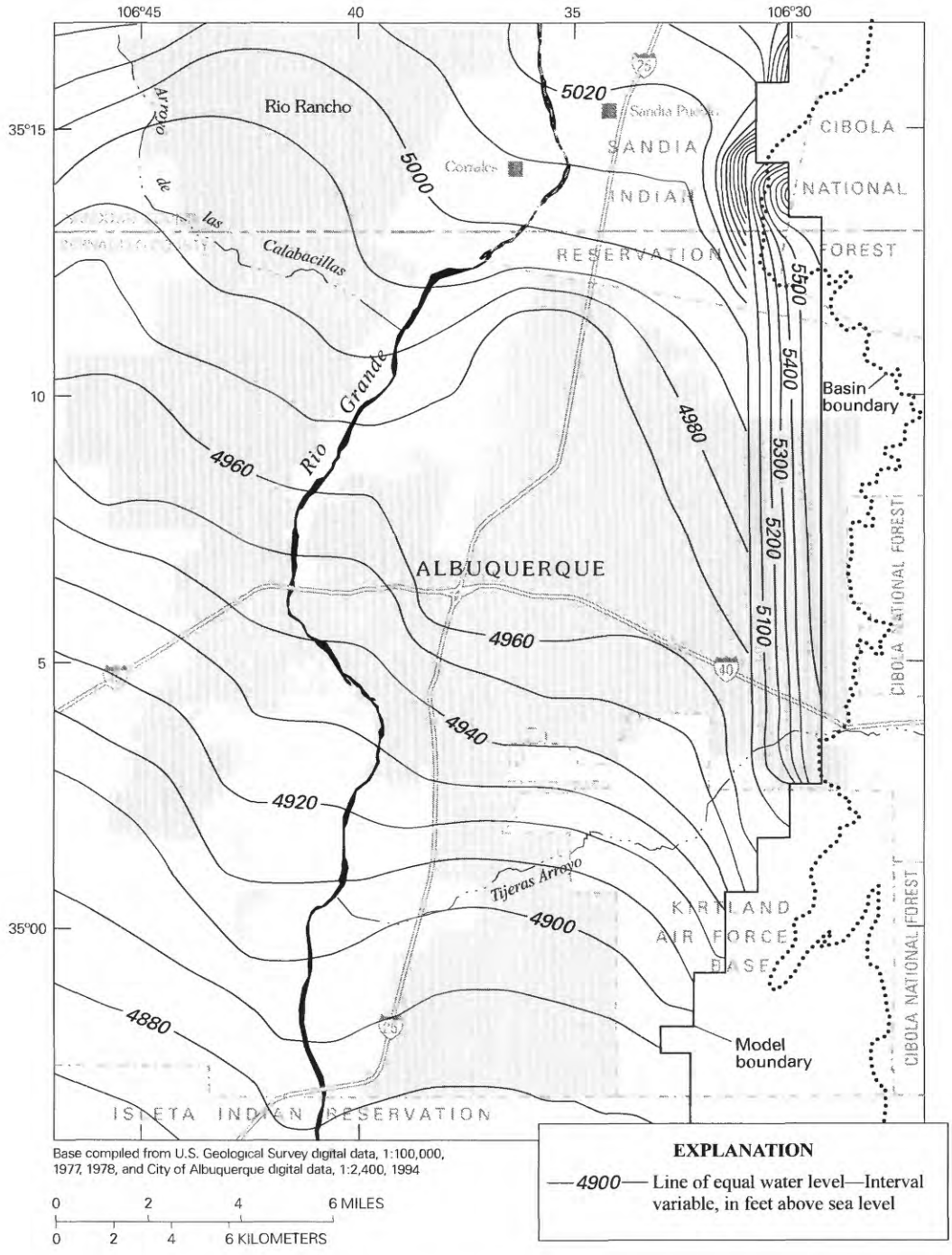

Figure 35. Simulated predevelpment water levels, in feet above sea level, in the vicinity of Albuquerque in layer 2 of the ground-water-flow model.

were plotted by placing a 10 by 10 grid of particles in every model cell and tracking the path lines backward to the source location. For path lines that reached underflow boundaries, the basin-entrance ages (table 3) were added to the MODPATH travel times. The ages for the entire grid of particles was then plotted to produce the images in figure 36. Several patterns emerge. Young water (less than 3,000 years) represented by the dark blue areas is present near the mountain fronts where recharge occurs at the land surface, and along the Rio Grande and Rio Puerco near where the rivers are losing water to the aquifer system. This general pattern mimics the pattern of ages observed in the basin (fig. 8). Older water represented by the yellow and red areas is present in the southern part of the basin and in areas next to basin boundaries where water is entering the basin as underflow. Very old water is also shown in the explicitly represented Cat Mesa Fault Zone because the flux inside that zone is so low that particles being tracked out require very long times.

A cross section of the simulated ages along row 75 is shown in figure 37. Although there is a general pattern of increasing simulated age with depth, the heterogeneity of the system in a few places creates local inversions where old water is predicted to occur above younger water that is moving through a more permeable zone. It should be noted that these ages are simulated using values of recharge that do not vary in time. Because some of the ages exceed 100,000 years, it is important to recognize that any variations in recharge over that time scale would give different age distributions for the aquifer system. The problem of time-varying recharge is addressed in the transient paleohydrologic simulation.

Hydrochemical Zones

The hydrochemical zones as identified by geochemical signatures (fig. 9) were also simulated using MODPATH and results from MODFLOW. The recharge regions were first divided into sections that roughly coincided with the areas identified as recharge sources by the geochemical signatures (table 1). MODPATH was then run in the same manner as for the creation of the age maps except that the source locations were plotted according to the starting locations of the particles. Results of the hydrochemical target-region observations are given at the end of table A3. A more complete map of source-delineation results is shown for layers 2 and 6 in figure 38. The final estimated model parameters reproduce all of the major zones identified in the geochemical survey. The red area in the center of figure 38 represents water that was recharge from the Rio Grande. This simulated zone is similar in total area to that of observed zone 12 (fig. 9), although the simulated zone extends farther into the center of the basin than the observed zone. One likely explanation is the steady-state assumption that recharge rates have been constant for more than 100,000 years. Water in the Rio Grande zone is about 10,000 years old at its western edge (figs. 8 and 9), suggesting this zone began forming after the climate change following the last glacial maximum. The fact that the western edge of the zone roughly parallels hydraulic-head contours within the city limits (figs. 4 and 9) also suggests this zone boundary may not have reached its potential farthest western extent from the Rio Grande. It is also possible that north-south-trending faults are partially blocking the movement of Rio Grande water farther west into the trough.

The earlier ground-water model of Kernodle and others (1995) did not predict the presence of any Rio Grande water in the aquifer system beyond the shallow system in the Inner valley under predevelopment conditions. This conclusion is not based on their model budget, which only records water leaving the Rio Grande itself, but on visual inspection of the simulated hydraulic heads (Kernodle and others, 1995, figs. 20 and 21). Tiedeman and others (1998) simulated several different hydrogeologic configurations to try to understand the origin of the trough and according to their model budgets, two of those configurations result in Rio Grande water leaving the Inner valley under predevelopment conditions. McAda and Barroll (2002) presented only one hydrogeologic configuration, but whether their model simulates Rio Grande water leaving the Inner valley is inconclusive based on their model budget or simulated predevelopment hydraulic-head map (their fig. 14). Source-area delineation mapping was not performed in any of the earlier modeling studies to show conclusively where Rio Grande water might have left the Inner valley.

The region of ground water that was simulated to come from the Rio Puerco also agrees with the geochemical survey, and the use of this area as an observation was important in the calibration of the amount of recharge estimated from the Rio Puerco. A cross section through row 75 of the simulated hydrochemical zones is shown in figure 37. The east and west basin boundary waters tend to remain along those boundaries, but the Rio Grande water penetrates down to about 1 kilometer, and the northern underflow waters occupy the central, deeper section of the basin.

Best-Fit Parameter Estimates

The combination of automated nonlinear regression runs and manual parameter adjustments led to the final parameter list in table 3. The best-fit values are listed there along with the assigned values for those parameters that were not estimated. After automatic convergence was attained, each estimated parameter value was varied individually to identify the point of minimum global error. An entire sweep of the parameters in this manner was, in effect, one manual iteration. Not all parameters required adjustment during a manual iteration to attain the minimum error. Three manual iterations were performed in all, resulting in a lowering of the minimum global error by about 20 percent. The estimated parameter values and their linear 95 percent confidence intervals are shown in figures 39–41. These confidence intervals should be considered as rough indicators of the confidence in the parameter estimates because in addition to the nonlinearity of the model, there is model error associated with the locations of the boundaries and zones that are not taken into account in the confi-

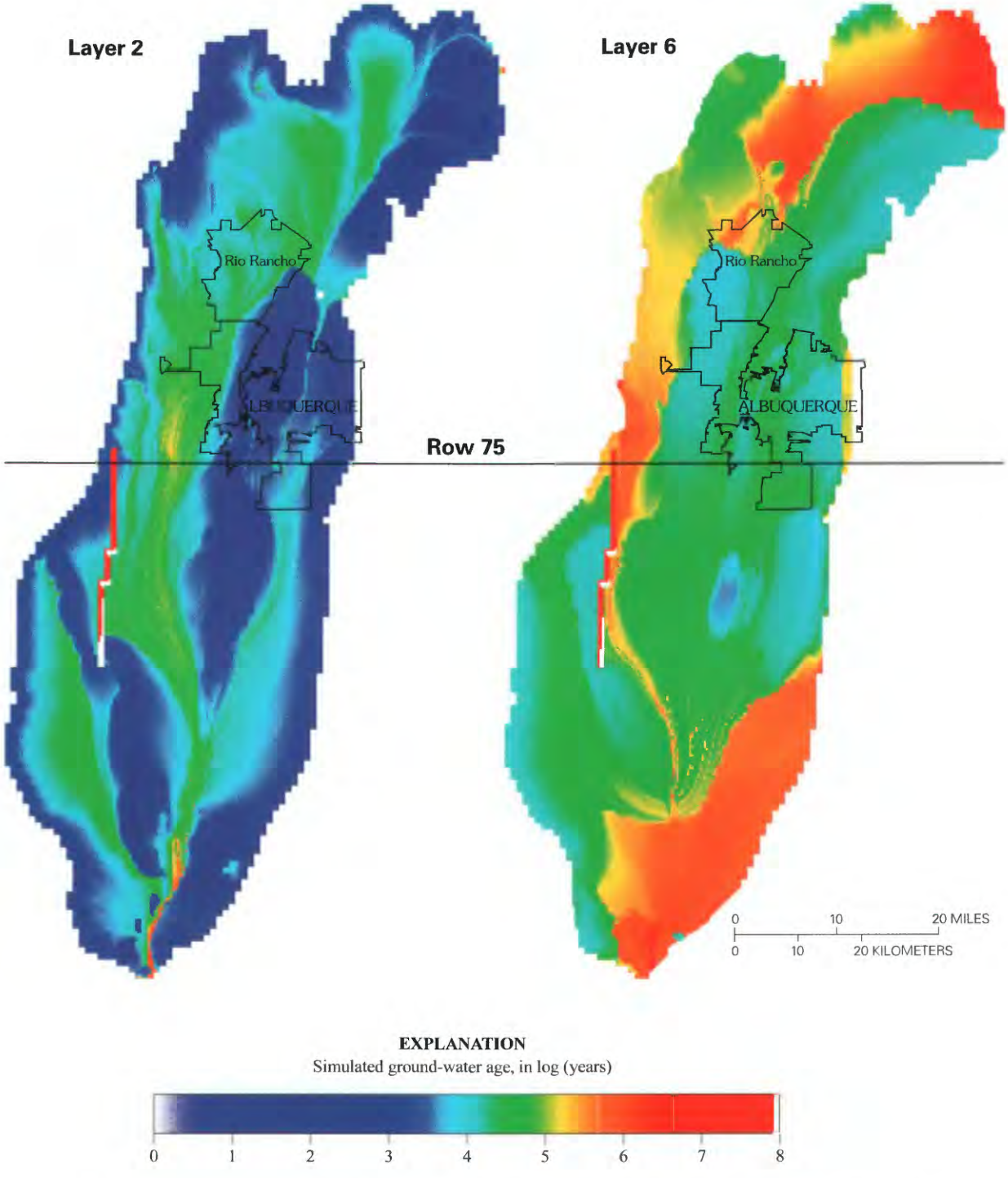

Figure 36. Simulated ground-water ages in layers 2 and 6 of the steady-state ground-water-flow model.

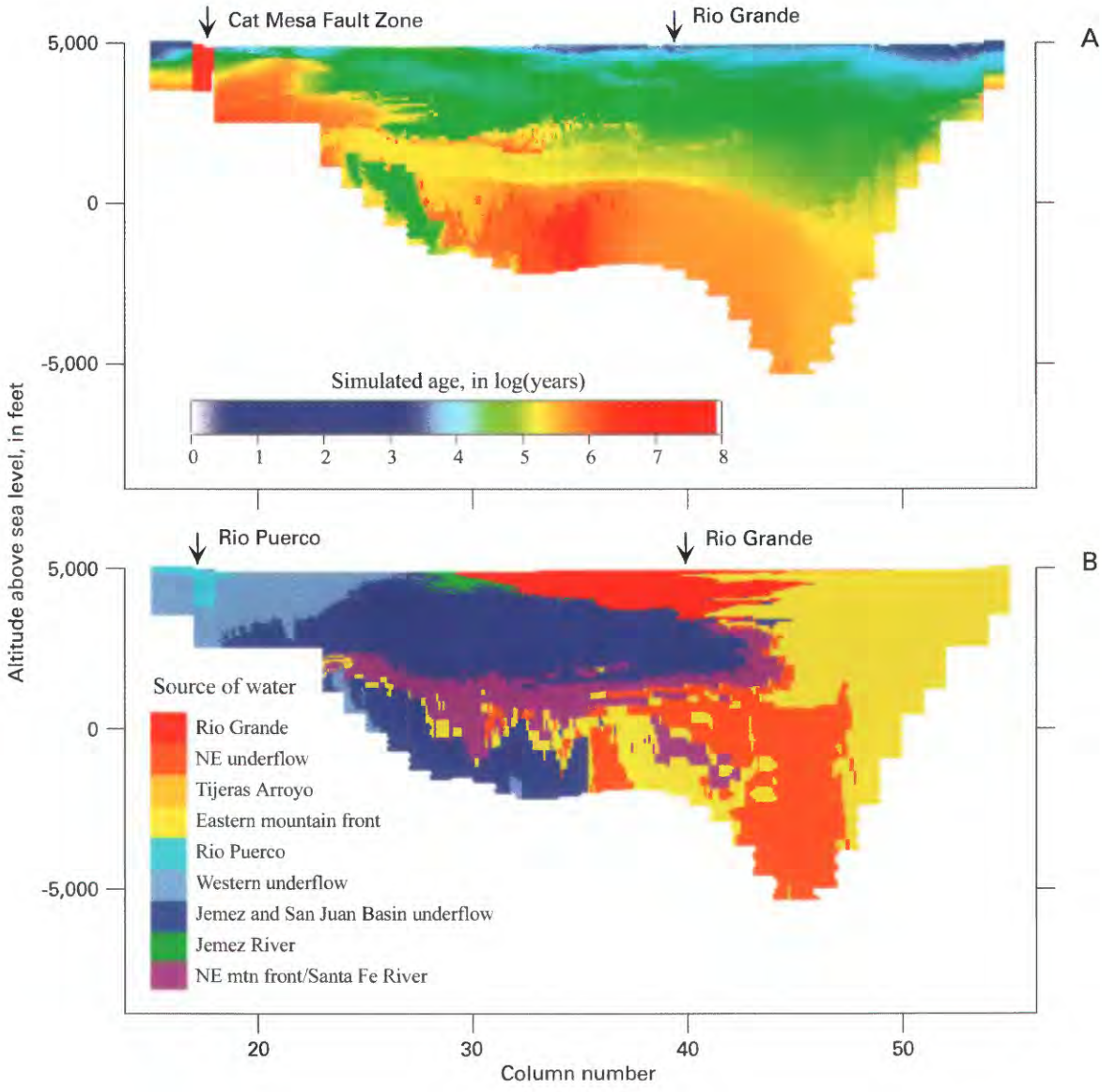

Figure 37. Simulated (A) ground-water ages and (B) source of water along row 75 of the steady-state ground-water-flow model (see fig. 36 for location of row 75).

dence interval calculations. The relative size of the interval in relation to other parameters is the most valuable information associated with the confidence interval calculations. A narrow band for the confidence interval indicates that, given the model is correct, the observed data provide more certainty that the estimated value is close to a true value, whereas a broad band indicates the available data cannot provide as much certainty. If there is likely model error (usually the case), then the interval more realistically represents the precision of the estimate, which is a function of how much information the observation data provide about the parameter value.

Uncertainty in the model parameters is also a function of parameter correlation. UCODE evaluates the correlation matrix during the sensitivity analysis. A correlation value of 1.0 or –1.0 indicates a perfect positive or negative correlation between parameters, respectively. A pair of such parameters is completely nonunique and indistinguishable. Similarly, correlation values of greater than 0.9 or less than –0.9 suggest strong correlation or nonuniqueness of parameters. Models dominated by head observations can typically have many highly correlated parameters (Poeter and Hill, 1997; Hill, 1998). Adding information to the model on advective path lines or travel times has been shown to reduce parameter correlation (Anderman and others, 1996; Poeter and Hill, 1997). For this model, the inclusion of travel times through the simulated ^{14}C activities resulted in a model with no highly correlated parameters. Out of 1,770 correlation values between parameters, only one value exceeded 0.8 and two values were less than –0.8. Nearly 1,200 values were between –0.2 and 0.2, indicating very little correlation.

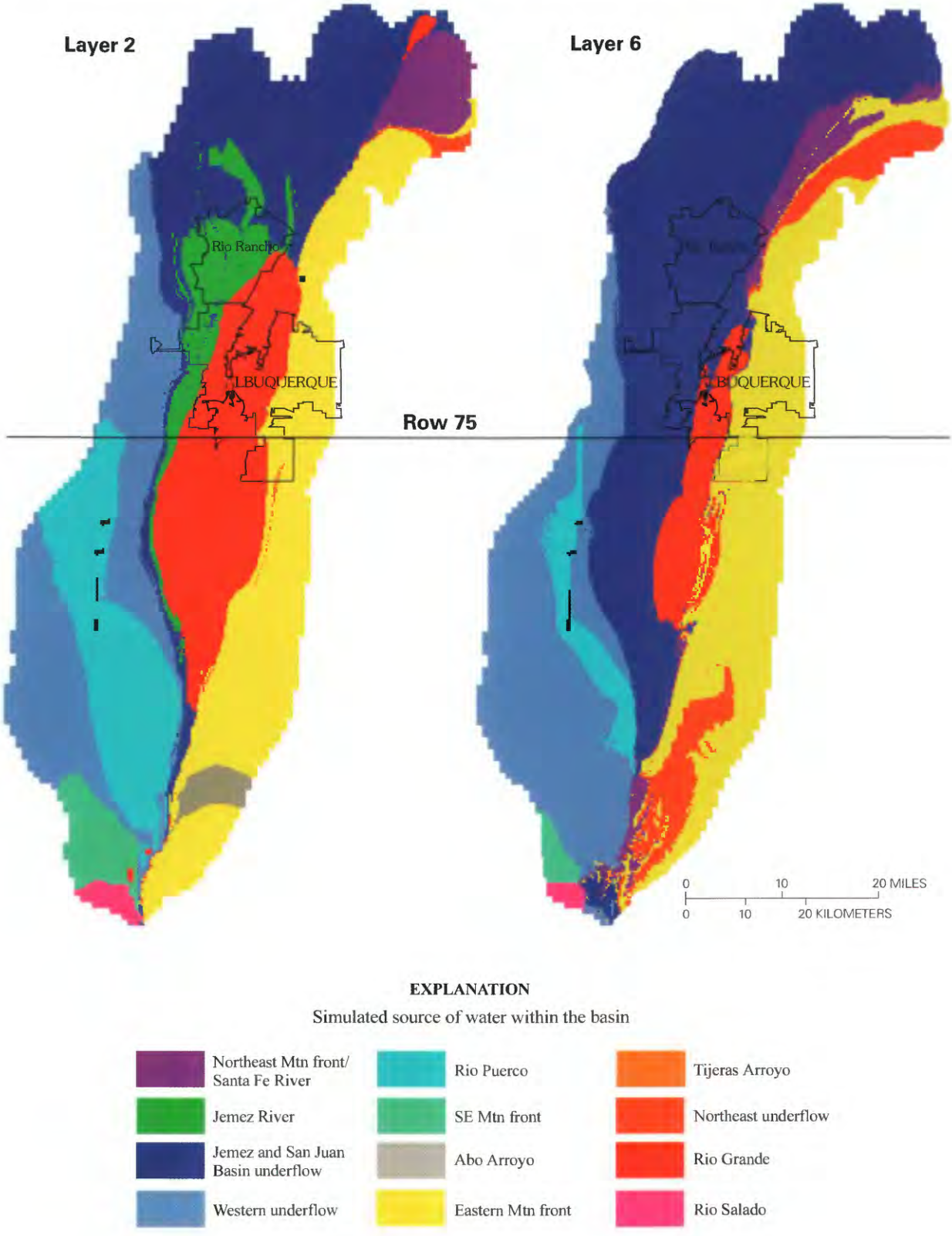

Figure 38. Simulated geochemical zones in layers 2 and 6 of the steady-state ground-water-flow model.

Table 3. Parameters of the ground-water-flow model and their optimized values.

Parameter name	Parameter description	Parameter location	Optimized parameter value*	Specified parameter value*
hcsfnw	hydraulic conductivity—Santa Fe Group northwest	figs. 18–27—northwest medium sand	1.66	
hcsfne	hydraulic conductivity—Santa Fe Group northeast	figs. 18–27—northeast medium sand	1.89	
hcsfsw	hydraulic conductivity—Santa Fe Group southwest	figs. 18–27—southwest medium sand	3.42	
hcsfse	hydraulic conductivity—Santa Fe Group southeast	figs. 18–27—southeast coarse sand	10.66	
hcsfcw	hydraulic conductivity—Santa Fe Group central west	figs. 18–27—west central medium sand	2.68	
hcsfce	hydraulic conductivity—Santa Fe Group central east	figs. 18–27—east central coarse sand	3.32	
hclsfn	hydraulic conductivity—lower Santa Fe—north section	figs. 18–27—northern medium sand	0.0079	
hclsfs	hydraulic conductivity—lower Santa Fe—south section	figs. 18–27—central medium sand	4.65	
hcsilt	hydraulic conductivity—silt layer	figs. 18–27—silts	0.435	
hcceja	hydraulic conductivity—Ceja gravels	figs. 18–27—Ceja gravels	1200	
hcdp3	hydraulic conductivity—deep section 3	figs. 18–27—piedmont slope deposits	1.04	
hcd4n	hydraulic conductivity—deep section 4—north	figs. 18–27—northern proximal volcanic sands	0.129	
hcd4s	hydraulic conductivity—deep section 4—south	figs. 18–27—southern proximal volcanic sands	0.502	
hcdp5	hydraulic conductivity—deep section 5	figs. 18–27—fine sand	0.15	
hcdp6	hydraulic conductivity—deep section 6	figs. 18–27—central fine and very fine sand	0.105	
hcalsd	hydraulic conductivity—river alluvium—Santo Domingo Basin	figs. 18–27—northern fluvial sand and gravel	5.38	
hcalal	hydraulic conductivity—river alluvium—Albuquerque region	figs. 18–27—central fluvial sand and gravel	24	
hcalbl	hydraulic conductivity—river alluvium—-Belen Basin	figs. 18–27—southern fluvial sand and gravel	160	
volcanics	hydraulic conductivity of volcanic rocks	figs. 18–27—extrusive and intrusive rocks	26	
fault1	Cat Mesa Fault Zone hydraulic conductivity	see figures 3, 18–27—faults		0.000001
fault2	West Sandia Fault Zone hydraulic conductivity	figs. 3, 18–27—faults	0.0535	
anisn	vertical anisotropy for northern basin except hcsfnw, hcsfne	see figure 16—Santo Domingo Subbasin	.000295	
anisc	vertical anisotropy for central basin except hcsfcw, hcsfce	see figure 16—Calabacillas Subbasin	.0012	
aniss	vertical anisotropy for southern basin except hcsfsw, hcsfse	see figure 16—Belen Subbasin	.00302	
ansfnw	vertical anisotropy for unit hcsfnw	figs. 17—northwest medium sand	0.000434	
ansfne	vertical anisotropy for unit hcsfne	figs. 18–27—northeast medium sand	0.000365	
ansfcw	vertical anisotropy for unit hcsfcw	figs. 18–27—west central medium sand	0.00284	
ansfce	vertical anisotropy for unit hcsfce	figs. 18–27—east central coarse sand	0.00129	
ansfsw	vertical anisotropy for unit hcsfsw	figs. 18–27—southwest medium sand	0.0016	
ansfse	vertical anisotropy for unit hcsfse	figs. 18–27—southeast coarse sand	0.00288	

Table 3. Parameters of the ground-water-flow model and their optimized values—Continued.

Parameter name	Parameter description	Parameter location	Optimized parameter value*	Specified parameter value*
analsd	vertical anisotropy for unit alalsd	figs. 18–27—northern fluvial sand and gravel	0.00051	
analal	vertical anisotropy for unit analal	figs. 18–27—central fluvial sand and gravel	0.0016	
analbl	vertical anisotropy for unit analbl	figs. 18–27—southern fluvial sand and gravel	0.0043	
hcpuercn	hydraulic conductance of the northern Rio Puerco riverbed	see figure 13	464	
hcpuercs	hydraulic conductance of the southern Rio Puerco riverbed	see figure 13	850	
hcjemez	hydraulic conductance of the Jemez River bed	see figure 13	180	
hcrivern	hydraulic conductance of the northern Rio Grande riverbed	figs. 18–27—northern fluvial sand and gravel		1,000,000
hcriverc	hydraulic conductance of the central Rio Grande riverbed	figs. 18–27—central fluvial sand and gravel	62,000	
hcrivers	hydraulic conductance of the southern Rio Grande riverbed	figs. 18–27—southern fluvial sand and gravel		1,000,000
sanjuan	underflow from the San Juan Basin	see figure 15	7,020	
jemez	underflow from the Jemez Mountains	see figure 15—Jemez east and west	1,970	
jemezmf	Jemez mountain front recharge	see figure 14		0
tijeras	Tijeras Arroyo recharge	see figure 14	15	
nnsandias	northernmost recharge along the Sandia Mountains	see figure 14—Sandia north	1,750	
nssandias	northern recharge along the Sandia Mountains	see figure 14—Sandia north central	0	
snsandias	southern recharge along the Sandia Mountains	see figure 14—Sandia south central	660	
sssandias	southernmost recharge along the Sandia Mountains	see figure 14—Sandia south	1,550	
manznitas	recharge along the Manzanitas	see figure 14	535	
manzanos	recharge along the Manzanos	see figure 14	1,700	
lospinos	recharge along the Los Pinos	see figure 14	2,200	
west	underflow from the western basin boundary	see figure 15—Sand Hill Fault Zone	1,610	
southwest	underflow from the southwestern basin boundary	see figure 15—Sierra Lucero	4,400	
hagan	underflow from the Hagan Embayment Basin	see figure 15	1,530	
sfriver	recharge from the Santa Fe River	see figure 14—northeast rivers	4,500	
santafe	underflow from the Santa Fe region	see figure 15—Española Basin	730	
aboarroyo	recharge from Abo Arroyo	see figure 14	900	
ladron	mountain front recharge from the Mt. Ladron region	see figure 14	800	
poros1	porosity of layer 1	see figure 12		0.36
poros2	porosity of layer 2	see figure 12		0.34
poros3	porosity of layer 3	see figure 12		0.32
poros4	porosity of layer 4	see figure 12		0.30

Table 3. Parameters of the ground-water-flow model and their optimized values—Continued.

Parameter name	Parameter description	Parameter location	Optimized parameter value*	Specified parameter value*
poros5	porosity of layer 5	see figure 12		0.28
poros6	porosity of layer 6	see figure 12		0.26
poros7	porosity of layer 7	see figure 12		0.24
poros8	porosity of layer 8	see figure 12		0.22
poros9	porosity of layer 9	see figure 12		0.20
age03	age of underflow at Jemez and San Juan Basin boundary	see figure 15	4,800	
age77	age of underflow at the Española Basin boundary boundary	see figure 15	7,140	
age06	age of recharge along the Mt. Ladron boundary	see figure 14	5,400	
age08	age of recharge along the Sandia model boundary	see figure 14—All four Sandia zones	1,950	
age15	age of recharge along the western model boundary	see figure 15—Sand Hill Fault Zone	100	
age16	age of recharge at the southeastern model boundary	see figure 15—Manzanos and Los Pinos	11,600	
age04	age of underflow along the southwestern model boundary	see figure 15—Sierra Lucero		0**

*hydraulic conductivity and riverbed conductance values are in feet per day; recharge and underflow values are in acre-feet per year; age values are in years

**although saline water underflow entering from the southwest is likely to be very old, Plummer and others (2003) showed that this water is diluted greatly by local recharge, which dominates the carbon-14 correction as well. Thus the age is set to zero to reflect local recharge.

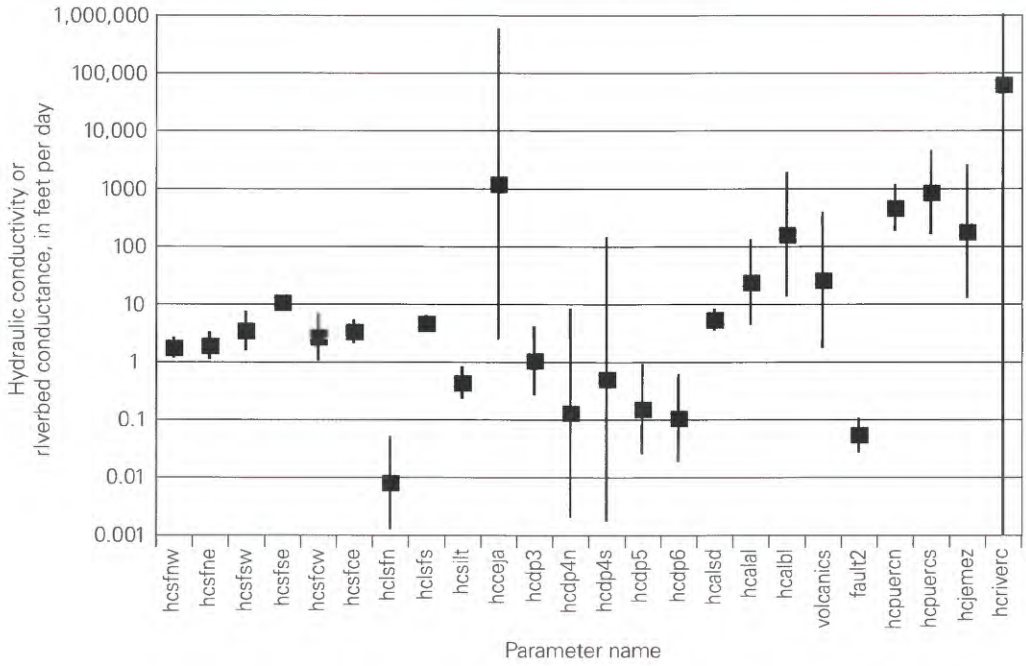

Figure 39. Optimized parameter values and 95 percent linear confidence intervals for hydraulic conductivity and riverbed conductance (see table 3 for parameter descriptions).

Hydraulic Conductivities

The estimated values for hydraulic conductivity and riverbed conductance are shown in figure 39. Values for the hydraulic conductivities of the Santa Fe Group fall mostly between 1 and 10 feet per day with some exceptions. These are values that are similar to estimates from previous models (Kernodle and others, 1995; Tiedeman and others, 1998) and to prior field measurements concerning the basin fill material (Thorn and others, 1993). Zones that have estimated hydraulic conductivity values significantly less than 1 foot per day are (1) the deeper Santa Fe unit to the north; (2) the silt layer in the central basin; (3) the deep units 4, 5 and 6; and (4) the West Sandia Fault Zone. Zones that have estimated values significantly greater than 10 feet per day are (1) the Ceja gravels, (2) the volcanic rocks, and (3) the alluvium associated with the paleochannel of the Rio Grande in the central and southern basin. The best-fit value for the Ceja gravels of greater than 1,000 feet per day exceeds all known field measurements, but the model could not estimate this value with any reasonable precision. Values for the Ceja gravels that were assumed in earlier models (100 feet per day or less) are well within the broad linear confidence interval shown in figure 39. Other parameters with high uncertainty were all of the deep units and Rio Grande alluvium. The riverbed conductances also were associated with high degrees of uncertainty. Some validation for the parameter values estimated for this model is given by the fact that the silt layer and the volcanic rock units had estimated values (low and high, respectively) that agree with their relative expected values. A valuable result of this study was not only estimates of parameter values but their uncertainties that reflect the current state of available data. Because the objective of this study was to estimate parameter values, and not provide a final model for management use, parameters with high uncertainty, such as the Ceja gravels, were not reassigned more reasonable values.

The best-fit values estimated for the vertical anisotropy in the hydraulic conductivity of the basin are shown in figure 40. The anisotropy (K_v/K_h) was estimated individually for 12 structural zones within the basin (fig. 16), and the values range from about 0.0003 to 0.004. Originally only three anisotropy zones were used, but the simulated observations were quite sensitive to their values, so an additional nine zones were ultimately added. These values are consistent with what might be expected for a layered system where the individual layers are isotropic and have values that vary by 2 to 4 orders of magnitude. Certain layers such as the silt, gravel, and volcanic layers would be expected to have values that vary by more than this, but they have been accounted for explicitly in separate zones.

Recharge Rates

The best-fit values estimated for recharge rates and initial underflow ages to the basin are shown in figure 41. Recharge was not estimated directly for the Rio Puerco and the Jemez River, but only through their riverbed conductance values (fig. 39). These conductance values translate into 3,600 acre-feet per year for Rio Puerco, but only 160 acre-feet per year for the Jemez River (table 4). The recharge for the Rio Puerco was similar to values used in earlier models, but the Jemez River recharge value was very much lower. The recharge from the Jemez River in the current study was constrained by the

observation of very old water just to the south of the Jemez River. It should be noted, however, that the confidence interval and therefore the uncertainty associated with this recharge estimate is very large. The model suggests that most of the ground water that originates outside the basin is coming from underflow from northern basins, at several thousand acre-feet per year.

Recharge from the eastern mountain front is estimated at about 8,500 acre-feet per year, with another 900 acre-feet per year leaking through Abo Arroyo. These numbers are somewhat lower than previous estimates that were based on rainfall-runoff equations, but are close to recent estimates of recharge along the eastern mountain front made using the chloride mass-balance method (Anderholm, 2001; table 4). Total recharge to the basin is estimated to be 55,000 acre-feet per year, with 20,000 acre-feet per year of the total coming from the floodplain of the Rio Grande. Kernodle and others (1995) showed Rio Grande leakage of 141,000 acre-feet per year, but most, if not all, of this is intercepted by evapotranspiration on the flood plain of the inner valley. Their model does not report a value leaving the inner valley, but visual inspection of their head contours strongly suggests this. The model of Tiedeman and others (1998) shows ground water leaving the inner valley, but only with certain hydrogeologic configurations of the ground-water trough. McAda and Barroll (2002) do not give estimates of ground-water fluxes leaving the inner valley, nor does a visual inspection of their hydraulic head map reveal whether ground water is leaving the inner valley. The basin-margin recharge estimated from this model, 35,000 acre-feet per year, is one-fourth of the estimates used in Kernodle and others (1995), and about half of that of McAda and Barroll (2002). The estimate for recharge from Tijeras Arroyo was very small (15 acre-feet per year), but the upper 95 percent linear confidence interval was 265 acre-feet per year. Some of the estimates for underflow recharge rates were accompanied with high uncertainty (very large confidence intervals).

Ages at Model Boundaries

Because it was difficult to obtain independent information on the age of ground water that enters the basin at different underflow boundaries, an attempt was made to estimate the ages at these boundaries in the parameter estimation procedure. Results of the estimates are given in figure 41. Most of the estimated values are accompanied by high uncertainty and broad confidence intervals. This indicates that the model could not estimate these values with any high degree of precision based on the data supplied. However, low sensitivity also indicates that the model error was not greatly affected by the value of the ages that were assigned at the boundary. This means that although the age at the boundary is a requirement in calculating travel times in the basin and underflow estimates, uncertainty in that age does not necessarily translate into greater uncertainty in the underflow estimates.

Model Fit

The overall goodness of fit of the model to the observation data was evaluated using summary measures and graphi-

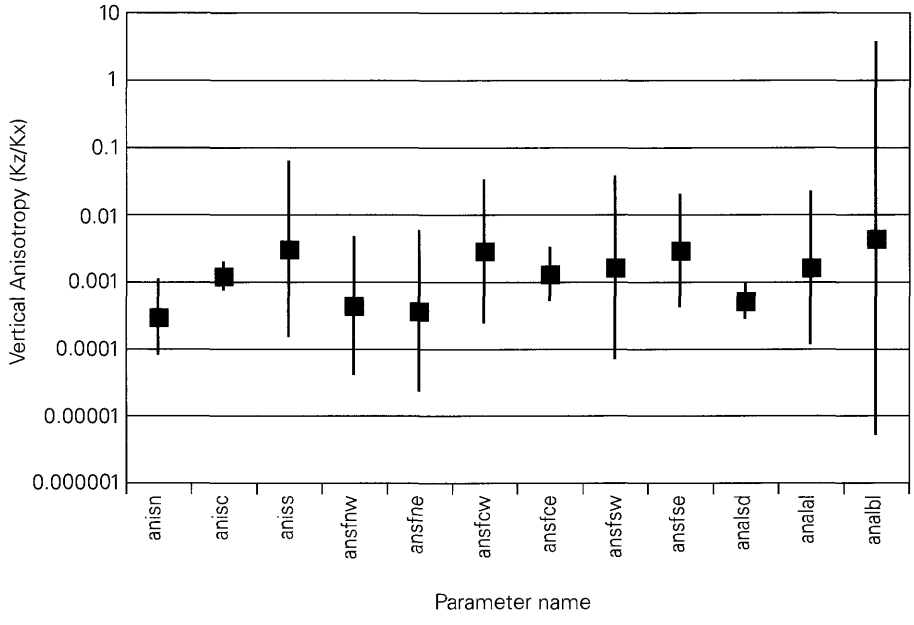

Figure 40. Optimized parameter values and 95 percent linear confidence intervals for anisotropy (see table 3 for parameter descriptions).

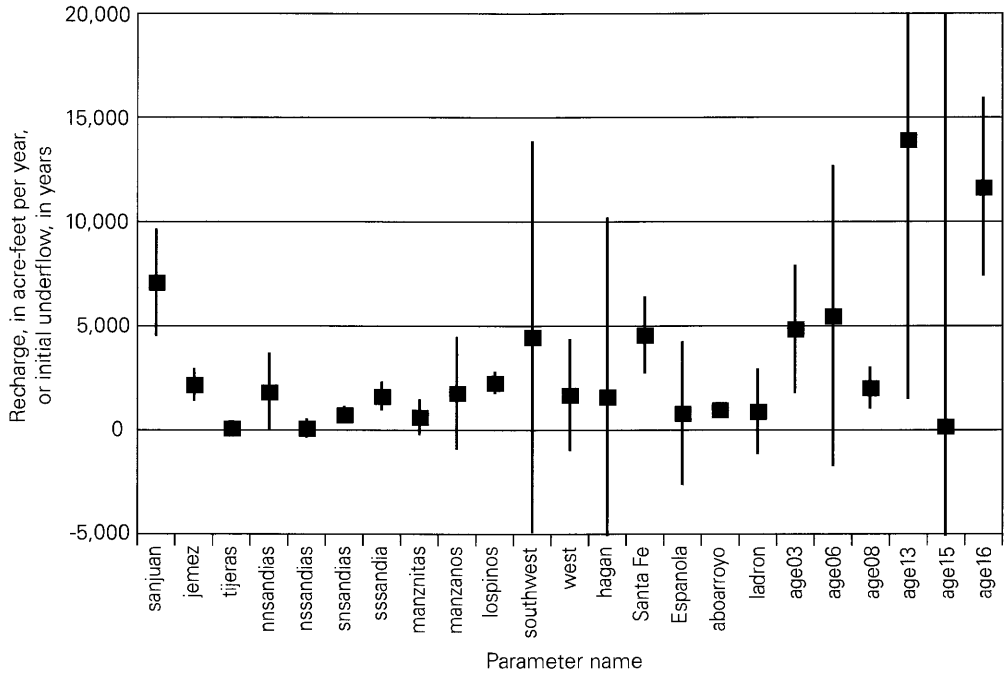

Figure 41. Optimized parameter values and 95 percent linear confidence intervals for recharge and initial underflow ages (see table 3 for parameter descriptions).

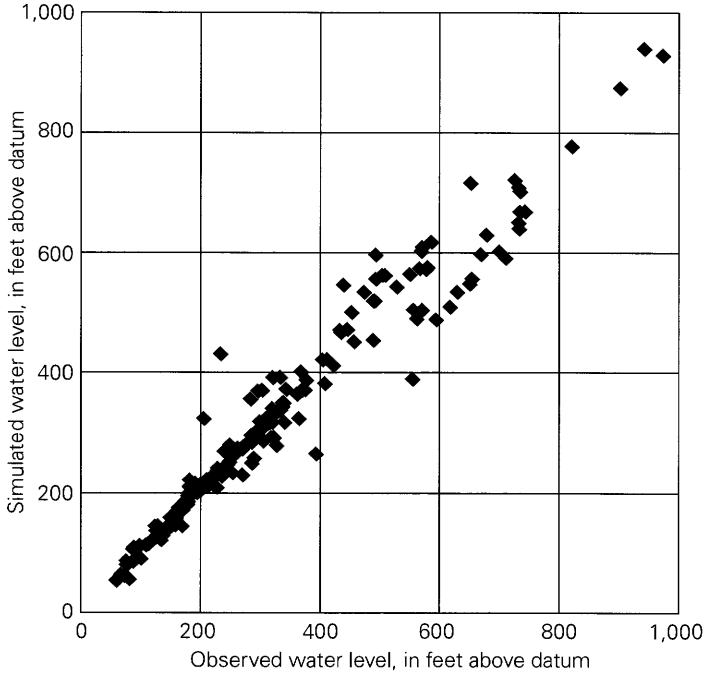

Figure 42. Observed water levels plotted against simulated water levels. Datum equals 4,650 feet above sea level.

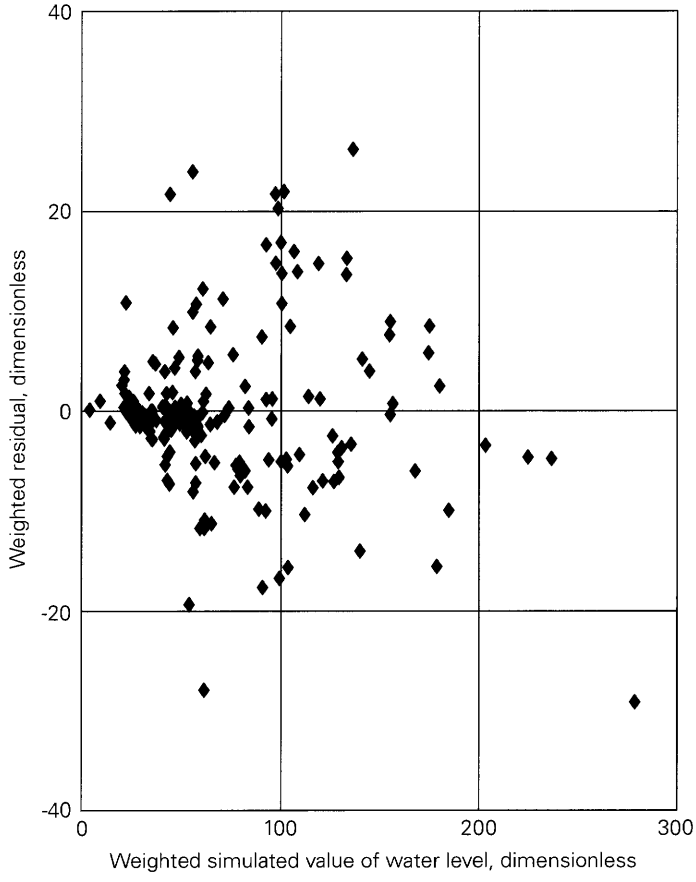

Figure 43. Weighted simulated values of water levels plotted against weighted residuals.

Table 4. Estimates of inflow and outflow from the Middle Rio Grande Basin from recent studies.

[All values are in acre-feet per year. nd = not determined, nr = not reported]

Region	Kernodle and others (1995)	Tiedeman and others (1998)	Anderholm (2001)	McAda and Barroll (2002)	This study
Inflows to the Middle Rio Grande Basin					
Inflows from external sources					
Adjacent basin underflows (fig. 15):					
Jemez West and East	14,300	7,000	nd	14,900	2,000
Western Boundary	4,700	4,700	nd	1,700	1,600
Southwest Boundary	7,500	2,400	nd	900	4,400
San Juan Basin	1,200	1,200	nd	1,000	7,000
Española Basin	6,000	12,600	nd	14,000	1,500
Total underflows	33,700	27,900	nd	32,500	16,500
Mountain front and tributary recharge (fig. 14):					
Northeast Rivers (Santa Fe)	7,600	7,700	nd	5,300	4,500
Tijeras Arroyo	10,600	6,200	1,800	700	15*
Abo Arroyo	15,400	15,400	1,300	1,300	900
Rio Puerco	5,600	1,700	nd	1,000	3,600
Jemez River	12,300	9,100	nd	15,000**	200
Rio Salado	7,200	7,200	nd	2,000	1,600
Sandia Mtn front	19,500	11,500	4,200	5,500	4,000
Southeast Mtn front	26,700	8,800	4,900	4,200	4,400
Total mtn. front and tributary recharge	104,900	67,600	nd	35,000	19,200
Total recharge from external sources	138,600	95,500	nd	67,500	35,700
Inflows from internal sources					
Inner Valley (Rio Grande flood plain)	nd	75,000***	nd	nd	20,000
Rio Grande	141,000	nr	nd	63,000**	nd
Total recharge from internal sources	141,000	75,000***		63,000**	20,000
Total inflow to the MRGB	279,600	170,500	nd	130,500	55,700
Outflows from the Middle Rio Grande Basin					
Total Inner Valley (Rio Grande flood plain)	nd	nr	nd	nd	55,700
Rio Grande	8,000	nr	nd	nd	nd
Evapotranspiration	261,000	170,000	nd	129,000	nd
Total outflow from the MRGB	269,000	170,000	nd	129,000	55,700

*Does not include the adjacent mountain front.

**Includes the Jemez Canyon Reservoir or Cochiti Lake.

***Includes canals and drains in the Inner Valley.

cal analyses. The standard error of regression is a measure of overall model fit to the calibration data, and is calculated as:

$$S = \left(\frac{S}{n-p} \right)^{\frac{1}{2}} \quad (5)$$

where S is the sum of the squared weighted residuals, n is the number of observations, and p is the number of parameters. A standard error of regression greater than one is an indication of model error, given that the weights correctly reflect the measurement errors (Hill, 1998, p. 18). For this model, the final sum of squared weighted residuals was 77,000, the number of observations was 409, and the number of parameters was 60, yielding a standard error of regression of 15. This number is significantly larger than 1, indicating model error, but given the complexity of the Middle Rio Grande Basin, this was expected. Only one model for the basin was calibrated in this study, so a value of s =15 cannot be compared to other models of the basin that were calibrated with the same data set. Earlier models of the basin by Tiedeman and others (1998) gave standard errors of regression between 3.4 to 4.0. The total error in the model for this current study was distributed as 72 percent to the ^{14}C activities, 15 percent to the water levels, and 13 percent to the hydrochemical-target regions. Thus, most of the error for this model was in the matching of the ^{14}C activities. The earlier models were calibrated against mostly water-level data, and thus a better model fit would be expected under those conditions.

One of the simplest ways of assessing model fit is to plot the observations against the simulated observations. For a perfect fit, all points should fall on the 1:1 diagonal line. The water-level observations for the model were plotted in this way (fig. 42), and show a strong trend along the 1:1 line. Another way to assess model fit and model bias is to plot the weighted residuals against the weighted simulated values. Ideally, these points should show a random distribution above and below zero for all weighted simulated values, indicating a lack of bias in the model error. The water-level residuals and simulated values were plotted in this way also (fig. 43), and show a random distribution above and below. Plots were also made of the ^{14}C observations to assess model fit and error. Observations plotted against simulated observations (fig. 44) show a substantially greater amount of scatter about the 1:1 line than the water-level observations. This poorer fit to the ^{14}C data was expected. Water levels represent a smoothly varying potential field that can be fit without much difficulty to the solution of the flow equation. Ground-water ages are a function of velocities that are in turn a function of the first derivatives of the ground-water-potential field, and are thus more difficult to fit. In addition, the multiple source areas in the Middle Rio Grande Basin create age patterns within the basin that are discontinuous (fig. 36), increasing further the complexity and difficulty in fitting age-related simulations to observations. Weighted residuals plotted against weighted simulated values for ^{14}C activities (fig. 45) show a similar number of values above and below the zero-residual line. The distribution, however, is not random because there are sloping envelopes within which the data must lie. The envelopes are present because the observations cannot lie outside of the range of 0–100 percent modern carbon.

A more detailed comparison of model fit to the data is accomplished through analysis of the spatial distribution of the water-level and ^{14}C activities residuals and weighted residuals. The water-level residuals and weighted residuals are plotted over a map of the Middle Rio Grande Basin to ascertain the regions of the basin where the model fit is good or poor (figs. 46, 47). The weighted residual plot shows the errors adjusted for the certainty in the observational data. In both cases it can be seen that the better fits to the data are in the center of the basin and along the Rio Grande. This is expected somewhat in that the Rio Grande acts as a line of constant head from which the head solution is not allowed to deviate substantially. The poorest matches to water levels occur in the northern section of the basin. Simulated water levels were consistently too low near the Jemez River and extreme northeast section of the basin, and too high in the Rio Rancho and northeast sections of the basin. The observed ground-water trough appears to extend farther north into the Rio Rancho region (fig. 4) than the current model simulates. Tiedeman and others (1998) also showed a poorer fit in the northern section of the basin. McAda and Barroll (2002) have similar magnitudes of residuals as this current model in the northern basin. This suggests that the hydrogeologic features in the north are different from those of the rest of the basin, and these differences are not included in the current models. To better simulate the northern section of the basin, a more regional model with a better representation of the hydrogeology may be required along with additional observation data.

The ^{14}C activities residuals and weighted residuals were also plotted over a map of the Middle Rio Grande Basin (figs. 48, 49). These plots show less spatial bias in the error than the water-level residual plots show. One apparent pattern is that near recharge areas, the simulated activities are often too large (simulated ages are too young), whereas in the center of the basin the simulated activities are often too small (simulated ages are too old). This may suggest ground-water flow through the basin was slower sometime in the recent past, but faster in the more distant past. This idea of a varying flux, or recharge, in the past is investigated further in the transient paleorecharge simulation.

Transient Paleorecharge Simulation

A transient ground-water-flow simulation was performed to investigate the effect of time-varying recharge rates over the past tens of thousands of years on simulated ^{14}C activities. A 30,000-year simulation was run using twelve 2,500-year time steps preceded by a near-steady-state condition. The near-steady-state condition was approximated by a 10-million-year time step. This long initial time step allowed MODPATH to

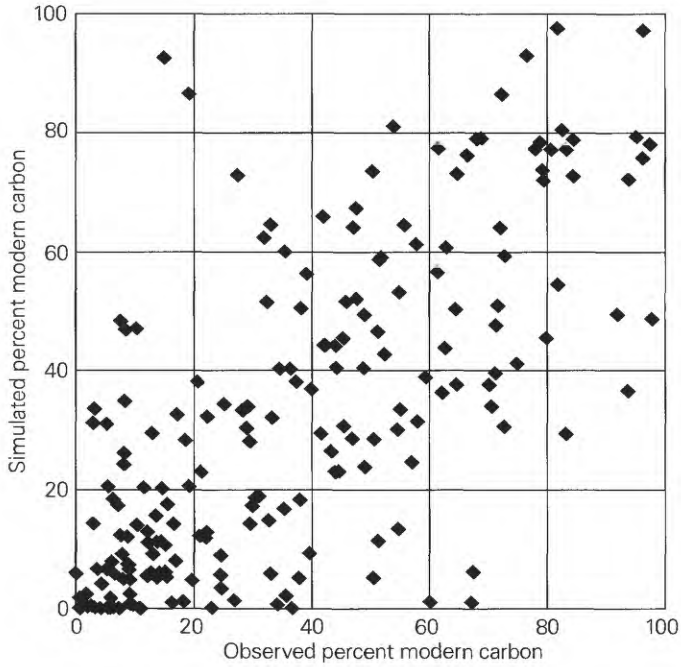

Figure 44. Observed plotted against simulated percent modern carbon.

track path lines back to recharge locations for path lines with very long travel times. Including the initial long time step, a total of 13 time steps were used. During each of the time steps, all recharge and underflow boundary cells were multiplied by a single recharge multiplier. The multipliers were all given an initial value of 1.0 to reproduce the conditions in the steady-state predevelopment simulation. The multipliers were then adjusted until an optimum fit was obtained between the observed data and the simulated observations. The nonlinear regression routine in UCODE was used initially to reduce the total sum of the squared errors, but eventually the individual recharge parameters were adjusted manually to obtain the best-fit recharge multiplier values. Results from this model were not used to report parameter estimates because none of the parameter estimates also in the predevelopment model changed during this simulation.

Results from the transient simulation suggest that recharge was greater before 15,000 years ago (fig. 50). The best-fit values for the recharge multipliers are greater than 10 for the period from 20,000 to 22,500 years ago. This time corresponds to the last glacial maximum that occurredapproximately 21,500 years ago. Evidence for a wetter climate during this period is also present in the Estancia Basin, just east of the Sandia Mountains, in the form of playa lake deposits (Bachhuber, 1992; Allen and Anderson, 2000). Simi-larly increased recharge during this time period is suggested from 14C flow-modeling and chloride results to the west in northeastern Arizona (Zhu, 2000; Zhu and others, 2003). The recharge multipliers have a best-fit value of 1.0 for the past 10,000 years, but have a value of 0.5 about 15,000 years ago. Although the relative changes in recharge rates are suggested by the transient simulation, the uncertainties associated with the values are quite high—especially the values before 20,000 years ago. An earlier simulation (Sanford and others, 2001) with longer time steps suggested that recharge during the glacial maximum was about five or six times greater than today. Some of the estimated increase in paleorecharge may be an artifact of not accounting for the vertical dispersion of ^{14}C in the basin as it is transported through the basin. This would have the effect of making deep water with small quantities of ^{14}C look younger than it really is, and the parameter estimation procedure would increase paleorecharge to account for this. In spite of this, all of the different results suggest greater recharge during the last glacial maximum and slightly less recharge just before or at the beginning of the Holocene. The exact amount of these changes in recharge, however, remains uncertain.

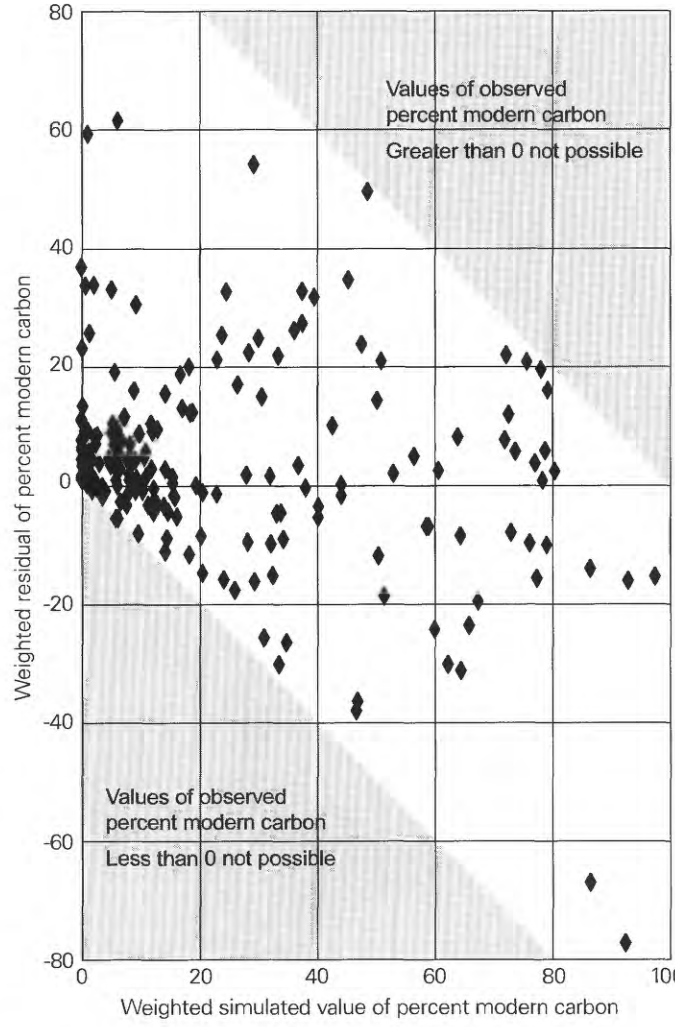

Figure 45. Weighted simulated values of percent modern carbon plotted against weighted residuals.

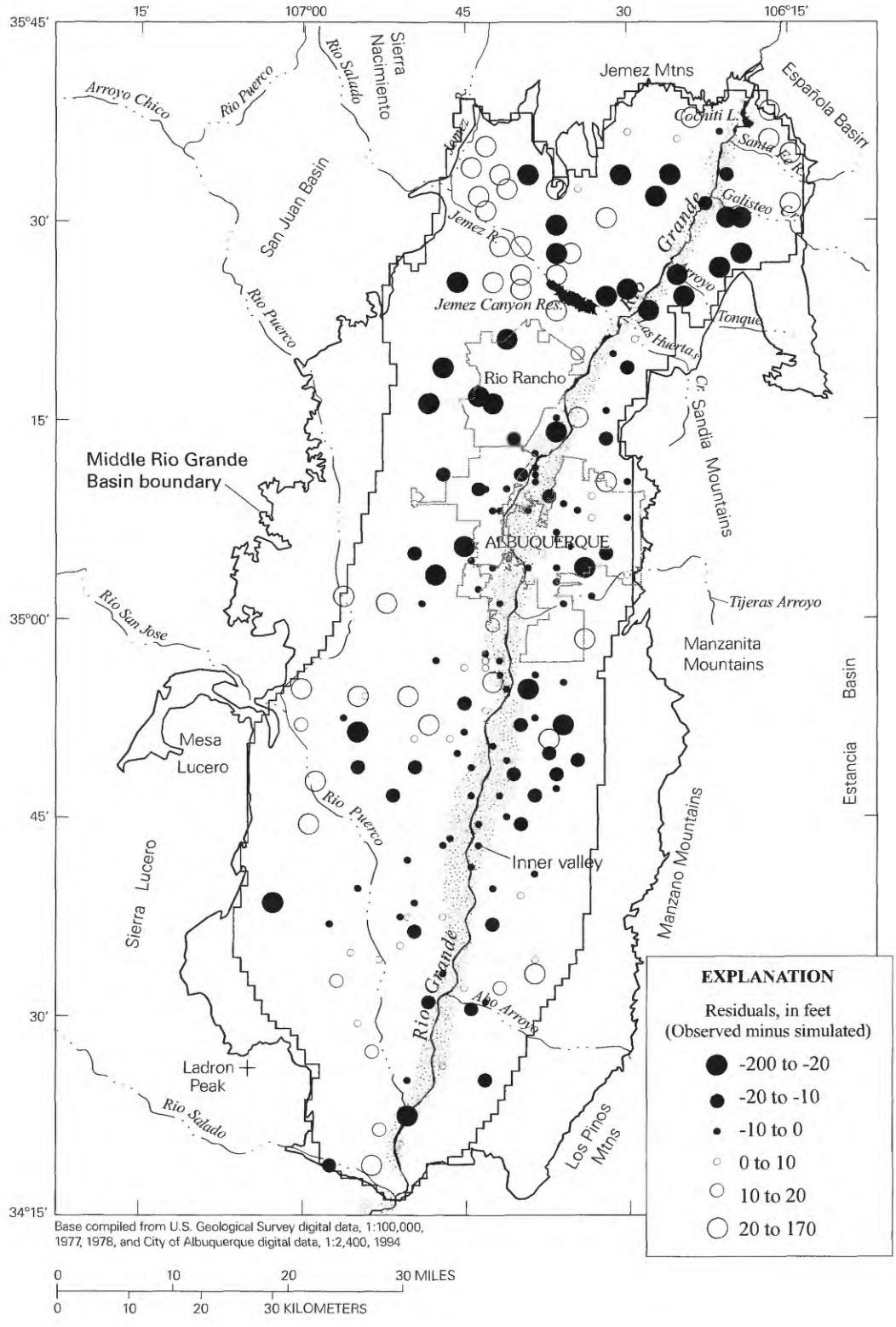

Figure 46. Spatial distribution of residuals between the observed and simulated water levels.

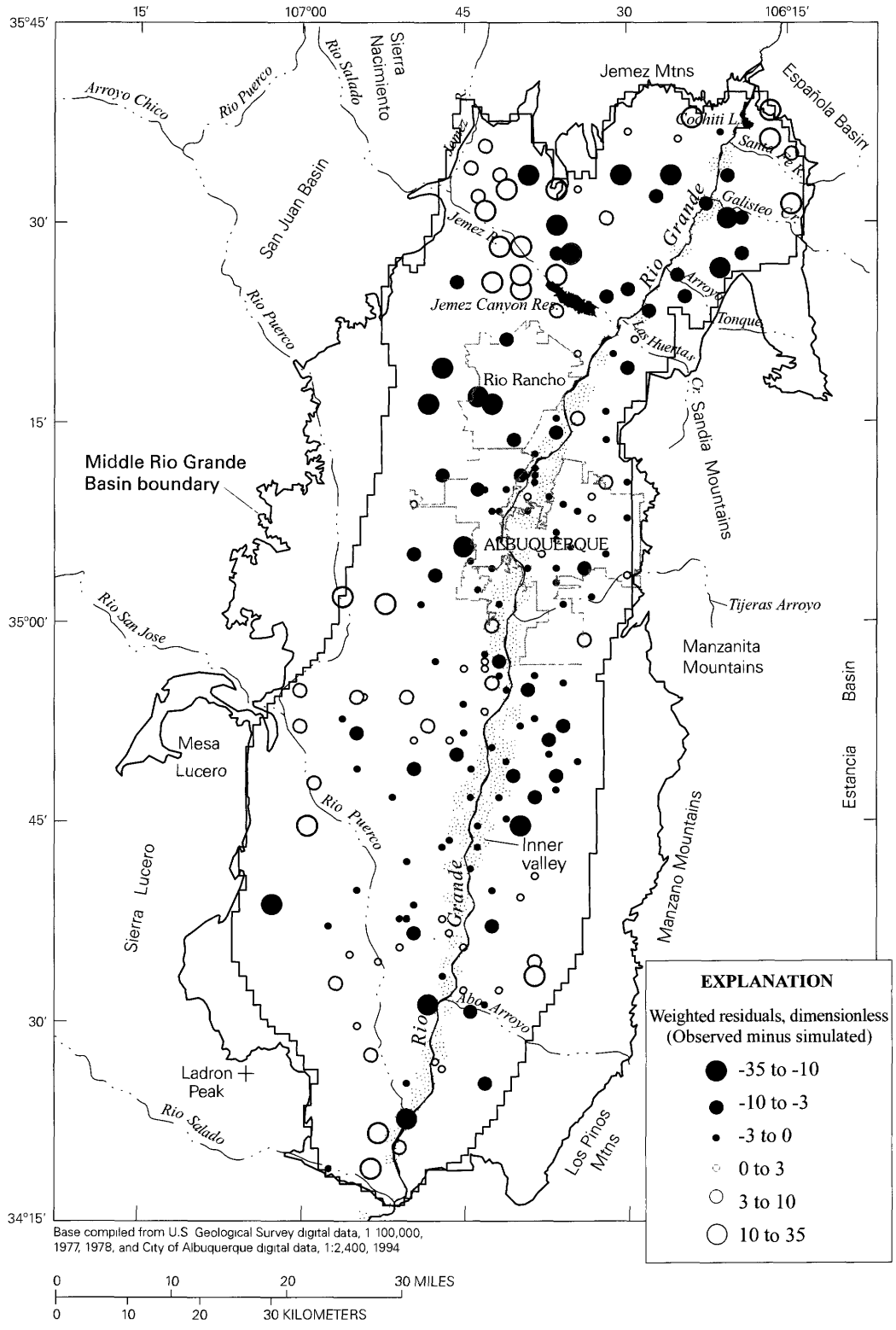

Figure 47. Spatial distribution of weighted residuals between the observed and simulated water levels.

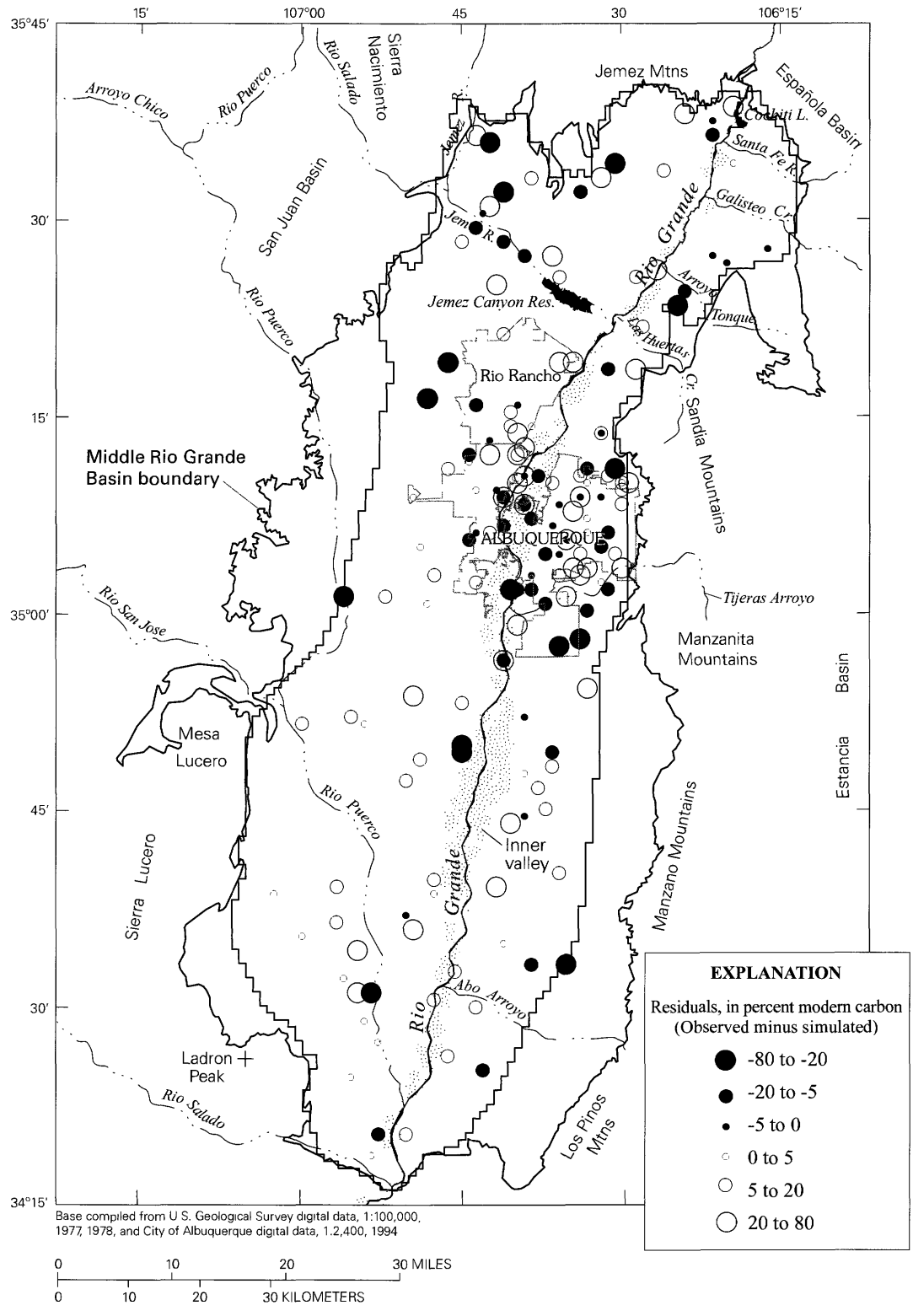

Figure 48. Spatial distribution of residuals between the observed and simulated ^{14}C activities.

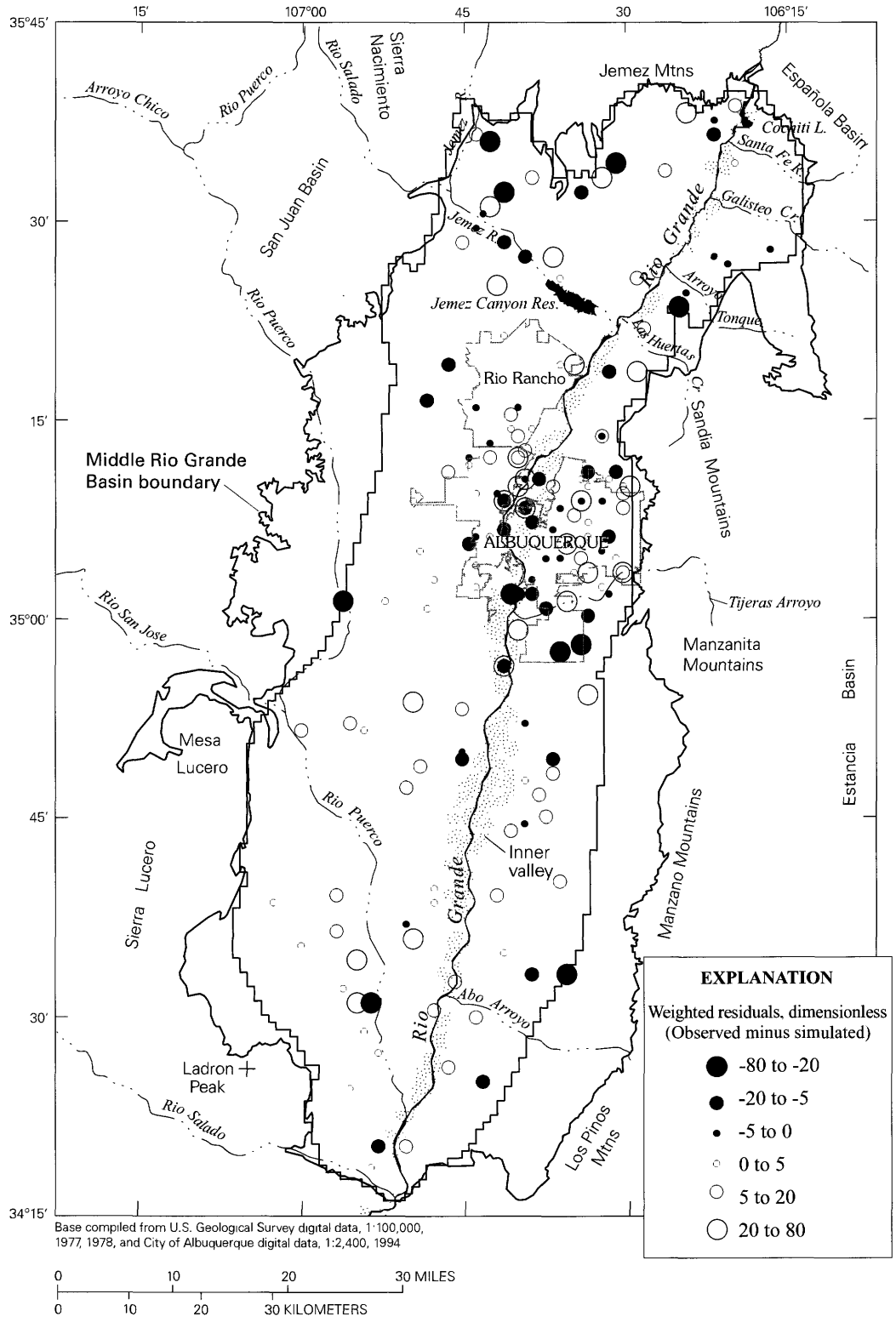

Figure 49. Spatial distribution of weighted residuals between the observed and simulated ^{14}C activities.

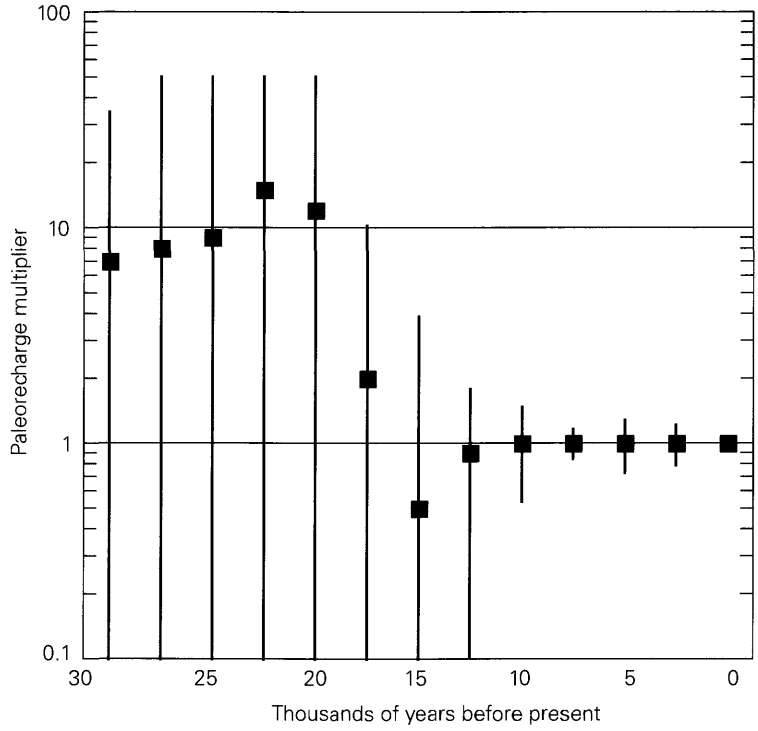

Figure 50. Optimized values of paleorecharge multipliers and their 95 percent linear confidence intervals.

SUMMARY AND CONCLUSIONS

The question of the availability of ground water as a long-term resource in the Middle Rio Grande Basin of central New Mexico was addressed recently by the characterization of the geohydrologic frameworks of the basin (Thorn and others, 1993) and the development of a ground-water-flow model by the USGS (Kernodle and others, 1995). In response to concerns from these studies, the USGS began a 6-year Middle Rio Grande initiative (1996–2001) to expand our understanding of basin hydrology (Bartolino and Cole, 2002). As part of that initiative, the present study used ^{14}C activities and the location of hydrochemical zones as observations to estimate parameters for a predevelopment ground-water-flow model of the Middle Rio Grande Basin. Water levels in the basin were simulated using MODFLOW, and travel times to wells and source-area delineation were simulated using MODPATH. The inverse modeling code UCODE was used to help estimate hydraulic conductivities of hydrogeologic units and modern and past recharge to the basin along the basin margins and tributary rivers. Some of the parameter values from this study were incorporated into an updated ground-water model of the basin (McAda and Barroll, 2002).

In the present study a three-dimensional geologic model of the basin (Cole, 2001b) was discretized into a three-dimensional MODFLOW grid of the basin. Major hydrogeologic units in the geologic model include volcanic rocks, and several units that represent the Santa Fe Group sediments, including ancestral gravels from the Rio Grande and some finer grained units that represent the middle and lower Santa Fe Group. The MODFLOW grid represented the hydrogeologic units with nine layers of variable thickness totaling more than 12,000 feet in places, and a uniform horizontal grid resolution of 1 square kilometer. Observations that were used to calibrate a steady-state model and then a transient paleohydrologic model included 200 water levels, 200 ^{14}C activities, and 9 hydrochemical-target regions. Observed water levels were compared with simulated water levels calculated with MODFLOW, ^{14}C activities were compared with simulated activities based on travel times to individual wells calculated with MODPATH, and the percentage of river water in the hydrochemical-target regions was compared with the percentage of simulated river water. The observed ^{14}C activities, corrected ages, and the extent of hydrochemical zones within the basin are described in detail by Plummer and others (2004).

Hydraulic conductivities estimated for the model were similar to values that had been estimated in the previous models of Kernodle and others (1995) and Tiedeman and others (1998). The estimates for the hydraulic conductivity of the Rio Grande alluvium ranged from 5 feet per day in the north

to 160 feet per day in the south, with values for the gravels beneath Albuquerque at 1,200 feet per day (but with a linear confidence interval extending well below 100 feet per day). In addition, the hydraulic conductivity of the volcanic rock unit was estimated to be 26 feet per day, and the hydraulic conductivity of a silty layer identified in the geologic model was estimated to be 0.44 feet per day. Estimates of vertical anisotropy for the various units ranged from 0.0003 to 0.004.

Basin-margin and tributary recharges estimated for the model were lower than values used in previous models. These values overall were estimated to be about 35,000 acre-feet per year of external recharge. The model calculated an additional 20,000 acre-feet per year leaking from the Rio Grande, bringing the total recharge to the basin to 55,000 acre-feet per year. The earlier model of Kernodle and others (1995) had assigned an external recharge of 138,600 acre-feet per year, and Tiedeman and others (1998) estimated an external recharge of 95,500 acre-feet per year. Although the latter value was from a calibrated model, the majority of observations were water-level measurements, with few flux-based observations to constrain flow or recharge rates. McAda and Barroll (2002) used a lower value of external recharge of 67,500 acre-feet per year, based partially on data from Anderholm (2001). The current model has 200 ground-water ages to constrain fluxes from external boundaries, and in so doing suggests some of the earlier inflow estimates from adjacent basins (Frenzel and Lyford, 1982; McAda and Wasiolek, 1988; Frenzel, 1995; Hawley and Grant, 1997) may have been too high. In addition, the rainfall-runoff methods used to estimate recharge in the earlier models do not account for runoff that enters the Rio Grande, or evapotranspiration of runoff once it enters the subsurface. Recharge estimates for the eastern mountain fronts have been made independently using the chloride mass-balance method (Anderholm, 2001). Estimates by the chloride method (11,200 acre-feet per year) were much closer to the estimates of this study (8,400 acre-feet per year) than to those of the previous models (greater than 40,000 acre-feet per year).

In the current study, a ground-water trough was simulated west of the Rio Grande with an associated zone of ground water derived from the Rio Grande. The trough and the Rio Grande-derived ground water were clearly observed in the predevelopment water-table map and hydrochemical zones. Rio Grande water was simulated under steady-state conditions in more of the trough than is observed, but this is consistent with the trough being a transient feature since the last glacial maximum and Rio Grande water in the trough dating to about 10,000 or so years. The earlier models with greater recharge did not reproduce these features very effectively.

A transient paleohydrologic model was calibrated to determine if the ^{14}C data as a whole contained information indicating that recharge rates had changed during the past 30,000 years. Paleolimnological evidence from central New Mexico has indicated that the climate in the region was wetter during the last glacial maximum (20,000–25,000 years ago). The transient simulation was for a period of 30,000 years, with an independent value of recharge estimated every 2,500 years. Although there is uncertainty in the results, especially before 20,000 years ago, the transient model suggested that recharge to the basin was substantially higher during the last glacial maximum than at present, and perhaps slightly lower just before the beginning of the Holocene period than at present.

REFERENCES CITED

Allen B.D., and Anderson, R.Y., 2000, A continuous, high-resolution record of the late Pleistocene climate variability from the Estancia basin, New Mexico: Geological Society of America Bulletin, v. 112, no. 9, p. 1,444–1,458.

Anderholm, S.K., 1988, Ground-water geochemistry of the Albuquerque-Belen Basin, central New Mexico: U.S. Geological Survey Water-Resources Investigations Report 86-4174, 37 p.

Anderholm, S.K., 2001, Mountain-front recharge along the eastern side of the Middle Rio Grande Basin, central New Mexico: U.S. Geological Survey Water-Resources Investigations Report 00-4010, 36 p.

Anderman, E.R., Hill, M. C., and Poeter, E. P., 1996, The use of advective-transport observations to improve ground-water flow parameter estimation: Ground Water, v. 34, no. 6, p. 1001–1009.

Athy, L.F., 1930, Density, porosity, and compaction of sedimentary rocks: Bulletin of the American Association of Petroleum Geologists, v. 14, p. 1–24.

Bachhuber, F.W., 1992, A pre-late Wisconsin paleolimnologic record from the Estancia Valley, central New Mexico, *in* Clark, P.U., and Lea, P.D., eds., The last interglacial-glacial transition in North America: Geological Society of America Special Paper 270, p. 289–307.

Bartolino, J.R., and Cole, J.C., 2002, Ground-water resources of the Middle Rio Grande Basin: U.S. Geological Survey Circular 1222, 132 p.

Bartolino, J.R., and Niswonger, R.G., III, 1999, Numerical simulation of vertical ground-water flux of the Rio Grande from ground-water temperature profiles, central New Mexico: U.S. Geological Survey Water-Resources Investigations Report 99-4212, 34 p.

Bartolino, J.R., and Sterling, J.M., 1999, Electromagnetic surveys in the Rio Grande flood plain, Middle Rio Grande Basin, New Mexico-Third-year status, *in* Bartolino, J.R., ed., U.S. Geological Survey Middle Rio Grande Basin Study—Proceedings of the Third Annual Workshop, Albuquerque, New Mexico, February 24–25, 1999: U.S. Geological Survey Open-File Report 99-203, p. 23–24.

Bexfield, L.M., and Anderholm, S. K., 2000, Predevelopment water-level map of the Santa Fe Group aquifer system in the Middle Rio Grande Basin between Cochiti Lake and San Acacia, New Mexico: U.S. Geological Survey Water-Resources Investigations Report 00-4249, 1 p.

Bexfield, L.M., and Anderholm, S. K., 2002, Spatial patterns and temporal variability of water quality from City of Albuquerque drinking-water supply wells and piezometer nests, with implications for the ground-water flow system: U.S. Geological Survey Water-Resources Investigations Report 01-4244, 101 p.

Bjorklund, L.J., and Maxwell, B. W., 1961, Availability of ground water in the Albuquerque area, Bernalillo and Sandoval Counties, New Mexico: New Mexico State Engineer Technical Report 21, 117 p.

Blaney, H.F., Ewing, P. A., Israelsen, O. W., Rohwer, C., and Scobey, F. C., 1938, Water utilization, in (U.S.) National Resources Committee, Regional Planning part VI—The Rio Grande joint investigations *in* the upper Rio Grande Basin in Colorado, New Mexico, and Texas, 1936–37: U.S. Government Printing Office v. 1, p. 293–427.

Bryan, K., 1938, Geology and ground-water conditions of the Rio Grande depression in Colorado and New Mexico, in (U.S.) National Resources Committee, Regional Planning part VI—The Rio Grande joint investigations in the upper Rio Grande Basin in Colorado, New Mexico, and Texas, 1936–37: U.S. Government Printing Office v. 1, p. 197–225.

Bureau of Reclamation, 1973, Progress report—Phreatophyte investigations—Bernardo evapotranspirometers: Middle Rio Grande Project Office, 50 p.

Cole, J.C., ed., 2001a, U.S. Geological Survey Middle Rio Grande Basin Study—Proceedings of the Fourth Annual Workshop, Albuquerque, New Mexico, February 2000: U.S. Geological Survey Open-File Report 00-488, 51 p.

Cole, J.C., 2001b, 3-D geologic modeling of regional hydrostratigraphic units in the Albuquerque segment of the Rio Grande rift, *in* Cole, J. C., ed., U.S. Geological Survey: Middle Rio Grande Basin Study—Proceedings of the Fourth Annual Workshop, Albuquerque, New Mexico, February 15–16, 2000, U.S. Geological Survey Open-File Report 00-488, p. 26–28.

Connell, S.D., Allen, B.D., and Hawley, J.W, 1998, Subsurface stratigraphy of the Santa Fe Group from borehole geophysical logs, Albuquerque area, New Mexico: New Mexico Geology, v. 20, no. 1, p. 2–7.

Constantz, J., 1998, Measurements of tributary, inter-arroyo, and mountain-front recharge on the Santa Fe River, Bear Canyon, and Abo Arroyo, New Mexico, *in* Slate, J.L., ed., 1998, U.S. Geological Survey Middle Rio Grande Basin Study—Proceedings of the Second Annual Workshop, Albuquerque, New Mexico, February 10–11, 1998: U.S. Geological Survey Open-File Report 98-337, p. 55–56.

Cooley, R.L., and Naff, R.L., 1990, Regression modeling of ground-water flow: U.S. Geological Survey Techniques of Water Resources Investigations, book 3, chap. B4, 232 p.

Cummins, B., 1997, Middle Rio Grande Water Assessment—Drilling, logging, monitoring, well installation, hydraulic conductivity tests, and infiltration gallery feasibility evaluation technical memoranda: U.S. Bureau of Reclamation, Albuquerque Area Office, Supporting document number 8, variously paged.

Deszcz-Pan, M., Rodriguez, B.D., Sawyer, D.A., Stone, B.D., Godbout, M., Doucette, J., Grauch, V. J. S., and Labson, V. F. , 1999, Application of electromagnetic surveys to geologic and hydrologic problems in the Middle Rio Grande Basin area, *in* Bartolino, J.R., ed., U.S. Geological Survey Middle Rio Grande Basin Study—Proceedings of the Third Annual Workshop, Albuquerque, New Mexico, February 24–25, 1999: U.S. Geological Survey Open-File Report 99-203, p. 35–36.

Driscoll, F. G., 1986, Groundwater and wells: Johnson Filtration Systems Inc., St. Paul, Minn., 1,089 p.

Freeze, R.A., and Cherry, J.A., 1979, Groundwater: Englewood Cliffs, Prentice-Hall, N.J., 604 p.

Frenzel, P.F., 1995, Geohydrology and simulation of ground-water flow near Los Alamos, north-central New Mexico: U.S. Geological Survey Water-Resources Investigations Report 95-4091, 92 p.

Frenzel, P.F., and Lyford, F.P., 1982, Estimates of vertical hydraulic conductivity and regional ground-water flow rates in rocks of Jurassic and Cretaceous age, San Juan Basin, New Mexico and Colorado: U.S. Geological Survey Water-Resources Investigations Report 82-4015, 59 p.

Giles, M.R., 1997, Diagenesis: A quantitative perspective—Implications for basin modeling and rock property prediction: Dorcrecht, Kluwer Academic Publishers, 526 p.

Gould, J., 1997, Middle Rio Grande Water Assessment—Middle Rio Grande channel permeameter investigations: U.S. Bureau of Reclamation, Albuquerque Area Office, supporting document number 11, variously paged.

Grauch, V.J.S., Sawyer, D.A., Keller, G.R., and Gillespie, C.L., 2001, Contributions of gravity and aeromagnetic studies to improving the understanding of the subsurface hydrogeology, Middle Rio Grande Basin, New Mexico. In Cole, J.C., ed., U.S. Geological Survey Middle Rio Grande Basin Study—Proceedings of the Fourth Annual Workshop, Albuquerque, New Mexico, February 15–16, 2000: U.S. Geological Survey Open-File Report 00-488, p. 3–4.

Haneberg, W.C., 1995, Depth-porosity relationships and virgin specific storage estimates for the upper Santa Fe Group aquifer system, central Albuquerque Basin, New Mexico: New Mexico Geology, v. 17, no. 4, p. 62–71.

Hawley, J.W., and Grant, P.R., Jr., 1997, Boundaries of the Albuquerque geohydrologic basin, north-central New Mexico [abs.]: New Mexico Geology, v. 19, no. 2, p. 60.

Hawley, J.W., and Haase, C.S., 1992, Hydrogeologic framework of the northern Albuquerque Basin: Socorro, New Mexico Bureau of Mines and Mineral Resources, Open-File Report 387, variously paginated.

Hawley, J.W., Haase, C.S., and Lozinsky, R.P., 1995, An underground view of the Albuquerque Basin, *in* Ortega-Klett, C.P., ed., The water future of Albuquerque and Middle Rio Grande Basin: Proceedings of the 39th Annual New Mexico Water Conference, November 3–4, 1994, New Mexico Water Resources Research Institute WRRI Report No. 290, p. 37–55.

Hearne, G.A., and Dewey, J. D., 1988, Hydrologic analysis of the Rio Grande Basin north of Embudo, New Mexico, Colorado and New Mexico: U.S. Geological Survey Water-Resources Investigations Report 86-4113, 244 p.

Hill, M.C., 1990, Preconditioned conjugate-gradient 2 (PCG2), a computer program for solving ground-water flow equations: U.S. Geological Survey Water-Resources Investigations Report 90-4048, 43 p.

Hill, M.C., 1992, A computer program (MODFLOWP) for estimating parameters of a transient, three-dimensional, ground-water flow model using nonlinear regression: U.S. Geological Survey Open-File Report 91-484, 358 p.

Hill, M.C., 1998, Methods and guidelines for effective model calibration: U.S. Geological Survey Water-Resources Investigations Report 98-4005, 90 p.

Hudson, M.R., Minor, S. A., Grauch, V.J.S., and Personius, S.F., 1999, Preliminary characterization of faults in the Middle Rio Grande Basin, *in* Bartolino, J. R., ed., 1999, U.S. Geological Survey Middle Rio Grande Basin Study—Proceedings of the Third Annual Workshop, Albuquerque, New Mexico, February 24–25, 1999: U.S. Geological Survey Open-File Report 99-203, p. 40–41.

Kalin, R.M., 2000, Radiocarbon dating of groundwater systems, *in* Cook, P. G., and Herczeg, A. L., eds., Environmental Tracers in Subsurface Hydrology: Boston, Kluwer Academic Publishers, p. 111–144.

Kelley, V.C., 1977, Geology of the Albuquerque Basin, New Mexico: Socorro, New Mexico Bureau of Mines and Mineral Resources Memoir 33, 60 p.

Kelley, V.C., and Kudo, A.M., 1978, Volcanoes and related basalts of Albuquerque Basin, New Mexico: Socorro, New Mexico Bureau of Mines and Mineral Resources, Circular 156, 29 p.

Kernodle, J.M., 1998, Simulation of ground-water flow in the Albuquerque Basin, Central New Mexico, 1901–1995, with projections to 2020: U.S. Geological Survey Water-Resources Investigations Report 96-209, 54 p.

Kernodle, J.M., McAda, D.P., and Thorn, C.R., 1995, Simulation of ground-water flow in the Albuquerque Basin, Central New Mexico, 1901–1994, with projections to 2020: U.S. Geological Survey Water-Resources Investigations Report 94-4251, 114 p.

Kernodle, J. M., Miller, R. S., and Scott, W. B., 1987, Three-dimensional model simulation of transient ground-water flow in the Albuquerque-Belen Basin, New Mexico: U.S. Geological Survey Water-Resources Investigations Report 86-4194, 86 p.

Kernodle, J. M., and Scott, W. B., 1986, Three-dimensional model simulation of steady-state ground-water flow in the Albuquerque-Belen Basin, New Mexico: U.S. Geological Survey Water-Resources Investigations Report 84-4353, 58 p.

Lee, W. T., 1907, Water resources of the Rio Grande Valley in New Mexico and their development: U.S. Geological Survey Water-Supply Paper 188, 59 p.

Logan, L. M., 1990, Geochemistry of the Albuquerque municipal area, Albuquerque, New Mexico: Socorro, New Mexico Institute of Mining and Technology, Independent study, 234 p.

Love, D. W., Reynolds, C. B., Hallett, B., Lozinsky, R. P., and Niemyjski, T., 1994, Sedimentation, deformation, and erosion related to Los Lunas volcanoes, central New Mexico (abs.): New Mexico Geology, v. 16, no. 3, p. 57.

Lozinsky, R.P., 1988, Stratigraphy, sedimentology, and sand petrology of the Santa Fe Group and pre-Santa Fe Tertiary deposits in the Albuquerque basin, central New Mexico: Socorro, New Mexico Tech, Ph.D. dissertation, 298 p.

Lozinsky, R.P., 1994, Cenozoic stratigraphy, sandstone petrology, and depositional history of the Albuquerque basin, central New Mexico, *in* Keller, G.R., and Cather, S.M., eds., Basins of the Rio Grande rift: Geological Society of America, Special Paper 291, p. 73–82.

Machette, M.N., Personius, S.F., Kelson, K.I., Haller, K.M., and Dart, R.L., 1998, Map and data for Quaternary faults in New Mexico: U.S. Geological Survey Open-File Report 98-521, 443 p.

McAda, D. P., 1996, Plan of study to quantify the hydrologic relations between the Rio Grande and the Santa Fe Group aquifer system near Albuquerque, central New Mexico: U.S. Geological Survey Water-Resources Investigations Report 96-4006, 58 p.

McAda, D. P., Barroll, P., and Sanford, W. E., 2001, Revision of the ground-water flow model of the Middle Rio Grande Basin, New Mexico, *in* Cole, J. C., ed., U.S. Geological Survey Middle Rio Grande Basin study—Proceedings of the Fourth Annual Workshop, Albuquerque, New Mexico, February 15–16, 2000: U.S. Geological Survey Open-File Report 00-488, p. 29–30.

McAda, D. P., and Barroll, P., 2002, Simulation of ground-water flow in the Middle Rio Grande Basin between Cochiti and San Acacia, New Mexico: U.S. Geological Survey Water-Resources Investigations Report 02-4200, 81 p.

McAda, D.P., and Wasiolek, M., 1988, Simulation of the regional hydrology of the Tesuque aquifer system near Santa Fe, New Mexico: U.S. Geological Survey Water-Resources Investigations Report 87-4056, 71 p.

McDonald, M. G., and Harbaugh, A. W., 1988, A modular three-dimensional finite-difference ground-water flow model: U.S. Geological Survey Techniques of Water-Resources Investigations, book 6, chap. A1, variously paged.

Medina, A., and Carrera, J., 1996, Coupled estimation of flow and solute transport parameters: Water Resources Research, v. 32, p. 3,063–3,076.

Meeks, T.O., 1949, The occurrence of ground water in the Tijeras Soil Conservation District, Bernalillo County, New Mexico: U.S. Department of Agriculture Regional Bulletin 109, Geological Series I. Soil Conservation Service Region 6, variously paged.

Minor, S.A., and Shock, N.A., 1998, Results from the Cochiti and Santo Domingo Pueblos, *in* Slate, J.L., ed., 1998, U.S. Geological Survey Middle Rio Grande Basin Study—Proceedings of the Second Annual Workshop, Albuquerque, New Mexico, February 10–11, 1998: U.S. Geological Survey Open-File Report 98-337, p. 22–23.

Nimmo, J.R., 1997, Recharging fluxes through layered alluvium—Centrifuge hydraulic property measurements interpreted by Darcian flow simulation, *in* Bartolino, J.R., ed., U.S. Geological Survey Middle Rio Grande Basin Study—Proceedings of the First Annual Workshop, Denver, Colorado, November 12–14, 1996: U.S. Geological Survey Open-File Report 97-116, p. 45.

Plummer, L.N., Bexfield, L.M., Anderholm, S.K., Sanford, W.E., and Busenberg, E., 2004, Geochemical characterization of ground-water flow in the Santa Fe Group aquifer system, Middle Rio Grande Basin, New Mexico: U.S. Geological Survey Water-Resources Investigations Report 03-4131, 395 p.

Poeter, E.P., and Hill, M.C., 1997, Inverse models—A necessary next step in groundwater modeling: Ground Water, v. 35, no. 2, p. 250–260.

Poeter, E.P., and Hill, M.C., 1998, Documentation of UCODE, a computer code for universal inverse modeling: U.S. Geological Survey Water-Resources Investigations Report 98-4080, 116 p.

Pollock, D.W., 1994, User's guide for MODPATH/MODPATH-PLOT, version 3—A particle tracking post-processing package for MODFLOW, the U.S. Geological Survey finite-difference ground-water flow model: U.S. Geological Survey Open-File Report 94-464, variously paged.

Raymo, M.E., and Ruddiman, W.F., 1992, Tectonic forcing of late Cenozoic climate: Nature, v. 359, no. 6391, p. 117–122.

Rodriguez, B.D., Deszcz-Pan, M., Sawyer, D., and Stone, B.D., 2001, Subsurface constraints on the hydrogeologic model of the Middle Rio Grande Basin, New Mexico, using airborne time-domain electromagnetic data, *in* Cole, J.C., ed., U.S. Geological Survey Middle Rio Grande Basin Study—Proceedings of the fourth Annual Workshop, Albuquerque, New Mexico, February 15–16, 2000: U.S. Geological Survey Open-File Report 00-488, p. 20–23.

Sanford, W.E., Plummer, N.L., and Bexfield, L.M., 1998, Using environmental tracer data to improve the U.S. Geological Survey MODFLOW model of the Middle Rio Grande Basin, *in* Slate, J. L., ed., U.S. Geological Survey Middle Rio Grande Basin Study—Proceedings of the Second Annual Workshop, Albuquerque, New Mexico, February 10–11, 1998: U.S. Geological Survey Open-File Report 98-337, p. 13–14.

Sanford, W. E., Plummer, N.L., McAda, D. P., Bexfield, L. M., and Anderholm, S. K., 2001, Estimation of hydrologic parameters for the ground-water model of the Middle Rio Grande Basin using carbon-14 and water-level data, *in* Cole, J. C., ed., U.S. Geological Survey Middle Rio Grande Basin Study—Proceedings of the Fourth Annual Workshop, Albuquerque, New Mexico, February 15–16, 2000: U.S. Geological Survey Open-File Report 00-488, p. 4–6.

Stewart, A.E., and Constantz, J., 2000, Determination of streamflow patterns to estimate stream loss along Abo Arroyo, New Mexico, *in* Cole, J. C., ed., U.S. Geological Survey Middle Rio Grande Basin Study—Proceedings of the Fourth Annual Workshop, Albuquerque, New Mexico, February 15–16, 2000: U.S. Geological Survey Open-File Report 00-488, p. 35–37.

Stone, B.D., 2001, Sedimentary, stratigraphic, and hydrologic consequences of syn-depositional faulting in the Rio Grande rift, *in* Cole, J.C., ed., U.S. Geological Survey Middle Rio Grande Basin Study—Proceedings of the Fourth Annual Workshop, Albuquerque, New Mexico, February 15–16, 2000: U.S. Geological Survey Open-File Report 00-488, p. 14–18.

Stone, B.D., and Allen, B.D., 1998, The 98th Street core—Key to analysis of Santa Fe Group stratigraphy and hydrogeology in the central Middle Rio Grande Basin, in Slate, J. L., ed., U.S. Geological Survey Middle Rio Grande Basin Study—Proceedings of the Second Annual Workshop, Albuquerque, New Mexico, February 10–11, 1998: U.S. Geological Survey Open-File Report 98-337, p. 41–46.

Stone, B.D., Cole, J.C., and Sawyer, D.A., 2001, Regional stratigraphic framework of the three-dimensional geologic model of the Rio Grande rift, *in* Cole, J.C., ed., U.S. Geological Survey Middle Rio Grande Basin Study—Proceedings of the Fourth Annual Workshop, Albuquerque, New Mexico, February 15–16, 2000: U.S. Geological Survey Open-File Report 00-488, p. 11–13.

Stonestrom, D.A., and Atkins, K.C., 1998, Environmental tracers of recharge at Abo Arroyo, Bear Canyon, and the Santa Fe River, Middle Rio Grande Basin, New Mexico, *in* Slate, J.L., ed., U.S. Geological Survey Middle Rio Grande Basin Study—Proceedings of the Second Annual Workshop, Albuquerque, New Mexico, February 10–11, 1998: U.S. Geological Survey Open-File Report 98-337, p. 57–59.

Stuiver, M., Reimer, P.J., Bard, E., Beck, J.W., Burr, G., Hughen, K.A., Kromer, B., McCormac, F.G., van der Plicht, J., and Spurk, M., 1998, INTCAL98 Radiocarbon age calibration, 24,000-0 cal BP: Radiocarbon, v. 40, no. 3, p. 1041.

Thompson, C.L., Stewart, A.E., and Constantz, J., 1999, Comparison of methods to determine infiltration and percolation rates along a reach of the Santa Fe River near La Bajada, New Mexico, *in* Bartolino, J.R., ed., 1999, U.S. Geological Survey Middle Rio Grande Basin Study—Proceedings of the Third Annual Workshop, Albuquerque, New Mexico, February 24–25, 1999: U.S. Geological Survey Open-File Report 99-203, p. 75–76.

Thorn, C.R., McAda, D.P., and Kernodle, J.M, 1993, Geohydrologic framework and hydrologic conditions in the Albuquerque Basin, central New Mexico: U.S. Geological Survey Water-Resources Investigations Report 93-4149, 106 p.

Tiedeman, C. R., Kernodle, J. M., and McAda, D. P., 1998, Application of nonlinear-regression methods to a ground-water flow model of the Albuquerque Basin, New Mexico: U.S. Geological Survey Water-Resources Investigations Report 98-4172, 90 p.

Titus, F. B., 1963, Geology and ground-water conditions in eastern Valencia County, New Mexico: Socorro, New Mexico Bureau of Mines and Mineral Resources Ground-Water Report 7, 113 p.

Waltemeyer, S. D., 1994, Methods for estimating streamflow at mountain fronts in southern New Mexico: U.S. Geological Survey Water-Resources Investigations Report 93-4213, 17 p.

Willis, W. S., 1993, Middle Rio Grande ground-water studies: Bureau of Reclamation, Middle Rio Grande Water Assessment, Technical Memorandum, June 30, 1993, variously paged.

Zhu, C., 2000, Estimate of recharge from radiocarbon dating of groundwater and numerical flow and transport modeling: Water Resources Research, v. 36, no. 7, p. 2,607–2,620.

Zhu, C., Winterle, J. R., and Love, E. I., 2003, Late Pleistocene and Holocene groundwater recharge from the chloride mass balance method and chlorine-36 data: Water Resources Research, v. 39., no. 7, 15 p., DOI 10.1029/2003WR001987.

Table A1. Information on wells from which water levels were used in the calibration of the ground-water-flow model.

Well name	Latitude	Longitude	Row number	Column number	Model layer	Well depth (feet)	Top of screen (feet)	Bottom of screen (feet)	Altitude of land surface (feet)	Depth to water (feet)	Altitude of water level (feet)	Water-level uncertainty (feet)
1940s Gentry #103	350108	1063542	73	47	1	215	200	210	5,150	195	4,955	10
1950s 4-Hills	350317	1063009	69	56	5	1,200	800	1,200	5,600	616	4,984	14
1950s Abo Arroyo 1	343205	1064150	127	38	1	173	168	173	4,957	169	4,788	12
1950s Abo Arroyo 2	343048	1064256	129	36	2	163	140	160	4,885	100	4,785	12
1950s Belen east 1	344132	1064421	110	34	2	80	20	70	4,814	7	4,807	12
1950s Belen east 2	344048	1063825	111	43	2	300	245	295	5,060	239	4,821	12
1950s Belen east 3	343910	1063955	114	41	2	260	235	255	5,019	209	4,810	12
1950s Belen north 1	344340	1064612	106	31	3	100	40	90	4,825	10	4,815	14
1950s Belen north 2	344300	1064343	107	35	3	105	20	105	4,819	8	4,811	10
1950s Belen north 3	344252	1064659	107	30	3	160	100	150	4,833	21	4,812	12
1950s Belen north 4	344147	1065029	109	25	3	556	500	550	5,231	418	4,814	12
1950s Belen south 1	343745	1064710	117	30	1	96	75	95	4,875	75	4,800	12
1950s Belen south 2	343635	1064630	119	31	3	100	40	90	4,785	8	4,777	10
1950s Belen south 3	343510	1064455	121	33	2	38	15	35	4,783	5	4,778	12
1950s Belen south 4	343304	1064650	125	30	3	123	30	123	4,769	5	4,764	10
1950s Belen south 5	343207	1064520	127	33	3	93	70	93	4,784	25	4,760	10
1950s Belen west 1	343720	1065055	117	24	3	500	440	490	5,198	393	4,805	12
1950s Belen west 2	343510	1065045	121	24	3	400	485	495	5,178	380	4,798	12
1950s Bernardo	342653	1064758	137	29	3	100	40	90	4,733	6	4,727	12
1950s Burton 5	350359	1063619	68	46	5	1,000	452	1,000	5,317	368	4,949	12
1950s Charles 4	350524	1063522	65	48	2	294	280	290	5,240	279	4,961	12
1950s Corrales N	351526	1063620	47	46	2	84	40	80	5,056	35	5,021	10
1950s Corrales S	351421	1063633	49	46	2	37	15	35	5,020	8	5,012	12
1950s Del Sol	350506	1063729	66	44	3	342	300	340	5,155	203	4,952	12
1950s East Matheson	350730	1063030	61	56	1	277	260	275	5,850	257	5,593	12
1950s HuntersRidge	351235	1063839	52	43	3	100	75	95	4,998	10	4,988	12
1950s Isleta Nest	345645	1064245	81	36	2	50	25	45	4,898	7	4,891	14
1950s Leavitt	350210	1064325	71	35	2	92	75	90	4,990	70	4,920	12
1950s Leyendecker	350853	1063543	59	47	2	302	147	302	5,157	186	4,971	12

Table A1. Information on wells from which water levels were used in the calibration of the ground-water-flow model—Continued.

Well name	Latitude	Longitude	Row number	Column number	Model layer	Well depth (feet)	Top of screen (feet)	Bottom of screen (feet)	Altitude of land surface (feet)	Depth to water (feet)	Altitude of water level (feet)	Water-level uncertainty (feet)
1950s LosLunas central1	345030	1064207	93	37	3	98	63	98	4,859	6	4,853	10
1950s LosLunas central2	344913	1064120	95	39	3	100	75	95	4,851	8	4,843	12
1950s LosLunas central3	344854	1064426	96	34	5	607	200	600	4,878	33	4,845	14
1950s LosLunas central4	344640	1064127	100	38	3	76	25	75	4,836	7	4,829	12
1950s LosLunas east1	344712	1063615	99	46	2	345	324	344	5,165	322	4,843	12
1950s LosLunas east2	344500	1064105	103	39	3	103	50	100	4,838	9	4,829	12
1950s LosLunas south1	344635	1064430	100	34	3	120	60	110	4,838	8	4,830	12
1950s LosLunas south2	344443	1064353	104	35	3	90	30	80	4,828	8	4,820	12
1950s LosLunas west1	344843	1065506	96	18	3	576	550	570	5,350	509	4,841	12
1950s LosLunas west2	344748	1065905	98	12	1	97	75	95	5,048	74	4,974	12
1950s LosLunas west3	344630	1065122	100	23	2	500	479	499	5,310	478	4,833	12
1950s LosLunas west4	344449	1065949	104	11	1	133	110	130	5,118	75	5,044	12
1950s Luz del Sol	350814	1064230	60	37	2	185	160	180	5,118	155	4,963	12
1950s Montano 4	350821	1063901	60	42	5	804	216	804	4,975	13	4,962	12
1950s MontanoNorth	350933	1063919	58	42	2	45	20	40	4,980	7	4,973	12
1950s Nor Este	351033	1063142	56	53	2	736	700	730	5,673	684	4,990	12
1950s North Kirtland	350355	1063344	68	50	4	900	452	900	5,354	401	4,953	12
1950s North La Joya	342215	1065001	145	25	2	100	40	90	4,735	17	4,718	14
1950s North of Isleta	345730	1064310	80	36	2	50	25	45	4,910	14	4,896	14
1950s NW Rio Bravo	350130	1064142	73	38	2	33	10	30	4,930	8	4,922	12
1950s ORL-2	350354	1063922	68	42	2	20	10	20	4,943	7	4,936	12
1950s Paseo2 north	351131	1063816	54	43	3	100	75	95	4,995	7	4,988	12
1950s Paseo2 south	351052	1063807	55	43	3	75	50	70	4,991	7	4,984	12
1950s Paseo2 verys	351012	1063807	56	43	2	60	30	50	4,988	10	4,978	12
1950s Ponderosa	350907	1063306	58	51	2	530	510	530	5,475	507	4,968	12
1950s Rio Puerco 1	343955	1065450	113	18	1	100	92	97	4,920	91	4,829	12
1950s Santa Barbara	350624	1063648	64	46	2	180	173	178	5,135	172	4,963	12
1950s Sierra Vista	350827	1064126	60	38	3	110	75	100	4,999	39	4,960	12

Table A1. Information on wells from which water levels were used in the calibration of the ground-water-flow model—Continued.

Well name	Latitude	Longitude	Row number	Column number	Model layer	Well depth (feet)	Top of screen (feet)	Bottom of screen (feet)	Altitude of land surface (feet)	Depth to water (feet)	Altitude of water level (feet)	Water-level uncertainty (feet)
1950s SisterCities	350930	1063655	58	45	3	110	80	100	4,977	9	4,968	12
1950s South Kirtland	350154	1063254	72	51	4	1,000	454	976	5,379	434	4,945	20
1950s South Matheson	350517	1063144	66	53	5	1,096	596	1,096	5,462	502	4,960	12
1950s Summer	351039	1062956	56	56	1	432	400	425	6,020	396	5,624	12
1950s SWAB 3 area	351045	1063943	55	41	3	74	50	70	4,990	8	4,982	12
1950s Thomas	350819	1063440	60	49	4	996	204	924	5,269	302	4,966	12
1950s VGP-1	345932	1064218	76	37	2	27	10	25	4,915	7	4,908	12
1950s Volandia	350632	1063615	63	46	2	189	175	185	5,140	175	4,965	12
1950s West Atrisco 3	350352	1064234	68	37	2	110	80	100	5,010	75	4,935	12
1950s West Bluff	350605	1064157	64	38	2	162	145	160	5,090	140	4,950	12
1950s West Kirtland	350305	1063647	70	46	5	1,000	395	940	5,303	356	4,947	14
1950s West Mesa 3	350440	1064432	67	34	3	500	300	500	5,220	284	4,936	14
1950s West Matheson	350754	1063321	61	51	5	1,092	624	1,092	5,445	479	4,966	12
98th Street deep	350530	1064452	65	33	7	1,544	1,534	1,539	5,320	422	4,900	2
Belen Airport S	343853	1064941	115	26	3	500	453	483	5,175	370	4,805	2
Cerro Colorado PW	350121	1065208	73	22	5	1,661	1,355	1,655	5,835	898	4,937	7
Domestic Well #06	343748	1065021	117	25	4	700	610	625	5,190	385	4,805	5
Domestic Well #08	342516	1064300	140	36	2	400	320	360	5,020	280	4,740	5
Domestic Well #09	343024	1064431	130	34	4	400	340	350	4,900	150	4,750	5
Domestic Well #10	343634	1064951	119	26	4	700	637	657	5,175	400	4,775	5
Domestic Well #11	343323	1063825	125	43	3	400	337	352	5,060	240	4,820	5
Domestic Well #12	344851	1064928	96	26	5	1,000	965	980	5,363	530	4,833	5
Domestic Well #13	344832	1063616	97	46	4	600	580	600	5,160	320	4,840	5
Domestic Well #20	344629	1063827	100	43	4	400	348	368	5,050	220	4,830	5
Domestic Well #27	350949	1064242	57	36	2	240	230	240	5,196	229	4,967	12
Domestic Well #29	344818	1064007	97	40	4	300	200	210	4,890	55	4,835	5
Domestic Well #31	350204	1065623	72	16	1	150	125	145	5,280	75	5,205	14
Domestic Well #32	342010	1065043	149	24	2	200	36	56	4,730	20	4,710	5
Domestic Well #35	342513	1065003	140	25	3	107	99	106	4,739	12	4,727	5

Table A1. Information on wells from which water levels were used in the calibration of the ground-water-flow model—Continued.

Well name	Latitude	Longitude	Row number	Column number	Model layer	Well depth (feet)	Top of screen (feet)	Bottom of screen (feet)	Altitude of land surface (feet)	Depth to water (feet)	Altitude of water level (feet)	Water-level uncertainty (feet)
Domestic Well #36	343706	1064223	118	37	4	375	353	373	4,980	200	4,780	5
Domestic Well #37	352121	1062855	36	57	2	100	75	95	5,130	23	5,107	5
Domestic Well #38	353329	1062040	13	70	3	138	131	138	5,225	24	5,201	5
Domestic Well #39	350953	1064103	57	39	2	184	160	180	5,125	154	4,971	12
Grasslands R	345000	1064555	94	32	2	200	175	195	4,990	140	4,850	2
Isleta Deep	345650	1064159	81	38	7	1,340	1,330	1,335	4,900	18	4,882	2
McLaughlin T	343428	1063833	123	43	3	400	335	355	5,052	253	4,799	2
MRN-1 (assume 40 ft dd)	345848	1063357	78	50	4	607	547	587	5,320	380	4,940	14
NM Highway Department	341839	1065316	152	20	1	212	173	212	4,900	168	4,732	5
Northeastern Well #01	353639	1062109	7	69	3	200	175	195	5,284	67	5,217	12
Northeastern Well #02	353622	1062451	8	63	2	650	625	645	5,820	589	5,231	12
Northeastern Well #03	353535	1061422	10	79	1	400	375	395	5,615	286	5,329	12
Northeastern Well #04	353610	1061656	8	76	1	200	175	195	5,461	110	5,351	12
Private Production Well #01	350336	1064751	69	29	4	1,292	820	1,290	5,725	834	4,891	7
Private Production Well #02	345205	1063942	90	41	2	100	80	90	4,905	37	4,868	12
Private Production Well #05	342608	1064647	138	30	4	300	238	258	4,757	19	4,738	5
Private Production Well #08	343103	1064827	129	28	4	300	224	249	4,830	92	4,738	2
Private Production Well #14	353041	1064255	18	36	1	10	5	10	5,390	5	5,385	10
Private Production Well #16	350112	1064902	73	27	5	1,350	1,242	1,292	5,680	781	4,899	7
Rabbit Hill	353533	1064253	9	36	1	220	195	215	5,655	102	5,553	10
Rio Grande Utility 5	343940	1064238	113	37	5	700	290	660	4,960	160	4,800	7
Rio Rancho Well 13	351630	1064812	45	28	5	1,920	1,343	1,721	6,055	1,101	4,954	12
Rio Rancho Well 15	352117	1064057	36	39	5	1,300	820	1,290	5,794	775	5,019	12
Rio Rancho Well 2	351340	1064014	50	40	5	751	508	751	5,266	295	4,971	12
Rio Rancho Well 7	351611	1064211	45	37	5	1,197	898	1,183	5,652	718	4,934	12
Rio Rancho Well 8	351653	1064353	44	35	5	1,618	982	1,599	5,827	880	4,947	12
Rio Rancho Well 9	351906	1064706	40	30	5	1,540	1,220	1,520	6,054	1,082	4,972	12
San Felipe B	352420	1062446	30	64	4	500	475	495	5,320	100	5,220	12

Table A1. Information on wells from which water levels were used in the calibration of the ground-water-flow model—Continued.

Well name	Latitude	Longitude	Row number	Column number	Model layer	Well depth (feet)	Top of screen (feet)	Bottom of screen (feet)	Altitude of land surface (feet)	Depth to water (feet)	Altitude of water level (feet)	Water-level uncertainty (feet)
Sandia ECW 2 E	351556	1063159	46	53	1	305	300	305	5,357	298	5,059	10
Sevilleta V	342107	1065304	147	21	3	300	210	220	4,860	137	4,723	2
Soil Amendment Facility	350854	1064927	59	26	5	1,463	1,116	1,429	5,866	922	4,944	7
Solar Powered Well	353842	1061655	4	76	1	600	575	595	5,895	534	5,361	12
SWAB 1	350449	1064931	66	26	4	1,200	980	1,179	5,775	862	4,913	5
SWAB 3 D	351051	1063953	55	41	6	1,100	870	1,050	4,995	23	4,962	5
SWAB 3 S	351051	1063953	55	41	5	1,100	350	590	4,995	23	4,968	5
SWAB2 D USGS F	351046	1064647	55	30	6	1,800	1,525	1,795	5,730	770	4,960	5
SWAB2 S USGS F	351046	1064647	55	30	3	1,800	800	955	5,730	780	4,950	5
Tierra Mirage D	351852	1062945	40	56	4	703	650	700	5,484	481	5,055	5
Tome Deep	344431	1063934	104	41	6	1,200	1,185	1,195	5,020	195	4,825	2
Volcano Cliffs H	351000	1064340	57	35	3	500	400	500	5,325	365	4,960	5
Windmill #03	343447	1065545	122	17	1	300	243	263	5,035	225	4,810	5
Windmill #04	345345	1064513	87	33	2	175	150	175	5,016	150	4,866	10
Windmill #05	345406	1065030	86	25	2	620	600	620	5,470	599	4,871	10
Windmill #07	345218	1070018	90	10	1	212	190	210	5,125	134	4,991	10
Windmill #09	352759	1063627	24	46	1	637	615	635	5,725	585	5,140	10
Windmill #10	343649	1065738	118	14	2	500	388	428	5,188	371	4,817	5
Windmill #17	342707	1065325	136	20	1	61	40	60	4,786	35	4,751	5
Windmill #18	342924	1065505	132	18	1	143	120	140	4,889	113	4,776	5
Windmill #23	343839	1070244	115	6	1	620	560	610	5,401	546	4,856	12
Windmill #31	343146	1065340	123	21	1	100	75	95	4,862	53	4,809	12
Windmill #33	343230	1065707	126	15	2	300	269	279	5,015	207	4,808	5
Windmill #34	344945	1063726	94	45	4	440	415	435	5,145	313	4,832	10
Windmill #35	345132	1065452	91	18	3	700	675	695	5,423	580	4,843	10
Windmill #37	353805	1062329	5	65	1	200	175	195	5,535	151	5,384	12
Windmill #41	352542	1064203	28	37	1	448	425	445	5,595	373	5,222	10
Windmill #42	352804	1064142	23	38	1	200	175	195	5,390	85	5,305	12
Windmill #43	353230	1063440	15	49	2	1,109	1,080	1,100	6,233	1,005	5,228	10

Table A1. Information on wells from which water levels were used in the calibration of the ground-water-flow model—Continued.

Well name	Latitude	Longitude	Row number	Column number	Model layer	Well depth (feet)	Top of screen (feet)	Bottom of screen (feet)	Altitude of land surface (feet)	Depth to water (feet)	Altitude of water level (feet)	Water-level uncertainty (feet)
Windmill #45	353340	1062547	13	62	4	600	575	595	5,635	546	5,089	12
Windmill #46	353013	1063158	19	53	1	700	650	700	5,930	650	5,280	50
Windmill #47	344939	1063426	95	49	2	500	475	495	5,295	451	4,844	12
Windmill #48	345111	1064641	92	31	3	250	225	245	5,030	189	4,841	12
Windmill #49	345144	1064515	91	33	2	184	160	180	4,995	132	4,863	10
Windmill #50	345235	1063844	89	43	2	123	100	120	4,977	115	4,862	10
Windmill #51	345314	1064255	88	36	2	50	25	45	4,880	13	4,867	12
Windmill #52	345421	1065358	86	19	4	885	860	880	5,504	654	4,850	10
Windmill #53	345442	1064107	85	39	2	23	10	20	4,890	5	4,885	10
Windmill #54	345511	1064207	84	37	3	138	57	134	4,890	10	4,880	8
Windmill #55	345522	1063537	84	47	1	440	312	323	5,221	317	4,904	10
Windmill #56	345604	1064130	83	38	3	102	20	96	4,890	10	4,880	8
Windmill #57	345629	1064304	82	36	3	260	235	255	5,071	184	4,887	10
Windmill #58	345643	1064723	81	29	2	430	400	420	5,273	387	4,886	10
Windmill #59	345207	1063535	90	47	2	445	425	440	5,260	427	4,833	10
Windmill #60	345046	1064945	92	26	2	437	420	435	5,263	420	4,843	10
Windmill #61	345158	1064819	90	28	2	401	375	395	5,230	352	4,878	10
Windmill #62	345427	1065505	86	18	1	780	755	775	5,665	687	4,978	10
Windmill #63	345442	1070026	85	10	1	271	245	265	5,143	128	5,015	10
Windmill #64	345225	1065558	89	16	2	720	695	715	5,570	601	4,969	10
Windmill #65	345556	1063834	83	43	3	442	415	435	5,260	381	4,879	10
Windmill #66	345433	1063854	85	42	3	460	432	456	5,235	356	4,879	10
Windmill #67	345111	1063707	92	45	2	355	340	350	5,160	318	4,842	10
Windmill #68	345610	1064513	82	33	1	378	355	375	5,260	339	4,921	10
Windmill #69	351504	1063418	47	49	2	96	61	96	5,060	35	5,025	8
Windmill #70	351716	1063433	43	49	1	40	50	50	5,035	7	5,028	10
Windmill #71	352003	1063431	38	49	2	230	205	225	5,265	192	5,073	10
Windmill #72	352003	1063120	38	54	4	212	190	210	5,085	22	5,063	10

Table A1. Information on wells from which water levels were used in the calibration of the ground-water-flow model—Continued.

Well name	Latitude	Longitude	Row number	Column number	Model layer	Well depth (feet)	Top of screen (feet)	Bottom of screen (feet)	Altitude of land surface (feet)	Depth to water (feet)	Altitude of water level (feet)	Water-level uncertainty (feet)
Windmill #73	352323	1063630	32	46	1	183	160	180	5,280	140	5,140	10
Windmill #74	352443	1063157	30	53	2	620	600	620	5,670	585	5,085	8
Windmill #75	352447	1063930	29	41	1	370	350	370	5,585	340	5,245	10
Windmill #76	352558	1063630	27	46	2	260	235	355	5,350	138	5,212	10
Windmill #77	352614	1063940	27	41	1	133	110	130	5,370	102	5,268	10
Windmill #78	352742	1063453	24	48	3	1,274	1,250	1,270	6,297	1,090	5,207	10
Windmill #79	352813	1063931	23	41	1	43	36	43	5,320	19	5,301	8
Windmill #80	352938	1063640	20	46	1	670	650	668	5,780	625	5,155	8
Windmill #81	352307	1062756	32	59	5	550	525	545	5,120	24	5,096	10
Windmill #82	352448	1062946	29	56	2	500	475	495	5,542	458	5,084	12
Windmill #83	352616	1062525	27	63	5	549	524	544	5,220	78	5,142	8
Windmill #84	353008	1062049	19	70	5	775	750	770	5,360	201	5,159	10
Windmill #85	353037	1061902	19	72	1	68	43	64	5,275	53	5,222	10
Windmill #86	353129	1062212	17	67	3	82	47	77	5,185	6	5,179	8
Windmill #87	352653	1062119	26	69	2	400	375	395	5,505	361	5,144	12
Windmill #88	353159	1062724	16	60	3	600	575	595	5,645	521	5,124	12
Windmill #89	353326	1063022	13	55	3	800	775	795	5,855	711	5,144	12
Windmill #90	353650	1062932	7	56	1	1,100	1,075	1,095	6,375	998	5,377	12
Windmill #91	352749	1061859	24	72	1	450	425	445	5,610	373	5,237	12
Windmill #92	353139	1061435	17	79	1	300	275	295	5,600	217	5,383	12
Windmill #93	353208	1064350	16	35	1	380	365	380	5,690	305	5,385	8
Windmill #94	353226	1064045	15	39	1	503	475	495	5,770	376	5,394	10
Windmill #95	353232	1063638	15	46	1	800	775	795	6,090	770	5,320	10
Windmill #96	353355	1063856	13	42	1	727	715	725	5,970	667	5,303	8
Windmill #97	353337	1064157	13	38	1	577	555	575	5,890	507	5,383	10
Windmill #98	353415	1064430	12	34	1	275	250	270	5,590	118	5,472	10
Windmill #99	352525	1064557	28	32	2	850	825	845	5,880	777	5,103	12
Windmill #100	351336	1063159	50	53	3	628	600	625	5,565	571	4,994	12
Windmill #101	341854	1065747	152	14	1	100	40	90	4,897	13	4,884	14

Table A2. Information on wells from which ^{14}C activities were used in the ground-water-flow model calibration.

Well Name	Latitude	Longitude	Row number	Column number	No. of path lines	Model layer(s)	Well depth (feet)	Depth to screen top (feet)	Depth to screen bottom (feet)	Screen length (feet)	Carbon-14 (pmC)	Uncertainty (pmC)	Raw C-14 age (years)	Implied Ao from reactions (pmC)	Corrected age (calendar years)
4 Hills-1	350340	1062940	69	55	1	1	70	25	65	40	93.95	6.0	516	93.95	0
98th St D	350530	1064452	65	33	1	6	1,544	1,534	1,539	5	0.13	0.1	54,935	63.15	51,135
98th St MD	350530	1064452	65	33	1	5	1,112	1,102	1,107	5	3.69	0.6	27,276	106.42	27,791
98th St MS	350530	1064452	65	33	1	4	749	739	744	5	0.79	0.8	40,018	82.70	38,448
98th St S	350530	1064452	65	33	1	2	438	388	433	45	43.25	6.0	6,929	91.94	6,234**
Belen 4	343917	1064747	115	28	3	3–4	504	150	504	354	14.55	3.5	15,935	126.57	17,882
Belen 5	344017	1064754	113	28	1	4	600	435	600	165	16.37	2.0	14,960	128.28	17,019
Burton 2	350421	1063613	67	46	4	3–5	857	425	845	420	47.73	5.0	6,114	107.04	6,677
Burton 5	350355	1063517	69	48	5	4–5	1,170	550	1,150	600	44.66	7.0	6,664	108.35	7,327
CEPC 02	353736	1062104	6	68	1	4	320	270	315	45	21.32	2.0	12,776	120.93	14,347
Cerro Colorado Landfill PW	350121	1065208	73	21	3	5	1,661	1,355	1,655	300	7.35	2.0	21,580	128.84	23,675
Charles 4	350559	1063339	64	50	5	3–5	1,055	456	1,032	576	51.39	7.0	5,503	105.68	5,960
College 2	350647	1064400	64	34	10	4–6	1,605	550	1,564	1,014	5.39	2.0	24,144	102.24	24,327
Coronado 1	351023	1063418	56	49	7	4–6	1,186	479	1,184	705	32.77	7.0	9,223	104.02	9,549
Del Sol D	350534	1063547	66	47	1	6	1,567	1,557	1,562	5	6.20	0.6	22,986	131.78	25,268
Del Sol M	350534	1063547	66	47	1	5	842	832	837	5	13.65	1.1	16,462	117.83	17,819
Del Sol S	350534	1063547	66	47	1	3	425	315	415	100	62.21	4.0	3,924	97.33	3,700
Domestic Well #03	344451	1063734	103	44	1	4	480	460	480	20	21.00	2.0	12,901	119.87	14,400
Domestic Well #05	351901	1063458	40	48	1	4	330	320	330	10	27.00	2.7	10,824	99.32	10,767
Domestic Well #06	343748	1065021	118	24	1	4	635	635	635	0	36.45	2.7	8,343	62.46	4,452
Domestic Well #07	350955	1063003	58	56	1	1	600	570	590	20	97.48	2.5	211	99.41	162
Domestic Well #08	342516	1064260	140	35	1	2	360	320	360	40	12.99	1.1	16,872	125.10	18,723
Domestic Well #09	343025	1064431	131	34	1	4	350	340	350	10	31.10	1.2	9,655	111.90	10,585
Domestic Well #10	343634	1064951	120	25	1	4	657	637	657	20	54.73	5.5	4,983	54.73	0
Domestic Well #11	343323	1063826	125	42	1	2	352	337	352	15	8.33	0.8	20,545	145.57	23,649
Domestic Well #12	344851	1064928	96	26	1	5	985	965	980	15	5.85	0.1	23,467	132.56	25,797
Domestic Well #13	344832	1063618	97	45	1	4	600	580	600	20	22.24	2.2	12,427	122.36	14,095
Domestic Well #14	351903	1062917	41	57	1	3	580	560	580	20	79.91	7.9	1,854	81.48	161
Domestic Well #15	342104	1065302	149	20	1	2	223	210	220	10	11.62	1.1	17,794	129.03	19,900
Domestic Well #16	351838	1063052	41	53	1	3	400	375	395	20	32.57	3.3	9,273	111.76	10,193
Domestic Well #18	351115	1063027	55	54	1	1	550	510	530	20	66.42	6.6	3,383	101.18	3,480
Domestic Well #20	344629	1063827	101	43	6	3	368	348	368	20	24.66	2.5	11,573	121.31	13,170
Domestic Well #21	344701	1065050	99	24	1	4	660	640	660	20	10.97	5.1	18,269	120.99	19,844
Domestic Well #22	351421	1063822	49	42	1	3	315	300	315	15	82.80	1.9	1,560	98.12	1,403
Domestic Well #23	343236	1064605	126	31	1	3	160	150	160	10	11.16	1.0	18,127	129.47	20,263
Domestic Well #25	350857	1062954	60	55	1	1	447	439	445	6	95.07	1.0	418	100.92	494
Domestic Well #27	350949	1064242	58	37	1	3	326	NA	NA	NA	43.37	4.3	6,906	98.64	6,793

Table A2 . Information on wells from which ^{14}C activities were used in the ground-water-flow model calibration—Continued.

Well Name	Latitude	Longitude	Row number	Column number	No. of patb lines	Model layer(s)	Well depth (feet)	Deptb to screen top (feet)	Depth to screen bottom (feet)	Screen length (feet)	Carbon-14 (pmC)	Uncertainty (pmC)	Raw C-14 age (years)	Implied Ao from reactions (pmC)	Corrected age (calendar years)
Domestic Well #28	351019	1064040	57	40	1	4	275	259	274	15	73.27	7.6	2,571	100.46	2,609
Domestic Well #29	344818	1064007	98	41	1	3	210	200	210	10	55.49	2.8	4,869	108.16	5,517
Domestic Well #30	343338	1063553	125	47	1	1	400	390	400	10	5.41	0.6	24,113	128.49	26,185
Domestic Well #31	350204	1065623	73	15	1	1	150	NA	NA	NA	36.33	5.2	8,370	76.15	6,118
Domestic Well #32	342011	1065043	149	24	1	3	130	120	130	10	10.82	2.6	18,383	132.34	20,700
Domestic Well #33	343524	1064120	122	39	1	4	480	460	480	20	15.81	1.6	15,248	130.49	17,448
Domestic Well #34	345934	1064033	77	40	1	3	109	NA	NA	NA	85.30	7.3	1,314	97.10	1,071
Eubank 1	350259	1063158	71	52	1	2	615	550	610	60	62.04	5.0	3,946	102.49	4,150
Garfield 1	350706	1063903	62	42	1	6	1,020	995	1,010	15	12.55	1.2	17,157	125.55	19,038
Garfield 2	350706	1063903	62	42	1	5	582	552	572	20	22.32	2.2	12,397	106.22	12,896
Garfield 3	350706	1063903	62	42	1	2	93	43	83	40	81.84	4.0	1,657	98.42	1,525
Gonzales 1	350641	1064232	64	37	6	4-5	970	350	950	600	47.04	6.0	6,235	103.95	6,555
Hunter Ridge Nest 1 Well 1	351200	1064008	53	40	1	6	1,518	1508	1,513	5	25.32	1.1	11,355	101.64	11,489
Hunter Ridge Nest 1 Well 2	351200	1064008	53	40	1	5	855	845	850	5	60.43	1.3	4,164	85.25	2,845
Hunter Ridge Nest 2 Well 1	351200	1064008	53	40	1	4	359	349	354	5	73.80	1.3	2,512	100.67	2,567
Isleta D	345650	1064159	82	38	1	6	1,340	1,330	1,335	5	2.71	1.1	29,828	130.26	32,013
Isleta MD	345650	1064159	82	38	1	6	815	805	810	5	35.76	1.7	8,501	83.79	7,039
Isleta MS	345650	1064159	82	38	1	3	185	175	180	5	72.32	2.8	2,679	91.61	1,955
Isleta S	345650	1064159	82	38	1	2	50	10	40	30	99.70	0.5	25	118.23	1,409
Kirtland 1	350302	1063332	70	49	2	3-4	1,199	550	800	250	59.38	3.0	4,309	104.37	4,662
Kirtland 11	350230	1063124	72	53	6	4-5	1,327	670	1,327	657	45.98	7.0	6,423	106.18	6,919
Kirtland 14	350301	1063546	70	46	6	2-5	1,000	380	1,000	620	48.86	7.0	5,921	106.72	6,458
Leavitt 1	350310	1064350	71	34	8	4-6	1,140	288	1,128	840	17.28	3.0	14,513	95.81	14,159
Leyendecker 1	350752	1063423	61	48	5	4-5	1,000	468	996	528	72.84	10.0	2,620	88.10	1,572
Lincoln D	351515	1064104	48	39	1	5	1,260	1,200	1,240	40	13.80	1.1	16,372	116.25	17,617
Lincoln M	351515	1064104	48	39	1	4	835	810	830	20	15.46	1.1	15,433	129.95	17,599
Lincoln S	351515	1064104	48	39	1	3	595	490	590	100	29.64	3.0	10,053	114.73	11,189
Lomas 1	350431	1063028	67	55	6	3-5	1,300	700	1,300	600	72.78	7.0	2,627	94.14	2,127
Los Lunas 3	344915	1064528	95	32	2	4-5	605	332	562	230	27.55	5.0	10,657	97.36	10,436
Los Lunas 4	345009	1064503	95	32	3	4	610	278	582	304	50.45	5.0	5,656	96.09	5,326
Love 1	350517	1063145	66	52	5	3-5	1,170	596	1,096	500	47.21	6.0	6,205	107.65	6,814
Matheson D	350653	1063116	64	53	1	6	1,520	1,460	1,500	40	35.35	2.2	8,596	109.35	9,335
Matheson M	350653	1063116	64	53	1	5	1,045	1,020	1,040	20	55.87	2.0	4,812	100.73	4,873
Matheson S	350653	1063116	64	53	1	2	705	600	700	100	64.88	3.0	3,576	101.60	3,708
Mesa Del Sol D	345758	1063642	80	46	1	6	1630	1,580	1,620	40	5.99	2.6	23,271	119.50	24,744
Mesa Del Sol M	345758	1063642	80	46	1	5	1,015	990	1,010	20	3.24	1.1	28,351	135.86	30,885
Mesa Del Sol S	345758	1063642	80	46	1	2	525	420	520	100	33.36	1.7	9,075	108.96	9,785

Table A2. Information on wells from which ^{14}C activities were used in the ground-water-flow model calibration—Continued.

Well Name	Latitude	Longitude	Row number	Column number	No. of path lines	Model layer(s)	Well depth (feet)	Depth to screen top (feet)	Depth to screen bottom (feet)	Screen length (feet)	Carbon-14 (pmC)	Uncertainty (pmC)	Raw C-14 age (years)	Implied Ao from reactions (pmC)	Corrected age (calendar years)
Montano-6D	350834	1063958	60	41	1	6	983	972	978	6	25.19	2.5	11,397	121.88	13,033
Montano-6MD	350834	1063958	60	41	1	6	836	826	831	5	37.95	2.7	8,010	107.34	8,595
Montano-6MS	350834	1063958	60	41	1	5	568	558	563	5	67.54	5.3	3,244	101.82	3,393
Montesa M	350056	1063701	74	44	1	5	708	698	703	5	18.63	2.6	13,891	121.61	15,509
Montesa S	350056	1063701	74	44	1	3	330	260	320	60	52.51	3.5	5,325	97.07	5,079
MRN-1	345848	1063357	79	49	1	3	607	547	587	40	42.23	2.7	7,126	107.49	7,723
NM Utilities 1	351137	1064417	54	33	4	4-5	1,050	648	1,050	402	13.91	4.0	16,307	132.17	18,612
NM Utilities 2	351215	1064216	53	36	4	3-5	1,000	350	800	450	50.94	6.0	5,576	108.27	6,233
NM Utilities 3	351302	1064247	51	36	7	4-6	1,364	650	1,351	701	15.59	7.0	15,364	123.90	17,136
NM Utilities 4	351215	1064413	53	33	6	4-6	1,357	692	1,339	647	7.36	6.0	21,569	131.68	23,844
Nor Este 1	351114	1063306	55	50	1	6	1,525	1,515	1,520	5	7.95	0.8	20,931	134.97	23,410
Nor Este 2	351114	1063306	55	50	1	5	1,193	1,183	1,188	5	17.12	1.1	14,590	120.06	16,101
Nor Este 3	351114	1063306	55	50	1	3	608	538	598	60	47.62	1.2	6,133	107.10	6,700
Open Space	350107	1063543	73	47	1	3	462	305	410	105	55.15	7.8	4,920	88.46	3,906
Paseo-2D	351057	1063842	56	43	1	3	150	135	145	10	76.69	5.4	2,194	99.58	2,159
Paseo-3D	351035	1063647	57	45	1	5	544	539	544	5	64.51	2.3	3,624	92.77	3,003
PL-2	350042	1063353	75	50	1	4	617	577	597	20	38.83	1.2	7,820	106.30	8,325
Ponderosa 1	350931	1063156	59	52	7	4-6	1,800	964	1,693	729	42.45	10.0	7,083	106.16	7,577
Private Production Well #01	350336	1064751	70	28	1	4	1,292	1,078	1,272	194	5.47	1.0	24,022	129.55	26,162
Private Production Well #02	345205	1063942	90	41	1	2	182	142	172	30	96.37	1.0	306	100.11	315
Private Production Well #03	353443	1061913	12	71	1	3	300	250	300	50	82.55	5.5	1,585	85.76	315
Private Production Well #04	353657	1062116	8	68	1	3	250	NA	NA	NA	51.93	5.0	5,417	107.27	5,997
Private Production Well #05	342608	1064647	138	30	1	4	258	238	258	20	7.46	1.0	21,457	139.07	24,183
Private Production Well #06	352713	1062056	25	68	2	4	800	520	760	240	29.21	5.0	10,173	52.51	4,848
Private Production Well #07	352558	1063638	28	46	1	2	440	200	380	180	62.74	5.0	3,854	102.98	4,096
Private Production Well #08	343103	1064827	130	28	1	3	249	224	249	25	9.23	0.9	19,697	132.98	22,053
Private Production Well #12	353856	1062001	4	71	3	3-4	805	356	690	334	92.03	8.0	687	99.64	657
Private Production Well #13	353106	1064214	18	36	1	1	572	392	552	160	71.20	3.3	2,808	99.80	2,791
Private Production Well #14	353041	1064255	19	35	1	1	320	260	320	60	37.39	2.2	8,132	106.43	8,648
Private Production Well #15	350319	1063014	69	55	5	1-5	1,200	650	1,180	530	82.70	10.0	1,570	81.88	-82
Private Production Well #16	350112	1064902	74	27	1	5	1,300	1,242	1,294	52	9.31	2.7	19,626	132.63	21,960
Private Production Well #17	352148	1062733	35	58	1	1	360	310	360	50	79.83	6.0	1,862	98.87	1,768
Private Production Well #19	351318	1063918	52	41	12	5-7	2,020	730	2,000	1,270	55.23	16.0	4,908	107.79	5,528
Private Production Well #20	352552	1062701	27	60	1	2	110	65	100	35	77.09	10.3	2,151	74.98	-229
Private Production Well #21	352552	1062701	27	60	1	5	557	517	547	30	58.84	1.2	4,384	82.73	2,817
Private Production Well #22	352506	1062400	30	64	1	3	286	268	286	18	69.34	2.8	3,027	101.17	3,123
Private Production Well #23	353701	1064358	8	34	1	1	81	19	81	62	93.79	5.0	530	93.79	0

Table A2. Information on wells from which ^{14}C activities were used in the ground-water-flow model calibration—Continued.

Well Name	Latitude	Longitude	Row number	Column number	No. of path lines	Model layer(s)	Well depth (feet)	Depth to screen top (feet)	Deptb to screen bottom (feet)	Screen length (feet)	Carbon-14 (pmC)	Uncertainty (pmC)	Raw C-14 age (years)	Implied Ao from reactions (pmC)	Corrected age (calendar years)
Rabbit Hill	353534	1064251	9	36	2	1-2	608	353	603	250	8.59	2.1	20,291	123.65	22,046
Rest Area	341841	1065317	152	19	1	1	212	173	212	39	80.73	5.4	1,770	78.98	-181
Ridgecrest 3	350413	1063313	69	50	8	4-6	1,475	620	1,436	816	70.25	10.0	2,919	99.26	2,858
Ridgecrest 4	350445	1063341	67	49	8	4-6	1,424	572	1,412	840	46.08	8.0	6,405	106.68	6,940
Rio Bravo 5 D	350140	1064016	72	40	1	5	515	500	510	10	3.11	0.6	28,690	134.08	31,114
Rio Bravo-1D	350137	1064105	73	39	1	3	149	139	144	5	15.11	1.5	15,622	127.11	17,605
Rio Bravo-1M	350137	1064105	73	39	1	3	104	94	99	5	33.21	3.3	9,113	106.59	9,640
Rio Bravo-4D	350135	1063906	73	42	1	3	149	139	144	5	34.64	3.3	8,764	109.02	9,478
Rio Grande Util 5	343940	1064238	114	37	3	4-5	670	290	660	370	33.18	5.0	9,120	108.40	9,787
Rio Grande Util 6	344355	1064060	105	39	2	4	602	330	590	260	51.34	5.0	5,511	101.75	5,655
Rio Rancho 10	351623	1063946	46	41	6	4-6	1,470	825	1,450	625	12.18	9.0	17,404	123.34	19,139
Rio Rancho 12	351915	1063529	40	46	10	4-6	1,487	435	1,487	1,052	11.66	10.0	17,765	107.44	18,358
Rio Rancho 13	351630	1064812	45	27	3	4-5	1,920	1,343	1,721	378	3.00	2.0	28,988	137.25	31,605
Rio Rancho 15	352117	1064057	36	38	4	3-5	1,310	820	1,290	470	18.27	5.0	14,053	100.62	14,104
Rio Rancho 2	351340	1064014	50	40	2	4-5	751	508	751	243	71.55	6.0	2,768	100.78	2,832
Rio Rancho 4	351459	1064034	49	39	3	4-5	990	670	990	320	19.77	4.5	13,400	113.15	14,422
Rio Rancho 8	351625	1064357	46	34	6	4-5	1,618	982	1,599	617	14.73	10.0	15,833	127.94	17,870
Rio Rancho 9	351923	1064707	40	30	4	3-5	1,540	1,120	1,520	400	7.72	5.0	21,174	130.03	23,345
San Jose 2	350338	1063832	70	42	7	4-6	1,000	264	996	732	29.10	10.0	10,205	113.24	11,233
Sandia D	351357	1063230	50	52	1	6	1,305	1,295	1,300	5	15.33	2.6	15,503	130.64	17,712
Sandia M	351357	1063230	50	52	1	5	1,025	1,015	1,020	5	10.43	1.6	18,687	126.43	20,625
Sandia Peak 1	351031	1063007	57	55	2	1	800	560	760	200	77.98	4.0	2,056	98.56	1,936
Sandia Peak 3	351031	1063007	57	55	2	1	603	383	583	200	83.23	5.0	1,517	98.04	1,354
Sandia S	351357	1063230	50	52	1	3	535	485	525	40	62.89	2.0	3,834	94.69	3,383
Santa Ana Bound-D	352708	1063944	26	41	1	5	800	730	750	20	6.47	0.6	22,634	92.40	21,981
Santa Ana Bound-M	352708	1063944	26	41	1	4	525	472	492	20	8.24	1.6	20,635	83.33	19,127
Santa Ana Bound-S	352708	1063944	26	41	1	1	252	190	210	20	5.54	0.6	23,917	106.22	24,416
Santa Barbara 1	350648	1063625	63	45	6	4-5	1,000	312	984	672	49.07	7.0	5,885	107.66	6,495
SH03 (UNM)	350950	1062948	57	56	1	1	495	420	490	70	96.31	4.0	311	96.31	0
Sierra Vista D	350910	1064148	59	38	1	7	1,644	1,634	1,639	5	1.89	0.3	32,807	93.42	32,244
Sierra Vista M	350910	1064148	59	38	1	5	928	918	923	5	34.24	1.7	8,860	77.55	6,758
Sierra Vista S	350910	1064148	59	38	1	2	210	140	200	60	68.85	2.8	3,085	92.91	2,478
Sister Cities 1	350908	1063444	59	49	1	6	1,308	1,298	1,303	5	8.03	0.6	20,848	131.16	23,091
Sister Cities 2	350908	1063444	59	49	1	5	799	789	794	5	66.26	6.8	3,402	91.67	2,683
Soil Amendment Facility	350855	1064928	59	25	3	4-5	1,463	1,116	1,429	313	4.50	2.0	25,636	129.43	27,768
SWAB Test Hole 1 D	350449	1064931	66	26	1	4	1,179	1,139	1,179	40	6.57	6.5	22,507	128.93	24,608
SWAB Test Hole 1 S	350449	1064931	66	26	1	4	1,121	980	1,121	141	9.12	2.0	19,796	132.19	22,103

Table A2. Information on wells from which ^{14}C activities were used in the ground-water-flow model calibration—Continued.

Well Name	Latitude	Longitude	Row number	Column number	No. of patb lines	Model layer(s)	Well deptb (feet)	Deptb to screen top (feet)	Depth to screen bottom (feet)	Screen length (feet)	Carbon-14 (pmC)	Uncertainty (pmC)	Raw C-14 age (years)	Implied Ao from reactions (pmC)	Corrected age (calendar years)
SWAB Test Hole 2 D	351046	1064648	55	30	2	6	1,805	1,525	1, 795	270	14.35	1.1	16,049	105.83	16,517
SWAB-3-760	351051	1063953	56	41	1	5	840	710	790	80	44.06	5.3	6,776	109.34	7,514
SWAB-3-980 (1St)	351051	1063953	56	41	1	6	1,055	870	1,050	180	44.08	7.7	6,772	108.41	7,439
Thomas 6	350720	1063305	62	50	7	4-6	1,536	760	1,520	760	44.21	6.0	6,747	106.64	7,279
Tome D	344431	1063934	104	41	1	6	1,200	1,185	1,195	10	8.80	1.6	20,091	121.72	21,716
Tramway East	351136	1063050	55	54	4	1-3	1,100	698	1,098	400	53.97	5.0	5,098	107.07	5,663
Vol Andia 2	350732	1063504	61	48	4	4-5	1,016	360	852	492	70.57	6.0	2,882	99.97	2,879
Vol Andia 5	350805	1063611	60	46	6	3-5	1,020	260	900	640	57.79	8.0	4,533	104.27	4,879
Volcano Cliff 1	350935	1064343	59	34	5	4-5	1,200	528	1,056	528	9.45	1.6	19,502	133.71	21,904
Walker 1	351025	1063140	56	53	7	4-6	1,723	991	1,711	720	41.64	7.0	7,243	104.78	7,629
Webster 1	351029	1063320	57	50	7	4-6	1,484	620	1,345	725	45.46	7.0	6,517	101.84	6,668
West Bluff Nest-1, W1	350638	1064137	63	38	1	6	1,095	1,085	1,090	5	2.00	0.1	32,339	105.31	32,767
West Bluff Nest-1, W2	350638	1064137	63	38	1	5	689	679	684	5	32.33	0.3	9,335	115.36	10,516
West Bluff Nest-2, W1	350638	1064137	63	38	1	3	328	318	323	5	63.51	7.3	3,753	103.56	4,042
West Mesa 3	350444	1064354	68	34	9	4-6	1,365	405	1,353	948	9.00	2.0	19,906	109.22	20,635
Windmill #02	342426	1065559	141	16	1	1	316	NA	NA	NA	40.02	2.7	7,571	108.02	8,208
Windmill #03	343447	1065545	123	17	1	1	268	NA	NA	NA	49.06	2.7	5,887	51.94	472
Windmill #04	345345	1064514	88	32	1	1	167	147	167	20	79.46	25.4	1,901	98.14	1,745
Windmill #05	345406	1065031	87	25	1	1	620	600	620	20	36.77	15.2	8,271	104.21	8,612
Windmill #07	345218	1070018	91	9	1	1	212	192	212	20	84.49	15.4	1,393	84.49	0
Windmill #08	345504	1063313	86	50	1	1	44	24	44	20	57.15	10.3	4,625	105.29	5,051
Windmill #09	352759	1063627	25	45	1	1	637	NA	NA	NA	39.70	5.3	7,637	106.86	8,185
Windmill #10	343649	1065738	119	14	1	1	428	388	428	40	9.69	1.6	19,295	128.17	21,347
Windmill #12	353302	1063856	14	42	1	1	727	715	725	10	38.08	2.7	7,981	100.02	7,983
Windmill #13	352811	1064523	23	32	1	1	240	125	135	10	84.47	3.0	1,395	87.66	306
Windmill #15	352633	1062018	26	70	1	1	55	NA	NA	NA	28.52	2.6	10,371	42.49	3,296
Windmill #17	342707	1065325	136	20	1	1	61	NA	NA	NA	29.76	5.1	10,019	29.63	-36
Windmill #18	342924	1065505	133	18	1	2	143	NA	NA	NA	8.14	1.6	20,736	96.16	20,412
Windmill #20	343539	1070055	121	9	1	1	439	NA	NA	NA	0.79	0.3	40,018	96.40	39,715
Windmill #21	343907	1065729	115	14	1	1	395	390	395	5	9.80	0.9	19,202	94.35	18,721
Windmill #23	343841	1070244	116	5	1	1	620	NA	NA	NA	4.24	0.6	26,128	104.84	26,518
Windmill #28	352345	1062516	32	63	1	1	175	NA	NA	NA	19.56	2.7	13,489	110.52	14,315
Windmill #29	352821	1061559	24	76	1	1	292	NA	NA	NA	19.54	2.7	13,497	125.35	15,365
Windmill #30	343053	1065518	129	17	1	4	440	NA	NA	NA	23.78	2.7	11,874	30.74	2,122
Windmill #31	343146	1065340	129	19	1	1	90	NA	NA	NA	32.88	2.7	9,195	63.07	5,385
Windmill #32	344012	1063617	112	46	1	1	380	NA	NA	NA	31.17	2.7	9,637	111.55	10,540
Windmill #33	343231	1065707	127	15	1	2	281	269	279	10	3.29	0.6	28,225	111.90	29,154

Table A2. Information on wells from which ^{14}C activities were used in the ground-water-flow model calibration—Continued.

Well Name	Latitude	Longitude	Row number	Column number	No. of patb lines	Model layer(s)	Well deptb (feet)	Deptb to screen top (feet)	Deptb to screen bottom (feet)	Screen length (feet)	Carbon-14 (pmC)	Uncertainty (pmC)	Raw C-14 age (years)	Implied Ao from reactions (pmC)	Corrected age (calendar years)
Windmill #34	344945	1063726	95	45	1	3	440	420	440	20	17.16	3.0	14,571	126.38	16,506
Windmill #35	345132	1065452	91	18	1	3	700	680	700	20	13.22	2.5	16,727	129.13	18,840
Windmill #36	345231	1065617	90	16	1	1	720	700	720	20	43.25	6.0	6,929	85.74	5,657
Windmill #37	353805	1062329	5	64	1	1	290	NA	NA	NA	97.90	2.0	175	98.01	9
Windmill #38	352556	1062929	28	57	1	3	535	NA	NA	NA	12.99	1.1	16,872	112.47	17,844**
Windmill #39	353458	1063037	12	54	1	1	260	NA	NA	NA	10.40	1.1	18,710	107.23	19,288**
Windmill #40	353338	1063228	14	52	1	1	100	NA	NA	NA	50.70	3.0	5,615	107.53	6,215
Windmill #41	352542	1064203	29	37	1	1	448	NA	NA	NA	71.29	5.5	2,798	94.89	2,364
Windmill #43	353230	1063440	16	49	1	1	1,109	NA	NA	NA	22.33	3.0	12,394	122.71	14,086
Windmill #44	352804	1064142	23	38	1	1	147	NA	NA	NA	51.55	3.0	5,478	83.60	3,997
Windmill #45	353340	1062547	14	61	1	2	555	NA	NA	NA	12.16	1.8	17,418	105.27	17,843**
Yale 1	350427	1063729	67	44	1	3-5	1,000	336	960	624	39.16	9.0	7,750	107.58	8,354
Zia Ball Park-D	353000	1064346	21	34	1	5	805	750	770	20	18.34	1.8	14,021	87.66	12,932**
Zia Ball Park-M	353000	1064346	21	34	1	4	550	486	506	20	20.68	2.1	13,028	80.27	11,212
Zia-BMT-D	353208	1064059	16	38	1	3	800	750	800	50	8.29	0.8	20,585	119.83	22,080

**These ages were the results of earlier adjustments and are, for the most part, only slightly different than the final ages reported in Plummer and others (2004).

Table A3. Observed and simulated values of water levels (italics), ^{14}C activities, and hydrochemical zones (bold).

Well name	Observed value*	Simulated value	Residual	sqrt (weight)	Weighted residual	Well name	Observed value*	Simulated value	Residual	sqrt (weight)	Weighted residual
Domestic #12	*183*	*199.5*	*-16.5*	*0.40*	*-6.6*	*1950 LL west3*	*183*	*193.4*	*-10.4*	*0.17*	*-1.7*
Domestic #10	*125*	*143.3*	*-18.3*	*0.40*	*-7.3*	*1950 LL east2*	*179*	*180.8*	*-1.8*	*0.17*	*-0.3*
Domestic #06	*155*	*152.9*	*2.1*	*0.40*	*0.8*	*1950 LL west4*	*394*	*264.3*	*129.7*	*0.17*	*21.6*
Domestic #13	*190*	*205.3*	*-15.3*	*0.40*	*-6.1*	*1950 LL sout2*	*170*	*175.2*	*-5.2*	*0.17*	*-0.9*
Domestic #20	*180*	*193.9*	*-13.9*	*0.40*	*-5.6*	*1950 Belen n1*	*165*	*171.0*	*-6.0*	*0.14*	*-0.9*
Domestic #11	*170*	*143.4*	*26.6*	*0.40*	*10.6*	*1950 Belen n2*	*161*	*167.4*	*-6.4*	*0.20*	*-1.3*
Domestic #09	*100*	*110.5*	*-10.5*	*0.40*	*-4.2*	*1950 Belen n3*	*162*	*168.7*	*-6.7*	*0.17*	*-1.1*
PP Well #05	*88*	*83.9*	*4.2*	*0.40*	*1.7*	*1950 Belen n4*	*164*	*173.8*	*-9.8*	*0.17*	*-1.6*
Domestic #08	*90*	*107.6*	*-17.6*	*0.40*	*-7.0*	*1950 Belen e1*	*157*	*160.0*	*-3.0*	*0.17*	*-0.5*
PP Well #08	*88*	*103.8*	*-15.8*	*1.00*	*-15.8*	*1950 Belen e2*	*171*	*171.2*	*-0.2*	*0.17*	*-0.0*
RG Utility 5	*150*	*157.1*	*-7.0*	*0.29*	*-2.0*	*1950 Puerco 1*	*179*	*185.6*	*-6.6*	*0.17*	*-1.1*
Grasslands R	*200*	*203.6*	*-3.6*	*1.00*	*-3.6*	*1950 Belen e3*	*160*	*158.3*	*1.7*	*0.17*	*0.3*
Belen Airport S	*155*	*155.5*	*-0.5*	*1.00*	*-0.5*	*Windmill #23*	*206*	*323.1*	*-117.1*	*0.17*	*-19.5*
McLaughlin T	*149*	*145.1*	*3.9*	*1.00*	*3.9*	*1950 Belen s1*	*150*	*142.7*	*7.3*	*0.17*	*1.2*
Sevilleta V	*73*	*60.8*	*12.2*	*1.00*	*12.2*	*1950 Belen w1*	*155*	*153.4*	*1.6*	*0.17*	*0.3*
NM Highway	*82*	*55.0*	*27.0*	*0.40*	*10.8*	*1950 Belen s2*	*127*	*134.7*	*-7.7*	*0.20*	*-1.5*
Domestic #35	*77*	*78.4*	*-1.4*	*0.40*	*-0.5*	*1950 Belen w2*	*148*	*140.4*	*7.6*	*0.17*	*1.3*
Domestic #36	*130*	*143.4*	*-13.4*	*0.40*	*-5.3*	*1950 Belen s3*	*128*	*126.4*	*1.6*	*0.17*	*0.3*
Domestic #29	*185*	*198.2*	*-13.2*	*0.40*	*-5.3*	*Windmill #31*	*159*	*154.0*	*5.0*	*0.17*	*0.8*
Windmill #33	*158*	*145.4*	*12.6*	*0.40*	*5.0*	*1950 Belen s4*	*114*	*113.8*	*0.2*	*0.20*	*0.0*
Windmill #17	*101*	*88.8*	*12.2*	*0.40*	*4.9*	*1950 Belen s5*	*110*	*111.3*	*-1.3*	*0.20*	*-0.3*
Windmill #18	*126*	*124.7*	*1.3*	*0.40*	*0.5*	*1950 Abo 1*	*138*	*128.1*	*9.9*	*0.17*	*1.6*
Domestic #32	*60*	*52.4*	*7.6*	*0.40*	*3.0*	*1950 Abo 2*	*135*	*120.1*	*14.9*	*0.17*	*2.5*
Windmill #03	*160*	*156.1*	*3.9*	*0.40*	*1.6*	*1950 Bernardo*	*77*	*84.4*	*-7.4*	*0.17*	*-1.2*
Windmill #10	*167*	*170.0*	*-3.0*	*0.40*	*-1.2*	*1950 N LaJoya*	*68*	*61.7*	*6.3*	*0.14*	*0.9*
Cerro CO PW	*287*	*247.9*	*39.1*	*0.29*	*11.2*	*Windmill #101*	*234*	*430.1*	*-196.1*	*0.14*	*-28.0*
PP Well #16	*249*	*250.9*	*-1.9*	*0.29*	*-0.6*	*Windmill #47*	*194*	*211.7*	*-17.7*	*0.17*	*-2.9*
Soil A Facility	*294*	*293.4*	*0.6*	*0.29*	*0.2*	*Windmill #48*	*191*	*207.9*	*-16.9*	*0.17*	*-2.8*
PP Well #01	*241*	*268.0*	*-27.0*	*0.29*	*-7.7*	*Windmill #49*	*213*	*210.8*	*2.2*	*0.20*	*0.4*
Tome Deep	*175*	*185.1*	*-10.1*	*1.00*	*-10.1*	*Windmill #50*	*212*	*220.8*	*-8.8*	*0.20*	*-1.8*
Windmill #46	*630*	*533.8*	*96.2*	*0.04*	*3.9*	*Windmill #51*	*217*	*223.2*	*-6.2*	*0.17*	*-1.0*
Isleta Deep	*232*	*236.9*	*-4.9*	*1.00*	*-4.9*	*Windmill #04*	*216*	*215.9*	*0.1*	*0.17*	*0.01*
MRN-1	*290*	*257.6*	*32.4*	*0.14*	*4.6*	*Windmill #52*	*200*	*211.9*	*-11.9*	*0.20*	*-2.4*
98th street D	*250*	*279.2*	*-29.2*	*1.00*	*-29.2*	*Windmill #53*	*235*	*233.8*	*1.2*	*0.20*	*0.2*
1950 LL cent1	*203*	*208.7*	*-5.7*	*0.20*	*-1.1*	*Windmill #54*	*230*	*233.2*	*-3.2*	*0.25*	*-0.8*
1950 LL cent2	*193*	*202.0*	*-9.0*	*0.17*	*-1.5*	*Windmill #55*	*254*	*232.8*	*21.2*	*0.20*	*4.2*
1950 LL cent3	*195*	*199.6*	*-4.6*	*0.14*	*-0.7*	*Windmill #56*	*230*	*240.0*	*-10.0*	*0.25*	*-2.5*
1950 LL west1	*191*	*203.7*	*-12.7*	*0.17*	*-2.1*	*Windmill #57*	*237*	*237.3*	*-0.3*	*0.20*	*-0.1*
1950 LL west2	*324*	*292.1*	*31.9*	*0.17*	*5.3*	*Windmill #58*	*236*	*227.3*	*8.7*	*0.20*	*1.7*
1950 LL east1	*193*	*200.2*	*-7.2*	*0.17*	*-1.2*	*PP Well #02*	*218*	*218.1*	*-0.1*	*0.17*	*-0.01*
1950 LL cent4	*179*	*186.8*	*-7.8*	*0.17*	*-1.3*	*Windmill #35*	*193*	*207.3*	*-14.3*	*0.20*	*-2.9*
1950 LL sout1	*180*	*185.3*	*-5.3*	*0.17*	*-0.19*	*Windmill #59*	*183*	*220.1*	*-37.1*	*0.20*	*-7.4*

Table A3. Observed and simulated values of water levels (italics), ^{14}C activities, and hydrochemical zones (bold)—Continued.

Well name	Observed value*	Simulated value	Residual	sqrt (weight)	Weighted residual	Well name	Observed value*	Simulated value	Residual	sqrt (weight)	Weighted residual
Windmill #34	*182*	*209.4*	*-27.4*	*0.20*	*-5.5*	*1950 WAtrsc3*	*285*	*287.2*	*-2.2*	*0.17*	*-0.4*
Windmill #60	*193*	*206.5*	*-13.5*	*0.20*	*-2.7*	*1950 Burton 5*	*299*	*305.5*	*-6.5*	*0.17*	*-1.1*
Windmill #05	*221*	*212.8*	*8.2*	*0.20*	*1.6*	*1950 NKirtland*	*303*	*309.4*	*-6.4*	*0.17*	*-1.1*
Windmill #61	*328*	*278.8*	*49.2*	*0.20*	*9.8*	*1950 4-Hills*	*334*	*391.5*	*-57.5*	*0.14*	*-8.2*
Windmill #62	*365*	*323.2*	*41.8*	*0.20*	*8.4*	*1950 WKirtland*	*297*	*296.4*	*0.6*	*0.14*	*0.1*
Windmill #63	*319*	*291.8*	*27.3*	*0.20*	*5.5*	*1950 Leavitt*	*270*	*272.8*	*-2.8*	*0.17*	*-0.5*
Windmill #64	*229*	*235.8*	*-6.8*	*0.20*	*-1.4*	*1950 SKirtland*	*295*	*298.6*	*-3.6*	*0.10*	*-0.4*
Windmill #65	*229*	*229.6*	*-0.6*	*0.20*	*-0.1*	*1950 Rio Bravo*	*272*	*275.5*	*-3.5*	*0.17*	*-0.6*
Windmill #66	*192*	*215.2*	*-23.2*	*0.20*	*-4.6*	*1950 VGP-1*	*258*	*263.6*	*-5.6*	*0.17*	*-0.9*
Windmill #07	*341*	*317.2*	*23.8*	*0.20*	*4.8*	*1940 Gntry103*	*305*	*285.6*	*19.4*	*0.20*	*3.9*
Windmill #67	*228*	*208.6*	*19.4*	*0.20*	*3.9*	*1950 N Isleta*	*246*	*246.7*	*-0.7*	*0.14*	*-0.1*
Windmill #68	*271*	*229.3*	*41.7*	*0.20*	*8.3*	*1950 Islta Nest*	*241*	*242.0*	*-1.0*	*0.14*	*-0.1*
Corrales N	*371*	*370.0*	*1.0*	*0.20*	*0.2*	*Windmill #69*	*375*	*370.8*	*4.2*	*0.25*	*1.0*
Corrales S	*362*	*363.5*	*-1.5*	*0.17*	*-0.3*	*Sandia ECW*	*409*	*380.8*	*28.2*	*0.20*	*5.6*
Windmill #100	*344*	*371.8*	*-27.8*	*0.17*	*-4.6*	*Windmill #70*	*378*	*386.7*	*-8.7*	*0.17*	*-1.5*
1950 H Ridge	*338*	*348.5*	*-10.5*	*0.17*	*-1.8*	*Windmill #71*	*423*	*410.9*	*12.1*	*0.20*	*2.4*
1950 Paseo2n	*338*	*343.7*	*-5.7*	*0.17*	*-1.0*	*Windmill #72*	*413*	*421.1*	*-8.1*	*0.20*	*-1.6*
1950 Paseo2s	*334*	*337.4*	*-3.4*	*0.17*	*-0.6*	*Windmill #73*	*490*	*453.1*	*36.9*	*0.20*	*7.4*
1950 SWAB 3	*332*	*335.9*	*-3.9*	*0.17*	*-0.7*	*Windmill #74*	*435*	*466.0*	*-31.0*	*0.25*	*-7.8*
1950 Nor Este	*340*	*349.6*	*-9.6*	*0.17*	*-1.6*	*Windmill #75*	*595*	*487.1*	*107.9*	*0.20*	*21.6*
1950 Summer	*974*	*928.6*	*45.4*	*0.17*	*7.6*	*Windmill #76*	*562*	*488.4*	*73.6*	*0.20*	*14.7*
1950 Paseo2v	*328*	*333.5*	*-5.5*	*0.17*	*-0.9*	*Windmill #77*	*618*	*508.8*	*109.2*	*0.20*	*21.8*
Domestic #39	*321*	*328.5*	*-7.5*	*0.17*	*-1.3*	*Windmill #78*	*557*	*503.5*	*53.5*	*0.20*	*10.7*
Domestic #27	*317*	*323.2*	*-6.2*	*0.17*	*-1.0*	*Windmill #09*	*490*	*518.0*	*-28.0*	*0.20*	*-5.6*
1950 MntanoN	*323*	*329.7*	*-6.7*	*0.17*	*-1.1*	*Windmill #79*	*651*	*546.7*	*104.3*	*0.25*	*26.1*
1950 SisterC	*318*	*317.4*	*0.6*	*0.17*	*0.1*	*Windmill #80*	*505*	*561.5*	*-56.5*	*0.25*	*-14.1*
1950 Pndrosa	*318*	*329.2*	*-11.3*	*0.17*	*-1.9*	*Windmill #81*	*446*	*470.9*	*-24.9*	*0.20*	*-5.0*
1950 Lyndckr	*321*	*316.8*	*4.2*	*0.17*	*0.7*	*San Felipe B*	*570*	*601.1*	*-31.1*	*0.17*	*-5.2*
1950 Sierra V	*310*	*319.3*	*-9.3*	*0.17*	*-1.6*	*Windmill #82*	*434*	*469.5*	*-35.5*	*0.17*	*-5.9*
1950 Mntano4	*312*	*315.8*	*-3.8*	*0.17*	*-0.6*	*Windmill #83*	*492*	*518.9*	*-27.0*	*0.25*	*-6.7*
1950 Thomas	*316*	*316.8*	*-0.8*	*0.17*	*-0.1*	*Windmill #84*	*509*	*561.2*	*-52.2*	*0.20*	*-10.5*
1950 Luz Sol	*313*	*315.6*	*-2.6*	*0.17*	*-0.4*	*Windmill #85*	*572*	*607.6*	*-35.6*	*0.20*	*-7.1*
1950 Wmath	*316*	*322.6*	*-6.6*	*0.17*	*-1.1*	*Windmill #86*	*529*	*542.6*	*-13.6*	*0.25*	*-3.4*
1950 Emath	*943*	*939.3*	*3.7*	*0.17*	*0.6*	*Windmill #87*	*494*	*595.5*	*-101.5*	*0.17*	*-16.9*
1950 Voland	*315*	*315.9*	*-0.9*	*0.17*	*-0.2*	*Windmill #88*	*474*	*533.7*	*-59.7*	*0.17*	*-9.9*
1950 Sbarb	*313*	*315.8*	*-2.8*	*0.17*	*-0.5*	*Windmill #89*	*494*	*554.6*	*-60.6*	*0.17*	*-10.1*
1950 WBluff	*300*	*303.4*	*-3.4*	*0.17*	*-0.6*	*Windmill #90*	*727*	*720.0*	*7.0*	*0.17*	*1.2*
1950 Charls4	*311*	*315.7*	*-4.7*	*0.17*	*-0.8*	*Windmill #45*	*439*	*545.5*	*-106.5*	*0.17*	*-17.8*
1950 Smath	*310*	*316.9*	*-6.9*	*0.17*	*-1.1*	*Windmill #91*	*587*	*616.5*	*-29.5*	*0.17*	*-4.9*
1950 Del Sol	*302*	*315.2*	*-13.2*	*0.17*	*-2.2*	*Windmill #92*	*733*	*649.6*	*83.4*	*0.17*	*13.9*
1950 WMesa3	*286*	*283.8*	*2.2*	*0.14*	*0.3*	*Rabbit Hill*	*903*	*874.1*	*28.9*	*0.20*	*5.8*
1950 ORL-2	*286*	*294.4*	*-8.4*	*0.17*	*-1.4*	*Windmill #41*	*572*	*503.6*	*68.4*	*0.20*	*13.7*

Table A3. Observed and simulated values of water levels (italics), ^{14}C activities, and hydrochemical zones (bold)—Continued.

Well Name	Observed value*	Simulated value	Residual	sqrt (weight)	Weighted residual	Well Name	Observed value*	Simulated value	Residual	sqrt (weight)	Weighted residual
PP Well #14	*735*	*667.1*	*67.9*	*0.20*	*13.6*	Domestic #21	10.91	0.02	10.89	1.00	10.89
Windmill #93	*735*	*701.1*	*33.9*	*0.25*	*8.5*	Belen-4	14.55	11.22	3.33	0.20	0.67
Windmill #94	*744*	*667.8*	*76.2*	*0.20*	*15.3*	Belen-5	16.37	0.93	15.44	0.20	3.09
Windmill #95	*670*	*596.5*	*73.5*	*0.20*	*14.7*	Windmill #02	40.02	36.79	3.23	1.00	3.23
Windmill #43	*578*	*571.2*	*6.8*	*0.20*	*1.4*	Burton2	47.73	52.02	-4.29	0.20	-0.86
Windmill #96	*653*	*715.8*	*-62.8*	*0.25*	*-15.7*	Burton5	44.70	23.01	21.60	0.20	4.32
Windmill #97	*733*	*707.1*	*25.9*	*0.20*	*5.2*	CEPO-02	21.32	22.92	-1.60	1.00	-1.60
Windmill #98	*822*	*777.7*	*44.3*	*0.20*	*8.9*	CerroCo-PW	7.35	0.00	7.35	0.20	1.47
Windmill #42	*655*	*555.5*	*99.5*	*0.17*	*16.6*	Charles-4	51.40	46.51	4.89	0.20	0.98
Windmill #99	*453*	*499.4*	*-46.4*	*0.17*	*-7.7*	Windmill #18	8.12	4.91	3.21	1.00	3.21
NE Well #01	*567*	*572.3*	*-5.3*	*0.17*	*-0.9*	Windmill #17	29.63	28.01	1.62	1.00	1.62
Windmill #37	*734*	*638.6*	*95.4*	*0.17*	*15.9*	PP Well #2	96.37	97.15	-0.78	0.20	-0.16
NE Well #02	*581*	*574.6*	*6.4*	*0.17*	*1.1*	PP Well #4	51.93	59.06	-7.13	1.00	-7.13
NE Well #03	*679*	*628.3*	*50.7*	*0.17*	*8.5*	Windmill #37	97.90	48.60	49.30	1.00	49.30
NE Well #04	*701*	*600.4*	*100.6*	*0.17*	*16.8*	PP Well #03	82.55	80.43	2.13	1.00	2.13
Solar Well	*711*	*590.2*	*120.8*	*0.17*	*20.1*	College-2	5.31	6.49	-1.18	0.20	-0.24
RR Well 2	*321*	*339.6*	*-18.6*	*0.17*	*-3.1*	Windmill #20	0.79	0.00	0.79	1.00	0.79
RR Well 7	*284*	*355.4*	*-71.4*	*0.17*	*-11.9*	Coronado-1	32.77	14.79	17.98	0.20	3.60
RR Well 8	*297*	*368.2*	*-71.2*	*0.17*	*-11.9*	Domestic #03	21.00	12.10	8.90	1.00	8.90
RR Well 9	*322*	*390.5*	*-68.5*	*0.17*	*-11.4*	Del-Sol-1-D	6.20	7.86	-1.66	1.00	-1.66
RR Well 13	*304*	*370.2*	*-66.2*	*0.17*	*-11.0*	Del-Sol-2-M	13.65	15.56	-1.91	1.00	-1.91
RR Well 15	*369*	*400.4*	*-31.4*	*0.17*	*-5.2*	Del-Sol-3-S	62.21	36.21	26.00	1.00	26.00
Tierra M D	*405*	*420.2*	*-15.2*	*0.40*	*-6.1*	Eubank-1	61.33	56.53	4.80	1.00	4.80
Domestic #37	*457*	*451.0*	*6.0*	*0.40*	*2.4*	Windmill #21	9.21	0.69	8.52	1.00	8.52
Domestic #38	*551*	*562.8*	*-11.8*	*0.40*	*-4.7*	Garfield-1	12.38	10.95	1.43	1.00	1.43
SWAB2 D	*310*	*316.3*	*-6.3*	*0.40*	*-2.5*	Garfield-2	22.08	11.86	10.22	1.00	10.22
SWAB2 S	*300*	*317.9*	*-18.0*	*0.40*	*-7.2*	Garfield-3	81.84	97.45	-15.61	1.00	-15.61
Volc Cliffs H	*310*	*323.0*	*-13.0*	*0.40*	*-5.2*	Domestic #22	80.70	77.11	3.59	1.00	3.59
SWAB 3 D	*312*	*322.8*	*-10.8*	*0.40*	*-4.3*	Domestic #05	27.00	1.33	25.67	1.00	25.67
SWAB 3 S	*318*	*327.5*	*-9.5*	*0.40*	*-3.8*	Gonzales-1	47.04	28.58	18.46	0.20	3.69
SWAB 1	*263*	*274.2*	*-11.2*	*0.40*	*-4.5*	Domestic #06	36.45	40.20	-3.75	1.00	-3.75
Domestic #31	*555*	*388.1*	*166.9*	*0.14*	*23.8*	Doemstic #07	97.48	78.08	19.40	1.00	19.40
4-Hills-1	93.95	72.16	21.79	1.00	21.79	Windmill #03	49.06	23.79	25.27	1.00	25.27
PP Well #15	81.88	54.39	27.49	0.20	5.50	Windmill #23	4.23	0.00	4.23	1.00	4.23
98thSt-DP	0.13	5.85	-5.72	1.00	-5.72	HuntRidg-11	24.66	5.63	19.03	1.00	19.03
98thSt-MD	3.69	6.59	-2.90	1.00	-2.90	HuntRidg-12	60.14	1.05	59.09	1.00	59.09
98thSt-MS	0.79	1.75	-0.96	1.00	-0.96	HuntRidg-21	72.13	64.06	8.07	1.00	8.07
98thSt-SH	6.37	0.11	6.26	1.00	6.26	PP Well #19	54.77	13.33	41.44	0.20	8.29
PP Well #1	5.47	0.09	5.39	0.20	1.08	Windmill #36	43.40	26.46	16.94	1.00	16.94
PP Well #16	9.12	7.36	1.77	0.20	0.35	Windmill #34	17.17	32.53	-15.36	1.00	-15.36
PP Well #17	79.29	73.74	5.56	1.00	5.56	Windmill #04	79.46	71.99	7.47	1.00	7.47
Windmill #15	28.30	33.19	-4.89	1.00	-4.89	Windmill #35	13.20	9.11	4.09	1.00	4.09

Table A3. Observed and simulated values of water levels (italics), ^{14}C activities, and hydrochemical zones (bold)—Continued.

Well Name	Observed value*	Simulated value	Residual	sqrt (weight)	Weighted residual	Well Name	Observed value*	Simulated value	Residual	sqrt (weight)	Weighted residual
Isleta D	2.71	0.42	2.29	1.00	2.29	NMUtility-4	7.18	17.35	-10.17	0.20	-2.04
Isleta MD	35.76	2.09	33.67	1.00	33.67	Nor-Este-1	7.64	12.21	-4.57	1.00	-4.57
Isleta MS	72.32	86.47	-14.15	1.00	-14.15	Nor-Este-2	16.70	14.17	2.53	1.00	2.53
Isleta S	118.23	117.66	0.57	1.00	0.57	Nor-Este-3	47.62	67.38	-19.76	1.00	-19.76
Domestic #08	13.00	29.41	-16.41	1.00	-16.41	PP Well #07	62.74	43.72	19.02	0.20	3.80
PP Well #23	93.79	36.49	57.30	0.20	11.46	Open-Space	55.15	33.40	21.75	1.00	21.75
Domestic #09	31.10	18.91	12.19	1.00	12.19	Domestic #29	54.94	53.08	1.86	1.00	1.86
Kirtland-01	59.38	38.82	20.56	0.20	4.11	Paseo-2D	76.69	92.91	-16.22	1.00	-16.22
Kirtland-11	45.98	51.56	-5.58	0.20	-1.12	Paseo-3D	64.51	50.31	14.20	1.00	14.20
Kirtland-14	48.86	40.32	8.54	0.20	1.71	PL-2	38.34	50.44	-12.10	1.00	-12.10
Leavitt 1	17.01	7.98	9.03	0.20	1.81	Ponderos-1	42.45	44.18	-1.73	0.20	-0.35
Leyendecker	72.84	30.51	42.33	0.20	8.47	Rabbit-Hill	8.59	46.75	-38.16	1.00	-38.16
Lincoln D	13.80	5.07	8.73	1.00	8.73	Domestic #12	5.85	0.06	5.79	1.00	5.79
Lincoln M	15.46	5.28	10.18	1.00	10.18	Domestic #30	5.28	30.99	-25.71	1.00	-25.71
Lincoln S	29.64	14.23	15.41	1.00	15.41	Rest-Area	78.90	78.38	0.52	1.00	0.52
Domestic #23	11.09	0.03	11.06	1.00	11.06	Ridgcrest-3	70.25	37.52	32.73	1.00	32.73
Lomas-1	72.78	59.29	13.49	0.20	2.70	Ridgcrest-4	45.53	30.73	14.80	1.00	14.80
Los-Lunas-3	27.55	72.89	-45.34	0.20	-9.07	RioBravo-5D	3.02	14.24	-11.22	1.00	-11.22
Los-Lunas-4	50.45	73.49	-23.04	0.20	-4.61	RioBravo-1D	15.11	92.49	-77.38	1.00	-77.38
Love-1	47.21	64.15	-16.94	0.20	-3.39	RioBravo-1M	33.21	64.53	-31.32	1.00	-31.32
Domestic #10	54.73	30.05	24.68	1.00	24.68	RioBravo-4D	34.64	40.19	-5.55	1.00	-5.55
Domestic #11	8.33	26.08	-17.75	1.00	-17.75	RioGrUtil-5	33.18	5.84	27.34	0.20	5.47
Matheson-D	35.35	16.74	18.61	1.00	18.61	RioGrUtil-6	51.34	11.36	39.98	0.20	8.00
Matheson-M	55.87	64.50	-8.63	1.00	-8.63	Domestic #31	35.55	59.98	-24.43	1.00	-24.43
Matheson-S	64.88	73.06	-8.18	1.00	-8.18	RioRancho10	12.18	12.88	-0.70	0.20	-0.14
Domestic #25	95.14	79.27	15.87	1.00	15.87	RioRancho12	24.80	3.35	21.45	0.20	4.29
MesaDelSol-D	5.99	1.75	4.24	1.00	4.24	RioRancho13	3.00	31.13	-28.13	0.20	-5.63
MesaDelSol-M	3.24	33.58	-30.34	1.00	-30.34	RioRancho15	18.27	1.09	17.18	0.20	3.44
MesaDelSol-S	33.36	32.05	1.31	1.00	1.31	RioRancho02	67.18	1.01	66.17	0.20	13.23
Montano-6DP	25.19	34.35	-9.16	1.00	-9.16	RioRancho04	19.77	4.68	15.09	0.20	3.02
Montano-6MD	37.95	5.08	32.87	1.00	32.87	RioRancho08	14.73	20.17	-5.44	0.20	-1.09
Montano-6MS	67.54	6.15	61.39	1.00	61.39	RioRancho09	7.72	48.25	-40.53	0.20	-8.11
Montesa-M	18.63	28.28	-9.65	1.00	-9.65	Domestic #32	10.82	0.00	10.82	1.00	10.82
Montesa-S	52.51	42.70	9.81	1.00	9.81	Domestic #13	22.24	12.88	9.36	1.00	9.36
Domestic #27	42.18	44.12	-1.94	1.00	-1.94	Windmill #05	36.77	0.00	36.77	1.00	36.77
MRN-1	42.08	65.89	-23.81	1.00	-23.81	Windmill #07	84.49	78.79	5.70	1.00	5.70
Domestic #28	71.77	50.91	20.86	1.00	20.86	Windmill #08	57.15	24.63	32.52	1.00	32.52
PP Well #05	7.46	0.00	7.46	1.00	7.46	PP Well #08	9.23	2.39	6.84	1.00	6.84
PP Well #06	29.21	33.91	-4.70	1.00	-4.70	PP Well #20	74.94	41.12	33.82	0.20	6.76
NMUtility-1	13.81	11.13	2.68	0.20	0.54	Windmill #28	19.25	86.50	-67.25	1.00	-67.25
NMUtility-2	50.57	5.16	45.41	0.20	9.08	PP Well #21	58.04	31.37	26.67	0.20	5.33
NMUtility-3	15.58	17.48	-1.90	0.20	-0.38	Windmill #38	12.99	5.98	7.01	1.00	7.01

Table A3. Observed and simulated values of water levels (italics), ^{14}C activities, and hydrochemical zones (bold)—Continued.

Well Name	Observed value*	Simulated value	Residual	sqrt (weight)	Weighted residual	Well Name	Observed value*	Simulated value	Residual	sqrt (weight)	Weighted residual
PP Well #22	68.06	78.93	-10.87	0.20	-2.18	Tome-D	8.80	12.03	-3.23	1.00	-3.23
SanJose-2	29.10	30.30	-1.20	0.20	-0.24	PP Well #12	92.03	49.36	42.67	0.20	8.53
Domestic #33	15.18	10.60	4.58	1.00	4.58	Tramway-E	53.97	81.04	-27.07	0.20	-5.41
Sandia-D	15.33	6.08	9.25	1.00	9.25	Domestic #34	83.31	29.33	53.98	1.00	53.98
Sandia-M	10.43	13.99	-3.56	1.00	-3.56	Windmill #33	3.27	0.13	3.14	1.00	3.14
SandiaPeak1	77.98	77.18	0.80	0.20	0.16	VolAndia-2	70.57	33.96	36.61	0.20	7.32
SandiaPeak3	83.23	77.13	6.01	0.20	1.22	VolAndia-5	57.78	61.23	-3.45	0.20	-0.69
Sandia-S	62.89	60.67	2.22	1.00	2.22	VolcanoCf-1	9.28	4.81	4.47	0.20	0.89
Windmill #09	39.70	9.23	30.47	1.00	30.47	Walker-1	41.64	29.39	12.25	0.20	2.45
SantaAna-B D	6.47	18.32	-11.85	1.00	-11.85	Webster-1	45.46	45.38	0.08	0.20	0.02
SantaAna-B M	8.24	24.19	-15.95	1.00	-15.95	WestBluf-11	2.00	0.28	1.72	1.00	1.72
SantaAna-B S	5.54	20.49	-14.95	1.00	-14.95	WestBluf-12	30.02	17.20	12.82	1.00	12.82
SantaBarb-1	49.07	49.39	-0.32	0.20	-0.06	WestBluf-21	61.51	77.36	-15.85	1.00	-15.85
Windmill #45	12.16	5.42	6.74	1.00	6.74	West-Mesa-3	8.89	7.37	1.52	0.20	0.30
Windmill #39	10.40	46.97	-36.57	1.00	-36.57	Domestic #20	24.66	8.85	15.81	1.00	15.81
Windmill #29	19.21	20.52	-1.31	1.00	-1.31	Yale-1	39.16	56.21	-17.05	0.20	-3.41
Domestic #14	79.91	45.39	34.52	1.00	34.52	Windmill #12	38.08	18.22	19.86	1.00	19.86
Domestic #15	11.62	20.31	-8.69	1.00	-8.69	Windmill #40	50.70	28.45	22.25	1.00	22.25
SH03(UNM)	96.31	75.65	20.67	1.00	20.67	Windmill #41	71.29	47.58	23.71	1.00	23.71
SierVista-D	1.89	2.44	-0.55	1.00	-0.55	Windmill #13	84.47	72.72	11.75	1.00	11.75
SierVista-M	34.24	0.65	33.59	1.00	33.59	Windmill #43	22.33	32.24	-9.91	1.00	-9.91
SierVista-S	68.85	79.09	-10.24	1.00	-10.24	Windmill #44	51.55	58.62	-7.07	1.00	-7.07
Domestic #16	32.57	51.45	-18.88	1.00	-18.88	Zia-Ball Park D	18.34	1.09	17.25	0.20	3.45
Sister Cities 1	7.97	9.10	-1.13	1.00	-1.13	Zia Ball Park M	20.70	38.03	-17.33	0.20	-3.47
Sister Cities 2	64.72	37.57	27.15	1.00	27.15	PP Well #13	71.20	39.52	31.68	1.00	31.68
Soil-Amend	4.50	4.16	0.34	0.20	0.07	PP Well #14	37.39	38.04	-0.65	1.00	-0.65
Windmill #30	23.12	0.06	23.06	1.00	23.06	Zia-BMT-D	8.30	34.81	-26.51	1.00	-26.51
Windmill #31	32.05	62.35	-30.30	1.00	-30.30	**rg2west**	2160	2790	-630	0.05	-28.64
Domestic #18	66.42	76.22	-9.80	1.00	-9.80	**rg2east**	1350	668	682	0.07	48.71
SWAB-1-D	6.57	5.81	0.76	1.00	0.76	**rg4west**	1890	3443	-1553	0.05	-81.74
SWAB-1-S	9.12	6.51	2.61	1.00	2.61	**rg4east**	900	779	121	0.11	13.44
SWAB-2-D	14.35	5.96	8.39	1.00	8.39	**rg6south**	500	502	-2	0.20	-0.40
SWAB3-760	44.06	22.97	21.09	1.00	21.09	**rp1north**	1800	1730	70	0.06	3.89
SWAB3-980	44.08	44.09	-0.01	1.00	-0.01	**rp2west**	540	599	-59	0.20	-11.80
Windmill #32	30.54	18.52	12.02	1.00	12.02	**rp2east**	1800	2138	-338	0.06	-18.78
Thomas-6	44.21	40.41	3.80	0.20	0.76	**rp3west**	1440	1794	-354	0.07	-25.29
Windmill #10	9.70	0.58	9.12	1.00	9.12						

*Water-level observed values are equal to the water-level altitude values (table A1) minus 4,650 feet. ^{14}C activity observed values are equal to the percent modern carbon values in table A2. Geochemical zone observed values are the estimated number of path lines that would originate from the river (table 2).

APPENDIX B. Computer Programs

A1. PROGRAM Prep.f

```
      common ilayer(3,80,156),tmult(13),und(6),age(6),
     1       rech(19),nc(6),ncr(17),rarray(80,156),
     2       irech(80,156),izone(19,19),izund(19,19),
     3       nzones(19),nzund(19),izoncd(80),vcond(80),
     4       thick(80,156,9),hcond(80,156,9),
     5       trans(80,156,2)
      character*1 a1
      character*20 name(6),form,tname
      OPEN(UNIT=15,FILE='UFLOWLAY2',STATUS='old')
      OPEN(UNIT=16,FILE='UFLOWLAY3',STATUS='old')
      OPEN(UNIT=17,FILE='UFLOWLAY4',STATUS='old')
      OPEN(UNIT=8,FILE='undflw.12',STATUS='UNKNOWN')
      OPEN(unit=9,FILE='params',STATUS='old')
      OPEN(unit=10,file='rechrg.map',status='old')
      OPEN(unit=11,file='rech001.18',status='unknown')
      OPEN(unit=12,file='recharge',status='unknown')
      OPEN(unit=13,file='age77',status='unknown')
      OPEN(unit=21,file='hcond1',status='unknown')
      OPEN(unit=22,file='hcond2',status='unknown')
      OPEN(unit=23,file='hcond3',status='unknown')
      OPEN(unit=24,file='hcond4',status='unknown')
      OPEN(unit=25,file='hcond5',status='unknown')
      OPEN(unit=26,file='hcond6',status='unknown')
      OPEN(unit=27,file='hcond7',status='unknown')
      OPEN(unit=28,file='trans8',status='unknown')
      OPEN(unit=29,file='trans9',status='unknown')
      OPEN(unit=31,file='vcon12',status='unknown')
      OPEN(unit=32,file='vcon23',status='unknown')
      OPEN(unit=33,file='vcon34',status='unknown')
      OPEN(unit=34,file='vcon45',status='unknown')
      OPEN(unit=35,file='vcon56',status='unknown')
      OPEN(unit=36,file='vcon67',status='unknown')
      OPEN(unit=37,file='vcon78',status='unknown')
      OPEN(unit=38,file='vcon89',status='unknown')
      OPEN(unit=41,file='ZONE1.array',status='unknown')
      OPEN(unit=42,file='ZONE2.array',status='unknown')
      OPEN(unit=43,file='ZONE3.array',status='unknown')
      OPEN(unit=44,file='ZONE4.array',status='unknown')
      OPEN(unit=45,file='ZONE5.array',status='unknown')
      OPEN(unit=46,file='ZONE6.array',status='unknown')
      OPEN(unit=47,file='ZONE7.array',status='unknown')
      OPEN(unit=48,file='ZONE8.array',status='unknown')
      OPEN(unit=49,file='ZONE9.array',status='unknown')
      OPEN(unit=51,file='thick1',status='unknown')
      OPEN(unit=52,file='thick2',status='unknown')
      OPEN(unit=53,file='thick3',status='unknown')
      OPEN(unit=54,file='thick4',status='unknown')
      OPEN(unit=55,file='thick5',status='unknown')
      OPEN(unit=56,file='thick6',status='unknown')
      OPEN(unit=57,file='thick7',status='unknown')
      OPEN(unit=58,file='thick8',status='unknown')
```

```
      OPEN(unit=59,file='thick9',status='unknown')
c
c  read in time recharge mulitpliers
c
      tmult0=1.0
      read(9,*) im1,tmult1
      read(9,*) im2,tmult2
      read(9,*) im3,tmult3
      read(9,*) im4,tmult4
      read(9,*) im5,tmult5
      read(9,*) im6,tmult6
      if (im1.eq.0) tmult1=0.5*(tmult0+tmult2)
      if (im3.eq.0) tmult3=0.5*(tmult2+tmult4)
      if (im5.eq.0) tmult5=0.5*(tmult4+tmult6)
      tmult( 1)=(2.*tmult6 + 0.*tmult6) / 2.
      tmult( 2)=(1.*tmult6 + 1.*tmult5) / 2.
      tmult( 3)=(2.*tmult5 + 0.*tmult5) / 2.
      tmult( 4)=(1.*tmult5 + 1.*tmult4) / 2.
      tmult( 5)=(2.*tmult4 + 0.*tmult4) / 2.
      tmult( 6)=(1.*tmult4 + 1.*tmult3) / 2.
      tmult( 7)=(2.*tmult3 + 0.*tmult3) / 2.
      tmult( 8)=(1.*tmult3 + 1.*tmult2) / 2.
      tmult( 9)=(2.*tmult2 + 0.*tmult2) / 2.
      tmult(10)=(1.*tmult2 + 1.*tmult1) / 2.
      tmult(11)=(2.*tmult1 + 0.*tmult1) / 2.
      tmult(12)=(1.*tmult1 + 1.*tmult0) / 2.
      tmult(13)=(2.*tmult0 + 0.*tmult0) / 2.
      iwelcb=79
c
c  read in the recharge code map
c
      DO 5 IY=1,156
        READ(10,4) (IRECH(IX,IY),IX=1,80)
    5 CONTINUE
    4 FORMAT(40I2)
      read(9,*) nrechp
      DO 9 irch=1,nrechp
        ncr(irch)=0
        read(9,*) nzones(irch),rech(irch)
        read(9,*) (izone(iz,irch),iz=1,nzones(irch))
        DO 8 IY=1,156
          DO 7 IX=1,80
            do 6 iz=1,nzones(irch)
              IF (izone(iz,irch).EQ.IRECH(IX,IY)) THEN
                ncr(irch)=ncr(irch)+1
              ENDIF
    6       CONTINUE
    7     CONTINUE
    8   CONTINUE
    9 CONTINUE
      read(9,*) rech(18)
      read(9,*) rech(19)
c
c  read in recharge rates in (in acre-feet per year)
c     and convert to feet/day per square kilometer
c
      do 10 irch=1,19
```

```
        rech(irch)=rech(irch)*43560./(3281.*3281.*365.24)
   10 continue
c
c   Construct recharge array into file
c
      rpcell=71.
      rjcell=31.
      rpincr=(rech(18)-rech(1))/rpcell
      rjincr=(rech(19)-rech(2))/rjcell
      ijrst=0
      irpst=0
      do 114 iy=1,156
        do 113 ix=1,80
          irr=irech(ix,iy)
          if (irr.ne.0) then
            do 222 irch=1,nrechp
              do 333 iz=1,nzones(irch)
                if (izone(iz,irch).eq.irr) then
                  rarray(ix,iy)=rech(irch)/ncr(irch)
                endif
  333         continue
  222       continue
          else
            rarray(ix,iy)=0.0
          endif
  113   continue
        if (iy.eq.3) ijrst=1
        if (ijrst.eq.1) rech(2)=rech(2)+rjincr
        if (iy.eq.72) irpst=1
        if (irpst.eq.1) rech(1)=rech(1)+rpincr
  114 continue
      do 115 ist=1,13
        do 115 iy=1,156
          write(12,116) (rarray(ix,iy),ix=1,80)
 115    continue
  116 format(1P8E11.4)
c
c   Construct main recharge file
c
      nrchop=3
      irchcb=79
      itop=1
      inrech=1
      iprn=-1
      ifile=71
      form="(8G11.0)            "
      write(11,11) nrchop,irchcb,itop
 11   format(3I10)
      do 15 istp=1,13
        write(11,11) inrech
        write(11,12) ifile,tmult(istp),form,iprn
 12     format(i10,f10.5,A20,i10)
 15   continue
c
c set number of cells along each reach
c
      name( 1)='San Juan Basin      '
```

```
      name( 2)='Jemez Mountains West'
      name( 3)='Jemez Mountains East'
      name( 4)='Hagan Basin          '
      name( 5)='Western Margin       '
      name( 6)='Southwestern Margin  '
c      name( 7)='Rio Salado           '
c      name( 8)='Ladron Peak          '
c      name( 9)='Rio Puerco North End'
c      name(10)='Jemez River NorthEnd'
c      name(11)='Jemez Arroyos Local  '
c      name(12)='Santa Fe and Arroyos'
c      name(13)='Jemez Mountains      '
c      name(14)='Tijeras Arroyo       '
c      name(15)='Abo Arroyo           '
c      name(16)='Las Huertas Creek    '
c      name(17)='North Sandia Front   '
c      name(18)='Sandia Mountain Frnt'
c      name(19)='Tijeras Arroyo Front'
c      name(20)='Hell Canyon Front    '
c      name(21)='Manzano Mountains    '
c      name(22)='Los Pinos Mountains  '
c      name(23)='Central Volcanics    '
c      name(24)='Rio Puerco South End'
c      name(25)='Jemez River SouthEnd'
c
c  read in the UFLOWLAY arrays
c
      ifile=15
      do 60 il=1,3
        do 50 iy=1,156
          read(ifile,777) (ilayer(il,ix,iy),ix=1,80)
  50    continue
        ifile=ifile+1
  60  continue
c
c  read in underflow fluxes (in acre-feet per year)
c     and underflow ages (in years), then convert
c     fluxes to cfd.
c
      read(9,*) nundp
c
c create underflow vectors from icode map arrays
c   one for each of the 13 stress periods
c   Jemez mountain west region first
c
c
      mxcell=0
      do 500 is=1,nundp
        nc(is)=0
        read(9,*) nzund(is),und(is)
        read(9,*) (izund(iz,is),iz=1,nzund(is))
        do 590 ix=1,80
          do 580 iy=1,156
            do 570 il=1,3
              do 560 iz=1,nzund(is)
                if (ilayer(il,ix,iy).eq.izund(iz,is)) then
```

```
                  nc(is)=nc(is)+1
                  mxcell=mxcell+1
                endif
  560         continue
  570       continue
  580     continue
  590   continue
  500 continue
      do 20 iund=1,nundp
        und(iund)=und(iund)*43560./365.24
   20 continue
      write(8,888) mxcell,iwelcb
      do 1000 it=1,13
      write(8,888) mxcell
        do 900 is=1,nundp
          do 890 ix=1,80
            do 880 iy=1,156
              do 870 il=1,3
                if (ilayer(il,ix,iy).ne.0) then
                  do 860 iz=1,nzund(is)
                    if (ilayer(il,ix,iy).eq.izund(iz,is)) then
                      flux=tmult(it)*und(is)/(3.0*nc(is))
                      tage=age(is)
                      tname=name(izund(iz,is))
                      iface=-1
                      write(8,888) il+1,iy,ix,flux,iface,tname
                    endif
  860             continue
                endif
  870         continue
  880       continue
  890     continue
  900   continue
 1000 continue
c
c read in conductivity parameters
c
      read(9,*) hcsfnw
      read(9,*) hcsfne
      read(9,*) hcsfsw
      read(9,*) hcsfse
      read(9,*) hclfnw
      read(9,*) hclfne
      read(9,*) hclfsw
      read(9,*) hclfse
      read(9,*) hcsilt
      read(9,*) hcceja
      read(9,*) hcdp3
      read(9,*) hcdp4
      read(9,*) hcdp5
      read(9,*) hcdp6
      read(9,*) hcalsd
      read(9,*) hcalal
      read(9,*) hcalbl
      read(9,*) anisnw
      read(9,*) anisne
```

```
      read(9,*) anissw
      read(9,*) anisse
      read(9,*) fault1
      read(9,*) fault2
      read(9,*) volcan
      read(9,*) sntafe
      write(13,*) sntafe
c
c create and write hcond files
c
      do 999 it=1,9
        read(40+it,1666) a1
        do 988 iy=1,156
          read(40+it,666) (izoncd(ix),ix=1,80)
          if (it.gt.1) read(50+it,606) (thick(ix,iy,it),ix=1,80)
          do 977 ix=1,80
            if (izoncd(ix).eq.0) then
              hcond(ix,iy,it)=0.0
            elseif (izoncd(ix).eq.3) then
              hcond(ix,iy,it)=hcdp3
            elseif (izoncd(ix).eq.4) then
              hcond(ix,iy,it)=hcdp4
            elseif (izoncd(ix).eq.5) then
              hcond(ix,iy,it)=hcdp5
            elseif (izoncd(ix).eq.6) then
              hcond(ix,iy,it)=hcdp6
            elseif (izoncd(ix).eq.8) then
              hcond(ix,iy,it)=hcsilt
            elseif (izoncd(ix).eq.10) then
              hcond(ix,iy,it)=hcceja
            elseif (izoncd(ix).eq.98.or.izoncd(ix).eq.99) then
              hcond(ix,iy,it)=volcan
            elseif (izoncd(ix).eq.80.or.izoncd(ix).eq.11) then
              if (iy.lt.43) then
                hcond(ix,iy,it)=hcalsd
              elseif (iy.gt.85) then
                hcond(ix,iy,it)=hcalbl
              else
                hcond(ix,iy,it)=hcalal
              endif
            elseif (izoncd(ix).eq.9) then
                vnw=alog10(hcsfnw)
                vne=alog10(hcsfne)
                vsw=alog10(hcsfsw)
                vse=alog10(hcsfse)
                hcsfn=vnw+ix*(vne-vnw)/80.
                hcsfs=vsw+ix*(vse-vsw)/80.
                hcsf=hcsfn+iy*(hcsfs-hcsfn)/156.
                hcond(ix,iy,it)=10**hcsf
            elseif (izoncd(ix).eq.7) then
                vnw=alog10(hclfnw)
                vne=alog10(hclfne)
                vsw=alog10(hclfsw)
                vse=alog10(hclfse)
                hcsfn=vnw+ix*(vne-vnw)/80.
                hcsfs=vsw+ix*(vse-vsw)/80.
```

```
                hcsf=hcsfn+iy*(hcsfs-hcsfn)/156.
                hcond(ix,iy,it)=10**hcsf
              endif
              if (ix.eq.55.and.iy.gt.50.and.iy.lt.75) then
                hcond(ix,iy,it)=fault2
              elseif (ix.eq.16.and.iy.gt.92.and.iy.lt.107) then
                hcond(ix,iy,it)=fault1
              elseif (ix.eq.17.and.iy.gt.87.and.iy.lt.94) then
                hcond(ix,iy,it)=fault1
              elseif (ix.eq.18.and.iy.gt.74.and.iy.lt.89) then
                hcond(ix,iy,it)=fault1
              endif
              if (it.ge.8) then
                trans(ix,iy,it-7)=hcond(ix,iy,it)*thick(ix,iy,it)
              endif
  977       continue
            if (it.lt.8) then
              write(it+20,899) (hcond(ix,iy,it),ix=1,80)
            else
              write(it+20,899) (trans(ix,iy,it-7),ix=1,80)
            endif
  988     continue
  999   continue
c
c create and write vcond files
c
        do 1999 it=1,8
          do 1988 iy=1,156
            do 1977 ix=1,80
              if (hcond(ix,iy,it).ne.0.) then
                term1=thick(ix,iy,it)/hcond(ix,iy,it)
              else
                term1=0.
              endif
              if (hcond(ix,iy,it+1).ne.0) then
                term2=thick(ix,iy,it+1)/hcond(ix,iy,it+1)
              else
                term2=0.
              endif
              if (term1.eq.0.and.term2.eq.0) then
                vcond(ix)=0.0
              else
                anison=anisnw+ix*(anisne-anisnw)/80.
                anisos=anissw+ix*(anisse-anissw)/80.
                aniso=anison+iy*(anisos-anison)/156.
                vcond(ix)=2.0*aniso/(term1+term2)
              endif
 1977       continue
            write(it+30,899) (vcond(ix),ix=1,80)
 1988     continue
 1999   continue
        stop
  606   format(10f9.1)
  666   format(80I2)
 1666   format(a1)
  777   format(80I1)
```

```
  888 format(3I10,F10.3,I10,5x,A20)
  899 format(1P10E11.4)
      end



A2.  PROGRAM  Getheads.f

      common /reals/ head(80,156,9),fx(200),fy(200),fz(200)
      common /integ/ ix1(200),ix2(200),iy1(200),iy2(200),
     1               iz1(200),iz2(200)
      common /charc/ name(200)
      character*13 a1
      character*3  a2,a3
      character*10 name
      open(unit=5,file="output",status="unknown")
      open(unit=6,file="water_well_points",status="unknown")
      open(unit=7,file="heads",status="unknown")
      open(unit=8,file="initheads",status="unknown")
      do 50 iw=1,200
        read(6,55) ix1(iw),ix2(iw),iy1(iw),iy2(iw),iz1(iw),
     1             iz2(iw),fx(iw),fy(iw),fz(iw),name(iw)
   50 continue
   55 format(6I5,3G10.0,2x,A10)
      do 250 iline=1,10000000
        read(5,2000) a1
        if (A1.EQ.'HEAD IN LAYER') THEN
          do 200 k=1,9
            do 100 il=1,9
              READ(5,3000) A3
  100       continue
            DO 150 J=1,156
              READ(5,*) ig,(heaD(I,J,k),I=1,80)
  150       CONTINUE
            READ(5,3000) A3
            READ(5,3000) A3
  200     continue
          GO TO 300
        ENDIF
  250 CONTINUE
c
c  trilinear interpolation between 8 cells
c
  300 DO 500 iw=1,200
        h1=head(ix1(iw),iy1(iw),iz1(iw))
        h2=head(ix1(iw),iy1(iw),iz2(iw))
        h3=head(ix1(iw),iy2(iw),iz1(iw))
        h4=head(ix1(iw),iy2(iw),iz2(iw))
        h5=head(ix2(iw),iy1(iw),iz1(iw))
        h6=head(ix2(iw),iy1(iw),iz2(iw))
        h7=head(ix2(iw),iy2(iw),iz1(iw))
        h8=head(ix2(iw),iy2(iw),iz2(iw))
        if (h2.eq.0.) h2=head(ix1(iw),iy1(iw),iz2(iw)+1)
        if (h1.eq.0.) h1=h2
        if (h4.eq.0.) h4=head(ix1(iw),iy2(iw),iz2(iw)+1)
        if (h3.eq.0.) h3=h4
```

```
        if (h6.eq.0.) h6=head(ix2(iw),iy1(iw),iz2(iw)+1)
        if (h5.eq.0.) h5=h6
        if (h8.eq.0.) h8=head(ix2(iw),iy2(iw),iz2(iw)+1)
        if (h7.eq.0.) h7=h8
        hx1=h1*(1.0-fx(iw))+fx(iw)*h5
        hx2=h2*(1.0-fx(iw))+fx(iw)*h6
        hx3=h3*(1.0-fx(iw))+fx(iw)*h7
        hx4=h4*(1.0-fx(iw))+fx(iw)*h8
        hxy1=hx1*(1.0-fy(iw))+fy(iw)*hx3
        hxy2=hx2*(1.0-fy(iw))+fy(iw)*hx4
        hxyz=hxy1*fz(iw)+hxy2*(1.0-fz(iw))
        WRITE(7,1000) name(iw), hxyz
  500 CONTINUE
      do 800 iz=1,9
        do 700 iy=1,156
          do 600 ix=1,80
            if (head(ix,iy,iz).eq.0.0) then
              if (iy.gt.20) then
                head(ix,iy,iz)=(160-iy)*3.0
              else
                head(ix,iy,iz)=(160-iy)*4.0
              endif
            endif
  600     continue
          write(8,900) (head(ix,iy,iz),ix=1,80)
  700   continue
  800 continue
      STOP
  900     format(14f9.4)
 1000 FORMAT(2x,A10,2x,F12.4)
 2000 FORMAT(14X,A13)
 3000 FORMAT(A3)
      END
```

A3. PROGRAM Post.f

```
      character*25 wnamea,wnameb
      open(unit=5,file='endyears',status='unknown')
      open(unit=6,file='c14ages',status='unknown')
      read(5,200) iz,ixa,iya,il,time,c14a,it,x,y,wnamea
      ikount=1
      c14t=c14a
  10  read(5,200) iz,ixb,iyb,il,time,c14b,it,x,y,wnameb
      if (wnameb.eq.' source area delineation ') go to 50
      if (wnamea.ne.wnameb) then
        c14=c14t/ikount
        write(6,300) ixa,iya,c14,wnamea
        ikount=1
        c14t=c14b
      else
        ikount=ikount+1
        c14t=c14t+c14b
      endif
      ixa=ixb
      iya=iyb
```

```
      wnamea=wnameb
      go to 10
   50 c14=c14t/ikount
      write(6,300) ixa,iya,c14,wnamea
c      iz1=0
      iz2=0
      iz3=0
      iz6=0
      iz7=0
      iza=0
      ip1=0
      ip2=0
      ip3=0
      ip4=0
      do 100 ip=1,58000
        read(5,200,end=400) iz,ixb,iyb,il,time,c14b,it,x,y
c      if (y.gt.120                          .and.iz.eq.12) iz1=iz1+1
      if (y.gt.80.and.y.lt.110.and.x.lt.45.and.iz.eq.12) iz2=iz2+1
      if (y.gt.80.and.y.lt.110.and.x.gt.45.and.iz.eq.12) iz3=iz3+1
      if (y.gt.50.and.y.lt.80 .and.x.lt.40.and.iz.eq.12) iz6=iz6+1
      if (y.gt.50.and.y.lt.80 .and.x.gt.40.and.iz.eq.12) iz7=iz7+1
      if (y.gt.20.and.y.lt.50             .and.iz.eq.12) iza=iza+1
      if (y.gt.60.and.y.lt.85             .and.iz.eq. 5) ip1=ip1+1
      if (y.gt.35.and.y.lt.60 .and.x.lt.15.and.iz.eq. 5) ip2=ip2+1
      if (y.gt.35.and.y.lt.60 .and.x.gt.15.and.iz.eq. 5) ip3=ip3+1
      if (y.gt.10.and.y.lt.35             .and.iz.eq. 5) ip4=ip4+1
  100 continue
  400 write(6,*) iz2
c      write(6,*) iz2
      write(6,*) iz3
      write(6,*) iz6
      write(6,*) iz7
      write(6,*) iza
      write(6,*) ip1
      write(6,*) ip2
      write(6,*) ip3
      write(6,*) ip4
      stop
  200 format(4i6,g10.0,g11.0,i5,2g9.0,A25)
  300 format(2I5,1pe11.4,A25)
      end
```